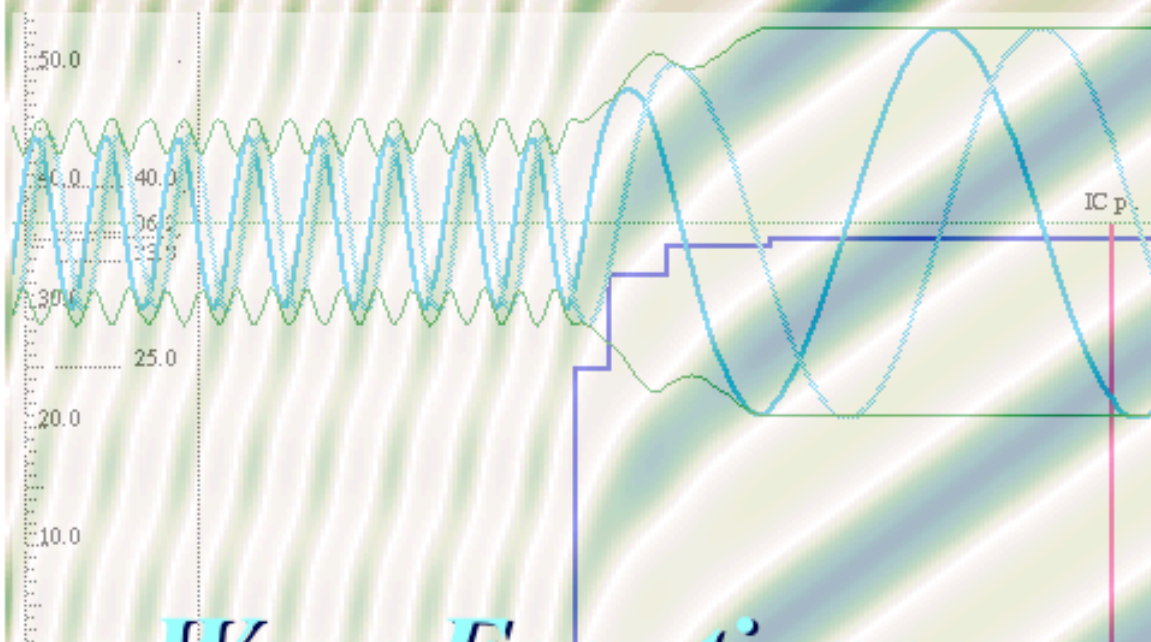


Quantum Theory for the Computer Age Unit 4



Wave Equations in Potentials

Unit 4 Wave Equations in Potentials

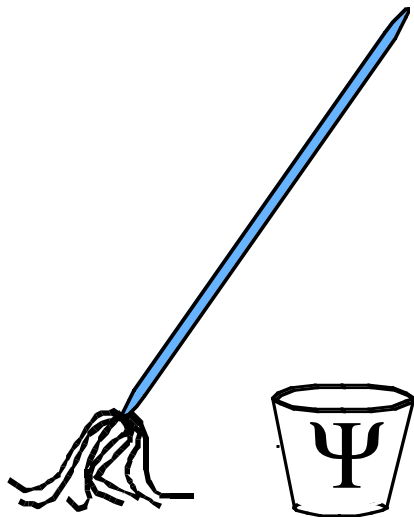
Unit 3 introduced the Schrodinger time equation using Fourier analysis and applied it to discrete systems with Fourier C_n symmetry. Unit 4 begins by relating the discrete wave analysis to difference equations and then differential equations. The best known such equations are Schrodinger's wave equation and time-independent potential equation. Such equations apply to systems of an arbitrary symmetry whose interaction with the environment is usually determined by a spatial potential function $V(x)$. Having such a potential goes against the relativistic symmetry and therefore Schrodinger theory is a low-energy approximation that treats time as an external parameter. In this Unit 4, the external environment is further approximated by representing the potential as a sequence of piecewise constant steps. Wave scattering depends on transmission and reflection amplitudes in crossing and scattering matrices (C-matrices and S-matrices) whose singularities represent resonances or bound states.

W. G. Harter
Department of Physics
University of Arkansas
Fayetteville

Hardware and Software by

HARTER-*Soft*

Elegant Educational Tools Since 2001



QM for AMOP

Chapter 11 Differential Wave Equations

W. G. Harter

UNIT 4 WAVE EQUATIONS IN POTENTIALS	1
CHAPTER 11. INTRODUCTION TO WAVE EQUATIONS	1
11.1 Discrete versus Continuous x and k Variables	2
11.2 Difference versus differential operators in coordinate space.....	4
(a) First differences and derivatives	4
(b) Second differences and derivatives.....	6
(c) Differential equations in Dirac notation: Green's operator	8
(d) Adjoint differential operator.....	9
(1) Self-Adjoint differential operator: Sturm-Liouville form	9
(2) Higher order difference and differential operators.....	10
11.3 Momentum and coordinate space operators : Fourier transforms.....	11
(a) Coordinate space and operators.....	11
(b) Wavevector operator k	12
(c) Momentum operator p.....	12
(d) Coordinate to momentum change-of-basis	13
11.4 Differential Wave Equations of Schrodinger.....	15
(a) Schrodinger Wave Equations in coordinate representation.....	15
(b) Free space wavefunction solutions	16
(c) Exponential and evanescent wavefunctions	18
(d) Schrodinger Wave Equations in momentum representation	19
11.5 Classical-Wave Analogies for Schrodinger equations	20
(a) Classical wave equation: “Phonon-like” to “photon-like” dispersion	21
(b) Classical gravity-waves: “Exciton-like” dispersion	22
(c) Shower-curtain model of Schrodinger equation	23
(d.) Klein-Gordon equations: Relativistic dispersion?	25
(e) “Hyper” Schrodinger equations and hyper-dispersion.....	26
Problems for Chapter 11	29
CHAPTER 12. INFINITE WELL STATES AND DYNAMICS	1
12.1 Infinite-Well Wavefunctions	1
(a) Eigenstate wavefunctions	1
(b) Superposition wavefunctions	2
(c) Energy expectation values.....	3
(d) Position expectation values.....	4
(e) Position moments: Dipole matrices	5
Moments of morphology	7
12.2 Wave Packet Shape and Dynamics	8
(a) Uncertainty relation and "Last-in-First-out" effect	9
(b) Wavepacket explodes! (Then revives)	10
(c) Bohr rotor waves: Relation to square well waves	12

(1) "Boxcar windows": Wavepackets that go "Bang!"15

(2) "Gaussian windows": Wavepackets that go "Poof!"17

(d) Brief history of revival structure and dynamics20

12.3 Infinite Well Dynamics vs. Bohr Waves21

(a) The Bohr image-wave21

(b) Flipped revivals.....22

(b) Cloned revivals23

Problems for Chapter 12.....25

CHAPTER 13. STEP POTENTIAL BARRIERS AND WELLS 1

13.1 Waves and Potential Barriers: Crossing Matrices1

(a) Single boundary potential barrier: C-matrix analysis2

(1) Probability current conservation6

(2) Momentum vs. frequency or energy normalization7

(b) Two boundary potential barriers8

Perfect transmission Case 1: Symmetric potential ($k = k'$)10

Perfect transmission Case 2: Geometric impedance matching ($k' = \sqrt{k k''}$)12

The "Stairway-to-Heaven"13

Units of Length, Energy and Frequency: meV to EeV15

13.2 Square wells: bound states vs. free state resonance.....17

(a) Ramsauer-Townsend resonances ($E > 0$)21

Nearly-grazing states ($E \sim 0$)22

(b) Bound state quantization ($E < 0$): The sine-line solution22

Continuum meets "discreteum"25

13.3 S-Matrix approach to free state resonance dynamics26

(a) Relating S-Matrix and C-matrix27

(b) S-Matrix and C-matrix for elementary barrier: U(2) Formulation28

(c) S-Matrix eigensolutions: Eigenchannels29

(d) U(2) and R(3) pictures of barrier wavestates31

(e) Linear combinations of barrier wavestates34

Remote boundary S-waves: "Sewing" waves together35

(f) Crossing and Scattering-matrices for square well and hump38

Resonance strength, variation and lifetime41

Problems for Chapter 13.....43

REVIEW TOPICS & FORMULAS FOR UNIT 446

One way to “tame” continuous differential operators and differential equations is to discretize them so they become matrix equations. Such “coarse-graining” is required for numerical computer solution. In Chapters 9 and 10, quantum wave equations were written as matrix equations. In this Chapter 11, the connection is made between matrix theory with Dirac notation and the continuum theory of differential wave equations and operator analysis. The most famous of the quantum wave equations are Schrodinger’s equations, one of the foundations of non-relativistic quantum theory. Again, coupled pendulum analogies as in Chapter 10 help us understand what is happening.

Unit 4 Wave Equations in Potentials

Chapter 11. Introduction to Wave Equations

We have waited until now, the fourth unit, to introduce the differential wave equations of quantum mechanics. Chief among these is the Schrodinger differential equation, which in 1927 revolutionized the existing Einstein-Bohr-Kellar semiclassical quantization theory. Bohr quantization seemed full of seemingly unavoidable approximations that the differential approach avoided easily. Also, the Schrodinger equation was welcomed by a generation of physicists trained in Newtonian, Hamiltonian, Maxwellian, and Lorentzian formalism for mechanics, electrodynamics, thermodynamics, and hydrodynamics, all of which had differential equations as the main course, indeed, their identifying icons.

We can only imagine how mysterious the non-classical aspects of the then-new quantum theory must have seemed then if we still find them mysterious scores of years later. Therefore, it is understandable why the appearance of a differential equation from which, in principle, all quantum phenomena could be deduced, would seem like a good and familiar thing. Since space and time had always been treated as a continuum, the use of differential equations came naturally, and still does today. The chances are good that as you read this page, even years after its copyright date, you will be holding one of just a few quantum texts that do not start off with Schrodinger differential equations. Most new texts are like old military manuals that forever fight the last war.

However, proactive researchers need to focus on the *future* engagements. New tools will be required to deal effectively with new problems. For one thing it is the *solutions* to the differential equations that we seek to understand, not just the equations themselves. While the Schrodinger equation is easy to solve for some old textbook problems, it turns out to be rather clumsy in much of modern research. For example, the full Euler-coordinate Schrodinger equation for a rotating asymmetric molecule like water (H_2O) would cover this page for just a rigid-rotor approximation; for the next small-vibration-approximation it would fill this chapter, and with all the electronic and nuclear degrees of freedom included it might fill a library. That's just the *equations*; not their solutions!

One goal of this chapter is to show connections between differential equations and the analogous discrete bra-ket matrices introduced in the preceding Chapters. Another goal is to use the differential equations and operators for the problems in which they are most suitable, namely, unbounded ones with *open boundary conditions*. Finally, a most important goal is to point the way toward more powerful analytical and computational techniques that replace differential analysis when it becomes impractical.

Modern digital computational techniques require a course-grain discretizing of the continuum. This fact, alone, requires satisfactory connection between finite-discrete spaces and ones that are infinite or continuous. However, there are also fundamental reasons for clarifying the relations between discrete and continuous spaces. Some of the resulting insights will be discussed in what follows.

11.1 Discrete versus Continuous x and k Variables

Let us review some of the types of quantum base-state systems studied so far. The latter part of Chapter 7 (Sec. 7.3a and 7.3b) introduced a finite *discrete* and *bounded* N -position coordinate $|x_p\rangle$ -state basis system for N discrete lattice points $\{x_0=0, x_1=a, x_2=2a, x_3=3a, \dots, x_{N-1}=(N-1)a, \}$

$$\{ |0\rangle, |1\rangle, |2\rangle, |3\rangle, \dots, |p\rangle, \dots, |N-1\rangle \} \text{ or } \{ |x_0\rangle, |x_1\rangle, |x_2\rangle, |x_3\rangle, \dots, |x_p\rangle, \dots, |x_{N-1}\rangle \}$$

This so-called *Hilbert* x_p -space is indexed by state *index* numbers $p = 0, 2, 3, \dots, N-1$, which are discrete ("quantized") and *bounded* by N (finite). But, they could be made *unbounded* by letting ($N=\infty$).

At the other extreme, Sec.7.1 and 7.2 introduced ∞ -state systems of *continuous* coordinate x .

$$\{ |-1.001\rangle, \dots, |4.17\rangle, \dots, |x''\rangle, |x'\rangle, \dots, |x\rangle, \dots \}.$$

These so-called *Banach* x -spaces are indexed by a real variable x which may be *bounded* to range only from $x = a$ to $x = b$ (typically from $x = 0$ to $x = L$) or may be *unbounded* and range from $x=-\infty$ to $x = +\infty$.

The wavevector or momentum base states $|k_m\rangle$ or $|k\rangle$ also came in four flavors. First there are the Bohr orbital states $|k_m\rangle$ that are indexed by a quantum number $m = 0, 1, 2, \dots, \infty$ that is discrete but unbounded. (Integer m is the number of 2π -waves in the Bohr circumference bounded by $x = 0$ to $x = L$).

Then there are the Bloch wave states $|k_m\rangle$ similarly indexed except $m = 0, 1, 2, \dots, N-1$ is bounded.

Then there are the two kinds of $|k\rangle$ states with continuous wavevector k obtained from the above by letting $L = \infty$ as in the Bohr system or by letting $N = \infty$ (with L fixed) as in the Bloch system. It might seem that this would lead to a large number of possible transformation matrix combinations beginning with $\langle x_p | k_m \rangle$ and ending with four kinds of $\langle x | k \rangle$. However, just four distinct types of transformations are possible overall. This is diagrammed in Fig. 11.1.1.

The X's mark off systems that are incompatible because their dimensions are different; obviously an N -dimensional basis cannot be transformed into an ∞ -dimensional one by a "square" transformation matrix. Neither can an unbounded continuum be mapped one-to-one onto its sub-set of integers that skip all the irrational numbers. Similarly, a bounded continuum is a subset of the whole (unbounded) continuum. Transformation matrices must satisfy orthonormality-completeness axioms-2 and 3. These have a unitary symmetry that makes them two sides of one coin, so to speak.

The O's mark off systems that have incompatible boundary conditions. A bounded x -continuum leads to unbounded but discrete k -set of Bohr orbitals through conditions (7.1.3) repeated below

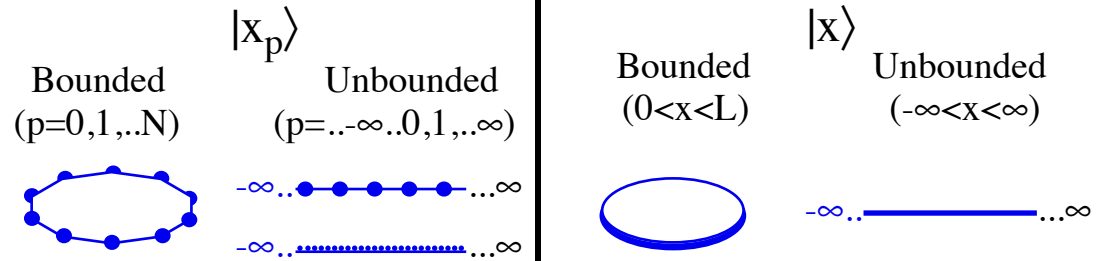
$$0 < x \leq L ; \quad \text{leads to: } k_m = \frac{2\pi}{L} m, \quad \text{where: } m = 0, \pm 1, \pm 2, \pm 3, \dots, \pm \infty \quad (7.1.3)_{\text{repeated}}$$

Similarly, an unbounded but discrete set of x -points (the infinite lattice: (7.1.3) with $L=aN=\infty$) leads to a bounded Bloch k -continuum, that is, the Brillouin zone bounded by $\pm k_{BZB}$ as defined in (9.3.9a).

$$x_p = p a = p L/N, \quad \text{where: } p = 0, 1, 2, 3, \dots, \infty; \quad \text{leads to: } -k_{BZB} \leq k < k_{BZB} = \pi/a \quad (11.1.1)$$

It is remarkable that a bounded continuum, irrationals and all, can be "counted" discretely by an infinite set of integers. Finer and finer wave zeros must eventually land close to all the numbers, rational or irrational.

Discrete Coordinate Bases | Continuous Coordinate Bases



Discrete Momentum Bases

$ k_m\rangle$ Bounded (m=0,1,..N)	Discrete Bloch System 	X	X	X
	Unbounded (m=0,1,..∞)	X	O	Discrete Bohr System
$ k\rangle$ Bounded (-k _{BZ} <k<k _{BZ})	X	Continuous Bloch System 	O	X
	Unbounded (-∞<k<∞)	X	X	Continuous Bohr System

Fig. 11.1.1 Comparison of discrete versus continuum systems

What we are discussing here is known as the *point-set topology* of our possible quantum spaces. This just means we're viewing the empty terrain or "real estate" and its effect on a quantum particle wave adding any structures such as potentials or force fields. Potentials are introduced later in this Chapter.

11.2 Difference versus differential operators in coordinate space

Most treatments of quantum mechanics (including Bohr's and Schrodinger's original development) begin with the x -continuum side of Fig. 11.1.1. Here we finally consider the x -differential equations that result from an x -continuum. However, the connection between the corresponding discrete x_p side of Fig. 11.1.1 will be maintained. The discrete side involves x_p -*difference equations*. If you plan to simulate continuum systems on a computer then this connection is essential.

(a) First differences and derivatives

The *first difference* $(\bar{\Delta} \psi)_p$ of a discrete function $\psi(x_p)$ is usually defined by

$$(\bar{\Delta} \psi)_p = \psi(x_{p+1}) - \psi(x_p) . \quad (11.2.1)$$

A matrix representation of $\bar{\Delta}$ acting on a $|\psi\rangle$ ket column of amplitudes

$$\{\langle x_0|\psi\rangle, \langle x_1|\psi\rangle \dots \langle x_p|\psi\rangle \dots\} = \{\psi(x_0), \psi(x_1) \dots \psi(x_p) \dots\} = \{\psi_0, \psi_1, \dots, \psi_p \dots\} \quad (11.2.2)$$

is the following.

$$\bar{\Delta}|\psi\rangle = \begin{pmatrix} \langle x_0|\bar{\Delta}|\psi\rangle \\ \langle x_1|\bar{\Delta}|\psi\rangle \\ \langle x_2|\bar{\Delta}|\psi\rangle \\ \langle x_3|\bar{\Delta}|\psi\rangle \\ \vdots \end{pmatrix} = \begin{pmatrix} -1 & 1 & & & \\ 0 & -1 & 1 & & \\ & 0 & -1 & 1 & \\ & & & 0 & -1 & \dots \\ & & & & \vdots & \ddots \end{pmatrix} \begin{pmatrix} \langle x_0|\psi\rangle \\ \langle x_1|\psi\rangle \\ \langle x_2|\psi\rangle \\ \langle x_3|\psi\rangle \\ \vdots \end{pmatrix} = \begin{pmatrix} \psi_1 - \psi_0 \\ \psi_2 - \psi_1 \\ \psi_3 - \psi_2 \\ \psi_4 - \psi_3 \\ \vdots \end{pmatrix} \quad (11.2.3)$$

This operation is analogous to the *first differential* $df(x)$ in continuum calculus.

$$df(x) = f(x+dx) - f(x) \quad (11.2.4a)$$

While this is an infinitesimal, the following *first derivative* is finite in a suitable limit sequence.

$$\frac{d\psi}{dx} = \frac{\psi(x+dx) - \psi(x)}{dx}, \text{ as: } dx \rightarrow 0 \quad (11.2.4b)$$

By analogy, the finite difference "derivative" or *first derivative* is defined

$$\left(\frac{\bar{\Delta}\psi}{\Delta x}\right)_p = \frac{\psi(x_{p+1}) - \psi(x_p)}{\Delta x} = \frac{\psi(x_{p+1}) - \psi(x_p)}{a} . \quad (11.2.5)$$

Finite differences have no problems with infinitesimal limits, but there is still a question of lattice location. One could define another operator $\bar{\Delta}$ that is the negative transpose of $\bar{\Delta}$ in (11.2.3).

$$\bar{\Delta} \psi = \psi(x_p) - \psi(x_{p-1}) \quad \text{where: } \bar{\Delta} = -\bar{\Delta}^T \quad (11.2.6a)$$

Its representation is

$$\bar{\Delta}|\psi\rangle = \begin{pmatrix} \langle x_0|\bar{\Delta}|\psi\rangle \\ \langle x_1|\bar{\Delta}|\psi\rangle \\ \langle x_2|\bar{\Delta}|\psi\rangle \\ \langle x_3|\bar{\Delta}|\psi\rangle \\ \vdots \end{pmatrix} = \begin{pmatrix} 1 & 0 & & & \\ -1 & 1 & 0 & & \\ & -1 & 1 & 0 & \\ & & & -1 & 1 & \dots \\ & & & & \vdots & \ddots \end{pmatrix} \begin{pmatrix} \langle x_0|\psi\rangle \\ \langle x_1|\psi\rangle \\ \langle x_2|\psi\rangle \\ \langle x_3|\psi\rangle \\ \vdots \end{pmatrix} = \begin{pmatrix} \psi_0 - \psi_{-1} \\ \psi_1 - \psi_0 \\ \psi_2 - \psi_1 \\ \psi_3 - \psi_2 \\ \vdots \end{pmatrix} . \quad (11.2.6b)$$

In continuum calculus no one would quibble about the difference between $\bar{\Delta}$ and $\bar{\Delta}$ since they could not differ by more than an infinitesimal. Indeed, the derivative could just as well be defined using the average $\bar{\Delta}$ of these two operators which is an *anti-symmetric* operator

$$\bar{\Delta} = \frac{\bar{\Delta} + \bar{\Delta}}{2} = -\bar{\Delta}^T \tag{11.2.7a}$$

$$\bar{\Delta}|\psi\rangle = \begin{pmatrix} \langle x_0 | \bar{\Delta} | \psi \rangle \\ \langle x_1 | \bar{\Delta} | \psi \rangle \\ \langle x_2 | \bar{\Delta} | \psi \rangle \\ \langle x_3 | \bar{\Delta} | \psi \rangle \\ \vdots \end{pmatrix} = \begin{pmatrix} 0 & \frac{1}{2} & & & \\ -\frac{1}{2} & 0 & \frac{1}{2} & & \\ & -\frac{1}{2} & 0 & \frac{1}{2} & \\ & & -\frac{1}{2} & 0 & \dots \\ & & & \frac{1}{2} & 0 & \dots \\ & & & & \vdots & \ddots \end{pmatrix} \begin{pmatrix} \langle x_0 | \psi \rangle \\ \langle x_1 | \psi \rangle \\ \langle x_2 | \psi \rangle \\ \langle x_3 | \psi \rangle \\ \vdots \end{pmatrix} = \frac{1}{2} \begin{pmatrix} \psi_1 - \psi_{-1} \\ \psi_2 - \psi_0 \\ \psi_3 - \psi_1 \\ \psi_4 - \psi_2 \\ \vdots \end{pmatrix} \tag{11.2.7b}$$

as follows.

$$(D\psi)_p = \left(\frac{\bar{\Delta}\psi}{\Delta x} \right)_p = \frac{\psi(x_{p+1}) - \psi(x_{p-1})}{2\Delta x} = \frac{\psi(x_{p+1}) - \psi(x_{p-1})}{2a} \xrightarrow{\Delta x \rightarrow 0} \frac{d\psi}{dx} \tag{11.2.7c}$$

While the alternative finite difference operator definitions all lead to the same limit in calculus, they only give slightly different results for unbounded or large- N discrete wave amplitudes. However, they give very different results for small- N discrete systems, particularly, near end points or boundaries.

The discrete and continuum representations of a derivative operator $\mathbf{D} \rightarrow \frac{d}{dx}$ are compared here.

$$\begin{aligned} \langle x_p | \mathbf{D} | \psi \rangle &= \sum_{q=a}^{q=b} \langle x_p | \mathbf{D} | x_q \rangle \langle x_q | \psi \rangle, & \langle x | \mathbf{D} | \psi \rangle &= \int_{y=a}^{y=b} dy \langle x | \mathbf{D} | y \rangle \langle y | \psi \rangle \\ &= (\mathbf{D}\psi)_p = \sum_{q=a}^{q=b} \mathbf{D}_{p,q} \psi_q, & = \mathbf{D}\psi(x) = \frac{d\psi}{dx} &= \int_{y=a}^{y=b} dy D(x,y) \psi(y) \end{aligned} \tag{11.2.8}$$

The continuum matrix element or *kernal* $D(x,y) = \langle x | \mathbf{D} | y \rangle$ of the \mathbf{D} operator follows from definition

$$\langle x | \mathbf{D} | \psi \rangle = \frac{d\psi(x)}{dx} = \frac{d\langle x | \psi \rangle}{dx} \tag{11.2.9a}$$

with $|\psi\rangle$ replaced by $|y\rangle$ and use Dirac's delta $\langle x | y \rangle = \delta(x,y)$. Anti-symmetry (11.2.7a) is added.

$$\langle x | \mathbf{D} | y \rangle = \frac{d\langle x | y \rangle}{dx} = \frac{d\delta(x,y)}{dx} = -\langle y | \mathbf{D} | x \rangle = -\frac{d\delta(y,x)}{dy} \tag{11.2.9b}$$

Now we check this strange kernal by substituting it into the integral (11.2.8) and integrating by parts.

$$\begin{aligned} \int_{y=a}^{y=b} dy \langle x | \mathbf{D} | y \rangle \psi(y) &= -\int_{y=a}^{y=b} dy \frac{d\delta(y,x)}{dy} \psi(y) \\ &= -\delta(y,x) \psi(y) \Big|_{y=a}^{y=b} + \int_{y=a}^{y=b} dy \frac{d\psi(y)}{dy} \delta(y,x) = \frac{d\psi(x)}{dx} \end{aligned} \tag{11.2.10}$$

This shows some more of the power of Dirac's notation and shows why the derivative of a Dirac delta function would cause an integral of a function to yield its derivative! The discrete-space versions of the δ -forms show that two neighboring function points need to be subtracted.

$$(\mathbf{D}\psi)_p = \frac{\psi_{p+1} - \psi_p}{a} = \sum_{q=a}^{q=b} \frac{\delta_{p+1,q} \psi_q - \delta_{p,q} \psi_q}{a} = \sum_{q=a}^{q=b} (\mathbf{D}\delta)_{p,q} \psi_q$$

Indeed, that is analogous to a Dirac-delta derivative. If the Dirac delta is a spike sticking up, as in Fig. 11.2.1a then its derivative is two spikes, as shown in Fig. 11.2.1b; the first one sticking up and the second one sticking down and moved infinitesimally forward to $x+dx$. It is actually the negative of this that must be integrated since we want the difference $-\psi(x)+\psi(x+dx)$ as (11.2.9-10) tells us, not $\psi(x)-\psi(x+dx)$.

(b) Second differences and derivatives

The *second difference* $(\Delta^2 \psi)_p$ of a discrete function $\psi(x_p)$ is defined using two first differences by

$$(\Delta^2 \psi)_p = (\bar{\Delta} \bar{\Delta} \psi)_p = \bar{\Delta} (\psi(x_{p+1}) - \psi(x_p)) = \psi(x_{p+1}) - 2\psi(x_p) + \psi(x_{p-1}). \quad (11.2.11a)$$

A matrix representation of Δ^2 acting on a $|\psi\rangle$ ket column of amplitudes

$$\{\langle x_0|\psi\rangle, \langle x_1|\psi\rangle \dots \langle x_p|\psi\rangle \dots\} = \{\psi(x_0), \psi(x_1) \dots \psi(x_p) \dots\} = \{\psi_0, \psi_1, \dots, \psi_p \dots\}$$

is the following

$$\Delta^2 |\psi\rangle = \begin{pmatrix} \langle x_0 | \Delta^2 | \psi \rangle \\ \langle x_1 | \Delta^2 | \psi \rangle \\ \langle x_2 | \Delta^2 | \psi \rangle \\ \langle x_3 | \Delta^2 | \psi \rangle \\ \vdots \end{pmatrix} = \begin{pmatrix} -2 & 1 & & & \\ & 1 & -2 & 1 & \\ & & 1 & -2 & 1 \\ & & & 1 & -2 & \dots \\ & & & & \vdots & \ddots \end{pmatrix} \begin{pmatrix} \langle x_0 | \psi \rangle \\ \langle x_1 | \psi \rangle \\ \langle x_2 | \psi \rangle \\ \langle x_3 | \psi \rangle \\ \vdots \end{pmatrix} = \begin{pmatrix} \psi_1 - 2\psi_0 + \psi_{-1} \\ \psi_2 - 2\psi_1 + \psi_0 \\ \psi_3 - 2\psi_2 + \psi_1 \\ \psi_4 - 2\psi_3 + \psi_2 \\ \vdots \end{pmatrix} \quad (11.2.11b)$$

Now three points are taken from the function space and the kernel will be a second derivative of the Dirac delta which has three spikes; two up spikes surrounding a down spike of twice the area. (See Fig. 11.2.1c)

$$\langle x | \mathbf{D}^2 | y \rangle = \frac{d^2 \langle x | y \rangle}{dx^2} = \frac{d^2 \delta(x, y)}{dx^2} = \langle y | \mathbf{D}^2 | x \rangle = \frac{d^2 \delta(y, x)}{dy^2} \quad (11.2.12a)$$

It is easy to verify that the integral representation of \mathbf{D}^2 is the usual second derivative.

$$\int_{y=a}^{y=b} dy \langle x | \mathbf{D}^2 | y \rangle \psi(y) = \int_{y=a}^{y=b} dy \frac{d^2 \delta(y, x)}{dy^2} \psi(y) = \frac{d^2 \psi(x)}{dx^2}. \quad (11.2.12b)$$

Furthermore, it is easy to see that $f(\mathbf{x}) \cdot \mathbf{D}^2$ for any function $f(x)$ gives a similar result. In Dirac notation we need to think of a function as a one-point functional evaluation. It is represented by left-multiplying \mathbf{D} by an abstract operator $f(\mathbf{x})$ that is diagonal in the $|x\rangle$ position state basis. That is,

$$f(\mathbf{x}) |x\rangle = f(x) |x\rangle \quad \text{and} \quad \langle y | f(\mathbf{x}) |x\rangle = f(x) \langle y | x \rangle = f(x) \delta(y, x) = f(x) \delta(x, y) \quad (11.2.13)$$

Then the following integral representations follow and correspond to the three parts of Fig. 11.2.1.

$$\int_{y=a}^{y=b} dy \langle x | h(x) \mathbf{1} | y \rangle \psi(y) = \int_{y=a}^{y=b} dy h(x) \delta(y, x) \psi(y) = h(x) \psi(x) \quad (11.2.14a)$$

$$\int_{y=a}^{y=b} dy \langle x | g(x) \mathbf{D} | y \rangle \psi(y) = \int_{y=a}^{y=b} dy g(x) \frac{d\delta(y, x)}{dy} \psi(y) = g(x) \frac{d\psi(x)}{dx} \quad (11.2.14b)$$

$$\int_{y=a}^{y=b} dy \langle x | f(x) \mathbf{D}^2 | y \rangle \psi(y) = \int_{y=a}^{y=b} dy f(x) \frac{d^2 \delta(y, x)}{dy^2} \psi(y) = f(x) \frac{d^2 \psi(x)}{dx^2} \quad (11.2.14c)$$

The first derivative is a bit more troublesome since the delta-derivative is anti-symmetric.

$$\delta'(x, y) = \delta'(x - y) = -\delta'(y - x) = -\delta'(y, x), \quad \text{or:} \quad \delta'(x - y) = \frac{d\delta(x - y)}{dx} = -\frac{d\delta(x - y)}{dy} = -\frac{d\delta(y - x)}{dx}$$

Odd derivatives are represented as asymmetric matrices or anti-symmetric matrices like (11.2.7b). So the delta-derivative is similarly lopsided.

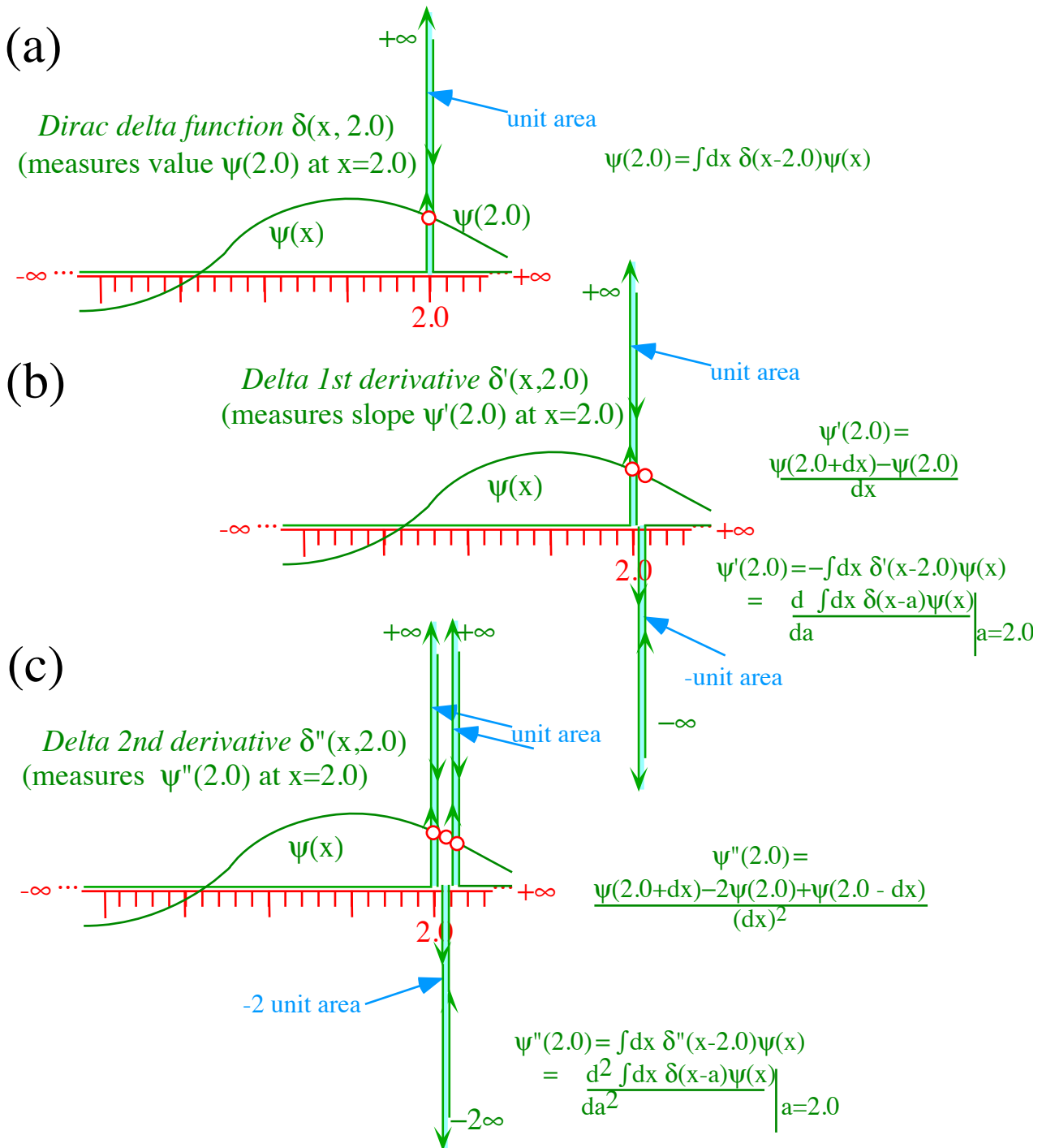


Fig. 11.2.1 Delta function derivatives and function evaluation (a) Zeroth, (b) First, and (c) Second

(c) Differential equations in Dirac notation: Green's operator

Summing (11.2.14) up gives a general linear second order differential equation and its integral operator representation

$$\int_{y=a}^{y=b} dy \langle x | \mathbf{L} | y \rangle \psi(y) = L \cdot \psi(x) = \langle x | \mathbf{L} | \psi \rangle \quad (11.2.15a)$$

where an *inhomogeneous differential equation*

$$L \cdot \psi(x) = f(x) \frac{d^2 \psi(x)}{dx^2} + g(x) \frac{d\psi(x)}{dx} + h(x) \psi(x) = s(x) \quad (11.2.15b)$$

has the following *kernal* or matrix element

$$\langle x | \mathbf{L} | y \rangle = f(x) \frac{d^2 \delta(y, x)}{dy^2} + g(x) \frac{d\delta(y, x)}{dy} + h(x) \delta(y, x) \quad (11.2.15c)$$

and is written in abstract Dirac notation as follows.

$$\mathbf{L} | \psi \rangle = | s \rangle \quad (11.2.15d)$$

The *source function* $s(x)$ or *inhomogeneity* is just another ket-vector represented in x -space by

$$s(x) = \langle x | s \rangle. \quad (11.2.15e)$$

The solution(s) to the equation $L \cdot \psi = s$ have the form

$$| \psi \rangle = | \varphi \rangle + \mathbf{G} | s \rangle, \quad (11.2.15f)$$

where ket $|\varphi\rangle$ is a solution to a *homogeneous equation* (True Schrodinger equations are homogeneous.)

$$\mathbf{L} | \varphi \rangle = \mathbf{0}, \quad (11.2.15g)$$

and \mathbf{G} is called the *Green's operator* and is a quasi-inverse to operator \mathbf{L} . In abstract operator notation

$$\mathbf{L} \cdot \mathbf{G} = \mathbf{1}, \quad (11.2.15h)$$

which in Dirac notation using completeness expands to the following integral representation

$$\int_{x'=a}^{x'=b} dx' \langle x | \mathbf{L} | x' \rangle \langle x' | \mathbf{G} | y \rangle = \langle x | \mathbf{1} | y \rangle = \delta(x, y) \quad (11.2.15i)$$

or converting back to a differential form using (11.2.15b-c), *Green's differential equation*.

$$L \cdot G(x, y) = f(x) \frac{d^2 G(x, y)}{dx^2} + g(x) \frac{dG(x, y)}{dx} + h(x) G(x, y) = \delta(x, y) \quad (11.2.15j)$$

The latter is an "almost homogeneous" equation with just one isolated delta "spike" source. The general solution sums *Green's function* $G(x, x') = \langle x | \mathbf{G} | x' \rangle$ over a *source distribution* $s(x) = \langle x | s \rangle$ of delta spikes to give a complete representation of general solution (11.2.15f).

$$\langle x | \psi \rangle = \langle x | \varphi \rangle + \int_{x'=a}^{x'=b} dx' \langle x | \mathbf{G} | x' \rangle \langle x' | s \rangle, \text{ or: } \psi(x) = \varphi(x) + \int_{x'=a}^{x'=b} dx' G(x, x') s(x') \quad (11.2.15k)$$

This ten-part equation shows many ways to represent a differential equation, which in Dirac notation are fairly easy to connect. Dirac's powerful notation goes a long way toward taking some of the mathematical mystery out of differential analysis. At the same time it begins to show how the equations can be related to discrete space analogs and course-grained numerical simulations. Linear differential equations and integral equations all boil down to (or up from) matrix operator equations in Dirac notation.

We don't need Green's function for solving the standard form $\mathbf{L}|\psi\rangle = \mathbf{0}$ of Schrodinger's equations because the source term is zero ($|s\rangle = \mathbf{0}$). However, approximation schemes exist which remove part of the Schrodinger operator and put it on the right hand side of the equation so it acts like a source or forcing term of a driven oscillator equation. Then the full solution (11.2.15k) is used.

(d) Adjoint differential operator

It is convenient for differential operators \mathbf{L} to be Hermitian or self-conjugate ($\mathbf{L}^\dagger = \mathbf{L}$). For Hamiltonian generators (Recall (9.2.8a)) $\mathbf{H}^\dagger = \mathbf{H}$ is mandated by axioms 1-4. The problem is: How do we define the "dagger" (\dagger) of a differential operator?

The key is in the matrix element or *kernal* (11.2.15c). The operator will have matrix elements that are transpose conjugates of the original matrix.

$$\langle x | \mathbf{L}^\dagger | y \rangle = \langle y | \mathbf{L} | x \rangle^* \quad (11.2.17)$$

Combining this with (11.2.15c) gives

$$\langle x | \mathbf{L}^\dagger | y \rangle = f^*(y) \frac{d^2 \delta(x, y)}{dx^2} + g^*(y) \frac{d \delta(x, y)}{dx} + h^*(y) \delta(x, y) \quad (11.2.18)$$

Putting this kernal into the integral (11.2.15a) gives

$$\begin{aligned} L^\dagger \cdot \psi(x) &= \langle x | \mathbf{L}^\dagger | \psi \rangle = \int_{y=a}^{y=b} dy \langle x | \mathbf{L}^\dagger | y \rangle \psi(y) \\ &= \int_{y=a}^{y=b} dy \left(f^*(y) \frac{d^2 \delta(x, y)}{dx^2} + g^*(y) \frac{d \delta(x, y)}{dx} + h^*(y) \delta(x, y) \right) \psi(y) \end{aligned} \quad (11.2.19)$$

Using (11.2.9a) and (11.2.12a) and integrating by parts yields the *adjoint differential operator* L^\dagger .

$$L^\dagger \cdot \psi(x) = \frac{d^2 (f^*(x) \psi(x))}{dx^2} - \frac{d (g^*(x) \psi(x))}{dx} + h^*(x) \psi(x) \quad (11.2.20a)$$

Assuming only real coefficient functions and expanding gives

$$L^\dagger \cdot \psi(x) = f(x) \frac{d^2 \psi(x)}{dx^2} + \left(2 \frac{df(x)}{dx} - g(x) \right) \frac{d \psi(x)}{dx} + \left(\frac{d^2 f(x)}{dx^2} - \frac{dg(x)}{dx} + h(x) \right) \psi(x) \quad (11.2.20b)$$

(1) *Self-Adjoint differential operator: Sturm-Liouville form*

For many quantum applications we must equate the adjoint (11.2.20b) to the original operator in (11.2.15b) so that the coefficient functions for a quantum operator are restricted.

$$g(x) = 2 \frac{df(x)}{dx} - g(x) \quad , \quad \text{and} \quad h(x) = \frac{d^2 f(x)}{dx^2} - \frac{dg(x)}{dx} + h(x) \quad (11.2.21)$$

Either restriction gives

$$\frac{df(x)}{dx} = g(x) \quad (11.2.22)$$

So the second order real *Hermitian* or *self-adjoint operator* must have the following form

$$\begin{aligned} L \cdot \psi(x) &= f(x) \frac{d^2 \psi(x)}{dx^2} + \frac{df(x)}{dx} \frac{d \psi(x)}{dx} + h(x) \psi(x) = L^\dagger \cdot \psi(x) \\ &= \frac{d}{dx} \left(f(x) \frac{d \psi(x)}{dx} \right) + h(x) \psi(x) \end{aligned} \quad (11.2.23)$$

11.3 Momentum and coordinate space operators : Fourier transforms

First, we need to review the meaning of coordinate bases $\{...|x\rangle...\}$ and operators associated with them. Then we will make the Fourier change of basis (7.2.4) and see how all this plays out in the new wavevector or momentum space basis $\{...|k\rangle...\}$.

(a) Coordinate space and operators

Anything that is done to a function $\psi(x) = \langle x|\psi\rangle$ should be thought of as a matrix operation \mathbf{M} on its ket vector $|\psi\rangle$ that maps it into a new vector

$$|\phi\rangle = \mathbf{M} |\psi\rangle, \quad (11.3.1)$$

which is represented as a new function

$$\phi(x) = \langle x|\phi\rangle = \langle x| \mathbf{M} |\psi\rangle. \quad (11.3.2)$$

Even just multiplying $\psi(x)$ by the x -coordinate to give $x\psi(x)$, or by a function $f(x)$ of the x -coordinate to give $f(x)\psi(x)$ is a *mapping operation* and is designated by bold-face type.

$$x\psi(x) = \langle x| \mathbf{x} |\psi\rangle \quad f(x)\psi(x) = \langle x| f(\mathbf{x}) |\psi\rangle \quad (11.3.3)$$

You might wonder, "How can I go through umpteen years of algebra and calculus and never see this?"

The reason is that in the continuum of coordinate bases $\{...|x\rangle...\}$ are eigenvectors ("own-vectors") of the \mathbf{x} -operator and all its functions $f(\mathbf{x})$.

$$\mathbf{x} |x\rangle = x |x\rangle \quad , \text{ or } f(\mathbf{x}) |x\rangle = f(x) |x\rangle \quad (11.3.4a)$$

Furthermore, the eigenbras $\langle x| = |x\rangle^\dagger$ have the same eigenvalue since x is real. (Recall (2.2.5).)

$$\langle x| \mathbf{x} = \langle x| x = x \langle x| \quad , \text{ or } \langle x| f(\mathbf{x}) = f(x) \langle x| \quad (11.3.4b)$$

So \mathbf{x} and $f(\mathbf{x})$ are Hermitian (self-† conjugate) operators if the function $f(x)$ is real, too.

$$\mathbf{x}^\dagger = \mathbf{x} \quad , \text{ and } f(\mathbf{x})^\dagger = f^*(\mathbf{x}^\dagger) = f(\mathbf{x}) \quad (11.3.4c)$$

This immediately gives (11.3.3).

$$\langle x| \mathbf{x} |\psi\rangle = \langle x|\psi\rangle x = x \langle x|\psi\rangle = x \psi(x) \quad , \text{ or } \langle x| f(\mathbf{x}) |\psi\rangle = f(x) \langle x|\psi\rangle = f(x)\psi(x) \quad (11.3.4d)$$

All \mathbf{x} -operators are diagonal in their own eigen-basis. (Oops, there's that bilingual redundancy again!) Matrix operator multiplication is reduced to plain old numerical multiplication.

You might wonder about a product like $f(x)\psi(x)$, "Which is the vector and which is the operator?" Good question! The answer can be both, one of them, or neither, depending on what you are doing! As you become more familiar with Dirac functional analysis notation, it will be easier to see how various operators and operatees (Is "operatee" a word yet. It should be.) play many different roles and switch them often. That will be a sign that you're getting proficient in your chosen career as a quantum mechanic!

(b) Wavevector operator \mathbf{k}

The empty infinite x -continuum is like the universe's most perfectly boring desert; miles and miles of nothing so much as a pop stand. That's what we call C_∞ -symmetry. No matter where you go, every point looks exactly the same as the last one. (Recall Sec. 8.2d which discussed the "roots" of e^{ikx} .) The analysis of C_N in Sec. 8.2 suggests how C_∞ -symmetry gives a diagonalizing transformation matrix

$$\langle x|k\rangle = \Psi_k(x) = e^{ikx} / \sqrt{2\pi} \quad (11.3.5)$$

also known as a *1-D plane-wave function* or *Fourier transform kernel* (7.2.4). The discussion in Sec. 7.2b listed some roles that this all-important exponential plays. Now we are using it as a transformation $\langle x|k\rangle$ or "ticket" to momentum space continuum bases $\{...|k\rangle...\}$.

The seemingly magic feature of symmetry analysis is that it gives the diagonalizing transformation (11.3.5) for the time evolution operator \mathbf{U} , or the Hamiltonian \mathbf{H} (Recall Sec. 9.3a) which describe physics in a C_∞ -symmetric desert. It does this without explicit knowledge of operators \mathbf{U} or \mathbf{H} . More will be said about this later. For now it is easier to see the diagonalization by simpler arguments.

To do this, let a *wavevector operator* \mathbf{k} play the same role in wavevector space $\{...|k\rangle...\}$ that the position operator \mathbf{x} plays in position space $\{...|x\rangle...\}$. That is, let \mathbf{k} be a diagonal operator satisfying

$$\mathbf{k} |k\rangle = k |k\rangle \quad , \text{ or } f(\mathbf{k}) |k\rangle = f(k) |k\rangle \quad (11.3.6a)$$

in analogy to (11.3.4) the eigenbras $\langle k| = |k\rangle^\dagger$ have the same real eigenvalue k .

$$\langle k| \mathbf{k} = \langle k| k = k \langle k| \quad , \text{ or } \langle k| f(\mathbf{k}) = f(k) \langle k| \quad (11.3.6b)$$

So \mathbf{k} and $f(\mathbf{k})$ are Hermitian (self-† conjugate) operators for any real function $f(k)$.

$$\mathbf{k}^\dagger = \mathbf{k} \quad , \text{ and } f(\mathbf{k})^\dagger = f^*(\mathbf{k}^\dagger) = f(\mathbf{k}) \quad (11.3.6c)$$

This immediately gives the k -space version of (11.3.3).

$$\langle k| \mathbf{k} |\psi\rangle = \langle k|\psi\rangle k = k \langle k|\psi\rangle = k\psi(k) \quad , \text{ or } \langle k| f(\mathbf{k}) |\psi\rangle = f(k) \langle k|\psi\rangle = f(k) \cdot \psi(k) \quad (11.3.6d)$$

(c) Momentum operator \mathbf{p}

The De Broglie relation (5.2.5c) equates momentum p with wavevector k times \hbar . The same applies to the operators:

$$\mathbf{p} = \hbar \mathbf{k}$$

A word of caution about notation: Boldface type \mathbf{k} here means a quantum operator for *one*-dimensional wavevector or momentum. Similar bold type is used in Chapter 6 to designate classical three-dimensional wavevectors \mathbf{k} . This is a common notation and may be an unfortunate source of confusion. Our solution is to denote quantum operators by a sans-serif \mathbf{k} and \mathbf{p} wherever they might be confused. Of course, this will be a real problem when we need to label three-dimensional quantum vector operator. One solution is "super-arrows" as in $\vec{\mathbf{k}}$. Fortunately, there is more elegant and powerful notation based on the theory of quantum *tensor operators* which will be treated in later chapters.

(d) Coordinate to momentum change-of-basis

There is another notational caveat. You must be extremely careful when using such powerful notation as Dirac has given us. The last line in (11.3.6d) gives a k -wavefunction as

$$\langle k|\psi\rangle = \psi(k)$$

in analogy to the usual x -wavefunction $\langle x|\psi\rangle = \psi(x)$. Does this mean just replace x with k in $\psi(x)$? The answer is no! no! no! **no! No! NO! NO-ooo!** This would be another example of "Dirac abuse" mentioned in Sec. 7.2. Instead, it means the *Fourier transform* (7.2.4c) of $\psi(x)$ repeated below.

$$\langle k|\psi\rangle = \int_{-\infty}^{+\infty} dx \langle k|x\rangle \langle x|\psi\rangle = \int_{-\infty}^{+\infty} dx \frac{e^{-ikx}}{\sqrt{2\pi}} \langle x|\psi\rangle = \frac{1}{\sqrt{2\pi}} \int_{-\infty}^{+\infty} dx e^{-ikx} \psi(x), \quad (11.3.7)$$

You see the trouble is not with Dirac. We get in trouble when we convert back to that old function notation of those musty Newtonian calculus books! Avoid using $\psi(k)$ for $\langle k|\psi\rangle$ and use $\psi(x)$ with care.

Now this change of basis between $\{...|k\rangle...\}$ and $\{...|x\rangle...\}$ needs to be applied to the wavevector (or momentum) operators. We ask, "How do \mathbf{k} and \mathbf{p} , which are diagonal in momentum space $\{...|k\rangle...\}$, get represented in the position coordinate basis $\{...|x\rangle...\}$?" A related question asks, "How does position operator \mathbf{x} look when represented in momentum k -space?"

First, the effect of \mathbf{k} on a general state, as represented in x -space, is found using x -completeness.

$$\langle x|\mathbf{k}|\psi\rangle = \int_{-\infty}^{+\infty} dx' \langle x|\mathbf{k}|x'\rangle \langle x'|\psi\rangle = \int_{-\infty}^{+\infty} dx' \langle x|\mathbf{k}|x'\rangle \psi(x') \quad (11.3.8)$$

Then the kernel $\langle x|\mathbf{k}|x'\rangle$ is expanded using the k -basis in which \mathbf{k} is diagonal (11.3.6a).

$$\begin{aligned} \langle x|\mathbf{k}|x'\rangle &= \int_{-\infty}^{+\infty} dk \int_{-\infty}^{+\infty} dk' \langle x|k\rangle \langle k|\mathbf{k}|k'\rangle \langle k'|x'\rangle \\ &= \int_{-\infty}^{+\infty} dk \int_{-\infty}^{+\infty} dk' \langle x|k\rangle (k') \langle k|k'\rangle \langle k'|x'\rangle \quad \mathbf{k}\text{-eigenvalue: } \mathbf{k}|k'\rangle = (k')|k'\rangle \end{aligned}$$

Fourier transformation matrix (11.3.5) and orthonormality $\langle k|k'\rangle = \delta(k-k')$ gives

$$\langle x|\mathbf{k}|x'\rangle = \int_{-\infty}^{+\infty} dk \int_{-\infty}^{+\infty} dk' \frac{e^{ikx}}{\sqrt{2\pi}} (k') \delta(k-k') \frac{e^{-ik'x'}}{\sqrt{2\pi}} = \int_{-\infty}^{+\infty} dk \frac{e^{ik(x-x')}}{2\pi} (k)$$

This can be written as an x -derivative of a Dirac delta $\langle x|x'\rangle = \delta(x-x')$.

$$\begin{aligned} \langle x|\mathbf{k}|x'\rangle &= \int_{-\infty}^{+\infty} dk \frac{e^{ik(x-x')}}{2\pi} (k) = \frac{1}{i} \frac{\partial}{\partial x} \int_{-\infty}^{+\infty} dk \frac{e^{ik(x-x')}}{2\pi} = \frac{-1}{i} \frac{\partial}{\partial x'} \int_{-\infty}^{+\infty} dk \frac{e^{ik(x-x')}}{2\pi} \\ &= \frac{1}{i} \frac{\partial}{\partial x} \int_{-\infty}^{+\infty} dk \langle x|k\rangle \langle k|x'\rangle = \frac{-1}{i} \frac{\partial}{\partial x'} \int_{-\infty}^{+\infty} dk \langle x|k\rangle \langle k|x'\rangle \quad (11.3.9) \\ &= \frac{1}{i} \frac{\partial}{\partial x} \langle x|x'\rangle = \frac{-1}{i} \frac{\partial}{\partial x'} \langle x|x'\rangle \end{aligned}$$

Putting the kernel $\langle x|\mathbf{k}|x'\rangle$ back into the integral (11.3.8) gives the following.

$$\begin{aligned} \langle x|\mathbf{k}|\psi\rangle &= \int_{-\infty}^{+\infty} dx' \frac{1}{i} \frac{\partial}{\partial x} \langle x|x'\rangle \psi(x') = \frac{1}{i} \frac{\partial}{\partial x} \int_{-\infty}^{+\infty} dx' \delta(x-x') \psi(x') \\ &= \frac{1}{i} \frac{\partial}{\partial x} \psi(x) \quad (11.3.10a) \end{aligned}$$

For momentum operator, multiply by the DeBroglie-Planck \hbar to make \mathbf{k} into $\mathbf{p} = \hbar\mathbf{k}$.

$$\langle x|\mathbf{p}|\psi\rangle = \frac{\hbar}{i} \frac{\partial}{\partial x} \psi(x) \quad (11.3.10b)$$

This is the desired *coordinate representation of the momentum operator \mathbf{p}* .

To test the operator \mathbf{p} apply it to the plane wave function $\langle x|k\rangle = \Psi_k(x) = e^{ikx} / \sqrt{2\pi}$ from (11.3.5)

$$\begin{aligned} \langle x|\mathbf{p}|k\rangle &= \frac{\hbar}{i} \frac{\partial}{\partial x} \Psi_k(x) = \frac{\hbar}{i} \frac{\partial}{\partial x} \frac{e^{ikx}}{\sqrt{2\pi}} = \hbar k \frac{e^{ikx}}{\sqrt{2\pi}} = p\Psi_k(x) \\ &= p\langle x|k\rangle \end{aligned} \quad (11.3.10c)$$

So plane wavefunction $\Psi_k(x)$ is indeed an eigenfunction of the \mathbf{p} operation. A matrix representation of the \mathbf{p} operator is not diagonal in the x -basis. Rather it is represented by (1)'s and (-1)'s off-diagonal as shown in (11.2.3), (11.2.6) or (11.2.24).

Without doing any more calculation it is easy to answer the question about the momentum or k -representation of the position operator \mathbf{x} in (11.3.4). The following

$$\langle k|\mathbf{x}|\psi\rangle = i \frac{\partial}{\partial k} \psi(k) \quad (11.3.11a)$$

is the desired *wavevector or momentum representation of the position operator \mathbf{x}* . To test the operator \mathbf{x} apply it to the kernel function $\langle k|x\rangle = e^{-ikx} / \sqrt{2\pi} = \Psi_x(k)$ which from (11.3.5) is an eigenfunction of \mathbf{x} .

$$\langle k|\mathbf{x}|\psi\rangle = i \frac{\partial}{\partial k} \Psi_x(k) = i \frac{\partial}{\partial k} \frac{e^{-ikx}}{\sqrt{2\pi}} = x \frac{e^{-ikx}}{\sqrt{2\pi}} = x\Psi_x(k) \quad (11.3.11b)$$

This is correct, apart from the terrible notation $\Psi_x(k)$ for the kernel $\langle k|x\rangle = \langle x|k\rangle^* = e^{-ikx} / \sqrt{2\pi}$. (Avoid such bad form that can enable "Dirac abuse" in Fourier transforms!) So the \mathbf{x} -operator is non-diagonal in the momentum representation.

Notice how both the \mathbf{x} and \mathbf{k} operator representations have imaginary (i) attached to their derivative definition. This is necessary to make them Hermitian self-conjugate operators $\mathbf{x}^\dagger = \mathbf{x}$ and $\mathbf{k}^\dagger = \mathbf{k}$ in (11.3.4c) and (11.3.6c), respectively, and thereby assure that their eigenvalues are real. A first derivative is an anti-symmetric operator $\bar{\Delta} = -\bar{\Delta}^\dagger$ matrix as pointed out in (11.2.7a) so the (i) is needed to "fix" it.

Now we are prepared to give a more rigorous derivation of the Schrodinger wave equations that were first obtained by semi-classical arguments in Chapter 5. (Recall equations (5.4.10) and (5.4.15).)

11.4 Differential Wave Equations of Schrodinger

In Sec. 9.2 there was introduced the abstract time evolution operator $\mathbf{U}(t;0)$ and its representation (9.1.3) in a discrete N -state basis. We now consider how it will be represented in a continuum basis such as the coordinate basis $\{...|x\rangle...\}$. This will be done by appealing to the Hamiltonian generating operator \mathbf{H} which generates the $\mathbf{U}(t;0)$ operator according to Schrodinger's *fundamental time equations* (9.2.5)

$$i\hbar \frac{\partial}{\partial t} \mathbf{U}(t,0) = \mathbf{H} \mathbf{U}(t,0), \quad (11.4.1a) \quad i\hbar \frac{\partial}{\partial t} |\Psi(t)\rangle = \mathbf{H} |\Psi(t)\rangle \quad (11.4.1b)$$

and satisfies the *energy eigenvalue equation* (9.3.1)

$$\mathbf{H} |\varepsilon\rangle = E |\varepsilon\rangle = \hbar\omega |\varepsilon\rangle. \quad (11.4.2)$$

The development of $\mathbf{U}(t;0)$ and \mathbf{H} shows from Planck's hypothesis that eigenvalues $E_k = \hbar\omega_k$ of \mathbf{H} are system energies, that is, \mathbf{H} is the *quantum energy operator*. We now develop a representation of energy operator \mathbf{H} in both the coordinate $|x\rangle$ -basis and in a momentum $|k\rangle$ -basis, just as we have already done for the position and momentum operators \mathbf{x} and $\mathbf{p} = \hbar \mathbf{k}$, respectively, in the preceding sections.

(a) Schrodinger Wave Equations in coordinate representation

Except for a brief description of classical analogies, it has been *differences* between classical and quantum mechanics that we have emphasized. In spite of all this a wonderfully simple axiom holds.

The quantum Hamiltonian energy operator $\mathbf{H}(\mathbf{x},\mathbf{p})$ is obtained directly from the classical Hamiltonian function $H(x,p)$ by replacing $x \rightarrow \mathbf{x}$ and $p \rightarrow \mathbf{p}$.

In other words (or equations), it is only necessary to replace the coordinate $q=x$ and momentum p in a classical Hamiltonian function $H(q,p)$ with the corresponding operators \mathbf{x} and \mathbf{p} and "Presto!" you have a correct working Hamiltonian operator \mathbf{H} to use in Schrodinger's time equation (11.4.1). Given classical

$$H(q,p) = H(x,p) = p^2/2M + V(x) \quad (11.4.3)$$

where $V(x)$ is a *potential energy PE function $V(x)$* , we immediately have

$$\mathbf{H}(\mathbf{q},\mathbf{p}) = \mathbf{H}(\mathbf{x},\mathbf{p}) = \mathbf{p}^2/2M + V(\mathbf{x}) \quad (11.4.4)$$

Sounds simple enough! Let us try it out using the coordinate $|x\rangle$ -basis first.

According to (11.3.10) the kinetic energy operator

$$\mathbf{T} = \mathbf{p}^2/2M = \hbar^2 \mathbf{k}^2/2M \quad (11.4.5a)$$

is $|x\rangle$ -represented by

$$\langle x | \mathbf{T} | \Psi \rangle = \langle x | \frac{\mathbf{p}^2}{2M} | \Psi \rangle = \frac{-\hbar^2}{2M} \frac{\partial^2}{\partial x^2} \Psi(x) \quad (11.4.5b)$$

so (11.4.1b) becomes *Schrodinger's time-dependent $\Psi(x,t) = \langle x | \Psi(t) \rangle$ wave equation*.

$$i\hbar \langle x | \frac{\partial}{\partial t} | \Psi \rangle = \langle x | \frac{\mathbf{p}^2}{2M} + V(\mathbf{x}) | \Psi \rangle, \quad \text{or:} \quad i\hbar \frac{\partial \Psi(x,t)}{\partial t} = \frac{-\hbar^2}{2M} \frac{\partial^2 \Psi(x,t)}{\partial x^2} + V(x) \Psi(x,t) \quad (11.4.5c)$$

Also, (11.4.2) becomes *Schrodinger's time-independent $\psi_\varepsilon(x) = \langle x | \varepsilon \rangle$ wave eigenequation*.

$$\langle x | \mathbf{H} | \varepsilon \rangle = E \langle x | \varepsilon \rangle, \quad \text{or:} \quad \frac{-\hbar^2}{2M} \frac{\partial^2 \psi_E(x)}{\partial x^2} + V(x) \psi_E(x) = E \psi_E(x) \quad (11.4.5d)$$

where the latter also follows from a simple substitution of the time-dependent wavefunction

$$\Psi(x,t) = e^{-i\omega t} \psi_E(x) = e^{-iEt/\hbar} \psi_E(x) = e^{-iEt/\hbar} \Psi(x,0) \quad (11.4.5e)$$

into (11.4.5c). The time-independent wave $\Psi_\epsilon(x)$ is a stationary state wave. Recall that eigenstates do not appear to move as far as mortals like us can tell; the absolute square of (11.4.5e) is, to us, dead as a doornail. However, most of the general wavefunctions $\Psi(x,t) = \langle x | \Psi(t) \rangle$ arising from (11.4.5c) will have a life! That is, their probability distributions

$$P(x,t) = |\Psi(x,t)|^2 = |\langle x | \Psi(t) \rangle|^2 \quad (11.4.6)$$

can easily dance the night away. The following chapters will show many examples.

(b) Free space wavefunction solutions

Without any potential function ($V(x)=0$) the Schrodinger wave equations are

$$i\hbar \frac{\partial \Psi(x,t)}{\partial t} = \frac{-\hbar^2}{2M} \frac{\partial^2 \Psi(x,t)}{\partial x^2}, \text{ and: } \frac{-\hbar^2}{2M} \frac{\partial^2 \Psi_E(x)}{\partial x^2} = \epsilon \Psi_E(x) \quad (11.4.7)$$

They should give the types of waves that are our old friends starting in Chapter 4. Indeed, substituting the plane moving wave (4.2.1a)

$$\Psi_k(x,t) = A e^{-i\omega t} \psi_k(x) = A e^{-i\omega t} e^{ikx} = A e^{i(kx-\omega t)} \quad (11.4.8)$$

into (11.4.7) along with $\psi_k(x) = e^{ikx}$ yields the following

$$-i\hbar \omega \frac{\partial e^{i(kx-\omega t)}}{\partial t} = \frac{-\hbar^2}{2M} \frac{\partial^2 e^{i(kx-\omega t)}}{\partial x^2}, \text{ and: } \frac{-\hbar^2}{2M} \frac{\partial^2 e^{ikx}}{\partial x^2} = E e^{ikx}$$

with frequency and energy eigenvalues that are just Planck and DeBroglie's rules.

$$\hbar \omega = \frac{\hbar^2}{2M} k^2 = \epsilon \quad (11.4.9a)$$

Either sign of the wavevector k gives the same energy ϵ or frequency ω .

$$k = \pm \sqrt{\frac{2ME}{\hbar^2}} = \pm \sqrt{\frac{2M\omega}{\hbar}} \quad (11.4.9b)$$

So a more general set of solutions are the monochromatic galloping waves (4.2.5) which have both $\pm ikx$.

$$\Psi_{gallop}(x,t) = A_{\rightarrow} e^{i(kx-\omega t)} + A_{\leftarrow} e^{i(-kx-\omega t)} \quad (11.4.10)$$

We insist on clockwise ($-i\omega t$) phasors as in Chapter 4 (Fig. 4.1.2). The two complex amps A_{\rightarrow} and A_{\leftarrow} define a general *one-dimensional (1D) free-space energy eigenfunction*.

The 1D wave (11.4.10) for a given energy $\epsilon = \hbar\omega$, constitutes a *two-state system* with base states $|k\rangle$ and $|-k\rangle$. It is a $U(2)$ system like the many analogous ones discussed in Chapter 1 and 4. The two complex parameters A_{\rightarrow} and A_{\leftarrow} amount to four real parameters including normalization, which is yet to be set. In Fig. 11.4.1 are several waves made by the program *BandIt*. The wave is set by adjusting two "master phasors" representing the constants A_{\rightarrow} and A_{\leftarrow} at an arbitrary point of origin, and they determine the magnitude, shape, and direction of a "galloping" wave. Having ($A_{\rightarrow}=1, A_{\leftarrow}=0$) gives right moving wave (11.4.8) shown on top. A typical galloping wave setting ($A_{\rightarrow}=0.8e^{i\pi/4}, A_{\leftarrow}=0.2$) produces a galloping wave with $SWR = (0.8-0.2)/(0.8+0.2) = 0.6$ shown in the center. At the bottom is a 50-50 standing wave with "master phasors" set to ($A_{\rightarrow}=0.5e^{i\pi/4}, A_{\leftarrow}=0.2e^{i\pi/12}$).

In spite of all the frantic phase galloping motion, these waves are actually stationary; their envelopes or interference moduli do not move since they are single-frequency (monochromatic) waves. Still the first two have a *current*. The current is proportional to $|A_{\rightarrow}|^2 - |A_{\leftarrow}|^2$ and is manifested by the relative phase between neighboring phasors in the time plots on the right hand side of Fig. 11.4.1. As (10.2.16) states, (See problem 10.2.1) the power factor for coupled oscillators is proportional to the sine of their relative phase lag. Each phasor in the upper right hand plot is about 45° ahead of its neighbor to the right, so it is continuously passing $\sin 45^\circ$ of "work" to the right. The phase lag and SWR is less for each of the two plots below, and it is zero for the standing wave, which has no current at all.

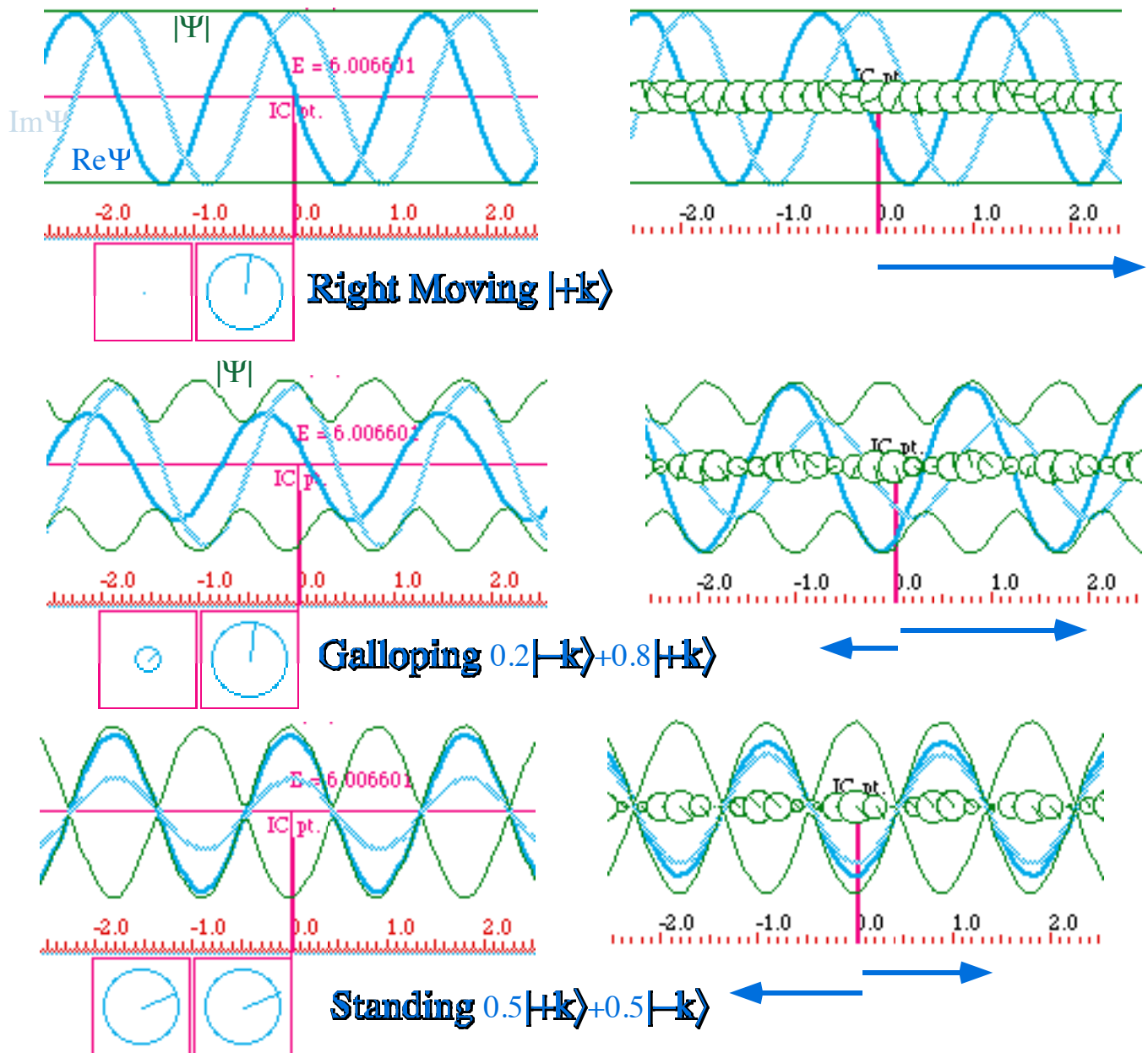


Fig. 11.4.1 Three general types of monochromatic free-space waves. (Plots by BandIt)

With any constant potential function ($V(x)=V$) the Schrodinger x -eigen-equation (11.4.5d) is

$$\frac{\partial^2 \psi_E(x)}{\partial x^2} + \frac{2M}{\hbar^2}(E - V)\psi_E(x) = 0 . \tag{11.4.7}$$

If energy E is above potential V , it has the sinusoidal wave form $\psi'' + k^2\psi = 0$ with *real wavevector* k .

$$\psi = Ae^{ikx} + B e^{-ikx} \qquad k = \pm \sqrt{\frac{2M}{\hbar^2}(E - V)} \quad (E > V) \tag{11.4.8}$$

(c) Exponential and evanescent wavefunctions

But, if energy ϵ is *below* potential V , the Schrodinger x -equation has the hyperbolic or exponential wave form $\psi'' - \kappa^2\psi = 0$ with an *imaginary wavevector* $k = i\kappa$ or *exponential extinction constant* $\kappa = -i k$.

$$\psi = Ae^{-\kappa x} + Be^{+\kappa x} \qquad \kappa = \pm \sqrt{\frac{2M}{\hbar^2}(V - E)} \quad (E < V) \tag{11.4.9}$$

If $B=0$ you get an *exponential wave* $\exp(-\kappa x)$ that dies in a potential barrier as shown in Fig. 11.4.2. Note that all phasors are synchronized to the same phase, but their area (probability) dies exponentially.

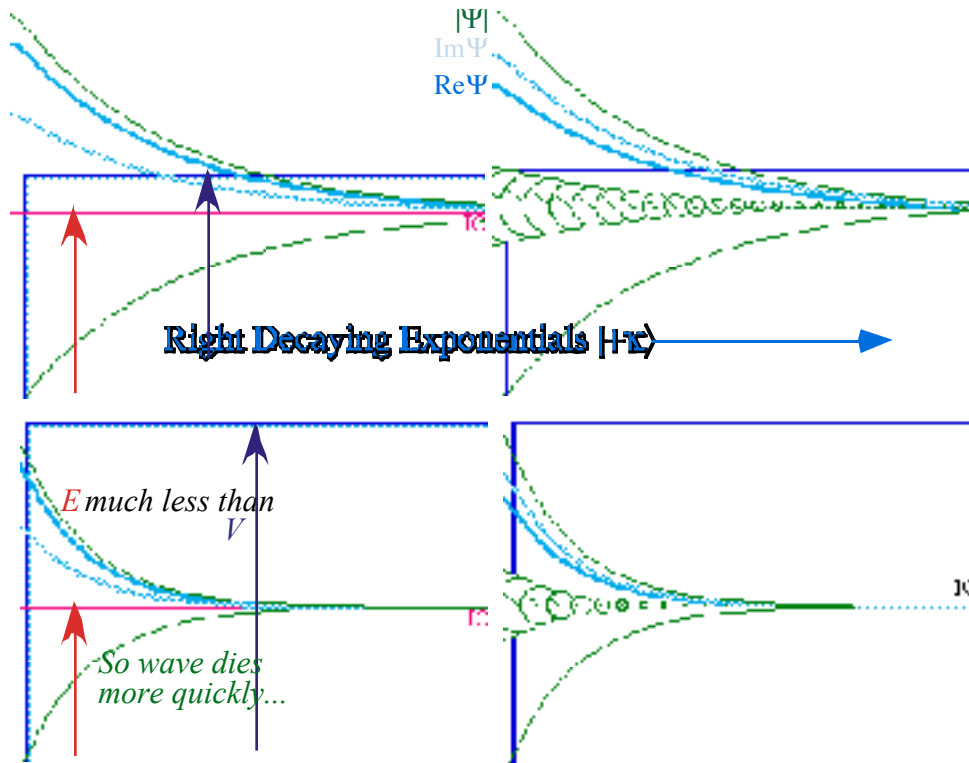


Fig. 11.4.2 Exponential waves $\exp(-\kappa x)$ dying to the right

Generally $(E < V)$ -waves are hyperbolic sine-cosine combinations known as *evanescent waves*.

$$\psi = \alpha \cosh \kappa x + \beta \sinh \kappa x \qquad \kappa = \pm \sqrt{\frac{2M}{\hbar^2}(V - E)} \quad (E < V) \tag{11.4.10}$$

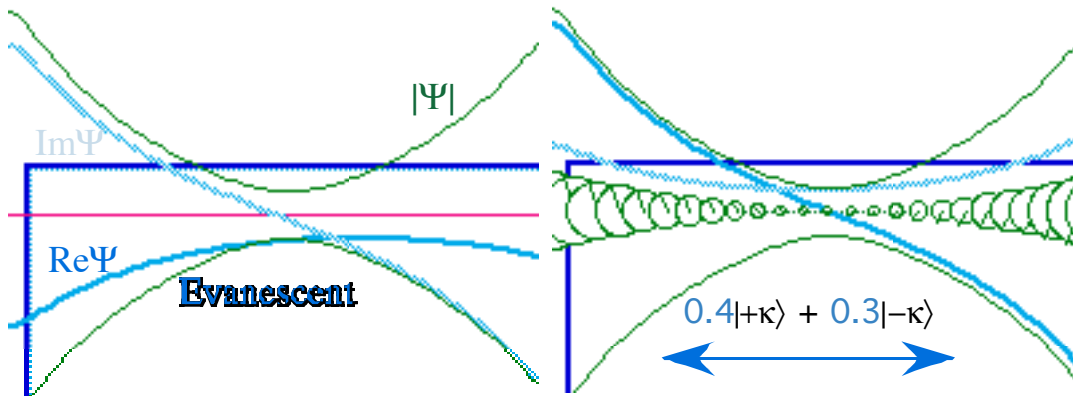


Fig. 11.4.3 Evanescent waves combine $\exp(-\kappa x)$ and $\exp(+\kappa x)$

Phasors in evanescent waves have regions where their phase varies with x so that they may communicate matter or energy through classically forbidden barriers in what is called a *tunneling* process. Tunneling paths between the quantum dots were hypothesized in Chapter 9. In Fig. 11.4.3, the relative phase between the two ends of a tunneling path may vary as shown in the following Chapter 12. The simple exponential waves in Fig. 11.4.2 have the same phase everywhere and therefore incapable of transmission.

Waves with above-barrier energy ($E > V$), such as in Fig. 11.4.1, curve toward the x -axis while the sub-barrier ($E < V$)-waves in Fig. 11.4.2-3 curve away from x . Grazing ($E = V$)-waves are straight lines.

(d) Schrodinger Wave Equations in momentum representation

The abstract time-independent Schrodinger eigenvalue equation (11.4.5) has the following form

$$\mathbf{H}|\varepsilon\rangle = E|\varepsilon\rangle \tag{11.4.11a}$$

based on the non-relativistic Hamiltonian or energy operator

$$\mathbf{H}(\mathbf{q}, \mathbf{p}) = \mathbf{H}(\mathbf{x}, \mathbf{p}) = \mathbf{p}^2/2M + V(\mathbf{x}) \tag{11.4.11b}$$

to give

$$(\mathbf{p}^2/2M + V(\mathbf{x}))|\varepsilon\rangle = E|\varepsilon\rangle \tag{11.4.11c}$$

where:

$$\mathbf{p} = \hbar \mathbf{k}$$

is the momentum or \hbar times the wavevector operator.

Now (11.4.11) in the momentum or wavevector- k basis is found by k -completeness.

$$\frac{\hbar^2}{2M} \langle k | \mathbf{k}^2 | \varepsilon \rangle + \int dk' \langle k | V(\mathbf{x}) | k' \rangle \langle k' | \varepsilon \rangle = E \langle k | \varepsilon \rangle \tag{11.4.12}$$

The kinetic term is very simple but the potential $V(\mathbf{x})$ requires an x -completeness expansion.

$$\frac{\hbar^2}{2M} k^2 \langle k | \varepsilon \rangle + \int dk' \int dx \langle k | x \rangle \langle x | V(\mathbf{x}) | k' \rangle \langle k' | \varepsilon \rangle = E \langle k | \varepsilon \rangle \tag{11.4.13a}$$

$$\frac{\hbar^2}{2M} k^2 \langle k | \varepsilon \rangle + \int dk' \int dx V(x) \langle k | x \rangle \langle x | k' \rangle \langle k' | \varepsilon \rangle = E \langle k | \varepsilon \rangle$$

Inserting transformation kernel $\langle x | k \rangle = e^{ikx}/\sqrt{2\pi}$ gives *Schrodinger's integral eigen-equation*.

$$\frac{\hbar^2}{2M} k^2 \langle k | \varepsilon \rangle + \int dk' V(k - k') \langle k' | \varepsilon \rangle = E \langle k | \varepsilon \rangle \tag{11.4.13b}$$

Here

$$V(k - k') = \langle k | V | k' \rangle = \frac{1}{2\pi} \int dx e^{-i(k-k')x} V(x) \tag{11.4.13c}$$

is a Fourier transform of the potential operator $V(\mathbf{x})$.

The momentum-space form of Schrodinger's equations is clearly more complicated unless the potential has a form that is easily Fourier transformed and simplifies the integral equation. The momentum representation becomes most useful for cases where the potential is isotropic or nearly so, that is, a constant almost everywhere. This is the situation in so-called *scattering theory*. More is said about this later when the k -equation returns with a vengeance of a jilted suitor in Chapter 16!

Many applications of Schrodinger equation involve a mass M hindered, trapped, or imprisoned in a more or less deep potential structure. This is the setting for the following chapter 12 that begins the saga of prisoner M ! But first, some classical analogies will be discussed to help with physical intuition regarding differences between trapped, propagating, and evanescent waves.

11.5 Classical-Wave Analogies for Schrodinger equations

An analogy between 2-state quantum systems and two coupled pendulums was shown in Chapter 10. Now we generalize the mechanical analogy to show that N -coupled pendulums correspond to N -state quantum systems, even ∞ -state continuous wave systems if you have an infinite number of pendulums. As was the case for $N=2$, the correspondence is appropriate in the absence of complex C -type chiral or "gauge" couplings such as the Coriolis or cyclotron magnetic field effects discussed in Sec. 10.2c.

Classical (Newton's or Hamilton's) oscillator equations are second order (acceleration) differential equations in time ($m\ddot{x} + \mathbf{K} \cdot \mathbf{x} = 0$), while Schrodinger's equation ($i\hbar|\dot{\Psi}\rangle + \mathbf{H} \cdot |\Psi\rangle = 0$) is first order in time. So the eigenvalues κ_j of the classical \mathbf{K} -spring matrix (divided by mass- m) are squares of the eigenmode frequencies. Classical mode frequencies have a square root form $\omega_j = \sqrt{(\kappa_j/m)}$ as shown by comparing quantum frequencies ($A \pm B$) in (10.2.7a) to mode eigenfrequencies $\sqrt{(A \pm B)}$ in (10.2.7b).

In contrast, the eigenvalues ϵ_j of the quantum Hamiltonian \mathbf{H} -matrix (divided by Planck's \hbar) are directly the eigenstate frequencies $\omega_j = \epsilon_j/\hbar$; no square root needed. The eigenvalues $A \pm B$ in (10.2.7a) or $H \pm S$ in (10.3.5) for C_2^B -symmetry ($pE=0$) are special cases of C_N -symmetry eigenvalues (9.3.5g).

$$\hbar\omega_m = \epsilon_m = H - 2S \cos(k_m a) \quad (11.5.1).$$

These are eigenvalues of a the \mathbf{H} -matrix in an N -by- N Schrodinger equation

$$i\hbar \frac{\partial}{\partial t} \begin{pmatrix} \vdots \\ \langle 0|\Psi\rangle \\ \langle 1|\Psi\rangle \\ \langle 2|\Psi\rangle \\ \langle 3|\Psi\rangle \\ \langle 4|\Psi\rangle \\ \vdots \end{pmatrix} = \begin{pmatrix} \ddots & \ddots & & & & & \\ & \ddots & \ddots & & & & \\ & & 2S & -S & & & \\ & & -S & 2S & -S & & \\ & & & -S & 2S & -S & \\ & & & & -S & 2S & \ddots \\ & & & & & -S & 2S & \ddots \\ & & & & & & \ddots & \ddots & \ddots \end{pmatrix} \begin{pmatrix} \vdots \\ \langle 0|\Psi\rangle \\ \langle 1|\Psi\rangle \\ \langle 2|\Psi\rangle \\ \langle 3|\Psi\rangle \\ \langle 4|\Psi\rangle \\ \vdots \end{pmatrix} \quad (11.5.2a)$$

We let $H=2S$ so the right hand side becomes $-S$ times the Δ^2 difference operator (11.2.11) in a matrix version of *Schrodinger's wave equation with zero potential* ($V(x)=0$). Recall that $\lim_{a \rightarrow 0} \frac{\Delta^2 \Psi}{a^2} = \frac{\partial^2 \Psi}{\partial x^2}$.

$$i\hbar \frac{\partial |\Psi\rangle}{\partial t} = -S a^2 \nabla^2 |\Psi\rangle \rightarrow i\hbar \frac{\partial \Psi(x,t)}{\partial t} = \frac{-\hbar^2}{2M} \frac{\partial^2 \Psi(x,t)}{\partial x^2}, \text{ where: } S = \frac{\hbar^2}{2Ma^2} \quad (11.5.2b)$$

This relates the tunneling parameter $S = \hbar^2/(2Ma^2)$ to mass M , \hbar , and inter-pendulum lattice space $a=L/N$.

(b) Classical gravity-waves: “Exciton-like” dispersion

The diagonal constant H in the Schrodinger equation sets the zero-value of the energy and frequency but has no observable effect in quantum experiments. (Remember: overall phase cancels out of $\Psi^*\Psi$.) Adding H to each diagonal element $2S$ shifts all eigenfrequencies upward together. But, since only differences (beats) between eigenfrequencies are observable, this change does not affect wave dynamics.

However, adding an H to the classically analogous problem has a very great effect. It is equivalent to adding gravitational restoring acceleration $H = g/\ell$ to each classical pendulum which previously had only a restoring term $2k_{12}/m = 2s$ due to its two neighbors on either side. This changes their wave behavior entirely. It is first noticed in the eigenfrequencies because they are square roots of the force \mathbf{K} -matrix eigenvalues. In place of (11.5.3c) we now have the following *general "exciton" dispersion relation*. At low wavevector $k \sim 0$, this resembles Bohr-Shrodinger dispersion $\omega \sim k^2$.

$$\omega_m = \sqrt{H + 2s - 2s \cos(k_m a)} = \sqrt{H + 4s \sin^2\left(\frac{k_m a}{2}\right)} \cong \sqrt{H} + \frac{sa^2}{2\sqrt{H}} k_m^2 + \dots \quad (11.5.4a)$$

An example is plotted in Fig. 11.5.2 and should be compared to the phonon example in Fig. 11.5.1. An obvious new feature is a *forbidden frequency gap* of $\sqrt{H} = \sqrt{g/\ell}$ at $k=0$. There the phase velocity is infinite. Phase velocity is not so ignorable a part of classical dynamics as it is for quantum waves!

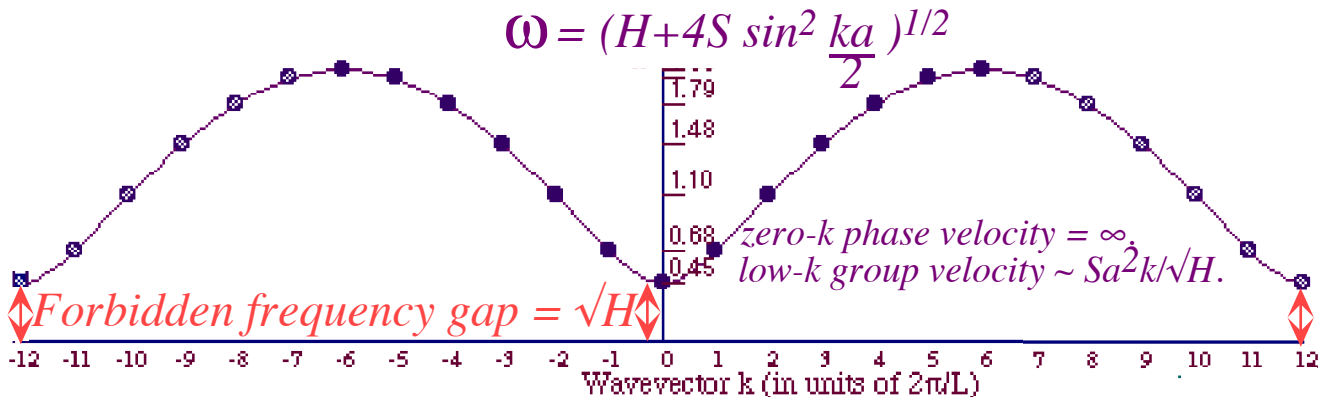


Fig. 11.5.2 General "exciton" dispersion for $N = 12$ classical coupled-pendulums-with-gravity.

The wave will not propagate in the gap where frequency is less than the individual frequency $\sqrt{g/\ell}$ of each uncoupled pendulum. This is true regardless of how strong we make the coupling $s = k_{12}/m$, the gap depends on the value of the local pendulum frequency $\sqrt{H} = \sqrt{g/\ell}$ only.

The low- ka ($ka \ll \pi$) approximation to the gravity pendulum's dispersion function is the following

$$\omega_m = \sqrt{H + 4s \sin^2\left(\frac{k_m a}{2}\right)} \cong \sqrt{H + sa^2 k_m^2} \quad (11.5.4b)$$

This has the same hyperbolic form as the waveguide dispersion function (6.3.5b) (Recall Fig. 6.3.2.)

$$\omega = \sqrt{c^2 k^2 + \omega_{cutoff}^2} \quad (6.3.5b)_{repeated}$$

Each approximates the relativistic dispersion function (5.2.8) and the Bohr $\omega \sim k^2$, as in Fig. 11.5.3.

Relativistic Schrodinger Quantum System

$$\frac{E}{\hbar} = \omega_{rel} = \sqrt{(Mc^2)^2 + (\hbar ck)^2}$$

$$\xrightarrow{k \ll Mc} \frac{Mc^2}{\hbar} + \frac{\hbar k^2}{2M} + \dots$$

Classical Curtain of Coupled Pendulums

$$\omega_{curtain} = \sqrt{(\omega_{local})^2 + 4s \sin^2 \frac{ka}{2}}$$

where:

$$\xrightarrow{ka \ll \pi} \omega_{local} + \frac{sa^2 k^2}{2\omega_{local}} + \dots \quad \omega_{local} = \sqrt{\frac{g}{l}}$$

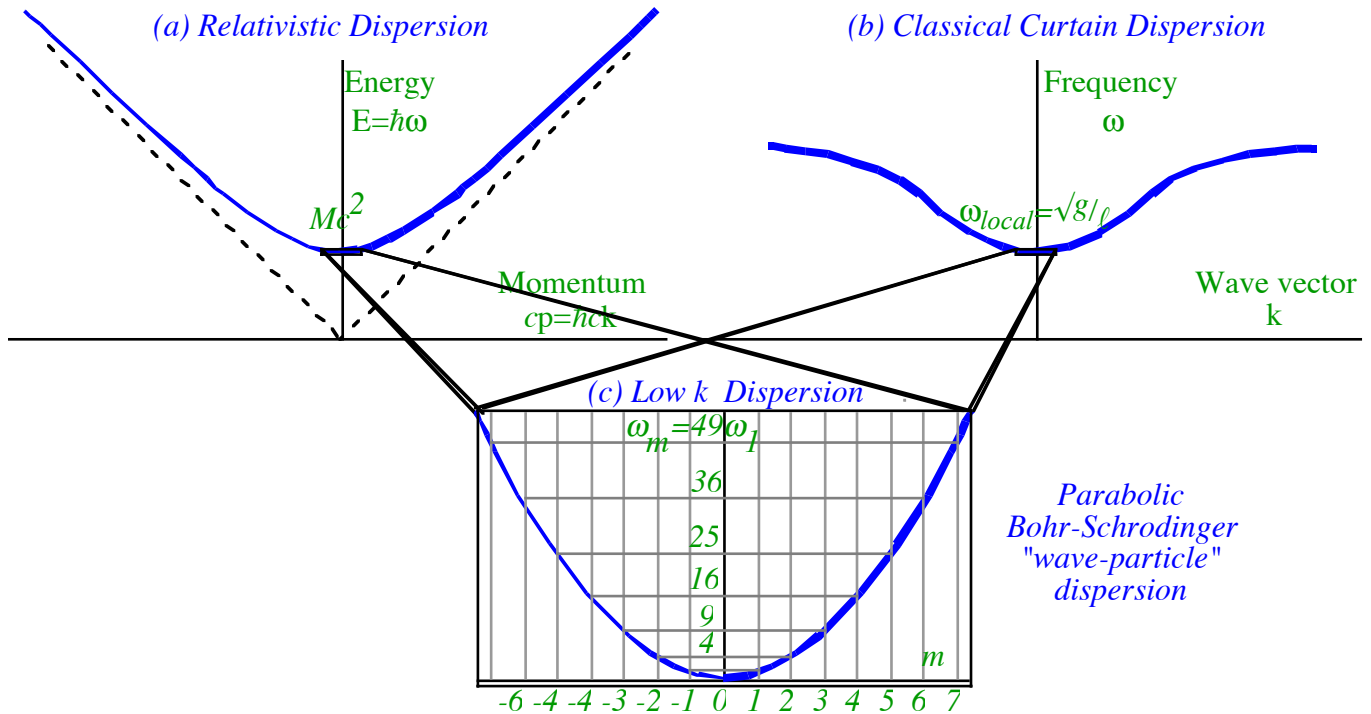


Fig. 11.5.3 Analogous dispersion functions at low k-values

(c) Shower-curtain model of Schrodinger equation

As stated in (5.2.5a) the cutoff or *proper* frequency μ for a matter wave to propagate is related to its rest energy mc^2 , that is $\mu = \omega_{cutoff} = mc^2/\hbar$. For the waveguide ω_{cutoff} is related to the waveguide width W : $\omega_{cutoff} = \pi c/W$. For the coupled pendulums ω_{cutoff} is equal to Galileo's pendulum frequency $\omega_{cutoff} = \sqrt{H} = \sqrt{g/l}$. A wave below ω_{cutoff} is evanescent and suffers exponential *extinction* away from its source. Suppose you grab a big stage curtain or a weighted shower curtain as sketched in Fig. 11.5.4. Swinging it back and forth slowly only moves the portion of the curtain closest to your hand; the response nearby is in phase with your hand but its amplitude dies off exponentially with distance as shown in Fig. 11.5.4a. (Note: The view here is, as usual, looking up from underneath the hanging pendulums or curtain.)

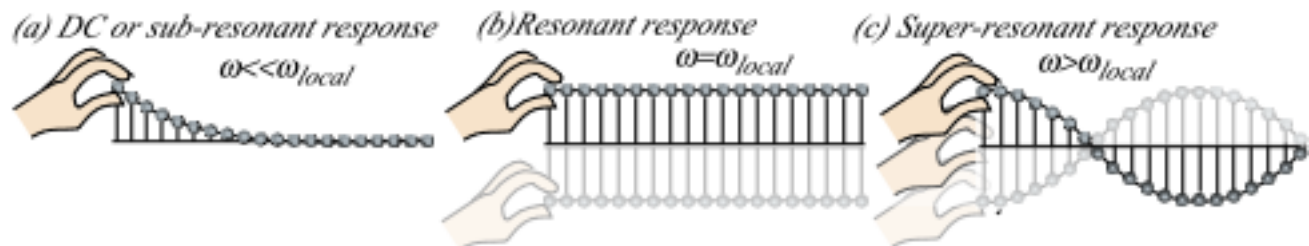


Fig. 11.5.4 Curtain motion around $\omega_{cutoff} = \omega_{local} = \sqrt{g/l}$ (a) Below ω_{cutoff} , (b) At ω_{cutoff} , (c) Above ω_{cutoff} .

However, if you wiggle with frequency at or above $\omega_{cutoff} = \sqrt{g/\ell}$ you will make waves go as far as the curtain extends! At resonance frequency ω_{cutoff} the entire curtain will swing rigidly as shown in Fig. 11.5.4b. Above ω_{cutoff} the waves may propagate as in Fig. 11.5.4c, if your wiggle phase-lag is small.

To simulate a non-uniform potential $V(x)$ of a Schrodinger equation, we may vary the local frequency of each oscillator, that is, vary with x of the pendulum lengths ℓ with position, that is pendulum length $\ell(x)$ goes up or down depending on location x of the pendulum. The bottom edge of the curtain rises as ℓ is shortened in proportion to the value $V(x)$ of a potential barrier as sketched below in Fig. 11.5.5. In other words, higher $V(x)$ means higher local frequency $V(x)/\hbar$ which is modeled by shorter pendulum length $\ell(x)$ as sketched in Fig. 11.5.5b. Shorter ℓ means higher local frequency $\omega_{local} = \sqrt{g/\ell}$.

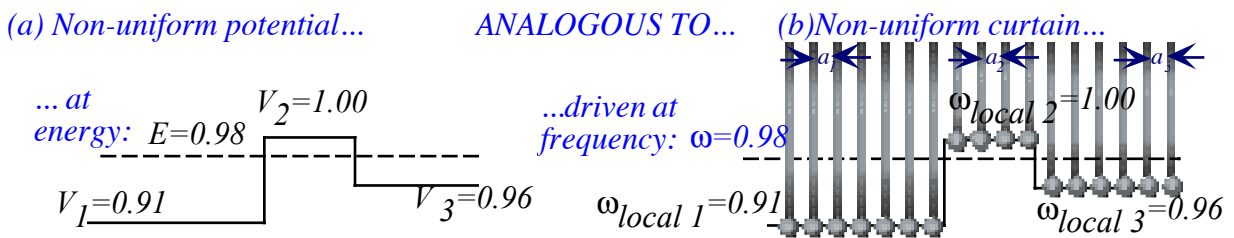


Fig. 11.5.5 Schrodinger-curtain analogy (a) Potential barriers, (b) Equivalent curtain segments.

The Schrodinger-curtain analogy requires $ka \ll 1$ (Wavelength is much longer than inter-pendulum spacing a .) as given by the corresponding dispersion relations above Fig. 11.5.3.

$$\begin{aligned}
 E - V &= \frac{p^2}{2M} = \frac{\hbar^2 k^2}{2M} \\
 \hbar\omega = E = V + \frac{\hbar^2 k^2}{2M} & \quad (11.5.5a) \\
 k &= \sqrt{\frac{2M(E - V)}{\hbar^2}}
 \end{aligned}$$

$$\begin{aligned}
 \omega - \omega_{local} &= \frac{sa^2 k^2}{2\omega_{local}} \\
 \omega = \omega_{local} + \frac{k^2}{2W} & \quad (11.5.5b) \\
 k &= \sqrt{2W(\omega - \omega_{local})} \quad \text{where: } W = \frac{\omega_{local}}{sa^2}
 \end{aligned}$$

Potential $V(x)$ or the analogous pendulum length $\ell(x)$ varies with x , but the factor $W = \sqrt{g/s^2 a^4 \ell}$ remains constant throughout. The W -factor is related to the Schrodinger mass factor M/\hbar^2 that is constant for all x . (The lattice spacing a or spring coupling constant s could vary in such a way to keep W constant.)

This analogy helps to clarify the *extinction* effect of a barrier on a wave whose energy $E = 0.98$ is below the center barrier top $V_2 = 1.00$ in Fig. 11.5.5a but above the left or right hand plateau potentials $V_1 = 0.91$ or $V_3 = 0.96$. The analogous pendulaum system in Fig. 11.5.5b is oscillating at a frequency $\omega = 0.98$ (Planck scale factor \hbar relates the analogous systems) which is high enough to support wave propagation everywhere except in the ω_{local2} barrier region where all the pendulums have a higher local frequency $\omega_{local2} = 1.00$ which prevents them from responding enthusiastically to $\omega < 1$. Only evanescent waves (Recall Fig. 11.4.3.) are possible inside the barrier at frequency $\omega = 0.98$.

Difference-differential *Schrodinger's equations with variable potential $V(x)$* follow from (11.2.11).

$$i\hbar \frac{\partial |\Psi\rangle}{\partial t} = (-Sa^2\nabla^2 + \mathbf{V})|\Psi\rangle \rightarrow i\hbar \frac{\partial \Psi(x,t)}{\partial t} = \frac{-\hbar^2}{2M} \frac{\partial^2 \Psi(x,t)}{\partial x^2} + V(x)\Psi(x,t) \quad (11.5.6a)$$

Here the tunneling parameter S is the same as before. (Recall (9.3.11) and discussion of "effective" mass.)

$$S = \frac{\hbar^2}{2Ma^2} \quad (11.5.6b)$$

The matrix form has diagonal terms V_p at each discrete position x_p to approximate $V(x)$ by $V_p = V(x_p)$.

$$i\hbar \frac{\partial}{\partial t} \begin{pmatrix} \vdots \\ \langle 0|\Psi\rangle \\ \langle 1|\Psi\rangle \\ \langle 2|\Psi\rangle \\ \langle 3|\Psi\rangle \\ \langle 4|\Psi\rangle \\ \vdots \end{pmatrix} = \begin{pmatrix} \ddots & & & & & & \\ & \ddots & & & & & \\ & & 2S+V_0 & -S & & & \\ & & -S & 2S+V_1 & -S & & \\ & & & -S & 2S+V_2 & -S & \\ & & & & -S & 2S+V_3 & -S \\ & & & & & -S & 2S+V_4 & \ddots \\ & & & & & & \ddots & \ddots \end{pmatrix} \begin{pmatrix} \vdots \\ \langle 0|\Psi\rangle \\ \langle 1|\Psi\rangle \\ \langle 2|\Psi\rangle \\ \langle 3|\Psi\rangle \\ \langle 4|\Psi\rangle \\ \vdots \end{pmatrix} \quad (11.5.6c)$$

It is instructive to compare the above with classically coupled pendulum equations,

$$\frac{\partial^2 |Y\rangle}{\partial t^2} = (Sa^2\nabla^2 - \mathbf{K})|Y\rangle \rightarrow \frac{\partial^2 Y(x,t)}{\partial t^2} = C^2 \frac{\partial^2 Y(x,t)}{\partial x^2} + K(x)Y(x,t), \quad (11.5.7a)$$

for N -coupled pendulums of inertia m connected by springs of constant k_{12} where, as before:

$$k_{12}/m = s = C^2/a^2. \quad (11.5.7b)$$

$$\frac{\partial^2}{\partial t^2} \begin{pmatrix} \vdots \\ \langle 0|Y\rangle \\ \langle 1|Y\rangle \\ \langle 2|Y\rangle \\ \langle 3|Y\rangle \\ \langle 4|Y\rangle \\ \vdots \end{pmatrix} = - \begin{pmatrix} \ddots & & & & & & \\ & \ddots & & & & & \\ & & 2s+K_0 & -s & & & \\ & & -s & 2s+K_1 & -s & & \\ & & & -s & 2s+K_2 & -s & \\ & & & & -s & 2s+K_3 & -s \\ & & & & & -s & 2s+K_4 & \ddots \\ & & & & & & \ddots & \ddots \end{pmatrix} \begin{pmatrix} \vdots \\ \langle 0|Y\rangle \\ \langle 1|Y\rangle \\ \langle 2|Y\rangle \\ \langle 3|Y\rangle \\ \langle 4|Y\rangle \\ \vdots \end{pmatrix} \quad (11.5.7c)$$

Spring term $2s$ adds to local Galilean gravity restoring acceleration K_p of each pendulum at point $x=x_p$.

$$K_p = k_p/m = g/l_p = K(x_p) \quad (11.5.7d)$$

(d.) Klein-Gordon equations: Relativistic dispersion?

If $K(x)$ and K_p are set equal to proper frequency $\mu^2 = (mc^2/\hbar)^2$ there results the *Klein-Gordon equation*.

$$\frac{1}{c^2} \frac{\partial^2 Y(x,t)}{\partial t^2} = \frac{\partial^2 Y(x,t)}{\partial x^2} - \left(\frac{mc^2}{\hbar}\right)^2 Y(x,t) \quad (11.5.8)$$

This equation was first presented by Schrodinger, Klein, and Gordon in 1926-1928 as a relativistic wave equation obtained from the energy momentum invariant (5.2.7).

$$E^2 - c^2 \mathbf{p} \bullet \mathbf{p} = E^2 - c^2 p^2 = (mc^2)^2 \quad (5.2.7) \text{repeated}$$

An energy operator is made from operator substitutions (11.3.10) as in the "crummy derivation" (5.4.10).

$$\mathbf{p} \rightarrow \frac{\hbar}{i} \frac{\partial}{\partial \mathbf{r}} = \frac{\hbar}{i} \nabla, \quad \frac{E}{c} \rightarrow \frac{\hbar i}{c} \frac{\partial}{\partial t}, \quad \left(\frac{E}{\hbar}\right)^2 = \frac{c^2 p^2}{\hbar^2} + \left(\frac{mc^2}{\hbar}\right)^2 \rightarrow \frac{-1}{c^2} \frac{\partial^2}{\partial t^2} = -\nabla^2 + \left(\frac{mc^2}{\hbar}\right)^2$$

It was proposed to add to this equation a non-constant potential $V(x)$ energy as in the following.

$$\frac{\hbar^2}{c^2} \frac{\partial^2 Y(x,t)}{\partial t^2} = \hbar^2 \frac{\partial^2 Y(x,t)}{\partial x^2} + (mc^2 + V)^2 Y(x,t)$$

Such a scheme is flawed. A scalar potential $V(x)$ can never be relativistically invariant, but must accompany an appropriately defined vector potential $\mathbf{A}(x)$. Then the quantity $V^2 - c^2 \mathbf{A}^2$ is a relativistic invariant as in the case of electromagnetic theory. Vector potential $\mathbf{A}(x)$ is introduced in Chapter 17.

(e) “Hyper” Schrodinger equations and hyper-dispersion

A general C_N -symmetric “quantum-dot” Hamiltonian described in Chapter 9 (Recall (9.2.7)) has tunneling amplitudes $-S, -T, -U$, and so forth, from each point to neighboring points $1, 2, 3, \dots, N-1$ steps away. Examples of $STU\dots$ “hyper-connectivity” are sketched in Fig. 9.2.1 and in Fig. 11.5.6 below.

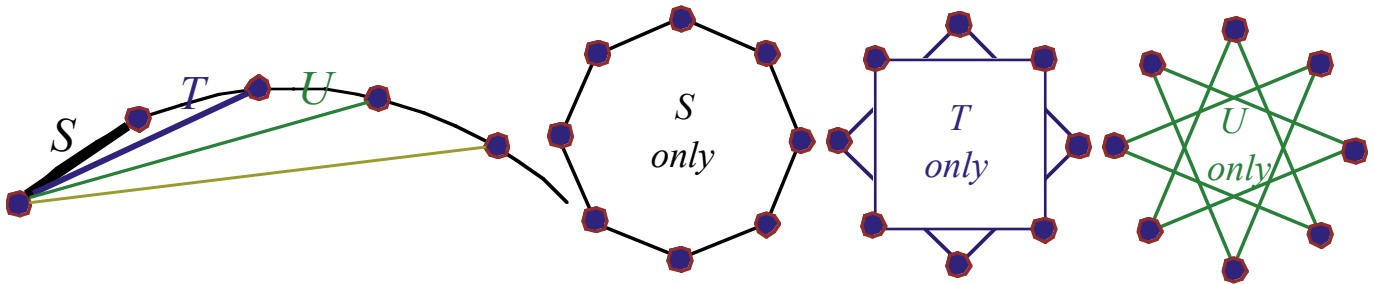


Fig. 11.5.6 Hyper-connecting tunneling amplitudes and examples for $N=8$ quantum dot structure.

$$i\hbar \frac{\partial}{\partial t} \begin{pmatrix} \vdots \\ \langle 0 | \Psi \rangle \\ \langle 1 | \Psi \rangle \\ \langle 2 | \Psi \rangle \\ \langle 3 | \Psi \rangle \\ \langle 4 | \Psi \rangle \\ \vdots \end{pmatrix} = \begin{pmatrix} \ddots & \ddots & & & & & & & \\ & \ddots & H & -S & -T & -U & & & \\ -T & -S & H & -S & -T & -U & & & \\ -U & -T & -S & H & -S & -T & -U & & \\ & -U & -T & -S & H & -S & -T & & \\ & & -U & -T & -S & H & \ddots & & \\ & & & -U & -T & \ddots & \ddots & & \end{pmatrix} \begin{pmatrix} \vdots \\ \langle 0 | \Psi \rangle \\ \langle 1 | \Psi \rangle \\ \langle 2 | \Psi \rangle \\ \langle 3 | \Psi \rangle \\ \langle 4 | \Psi \rangle \\ \vdots \end{pmatrix} \tag{11.5.10a}$$

If S, T, U, \dots are real, discrete Δ^k difference operators (11.2.24) could combine to give the matrix above.

$$i\hbar \frac{\partial | \Psi \rangle}{\partial t} = (\delta_0 - \delta_2 \Delta^2 - \delta_4 \Delta^4 - \delta_6 \Delta^6 - \dots) | \Psi \rangle \tag{11.5.10b}$$

Corresponding C_∞ -symmetric continuum differential equations involve a combination of higher order x -derivatives. *Bilateral B-type* symmetry (Sec. 10.2b) has real S, T, U and only even-order derivatives.

$$i\hbar \frac{\partial \Psi(x,t)}{\partial t} = d_0 \Psi(x,t) + d_2 \frac{\partial^2 \Psi(x,t)}{\partial x^2} + d_4 \frac{\partial^4 \Psi(x,t)}{\partial x^4} + d_6 \frac{\partial^6 \Psi(x,t)}{\partial x^6} + \dots \tag{11.5.10c}$$

Real constant coefficients d_k of derivatives are functions of tunneling amplitudes $STU\dots$ and vice-versa. So far, we have only dealt with zeroth and second x -derivatives in the standard Schrodinger equation.

$$i\hbar \frac{\partial \Psi(x,t)}{\partial t} = V \Psi(x,t) + \frac{-\hbar^2}{2M} \frac{\partial^2 \Psi(x,t)}{\partial x^2} \quad (11.5.10d)$$

If potential V is constant, the dispersion function reduces to a quadratic (Bohr-ring!) $\omega = (\hbar^2/2M)k^2$.

If connectivity is C_∞ -symmetric so all S, T, U, \dots or $\delta_1, \delta_2, \delta_3, \dots$, or d_1, d_2, d_3, \dots are independent of x or x_p , then $\Psi = e^{ikx}$ will be eigenfunctions for all δ_k or d_k . Real S, T, U, \dots give B -type symmetry and B -hyperconnectivity allows us to make any *even* dispersion function ($\omega_m(-k_m) = \omega_m(k_m)$). (Recall making revival Hamiltonians (9.4.6) where the objective was to *recover* a Bohr-ing $\omega \sim k^2$ dispersion.) Here, putting $\Psi = e^{ikx}$ into the hyper-Schrodinger equation (11.5.10d) yields $\omega(k)$ as a power series in k .

$$\omega(k) = d_0 + d_2 \frac{k^2}{2!} + d_4 \frac{k^4}{4!} + d_6 \frac{k^6}{6!} + \dots \quad (11.5.10e)$$

Equivalently, a quantum-dot equation yields $\omega_m(k_m)$ as a Fourier cosine series (9.3.5d) in k_m .

$$\omega_m = H + 2|S| \cos(k_m a) + 2|T| \cos(2k_m a) + 2|U| \cos(3k_m a) + \dots \quad (11.5.10f)$$

In the high- N and low- k limit, the series (e) and (f) should converge on the same dispersion function.

Complex tunneling amplitudes S, T, U, \dots correspond to C -type symmetry (Sec. 10.2c) and give anti-symmetric Hamiltonian matrix components and asymmetric dispersion functions. ($\omega_m(-k_m) \neq \omega_m(k_m)$) Cosine series are not sufficient. Complex $e^{iMk_m a}$ Fourier series dispersion functions (9.3.5c) arise.

$$\hbar \omega_m = H + S e^{-ik_m a} + S^* e^{ik_m a} + T e^{-i2k_m a} + T^* e^{i2k_m a} + U e^{-i3k_m a} + \dots \quad (11.5.11)$$

This has odd (sine) terms which give odd powers of k in the continuum dispersion function.

$$\omega(k) = d_0 + d_1 k + d_2 \frac{k^2}{2!} + d_3 \frac{k^3}{3!} + d_4 \frac{k^4}{4!} + d_5 \frac{k^5}{5!} + d_6 \frac{k^6}{6!} + \dots \quad (11.5.12)$$

A C -type hyper-Schrodinger equation has odd-order derivatives. (*Odd- k d_k are imaginary so $\mathbf{H}^\dagger = \mathbf{H}$* .)

$$i\hbar \frac{\partial \Psi(x,t)}{\partial t} = d_0 \Psi(x,t) + d_1 \frac{\partial \Psi(x,t)}{\partial x} + d_2 \frac{\partial^2 \Psi(x,t)}{\partial x^2} + d_3 \frac{\partial^3 \Psi(x,t)}{\partial x^3} + d_4 \frac{\partial^4 \Psi(x,t)}{\partial x^4} + \dots \quad (11.5.13)$$

A first order Schrodinger derivative term arises from an electromagnetic vector potential \mathbf{A} .

$$\begin{aligned} i\hbar \frac{\partial \Psi(x,t)}{\partial t} &= V \Psi(x,t) + \frac{\hbar^2}{2M} (\mathbf{p} - e\mathbf{A})^2 \Psi(x,t) \\ &= \left(V + \frac{e^2 \hbar^2}{2M} A^2 \right) \Psi(x,t) - i \frac{\hbar^2}{M} \mathbf{A} \cdot \frac{\partial \Psi(x,t)}{\partial \mathbf{x}} - \frac{\hbar^2}{2M} \frac{\partial}{\partial \mathbf{x}} \cdot \frac{\partial \Psi(x,t)}{\partial \mathbf{x}} \end{aligned} \quad (11.5.14)$$

The canonical electromagnetic momentum ($\mathbf{p} - e\mathbf{A}$) will be discussed in Chapter 17. This is a first step toward putting quantum theory back into its natural relativistic setting. (However, treating time as a separate parameter, as in any of these Schrodinger equations, can never yield fully relativistic theory.)

With no translation or C_∞ -symmetry, each coefficient d_k , starting with $d_0 = V(x)$, may be a function of x . Having such *asymmetric* or A -type symmetry (Sec. 10.2a) destroys a Fourier-symmetry based dispersion (11.5.12). A -eigenfunctions localize or “puddle” around potential anisotropy due to $d_0 = V(x)$ or kinetic anisotropy due to $d_1 = -i(\hbar^2/M)A(x)$ or higher kinetic $d_k(x)$ -hyper-connectivity terms in (11.5.13).

In curved (q_1, q_2, \dots) coordinates, Schrodinger equations will have coordinate- q -dependent connectivity terms $d_{k,l,\dots}(q_m)$. Generally, these are restricted to second order ($k+l=2$).

$$i\hbar \frac{\partial \Psi(q_m, t)}{\partial t} = \sum_{k,l} d_{k,l,\dots}(q_m) \frac{\partial^{k+l} \Psi(q_m, t)}{\partial q_1^k \partial q_2^l \dots} \quad (11.5.15)$$

The two state systems avoid consideration of hyper-connectivity by having only nearest neighbors! So an ($N=2$)-state mechanical analogy is much simpler than any of the Schrodinger equations or their discrete matrix versions considered above. The *ABCD* analogy for an ($N>2$)-level system does not simply reduce to difference or differentials that are only second-order-in- x . (See exercise 11.5.2.)

Problems for Chapter 11

Topology slopology

11.1.1. The Discrete Bloch Problem is the name we chose for a C_N “qudot” system. By changing number N of dots and lattice spacing a between them it is possible to approach each of the other three cases in Fig. 11.1.1.

Do so for each case (CBI) Continuous Bloch, (DBo) Discrete Bohr, and (CBo) Continuous Bohr.

Recycled differences

11.2.1. The differential-difference operators $\bar{\Delta}^q$ in (11.2.24) can be written so they apply to a cyclic C_N ring of N -qudots. The key idea is that all such operators be invariant to C_N symmetry operator powers \mathbf{r}^p .

- (a) Construct matrix $\bar{\Delta}^q$ for $q=1$ and $N=6$ so $\bar{\Delta}^1 = (\mathbf{r}^{-1} - \mathbf{r})/2$ with $\mathbf{r}^{-1} = \mathbf{r}^5$ defined in discussion of C_6 after (8.1.5).
- (b) Write the matrix for $\bar{\Delta}^2$, that is $\bar{\Delta}^q$ for $q=2$. Is this definition consistent in that $(\bar{\Delta}^1)^2 = \bar{\Delta}^2$?
- (c) Derive similar $N=6$ matrix “derivatives” $\bar{\Delta}^q$ for $q=3-6$.
- (d) Instead define Δ^2 as in (11.2.26) and express it in terms of \mathbf{r}^p from C_6 . What Δ^q matrices result from powers?
- (e) Using results of (d) write Hamiltonian \mathbf{H} in (9.2.7) in terms of Δ^q . Write as a “differential” equation (9.3.5b).

What adjoint

11.2.2. Consider a driven (by $a(t)$), damped (by Γ), harmonic (frequency ω_0) oscillator equation.

$$\mathbf{H} \cdot \mathbf{x} = \mathbf{a} \quad \text{or:} \quad H \cdot x(t) = \left(\frac{d^2}{dt^2} + 2\Gamma \frac{d}{dt} + \omega_0^2 \right) \cdot x(t) = a(t)$$

- (a) Under what conditions, if ever, is operator H self adjoint? Derive adjoint operator H^\dagger .
- (b) Find Green’s function such that $H \cdot G(t) = \delta(t-0)$ or $\mathbf{H} \cdot \mathbf{G} = \mathbf{1}$.
- (c) Represent equations in frequency basis (Fourier transform) and give frequency representation of \mathbf{G} . Hint: See Appendix 1.B.

x Commute per x

11.3.1. Consider expressions and effects of the commutator $\mathbf{C} = [\mathbf{x}, \mathbf{p}] = \mathbf{x}\mathbf{p} - \mathbf{p}\mathbf{x}$ or $\mathbf{C}/\hbar = [\mathbf{x}, \mathbf{k}] = \mathbf{x}\mathbf{k} - \mathbf{k}\mathbf{x}$

- (a) Derive the coordinate representation of the operator \mathbf{C} and apply it to a function $\phi(x)$. Discuss.
- (b) Derive the momentum representation of the operator \mathbf{C} and apply it to a function $\phi(p)$. Discuss.

Boosts and Roosts

11.3.2. We have noted that energy operator \mathbf{H} is a generator of time translation or evolution operator $\mathbf{U} = \exp(-i\mathbf{H}t)$. What do other operators such as \mathbf{x} and \mathbf{p} generate? (Here we take $\hbar=1$)

- (a) Apply operator $\mathbf{T} = \exp(-i\mathbf{p}a)$ to a function $\psi(x)$ of coordinate x . Check for case of plane wave $\psi(x) = e^{ikx}$.
- (b) Apply operator $\mathbf{B} = \exp(i\mathbf{x}b)$ to a function $\phi(p)$ of momentum $p=k$. Check for case of plane wave $\phi(p) = e^{ikx}$.

Dying to keep the phase

11.4.1. Exponential and evanescent waves keep time (phase) differently as shown in Fig. 11.4.2-3.

- (a) Consider an exponential “right-dying” plane wave $\psi(x,t) = e^{-\kappa x - i\omega t}$. Are its phasors synchronized at each t ?
- (b) Consider an evanescent “growing-dying” plane wave $\psi(x,t) = Ae^{-\kappa x - i\omega t} + Be^{+\kappa x - i\omega t}$. Can its phasors be synchronized? For what A or B? Write the wave as a combination of hyper-cosine and hyper-sine functions.
- (c) Consider the 50-50 cases of the “growing-dying” wave in (b). Derive “expo-hyperine” identities analogous to the expo-cosine or expo-sine identities used in Chapter 4.

Getting hyper

11.5.1. Compare que-dot equations (11.5.10a), difference-eqs. (11.5.10b) and hyper Schrodinger eqs. (11.5.10c).

- (a) Derive coefficients δ_k in terms of S, T, and U and vice-versa.
- (b) Derive coefficients d_k in terms of S, T, and U and vice-versa.
- (c) Compare resulting dispersion relations (11.5.10e) and (11.5.10f). Relate them in the high-N-low-k limit.

Getting more hyper

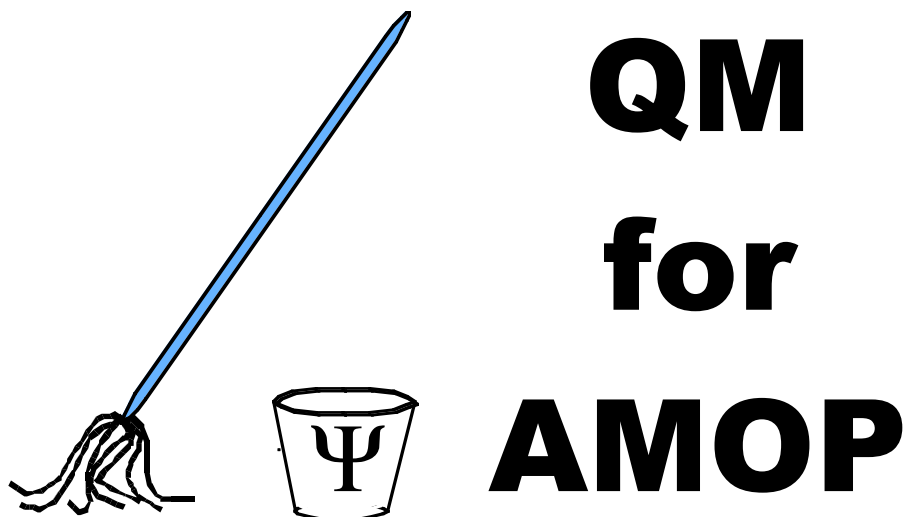
11.5.2. Generalize the ABCD analogy in Ch. 10 between 2-state Schrodinger and 2-pendulum Hamilton equations.

- Write a general N-state Schrodinger equation (N=3 or 4 is a start) as real equations as in (10.1.2).
- Find a classical Hamiltonian would give the real equations (a).
- For an all real quantum Hamiltonian (Zero C-type components) find the Newton's equations as in (10.1.5).
- Show how C_N symmetry would simplify the results of (a-c).
- Write (a)-(d) equations as difference and differential equations as done, for example, in (11.5.10).

Curtain Call

11.5.3. This problem relates to the analogy between classical coupled pendulums and quantum waves which are evanescent or propagating. Suppose a curtain stretched by a tension of $1N$ across a 10 meter stage, connects a thousand loosely connected lead weights each hanging from the ceiling 9.8 meters above. (First, show that classical coupled pendulum equations give an approximate dispersion function of the form: $\omega(k) \sim \omega_{CUT} + Ak^2$.)

- You are holding one end while your partner stage-hand is at the other. You notice that if you swing your end at precisely $\omega = 2(\text{radian})/\text{sec.}$, the resulting waves take exactly 5 seconds to cross the stage to your partner who absorbs them. (Does this give V_{phase} or V_{group} ? Explain. Note the word "precisely".) Use this to find A and ω_{CUT} in numeric dispersion formula and related formulas for the group and phase velocities and wave length as a function of angular frequency ω . Give the numerical values for these quantities for $\omega = 1.0, 1.5, 2.0$ and 3.0 .
- Suppose you gently pull your end of the curtain toward the audience and hold it at one meter from its resting point. Describe the curve the curtain makes and tell how much of the curtain has been pulled more than 5 cm. from its resting point. ($e^{-3} = 0.05$.)
- If you gently swing your end at a steady frequency ω with a 1 meter amplitude, what is the smallest frequency ω needed to cause at least a 5 cm. swing amplitude at the location of your partner on the other side.



Chapter 12
Infinite Well States
And
Dynamics

W. G. Harter

CHAPTER 12. INFINITE WELL STATES AND DYNAMICS1

12.1 Infinite-Well Wavefunctions1

- (a) Eigenstate wavefunctions1
- (b) Superposition wavefunctions2
- (c) Energy expectation values3
- (d) Position expectation values4
- (e) Position moments: Dipole matrices5
 - Moments of morphology7

12.2 Wave Packet Shape and Dynamics8

- (a) Uncertainty relation and "Last-in-First-out" effect9
- (b) Wavepacket explodes! (Then revives)10
- (c) Bohr rotor waves: Relation to square well waves13
 - (1) "Boxcar windows": Wavepackets that go "Bang!"15
 - (2) "Gaussian windows": Wavepackets that go "Poof!"17
- (d) Brief history of revival structure and dynamics20

12.3 Infinite Well Dynamics vs. Bohr Waves21

- (a) The Bohr image-wave21
 - The buck stops here!21
- (b) Flipped revivals22
- (b) Cloned revivals23

Problems for Chapter 12.25

Now for the saga of prisoner M, a tiny mass trapped in a maximum-security prison made of infinite potential walls! This is the simplest Schrodinger model besides the Bohr orbitals discussed in Chapter 9, in fact it is subset contained within the Bohr problem. The infinite well provides a setting for introducing expectation values of energy and dipole transition and it helps clarify concepts of uncertainty and Fourier dynamics (revivals) introduced previously. This maximum-security prison prepares one for the other lesser-or-minimum-security prisons such as finite square well, oscillator, and Coulomb whose discussions occupy later Chapters. It will seem like all the particles spend most of their time in jail. Schrodinger analysis does seem to encourage a lot of recidivism!

Chapter 12. Infinte Well States and Dynamics

12.1 Infinite-Well Wavefunctions

Suppose a potential that is zero only in a finite well region of width W between walls at $x=0$ and $x=W$. Outside $V(x)$ is made extremely high so it is effectively an infinite prison that makes the mass M inside to bounce back and forth forever between the walls. Poor prisoner M !

(a) Eigenstate wavefunctions

However, eigenwaves for M in the prison may not be so different from what they may have been before the walls were put up. The difference now is that ψ must be a standing wave like the lowest plot of Fig. 11.4.1, and the energy must be such that points $x=0$ and $x=W$ lie under *wave nodes*. If the wave is zero *in* the walls it must be zero *at* the walls. These are the *infinite square-well boundary conditions*.

$$\psi_{\infty \text{ well}}(x) = A_{\rightarrow} e^{ikx} + A_{\leftarrow} e^{-ikx} = \begin{cases} 0 & \text{for: } x=0, \text{ or: } A_{\rightarrow} + A_{\leftarrow} = 0 \\ 0 & \text{for: } x=W, \text{ or: } A_{\rightarrow} e^{ikW} + A_{\leftarrow} e^{-ikW} = 0 \end{cases} \quad (12.1.1a)$$

Solving gives amplitude conditions and quantization conditions for sine standing wave eigenfunctions.

$$A_{\rightarrow} = -A_{\leftarrow} \qquad kW = n\pi \quad \text{or: } k = n\pi/W \qquad (12.1.1b)$$

$$\langle x | \epsilon_n \rangle = \psi_n(x) = A \sin(k_n x) = A \sin\left(\frac{n\pi x}{W}\right) \quad (n=1,2,3,\dots,\infty) \quad (12.1.1c)$$

These are plotted in Fig. 12.1.1 on the three lowest energy eigenvalue levels to which they belong.

$$\epsilon_n = \frac{\hbar^2}{2M} k^2 = \frac{\hbar^2 n^2 \pi^2}{2MW^2} = (1^2, 2^2, 3^2, \dots, \text{or } n^2) \frac{\hbar^2}{8MW^2} \quad (12.1.1d)$$

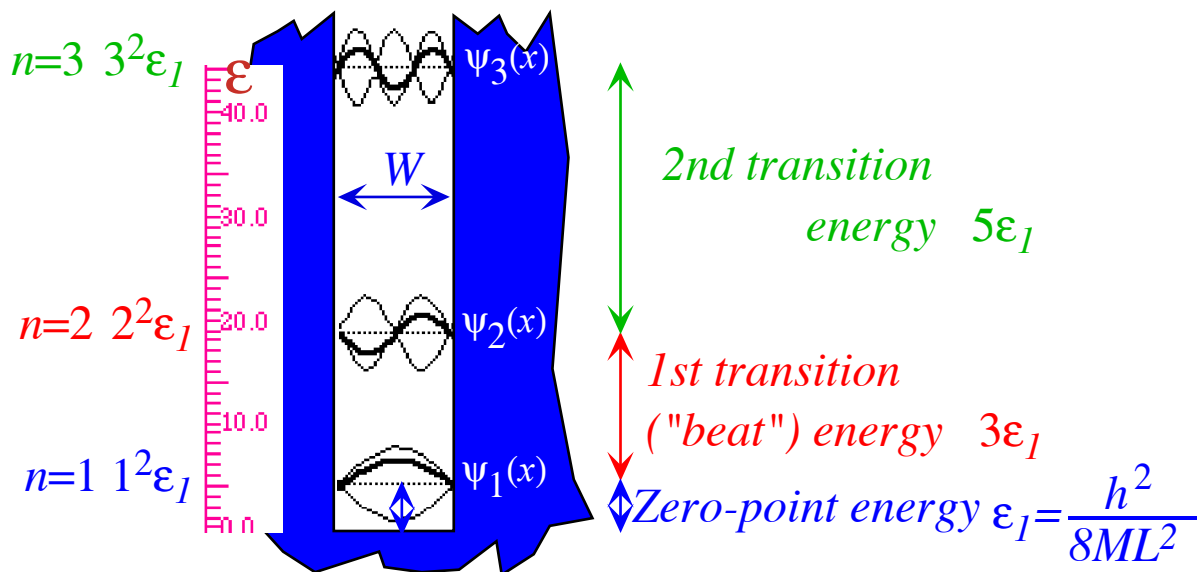


Fig. 12.1.1 Asleep in prison. Infinite square well standing waves have stationary envelopes.

Imposition of boundary conditions (12.1.1b) on prisoner M causes severe restrictions. The infinite continuum of energy and k -values is reduced to a discrete semi-infinite spectrum like the Bohr spectrum sketched in Fig. 7.1.1. However, unlike a Bohr or free-space spectrum, double energy degeneracy is

halved; only singlet sine waves remain while all cosine waves, including the $n=0$ state, are forbidden. This rules out moving or galloping wave eigenstates. Recall that zero-quanta were forbidden for the optical cavity (the "photon prison") in Fig. 6.3.7. Imprisoned spectra start counting with $n=1$, and the very first energy level is non-zero and called a *zero-point energy*. For the infinite square well it is $h^2/(8MW^2)$.

(b) Superposition wavefunctions

While none of the $\langle x | \psi_n \rangle$ waves in Fig. 12.1.1, by themselves, move any but their invisible phases, combinations like $\alpha \langle x | \psi_m \rangle + \beta \langle x | \psi_n \rangle$ do appear to bounce back and forth at a "beat" frequency equal to the difference $|\omega_m - \omega_n|$. For example, consider a wave state $\langle x | \Psi(t) \rangle$ that is a 50-50 combination

$$\langle x | \Psi(t) \rangle = \langle x | \psi_1 \rangle \langle \psi_1 | \Psi(t) \rangle + \langle x | \psi_2 \rangle \langle \psi_2 | \Psi(t) \rangle = \langle x | \psi_1 \rangle (e^{-i\omega_1 t}) + \langle x | \psi_2 \rangle (e^{-i\omega_2 t}) \quad (12.1.2)$$

of the first two waves $\langle x | \psi_1 \rangle$ and $\langle x | \psi_2 \rangle$ in Fig. 12.1.1. Its envelope "sloshes" at a beat frequency of

$$\omega_{beat} = \omega_2 - \omega_1 = \frac{\epsilon_2 - \epsilon_1}{\hbar} = \frac{2^2 - 1^2}{\hbar} \frac{h^2}{8MW^2} = 3 \frac{2\pi h}{8MW^2} = 3\omega_1 \quad (12.1.3)$$

as shown below in Fig. 12.1.2. Poor M is up and pacing back and forth in the cell. No rest for the wicked!

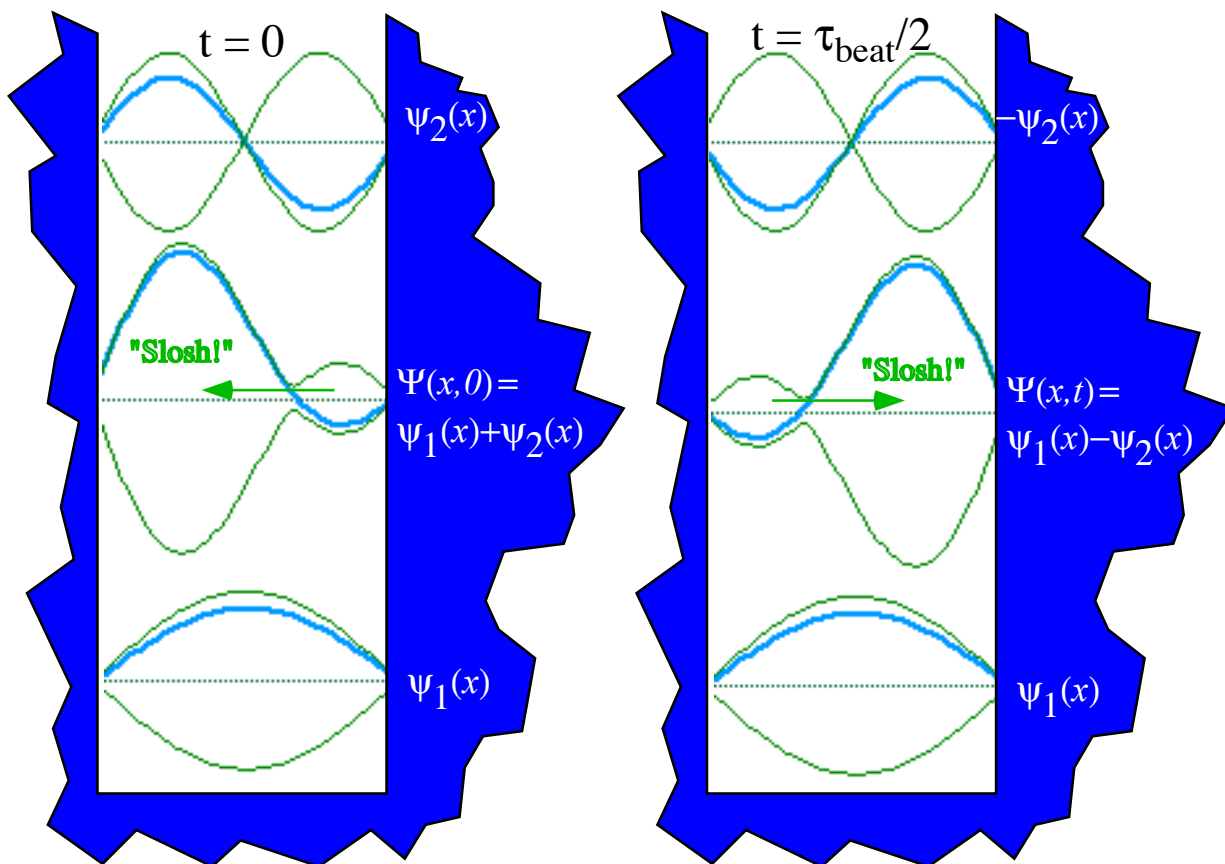


Fig. 12.1.2 Exercise in prison. Infinite square well eigensolution combination "sloshes" back and forth.

It is important to clearly visualize the dynamics of a combination wave such as is plotted in Fig. 12.1.2. If, at time $t=0$, the two components of (12.1.2) were in phase, the combination wave would be the sum of $\psi_1(x) + \psi_2(x)$ that is biased or "sloshed" to the left side of the cell. Half a beat-period later the sum becomes a difference as slower $\psi_1(x)$ falls π behind $\psi_2(x)$ to give $-\psi_1(x) + \psi_2(x)$ "sloshed" to the right.

Because $\langle x | \Psi(t) \rangle$ is a combination of $\langle x | \psi_1 \rangle$ and $\langle x | \psi_2 \rangle$ it seems reasonable that M has a kinetic energy that lies somewhere between the allowed quantum levels ϵ_1 and ϵ_2 of its component eigenstates as drawn in Fig. 12.1.2. Roughly speaking, M is somewhere between sleeping on the floor (ϵ_1) and sleeping in the first excited state or second level (ϵ_2). A quantum system is not restricted to its energy eigenvalues, "quanta" ϵ_m are just values at which it can "sleep" or "play dead." It may have any energy between its ϵ_m -values and have it in many ways, as long as it stays "awake!" This generalized energy is called the *energy expectation value* $\langle \epsilon \rangle$ and will be defined shortly.

Suppose poor sleepless M is really pacing back and forth along the full width W of the cell. In fact, he stops well short of each wall when pacing at low energy, and only really "smacks" the cell wall when he's really mad and pacing at high energy. Precise definition of this uses the *position expectation value* $\langle x \rangle$ to be defined shortly along with that of energy. But, if we assume M paces at the beat frequency (12.1.3) and at a constant speed v (he is, after all, on a flat $V=0$ prison floor in between the walls) and covers a distance $2W$ in one beat period then he will have an average speed of about

$$v = \frac{2W}{\tau_{beat}} = \frac{2W \omega_{beat}}{2\pi} = \frac{3h}{4MW} \quad (12.1.4a)$$

and an approximate energy of

$$E = \frac{1}{2} Mv^2 = \frac{1}{2} M \left(\frac{3h}{4MW} \right)^2 = \frac{9}{4} \frac{h^2}{8MW^2} \quad (12.1.4b)$$

that is, $2^{1/4}$ of the quantum ground state (zero-point) energy ϵ_1 , and a little shy of half way between ϵ_1 and ϵ_2 , which is $2^{1/2}$, the exact value as we'll see soon. Now let's see if we can figure out exactly what prisoner M is up to! (Cons must be watched precisely even while incarcerated.)

(c) Energy expectation values

Prisoner M "wakes up" and "paces" when in a *combination state* of at least two eigenstates such as

$$|\Psi(t)\rangle = |\psi_1\rangle\langle\psi_1 | \Psi(t)\rangle + |\psi_2\rangle\langle\psi_2 | \Psi(t)\rangle = \alpha(t)|\psi_1\rangle + \beta(t)|\psi_2\rangle \quad (12.1.5a)$$

where coefficients $\langle\psi_1 | \Psi(t)\rangle = \alpha(t) = \alpha(0) e^{-i\omega_1 t}$, and $\langle\psi_2 | \Psi(t)\rangle = \beta(t) = \beta(0) e^{-i\omega_2 t}$ (12.1.5b) preserve normalization, that is

$$|\alpha(t)|^2 + |\beta(t)|^2 = 1 \quad (12.1.5c)$$

Indeed, they should, since $|\alpha(t)|^2$ (or $|\beta(t)|^2$) is the probability for prisoner M to be found sleeping on the floor-level- ϵ_1 (or first bunk level- ϵ_2 , respectively) if the warden wanders by with his flashlight. We have been assuming that M has only enough strength to get up to the first bunk. Bad assumption, perhaps, and we will modify it shortly.

However, if M is confined to the two lowest levels then his energy may be easily computed by summing the probabilities for being in each level times the energy of the level.

$$\begin{aligned} E_{\Psi_{average}} = \langle E \rangle_{\Psi} &= \sum_{n=1}^2 (\text{Energy of state } n) (\text{Probability of state } n) \\ &= \sum_{n=1}^2 (\epsilon_n) \left(\langle \epsilon_n | \Psi \rangle^* \langle \epsilon_n | \Psi \rangle \right) \end{aligned} \quad (12.1.6)$$

For this case the sum reduces to

$$\langle E \rangle_{\Psi} = \varepsilon_1 |\alpha|^2 + \varepsilon_2 |\beta|^2 \left(= \frac{\varepsilon_1 + \varepsilon_2}{2} = \frac{5\varepsilon_1}{2} \text{ for: } \alpha = \frac{1}{\sqrt{2}} = \beta \right), \quad (12.1.7)$$

or for a 50-50 combination, exactly $2^{1/2}$ times the quantum ground state (zero-point) energy ε_1 , and exactly half way between ε_1 and ε_2 . So our previous estimate of $2^{1/4}$ for M 's energy was a little bit low.

The general formula for energy expectation is (12.1.6) summed over all eigenstates.

$$E_{\Psi \text{ average}} = \langle E \rangle_{\Psi} = \sum_{n=1}^{\infty} \varepsilon_n \langle \varepsilon_n | \Psi \rangle^* \langle \varepsilon_n | \Psi \rangle = \sum_{n=1}^{\infty} \varepsilon_n \langle \Psi | \varepsilon_n \rangle \langle \varepsilon_n | \Psi \rangle \quad (12.1.8a)$$

Notice that conjugation axiom-2 makes this sum into a matrix element of the spectral decomposition of the Hamiltonian \mathbf{H} operator in terms of its eigenvector ket-bras $|\varepsilon_m\rangle \langle \varepsilon_m| = |\varepsilon_m\rangle \langle \varepsilon_m|$.

$$E_{\Psi \text{ average}} = \langle E \rangle_{\Psi} = \langle \Psi | \mathbf{H} | \Psi \rangle, \text{ where: } \mathbf{H} = \sum_{n=1}^{\infty} \varepsilon_n |\varepsilon_n\rangle \langle \varepsilon_n| \quad (12.1.8b)$$

This is the "professional" formula for the *energy expectation value* of any state $|\Psi\rangle$. It goes along a similar formula for "existence" or *number expectation value* based on the completeness axiom-4.

$$N_{\Psi \text{ average}} = \langle N \rangle_{\Psi} = \langle \Psi | \mathbf{1} | \Psi \rangle = \langle \Psi | \Psi \rangle, \text{ where: } \mathbf{1} = \sum_{n=1}^{\infty} |\varepsilon_n\rangle \langle \varepsilon_n| \quad (12.1.9a)$$

The latter is just a simple "bed-count" of prisoner(s) M . Here, it had better be equal to "1" or the warden is going to be in big trouble. This is, after all, an infinitely maximum-security prison! Later, we will consider more realistic prisons that are not so escape-proof. For this one, however, we *assume* there is exactly one prisoner and that sets the *norm* or *normalization* of all the states $|\varepsilon_m\rangle$ and $|\Psi\rangle$.

$$\langle \varepsilon_m | \varepsilon_m \rangle = 1 = \langle \Psi | \Psi \rangle \quad (12.1.9b)$$

Normalization of base-eigenstates is required by orthonormality axiom-2 but not necessarily for general combination states like $|\Psi\rangle$.

(d) Position expectation values

While prisoner M paces back and forth in state $|\Psi\rangle$ we can imagine (the warden) wanting to know his position in that dark cell with as much accuracy as possible. However, this is a quantum prison with all the problems and strange behavior introduced so far. Chief among these is the fact that quantum theory has nothing to say about individual observations of prisoner M . Let us all say this again for emphasis: "About each observation, quantum theory tells you nothing!..zip!..nada!..diddley-squat!..fuggedaboutit!" To a classicist warden, quantum mechanics might seem like not a theory at all,..just sheer rubbish!

What saves quantum mechanics is sheer numbers and its *statistical* predictions. To be useful, quantum theory needs thousands and thousands of prison cells each with a prisoner M in state $|\Psi(t)\rangle$. (This is apparently a goal of many modern politicians.) Or else, a single prisoner M has to be put in cell state $|\Psi(t)\rangle$ and analyzed over and over again for each value of time t . (The social-psychological approach.)

Fortunately for quantum theory, photons, electrons, and other atomic particles are relatively cheap and plentiful so massively sequential or parallel experiments are easily done. So we may accumulate huge statistical distributions to check a quantum theory. For example, in the case of prisoner M in state $|\Psi\rangle = |\Psi(t)\rangle$ it is possible to accurately predict the *position expectation value* $\langle x \rangle$ defined as follows.

$$x_{\Psi \text{ average}} = \langle x \rangle_{\Psi} = \langle \Psi | \mathbf{x} | \Psi \rangle, \text{ where: } \mathbf{x} = \int_{-\infty}^{\infty} dx x |x\rangle \langle x| \quad (12.1.10a)$$

Like $\langle E \rangle$ and \mathbf{H} , $\langle x \rangle$ is based on the spectral decomposition of position operator \mathbf{x} which yields

$$\begin{aligned} x_{\Psi_{average}} = \langle x \rangle_{\Psi} &= \langle \Psi | \mathbf{x} | \Psi \rangle = \int_{-\infty}^{\infty} dx x \langle \Psi | x \rangle \langle x | \Psi \rangle = \int_{-\infty}^{\infty} dx x \langle x | \Psi \rangle^* \langle x | \Psi \rangle \\ &= \int_{-\infty}^{\infty} dx \Psi^*(x) x \Psi(x) \end{aligned} \quad (12.1.10b)$$

This is the sum ($\int dx$) over position x times the probability $\langle x | \Psi \rangle^* \langle x | \Psi \rangle = \Psi^*(x) \Psi(x)$ for each position.

Moreover, the functional spectral decomposition yields the *functional position expectation value* $\langle f(x) \rangle$

$$\begin{aligned} \langle f(x) \rangle_{\Psi} &= \langle \Psi | f(\mathbf{x}) | \Psi \rangle = \int_{-\infty}^{\infty} dx f(x) \langle \Psi | x \rangle \langle x | \Psi \rangle = \int_{-\infty}^{\infty} dx f(x) \langle x | \Psi \rangle^* \langle x | \Psi \rangle \\ &= \int_{-\infty}^{\infty} dx \Psi^*(x) f(x) \Psi(x) \end{aligned} \quad (12.1.10c)$$

This includes as a special case the *number expectation value*.

$$\begin{aligned} \langle N \rangle_{\Psi} &= \langle \Psi | \mathbf{1} | \Psi \rangle = \int_{-\infty}^{\infty} dx \langle \Psi | x \rangle \langle x | \Psi \rangle = \int_{-\infty}^{\infty} dx \langle x | \Psi \rangle^* \langle x | \Psi \rangle \\ &= \int_{-\infty}^{\infty} dx \Psi^*(x) \Psi(x) \end{aligned} \quad (12.1.10d)$$

The latter is x -representation of the "bed-count" of prisoner(s) M , and it had better be equal to "1" here in the "maximum-security" case every time the warden looks.

$$\langle N \rangle_{\Psi} = 1 = \int_{-\infty}^{\infty} dx \Psi^*(x) \Psi(x) \quad (12.1.10e)$$

In other words, in a "strict" prison we demand unit *normalization* of all states.

The above equations provide the means for developing a complete statistical analysis of the prisoner M population and dynamics. $\langle f(x) \rangle$ formulas give the values and time behavior not only of the average or mean position $\langle x \rangle$ of prisoner(s) M each time the warden uses his flashlight, but also the (possibly time-dependent) *mean square* $\langle x^2 \rangle$, *mean-cube* $\langle x^3 \rangle$, and so forth. These are "moments" that will warm the heart of the coldest statistician, and the body count $\langle N \rangle = \langle x^0 \rangle$ is just another precious moment.

There's more. A similar formulation (12.1.10) gives the momentum operator \mathbf{p} and its moments $\langle p^0 \rangle$, $\langle p \rangle$, $\langle p^2 \rangle$, and distributions. This yields statistics about where the prisoner was going when caught each time by the glare of the warden's hated flashlight.

(e) Position moments: Dipole matrices

Evaluation of position expectation values $\langle \Psi | \mathbf{x} | \Psi \rangle$ or moments $\langle \Psi | f(\mathbf{x}) | \Psi \rangle$ can be done in any basis. The energy eigenfunction basis leaps to mind as one possibility. Using its completeness gives

$$\langle x \rangle_{\Psi} = \langle \Psi | \mathbf{x} | \Psi \rangle = \sum_{m=1}^{\infty} \sum_{n=1}^{\infty} \langle \Psi | \varepsilon_m \rangle \langle \varepsilon_m | \mathbf{x} | \varepsilon_n \rangle \langle \varepsilon_n | \Psi \rangle \quad (12.1.11)$$

This will require some *dipole matrix elements* $\langle \varepsilon_m | \mathbf{x} | \varepsilon_n \rangle$ that may be evaluated in the coordinate $|x\rangle$ -basis. First, the x -completeness relation is used twice to expand both sides of the matrix element. Then the x -eigenvalue relation $\mathbf{x}|x\rangle = x|x\rangle$ and orthonormality $\langle x' | x \rangle = \delta(x'-x)$ are used.

$$\begin{aligned} \langle \varepsilon_m | \mathbf{x} | \varepsilon_n \rangle &= \int_{-\infty}^{\infty} dx' \int_{-\infty}^{\infty} dx \langle \varepsilon_m | x' \rangle \langle x' | \mathbf{x} | x \rangle \langle x | \varepsilon_n \rangle \\ &= \int_{-\infty}^{\infty} dx' \int_{-\infty}^{\infty} dx \langle \varepsilon_m | x' \rangle x \delta(x'-x) \langle x | \varepsilon_n \rangle \end{aligned} \quad (12.1.12a)$$

The $\delta(x'-x)$ kills one integral. Wavefunctions (12.1.1c) are inserted.

$$\langle \varepsilon_m | \mathbf{x} | \varepsilon_n \rangle = \int_{-\infty}^{\infty} dx x \langle x | \varepsilon_m \rangle^* \langle x | \varepsilon_n \rangle = \frac{1}{norm.} \int_0^W dx x \sin k_m x \sin k_n x \quad (12.1.12b)$$

Finally, the normalization constant *norm.* needs to be found using (12.1.10e).

$$1 = \langle \varepsilon_n | \mathbf{1} | \varepsilon_n \rangle = \frac{1}{norm.} \int_0^W dx \sin^2 k_n x, \text{ where: } k_n = \frac{n\pi}{W} \quad (12.1.12c)$$

Using identity $\sin^2 x = (1 - \cos 2x)/2$ and the vanishing of full-wave cosine integral gives $norm. = W/2$.

$$\langle \varepsilon_m | \mathbf{x} | \varepsilon_n \rangle = \frac{2}{W} \int_0^W dx x \sin k_m x \sin k_n x \quad (12.1.12d)$$

Note the change of integration limits. We don't have to integrate over the entire universe ($-\infty$ to ∞) when the wavefunction is zero everywhere except in the prison cell (0 to W). (Now we are dealing with a maximum-security prison; later we will deal with "softer" incarcerations.)

Also, note that our origin point ($x=0$) is on the left side of a symmetric cell. Symmetry arguments would be better served if we chose it in the center ($x=W/2$). For example, if we define $\mathbf{X} = \mathbf{x} - (W/2)\mathbf{1}$ you could tell right away that $\langle \varepsilon_n | \mathbf{X} | \varepsilon_n \rangle$ is zero by noting its C_2 -symmetry under reflection $\mathbf{R}: x \rightarrow -x$.

$$\langle \varepsilon_n | \mathbf{X} | \varepsilon_n \rangle = \langle \varepsilon_n | -\mathbf{X} | \varepsilon_n \rangle = 0 \quad \text{or:} \quad \langle \varepsilon_n | \mathbf{x} | \varepsilon_n \rangle = W/2 \quad (12.1.13)$$

The conclusion is fairly self-evident, too. All eigenfunctions, that is, all "sleeping prisoners" in Fig. 12.1.1 are located (on the average) dead center ($x=W/2$) in their symmetric cell bunks. (Later, we will see what happens when you tip the prison one way or the other!) Furthermore, all eigenfunctions are either even (+) parity (for $n=1,3,5,\dots$) or else odd (-) parity (for $n=2,4,6,\dots$), that is, just the opposite of their numerical quantum numbers.

Evaluation of matrix (12.1.12d) will be done without symmetrizing just to show that it is still fairly easily performed even while we're being fairly stupid.

$$\begin{aligned} \langle \varepsilon_m | \mathbf{x} | \varepsilon_n \rangle &= \frac{2}{W} \int_0^W dx x \sin k_m x \sin k_n x = \frac{2}{W} \int_0^W dx x \left(\frac{e^{ik_m x} - e^{-ik_m x}}{2i} \right) \left(\frac{e^{ik_n x} - e^{-ik_n x}}{2i} \right) \\ &= \frac{2}{-4W} \int_0^W dx x \left(e^{i(k_m+k_n)x} - e^{i(k_m-k_n)x} + c.c. \right) \end{aligned}$$

Carrying out the integrals gives

$$\begin{aligned} \langle \varepsilon_m | \mathbf{x} | \varepsilon_n \rangle &= \\ &= \frac{-1}{2W} \left[\frac{2x \sin(k_m+k_n)x}{k_m+k_n} - \frac{2x \sin(k_m-k_n)x}{k_m-k_n} \right]_0^W \\ &= \frac{-1}{2W} \left[\frac{2W \sin(k_m+k_n)W}{k_m+k_n} - \frac{2W \sin(k_m-k_n)W}{k_m-k_n} \right. \\ &\quad \left. + \frac{2 \cos(k_m+k_n)W - 2}{(k_m+k_n)^2} - \frac{2 \cos(k_m-k_n)W - 2}{(k_m-k_n)^2} \right] \quad (12.1.14) \end{aligned}$$

Boundary-restricted wavevectors $k_n = n\pi/W$ make all sines zero and all cosines ± 1 , that is,

$$\cos(k_m+k_n)W = (-1)^{m+n} = \cos(k_m-k_n)W$$

Our failure to heed symmetry bothers us with $(m=n)$ -terms of $\sin(0)/_{(0)}$ that just give the $W/2$ in (12.1.13).

Ignoring these gives the necessary off-diagonal *dipole matrix elements*.

$$\langle \varepsilon_m | \mathbf{x} | \varepsilon_n \rangle = \frac{1 - (-1)^{m+n}}{2W} \left[\frac{2}{(k_m + k_n)^2} - \frac{2}{(k_m - k_n)^2} \right] = \frac{1 - (-1)^{m+n}}{W\pi^2} \left[\frac{W^2}{(m+n)^2} - \frac{W^2}{(m-n)^2} \right]$$

$$= \begin{cases} \frac{8W \cdot m \cdot n}{\pi^2 (m^2 - n^2)^2} & \text{for: } m=n \pm 1, 3, 5\dots \\ 0 & \text{for: } m=n \pm 2, 4, 6\dots \end{cases} \quad (12.1.15a)$$

Finally, the location of the pacing prisoner M can be statistically determined with great accuracy using (12.1.11). (Some theory! Now it'll tell you exactly where the prisoner might be!) For simplicity we'll first consider the usual combo (12.1.5) of the lowest two states. The x -expectation is

$$\langle \Psi | \mathbf{x} | \Psi \rangle = \langle \Psi | \varepsilon_1 \rangle \langle \varepsilon_1 | \mathbf{x} | \varepsilon_1 \rangle \langle \varepsilon_1 | \Psi \rangle + \langle \Psi | \varepsilon_1 \rangle \langle \varepsilon_1 | \mathbf{x} | \varepsilon_2 \rangle \langle \varepsilon_2 | \Psi \rangle + \langle \Psi | \varepsilon_2 \rangle \langle \varepsilon_2 | \mathbf{x} | \varepsilon_1 \rangle \langle \varepsilon_1 | \Psi \rangle + \langle \Psi | \varepsilon_2 \rangle \langle \varepsilon_2 | \mathbf{x} | \varepsilon_2 \rangle \langle \varepsilon_2 | \Psi \rangle$$

$$= \alpha^* \langle \varepsilon_1 | \mathbf{x} | \varepsilon_1 \rangle \alpha + \alpha^* \langle \varepsilon_1 | \mathbf{x} | \varepsilon_2 \rangle \beta + \beta^* \langle \varepsilon_2 | \mathbf{x} | \varepsilon_1 \rangle \alpha + \beta^* \langle \varepsilon_2 | \mathbf{x} | \varepsilon_2 \rangle \beta$$

(A 2 by 2 matrix expression would be simpler.) Inserting (12.1.14) and putting those $W/2$ terms gives

$$\langle \Psi | \mathbf{x} | \Psi \rangle = \left(|\alpha|^2 + |\beta|^2 \right) \frac{W}{2} + \langle \varepsilon_1 | \mathbf{x} | \varepsilon_2 \rangle \left(\alpha^* \beta + \beta^* \alpha \right)$$

$$= \frac{W}{2} + \frac{8W \cdot m \cdot n}{\pi^2 (m^2 - n^2)^2} |\alpha(0)\beta(0)| \left(e^{i\omega_1 t} e^{-i\omega_2 t} + e^{i\omega_2 t} e^{-i\omega_1 t} \right) \quad (12.1.15b)$$

$$= \frac{W}{2} + \frac{8W \cdot 1 \cdot 2}{\pi^2 (1^2 - 2^2)^2} 2 |\alpha(0)\beta(0)| \cos(\omega_1 - \omega_2) t$$

The maximum pacing amplitude is had by choosing a 50-50 (1-2)-combo, that is, $\alpha(0) = \beta(0) = 1/\sqrt{2}$. Then prisoner M is expected to "slosh" according to...

$$\langle \Psi | \mathbf{x} | \Psi \rangle = \frac{W}{2} + \frac{16W}{\pi^2 9} \cos(\omega_1 - \omega_2) t = \frac{W}{2} + 0.18W \cos(\omega_1 - \omega_2) t \quad (12.1.15c)$$

Poor prisoner M ! His quantum pacing is restricted to 18% of his cell width from the center. If you look at the plot in the center of Fig. 12.1.2, it seems to be evidence of such cruel and unusual penury. The peak's "slosh" amplitude is only about 25% of W and it has a "tail" on the opposite side that reduces $\langle x \rangle$ even more. Also, the sloshing lump is so fat it takes up half the cell and cannot get very close to the wall without deforming significantly. (Prison life has fattened prisoner M . Maybe the food is not so bad.) The next Section 12.2 is devoted to putting M on a diet and slimming him down somehow.

Moments of morphology

It should be clear that the position expectation value $\langle \Psi | \mathbf{x} | \Psi \rangle$ by itself is a rather incomplete descriptor of the morphology of prisoner M . For a Newtonian particle, it's all you need, but for a quantum wave it only gives the centroid of a wavepacket blob that can take on many shapes and sizes. Instead, shape analysis will require many higher moments $\langle \Psi | \mathbf{x}^m | \Psi \rangle$ or moment functions $\langle \Psi | f(\mathbf{x}) | \Psi \rangle$. An obvious choice for moment functions are $f(x) = \sin mx$, the eigenfunctions themselves, but that leads back to Fourier analysis of wave packets. We return to that next.

12.2 Wave Packet Shape and Dynamics

By combining more and higher energy eigenstates it becomes possible to slim down the wavefunction of prisoner M to the point that he can approach arbitrarily close to either wall. But, then something else happens to severely affect his new slim figure. It is called *wavepacket dynamics*.

Before we discuss the ruinous effects of wavepacket spreading, let's see how slim we can make the wave function. In principle, we can make it infinitely thin, provided we could pay for the energy needed to make a *Dirac delta-wavefunction* $\Psi(x)=\delta(x-a)$. Such an anorexic shape will require exercising prisoner M to the extreme and will have extraordinary side effects.

A key to this extraordinary slenderizing is $|x\rangle$ -orthonormality and $|\epsilon_n\rangle$ -completeness

$$\delta(x-a) = \langle x|a\rangle = \sum_{n=1}^{\infty} \langle x|\epsilon_n\rangle \langle \epsilon_n|a\rangle = \sum_{n=1}^{\infty} a_n \sin k_n x \quad , \quad (12.2.1a)$$

where the constant coefficients

$$a_n = \langle \epsilon_n|a\rangle = (2/W) \sin k_n a \quad (k_n = n\pi/W) \quad (12.2.1b)$$

depend on the position ($0 < a < W$) where we would like to put this "slim-jim" wonder-wave. Note that it can't stand exactly at the walls because $\sin k_n a$ goes to zero for $a = 0$ and $a = W$, but it can get close.

This is a situation that happens quite often in continuum quantum theory. The sum (12.2.1) is infinite and discrete and makes an infinitely sharp feature in a bounded continuum. Here you get what you pay for, and no one can afford the time or energy it takes to make prisoner M infinitely thin. So (12.2.1) becomes an approximate or *truncated* sum that just stops when we tire of summing. A 30 term truncation of (12.2.1a) for ($a=0.2W$) is shown in Fig. 12.2.1. (It is scaled down by a factor of 30.)

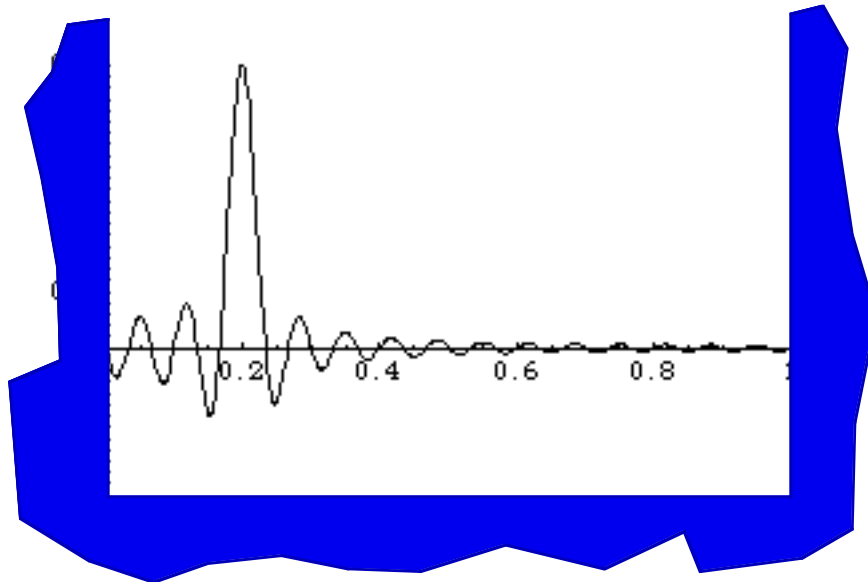


Fig. 12.2.1 Greetings from prisoner M ! Initial wavepacket combination (12.2.1) of 30 energy states.

Now let's see what happens if we pay for a few more terms! We'll redo the pulse wave analysis that was done for optical waves in Chapter 5 equation (5.3.5).

(a) Uncertainty relation and "Last-in-First-out" effect

By summing over 100 levels the profile of the prisoner M wave becomes quite svelte, as seen in Fig. 12.2.2. The ultimate shape of this kind of delta function is beginning to emerge. About its center, it has a distinctive shape of the *elementary diffraction function* $\sin kx/x$ that is seen often in spectral theory.

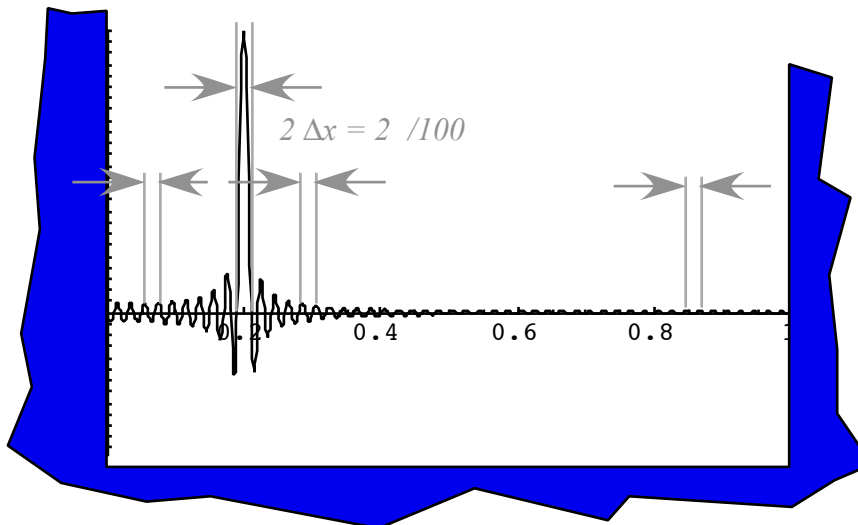


Fig. 12.2.2 Ultra-thin prisoner M. Initial wavepacket combination (12.2.1) of 100 energy states.

You can derive this shape approximately by converting the k_n -sum (12.2.1) into a k -integral.

$$\Psi(x) = \frac{2}{W} \sum_n^{N_{\max}} \sin k_n a \sin k_n x \rightarrow \frac{2}{W} \int_0^{K_{\max}} dk \frac{\Delta n}{\Delta k} \sin ka \sin kx = \frac{2}{W} \frac{W}{\pi} \int_0^{K_{\max}} dk \sin ka \sin kx \quad (12.2.2)$$

The approximate result is a function that wiggles just as much as the maximum k -value K_{\max} allows.

$$\begin{aligned} \Psi(x) &\cong \frac{2}{\pi} \int_0^{K_{\max}} dk \sin ka \sin kx = \frac{1}{\pi} \int_0^{K_{\max}} dk (\cos k(x-a) - \cos k(x+a)) \\ &\cong \frac{\sin K_{\max}(x-a)}{\pi(x-a)} - \frac{\sin K_{\max}(x+a)}{\pi(x+a)} \cong \frac{\sin K_{\max}(x-a)}{\pi(x-a)} \quad \text{for: } x \approx a \end{aligned} \quad (12.2.3)$$

You might call this the *"last-in-first-out" effect*. The last K_{\max} -value dominates while the lesser values get "smothered" by interference with neighboring values above and below them. Note that $\Psi(x)$ peaks at $(x=a)$ and plummets to zero on either side at $(x=a \pm \Delta x)$ with *half-width* Δx inversely related to K_{\max} by

$$\sin K_{\max}(\Delta x) = 0, \text{ which implies: } (\Delta x)K_{\max} = \pm \pi, \text{ or: } \Delta x = \pm \pi / K_{\max}. \quad (12.2.4)$$

This is another example of the celebrated *Heisenberg uncertainty relation* which estimates the product of widths Δx and Δk (or $\Delta p = \hbar \Delta k$) of coordinate and wavevector (or momentum) distributions.

$$\Delta x \cdot |K_{\max}| = \Delta x \cdot \Delta k = \pi \quad \text{or: } \Delta x \cdot \Delta p = \pi \hbar = h/2 \quad (12.2.5)$$

Simply stated: the more accurately the warden determines M 's position or where prisoner M is, the less he knows about M 's momentum or where he's going. Crudely stated: a fat prisoner M mostly sits around like a big couch potato and only sloshes his beer gut like Fig. 12.1.2. A thin prisoner M like Fig. 12.2.2 is a high energy "bundle of nerves" or *wavepacket* which, as we will see next, is about to explode like a bomb!

(b) Wavepacket explodes! (Then revives)

Prisoner M 's svelte figure doesn't last. In an instant he is blown all over his cell as shown in Fig. 12.2.3. M 's one-hundred energy states or ten thousand zero-point energy units ε_1 ($\varepsilon_{100} = 100^2 \varepsilon_1$) go about two miles high if the ε_1 level is a foot off the cell floor. So it's not surprising that M goes off with a bang!

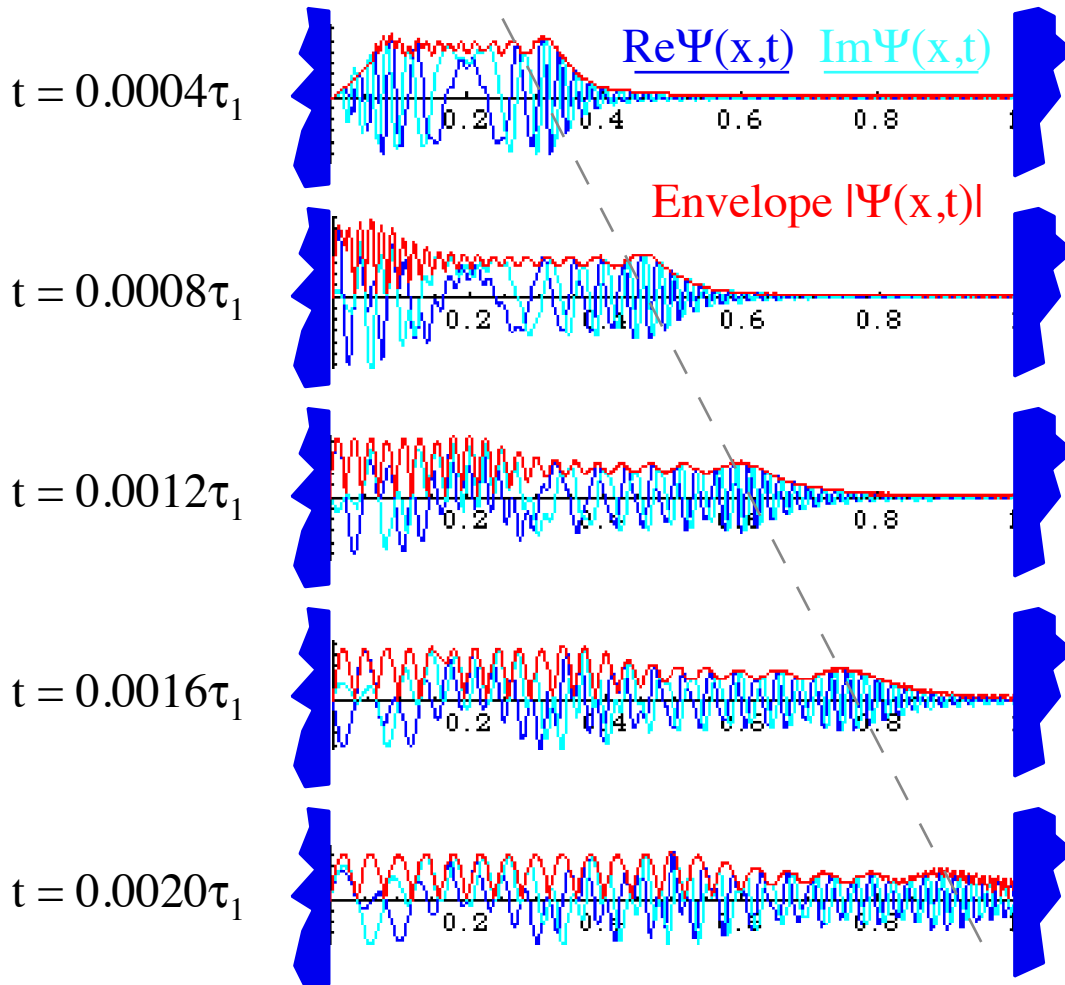


Fig. 12.2.3 Ultra-thin prisoner M exploding. Wavepacket in Fig. 12.2.2 disintegrates.

Time is given in terms of a fundamental unit of time that is the period τ_1 of the slowest phasor belonging to ground or "zero-point" level in Fig. 12.2.2. The *fundamental zero-point period* $\tau_1 = 1/\nu_1$ is

$$\tau_1 = \frac{2\pi}{\omega_1} = \frac{2\pi\hbar}{\varepsilon_1} = \frac{h}{\hbar^2 / 8MW^2} = \frac{8MW^2}{h} \quad (12.2.6)$$

Notice in Fig. 12.2.3 the highest ($n=100$) energy wave which was "last-in" is now "first-out" and makes a group "shock" wave that races across the cell toward the right wall at $x=W$. The speed of that wave is the group velocity or classical particle velocity at the highest energy ε_{100} . The ε_n -level *classical velocity* is

$$V_n = \frac{d\omega_n}{dk} = \frac{1}{\hbar} \frac{d\varepsilon_n}{dk} = \frac{1}{\hbar} \frac{\hbar^2}{2M} \frac{dk^2}{dk} = \frac{\hbar 2k_n}{2M} = \frac{\hbar n\pi}{MW} = \frac{\hbar n}{2MW} \quad (12.2.7)$$

Related to this is the ϵ_n -level classical round trip time $T_n(2W)$ or the time for the "particle" or "shock" wave associated with quantum level ϵ_n to go distance $2W$ back and forth across a width- W -cell.

$$T_n(2W) = \frac{2W}{V_n} = 2W \frac{2mW}{\hbar n} = \frac{4mW^2}{\hbar n} = \frac{1}{2n} \frac{8mW^2}{\hbar} = \frac{\tau_1}{2n} \quad (12.2.8)$$

The time sequence in Fig. 12.2.3 shows the group going a distance of $0.8W$ from $x=0.2W$ to $x=W$ in a time $0.002\tau_1$ or 0.8 of the ϵ_n -level classical one-way trip time $T_n(W)$ for a "particle" to cross the cell once.

$$T_n(W) = T_n(2W) / 2 = \frac{\tau_1}{4n} (= 0.0025 \tau_1 \text{ for } n=100) \quad (12.2.9)$$

The "break-away" wave speeding at V_{100} to the right in Fig. 12.2.3 is due to the "last-in-first-out" k -value $K_{max}=k_{100}$ which shapes the initial wave pattern in Fig. 12.2.2 according to (12.2.3) and gives the break-away "shock" of 100 half-waves per cell width W moving under a smooth group envelope. Its front end reflects from $x=W$ at $t=0.0020\tau_1$ and starts to make a jagged interference envelope. The left break-away wave reflects from $x=0$ immediately, after which its interference envelope stretches like an accordion.

There is something else quite wonderful. According to (12.2.8), the fundamental zero-point period τ_1 is exactly enough time for a "particle" or group wave in the ϵ_n -level to make $2n$ round trips.

$$\tau_1 = 2n T_n(2W) = \frac{8mL^2}{\hbar} \quad (12.2.10)$$

So, in one fundamental period τ_1 the ground ϵ_1 -level particle makes 2 round trips, the first excited ϵ_2 -level particle makes 4 round trips, the next excited ϵ_3 -level particle makes 6 round trips, ..., and the 100-th excited ϵ_{100} -level particle makes 200 round trips, all in exactly the same time τ_1 .

Prisoner M may look like he is exploding randomly, but he is executing a dance whose timing would be the envy of the Moscow Ballet! After 50 round-trips across the stage, M 's wave performs a partial revival as it piles up into an upside down-delta function around $x=0.8W$. Then, after 100 round trips M undergoes a full revival and "unexplodes" into his original spike at $x=0.2W$, as seen in Fig. 12.2.4.

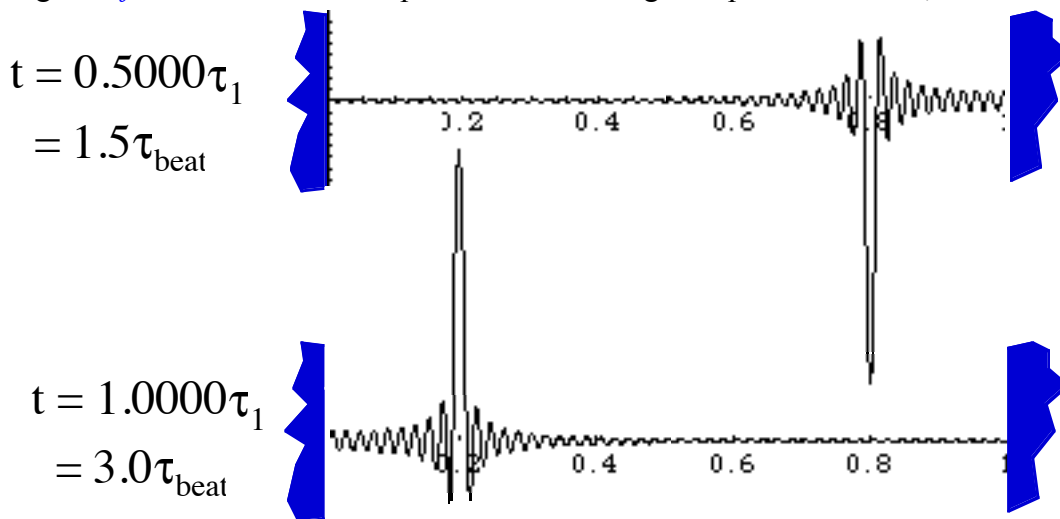


Fig. 12.2.4 Revival for prisoner M . Exploded wavepacket in Fig. 12.2.3 re integrates twice per τ_1 period.

The wave packet of the energized M performs its perfect wavefunction revival in a time that is three times the beat period of the low energy "couch-potato" combination in Fig. 12.1.2. The high energy

revival is of the wavefunction. The low energy combination in Fig. 12.1.2 only revives its probability envelope in $\tau_1/3$. It still takes a full τ_1 to get the wavefunction back to the initial shape.

The full wavefunction revival is a consequence of the integral values of the energy spectrum (12.1.1d) shown in Fig. 12.1.1. As will be shown, it is closely related to the Bohr revivals discussed in Chapter 9. All eigenphases complete an integral number of complete 2π rotations in the time τ_1 it takes the lowest phasor to complete a single 2π rotation. So all phases return to initial settings at exactly τ_1 , as does the envelope or probability distribution made from their sum. More remarkably, the envelope can perform full or partial revivals in even shorter times while performing a kind of "dance of deltas" as in Fig. 12.2.5. Here the initial delta is put in the exact center ($x=0.5W$) instead of at $x=0.2W$, and this gives a beautiful series of q *kaleidoscope deltas* at rational relatively prime time fractions (p/q) of τ_1 . Views at periodic fractional times are called *stroboscopic pictures*. To understand this kaleidoscopic and stroboscopic behavior we review how it happens for Bohr orbitals that also have a quadratic spectrum.

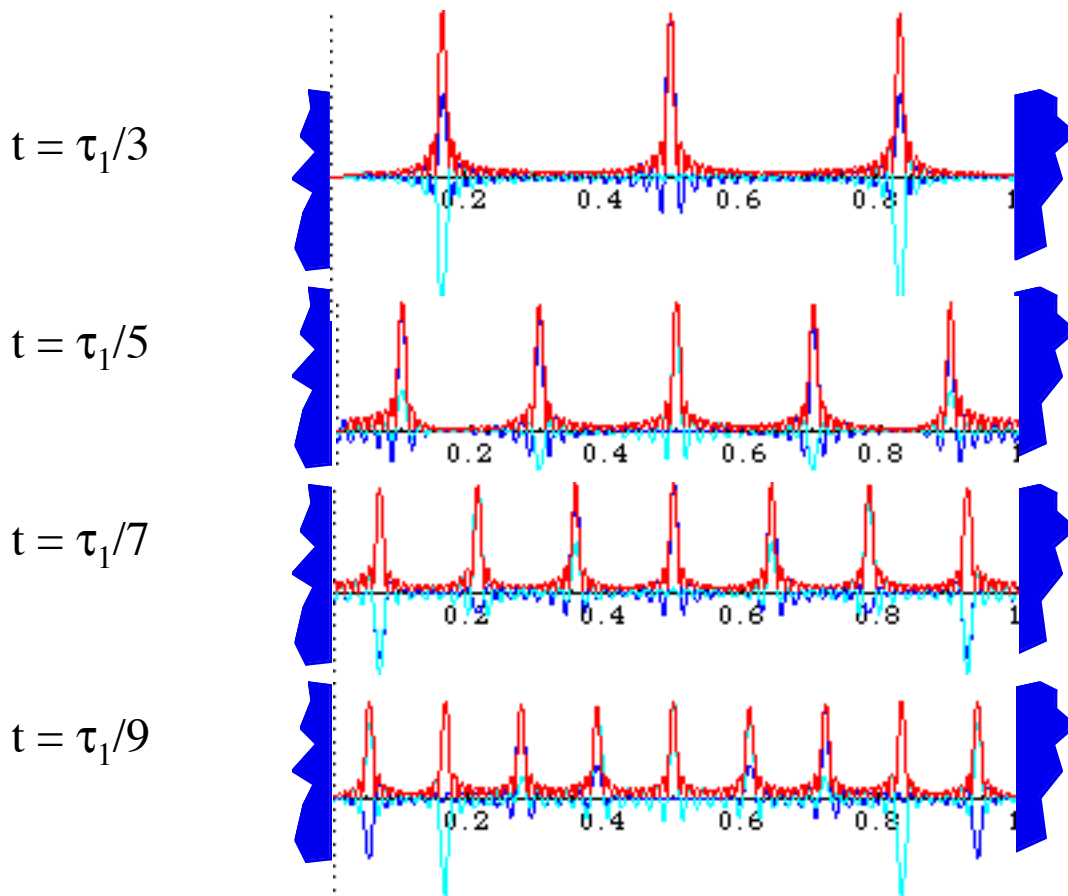


Fig. 12.2.5 The "Dance of the deltas." Mini-Revivals for prisoner M 's wavepacket envelope function.

We shall see that this behavior is closely related to the Bohr-revivals in Fig. 5.6.5 of Ch. 5.

(c) Bohr rotor waves: Relation to square well waves

Now suppose that prisoner M is moved (because of good behavior and his stunning dance moves) from his width- W cell into a less restrictive environment consisting of a circle of circumference $L=2\pi R$

and radius R , that is, to a *Bohr-rotor*. Bohr rotor wavefunctions and levels were first plotted in Fig. 7.1.1. The equation for their energy eigenvalues was first given by (5.6.10) in Chapter 5 and is repeated below.

$$E_m = \hbar\omega_m = \frac{(\hbar k_m)^2}{2M}, \text{ where: } p_m = \hbar k_m = \hbar \frac{2\pi}{L} m \quad (m=0, \pm 1, \pm 2, \dots) \quad (12.2.11a)$$

Notice that, like (12.1.1d), the energy values are also quadratic in the Bohr rotor quantum number m .

$$E_m = \frac{\hbar^2}{2M} k^2 = \frac{2\hbar^2 m^2 \pi^2}{ML^2} = (0, 1^2, 2^2, 3^2, \dots \text{ or } m^2) \frac{h^2}{2ML^2} = \frac{\hbar^2 m^2}{2MR^2} \quad (12.2.11b)$$

In fact the Bohr rotor momentum or wavevector and energy are *the same* for a given quantum number m if the circumference L is twice the linear cell width W , that is $L=2W$ as shown in Fig. 12.2.6.

To better understand the relation between an infinite square well and a Bohr rotor we sketch in Fig. 12.2.6 one example of each system arranged so that their eigensolutions match as closely as possible. The square well in Fig. 12.2.6a has a width W that is exactly half the length $L=2W$ of the Bohr rotor in Fig. 12.2.6b. The sine wave solutions of the Bohr rotor are arranged so that their wavefunctions on the front half-range ($0 < x < W$) or ($0 < \phi < \pi$) are identical to the square-well waves in the same region of Fig. 12.2.6a. The Bohr-rotor cosine waves, including the ($m=0$)-wave, are plotted with dashed lines of Fig. 12.2.6b but are absent from the square well in Fig. 12.2.6a. The remaining Bohr-rotor sine waves are identical in form, momentum, and energy to the infinite square-well sine wave solutions in the front range ($0 < \phi < \pi$) only. Note that the rotor has a zero-quantum state with zero energy and a constant wavefunction $\Psi_0 = A \cos 0x = A$. The fundamental frequency for the Bohr waves is equal to the difference between the first and zero-th levels. This equals the first beat frequency *and* the first frequency eigenvalue, as follows.

$$\omega_{beat} = \omega_1 - \omega_0 = \frac{E_1 - E_0}{\hbar} = \frac{1^2 - 0^2}{\hbar} \frac{h^2}{2ML^2} = 2\pi \frac{h}{2ML^2} = \frac{\hbar}{2MR^2} = \omega_1 \quad (12.2.12)$$

This is the same as the fundamental ω_1 for the linear cell of width $W=L/2$. The fundamental time unit is

$$\tau_1 = \frac{2\pi}{\omega_1} = \frac{2ML^2}{h} = \frac{8MW^2}{h} \quad (12.2.13)$$

The time τ_1 above and in (3.2.25) is enough time for two round trips of total length $4W=2L$ up and down a linear cell, or as we will see, for a rotor to go a distance $2L$ or twice around circumference of length L .

Excited Bohr energy levels are doubly degenerate because there are negative as well as positive values of the m -quantum number in (12.2.1). This means that the full $U(2)$ freedom of choice for standing, moving, and galloping waves exists at each excited level. (The ground $m=0$ level is the one exception. It has only a single constant wave of zero energy and momentum; the penultimate "couch-potato" of the quantum world; asleep on its circular sofa and snoring at zero frequency. The infinite square-well prison allows no such luxury!)

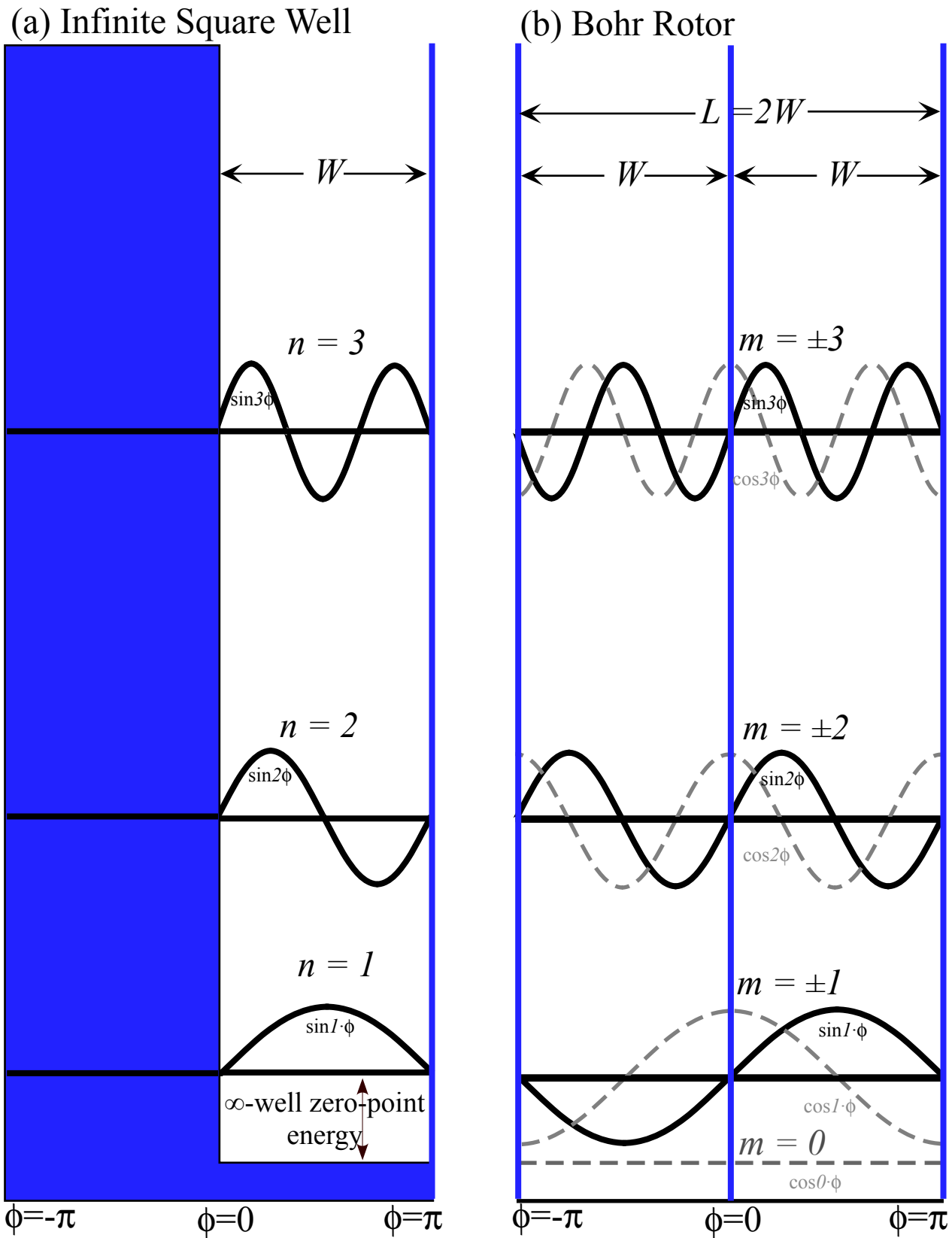


Fig. 12.2.6 Comparison of eigenfunctions for (a) Infinite square well, and (b) Bohr rotor.

All waves in the front range ($0 < x < W$) of the Bohr-rotor system can be made to duplicate exactly what happens to the infinite-square-well in its front range. In order to do this, the waves in the back range ($-W < x < 0$) of the Bohr-rotor (where all infinite-square-well waves vanish) must be perfectly *inverted* copies of the waves in the front range ($\Psi(x \pm W) = -\Psi(x) = \Psi(-x)$) since sine waves are odd to inversion.

Both the rotor and infinite-well have quadratic $\omega_m = \omega_1 m^2$ spectra. To understand infinite-well revivals we first review the less restrictive Bohr system. Complex $e^{im\phi}$ waves are actually simpler than $\sin m\phi$ waves of the well. A delta function of Bohr angle $\phi = 2\pi x/L$ uses ortho-completeness axioms 3 and 4.

$$\psi_{\phi_0}(\phi) = \delta(\phi - \phi_0) = \langle \phi | \phi_0 \rangle = \sum_{n=-\infty}^{\infty} \langle \phi | n \rangle \langle n | \phi_0 \rangle \quad (12.2.14a)$$

This is a "spike" at position $x = x_0 = \phi_0 L/2\pi$. In terms of the Bohr orbital waves, $\delta(\phi - \phi_0)$ becomes

$$\psi_{\phi_0}(\phi) = \delta(\phi - \phi_0) = \sum_{n=-\infty}^{\infty} \frac{e^{in\phi}}{\sqrt{2\pi}} \frac{e^{-in\phi_0}}{\sqrt{2\pi}} = \frac{1}{2\pi} \sum_{n=-\infty}^{\infty} e^{in(\phi - \phi_0)} \quad (12.2.14b)$$

Each amplitude $\langle n | \phi_0 \rangle$ is a preset constant, but eigenfunction $\langle \phi | n \rangle$ or eigenket $|n\rangle$ has eigenfrequency ω_n .

$$|n(t)\rangle = e^{-i\omega_n t} |n(0)\rangle = e^{-i\omega_n t} |n\rangle, \text{ or: } \langle \phi | n(t)\rangle = e^{-i\omega_n t} \langle \phi | n\rangle = e^{i(n\phi - \omega_n t)} \quad (12.2.14c)$$

Level- n has energy $\epsilon_n = \hbar\omega_n$. Inserting this into (12.2.14a) gives the time behavior of a delta wave.

$$\psi_{\phi_0}(\phi, t) = \sum_{n=-\infty}^{\infty} \frac{e^{i(n\phi - \omega_n t)}}{\sqrt{2\pi}} \frac{e^{-in\phi_0}}{\sqrt{2\pi}} = \frac{1}{2\pi} \sum_{n=-\infty}^{\infty} e^{i(n\phi - n\phi_0 - n^2\omega_1 t)} \quad (12.2.15a)$$

NOTE: only the state factor $\langle \phi | n \rangle$ gets the Planck time-phase factor $e^{-i\omega_n t} = e^{-in^2\omega_1 t}$ while the coefficient $\langle n | \phi_0 \rangle$ is fixed by the initial x_0 -position state's overlap with the eigenstate $|n\rangle$ at initial time $t=0$.

It is impossible excite an infinite number of levels. (Even a hundred is costly.) We may arbitrarily cut off the sum at some value $n = N_{CUT}$ (such as $N_{CUT} = 30$ in Fig. 12.2.1), or we may multiply the terms by a *weighting* or *windowing function* $W(n)$ that vanishes for high n . Let us consider some possibilities.

(1) "Boxcar windows": Wavepackets that go "Bang!"

Consider first a square window or "Boxcar" weight function. It is the same as a simple cut-off.

$$\psi_{\phi_0}(\phi, t) = \sum_{n=-\infty}^{\infty} W(n) e^{i(n\phi - n\phi_0 - n^2\omega_1 t)} \quad \text{where: } W(n) = \begin{cases} A & \text{if: } |n| \leq N_{CUT} \\ 0 & \text{if: } |n| > N_{CUT} \end{cases} \quad (12.2.15b)$$

A sharp cut-off by a boxcar window produces a ringing $\sin x/x$ wavefunction as described in (12.2.3).

Such a wave goes off with a "bang" like the one shown earlier in Fig. 12.2.3. Fig. 12.2.7 shows the magnitude $|\Psi(x, t)|$ of a Bohr-rotor equivalent wave with $N_{CUT} = 16$ plotted using shading at each space-point x (horizontal axis) and time t (vertical axis). The white regions correspond to nodal regions in which the destructive interference of the 16 excited waves gives probability that is small or zero. Interference patterns begin to develop after the left-and-right-moving shock fronts meet each other at the opposite side ($\phi = \pm\pi$) of the Bohr-rotor ring space. The group velocity of the fastest ($m = N_{CUT}$) waves is for ($m \gg 1$).

$$V_{group}(m) = \frac{d\omega_m}{dk_m} = \frac{d\omega_m}{dm} \frac{dm}{dk_m} = \frac{\hbar}{2M} \frac{d}{dm} \left(\frac{2\pi m}{L} \right)^2 \frac{L}{2\pi} = \frac{\hbar 2\pi}{2ML} 2m = \frac{L}{\tau_1} 2N_{CUT} \quad (12.2.16)$$

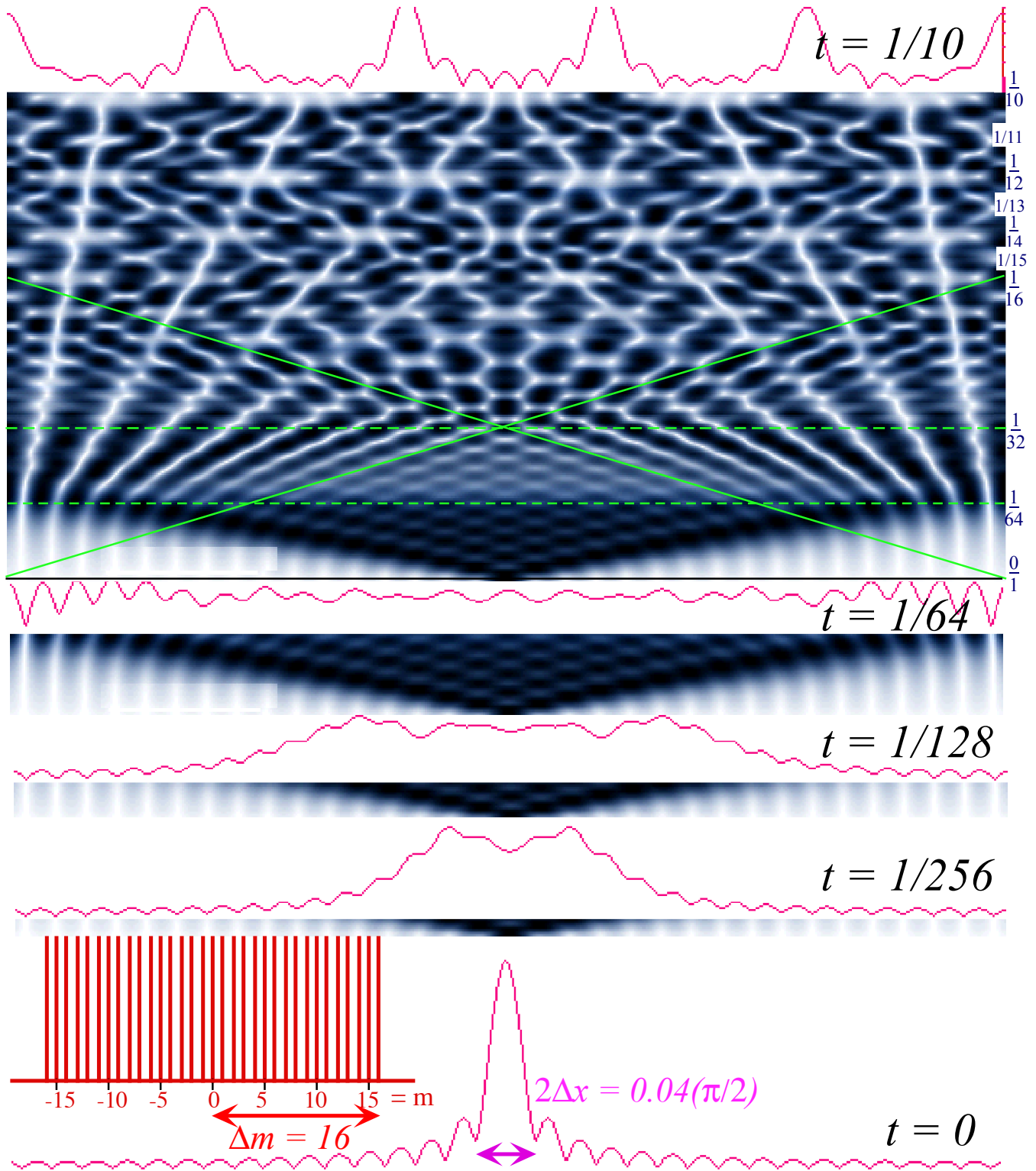


Fig. 12.2.7 (a) Initial evolution for $\Delta x = 0.03$ and $\Delta m = 16$ "boxcar" wavepacket for Bohr rotor.

The maximum V_{group} is 32 Bohr L -laps per Bohr time units τ_I , or 1/2 circumference L in $1/64$ -th τ_I . The interference starts in Fig. 12.2.7 at time fraction $1/64$ just before $t/\tau_I = 1/50$. Then a series of fractional revivals are seen starting at time fraction $1/32$ which is enough time for the fastest waves to make a full circle. The $1/32$ revival has 16 zeros (or peaks), the $1/16$ revival has 8 zeros (or peaks), the $1/14$ revival

has 7 zeros (or peaks), the $1/12$ revival has 6 zeros (or peaks), and the $1/10$ revival has 5 zeros and peaks as shown clearly at the top of Fig. 12.2.7. Meanwhile, the odd-fraction revivals in between such as the $1/13$ revival has 13 zeros (or peaks) and the $1/11$ revival has 11 zeros (or peaks), but these are more difficult to spot due to ringing side-bands around each peak. Now we tame wavepacket sidebands as was done for optical wave pulses in equation (5.3.6) of Chapter 5.

(2) "Gaussian windows": Wavepackets that go "Poof!"

We tame the "last-in-first-out" dominance of the $m=N_{CUT}$ component by using a smooth window function so all m -components have $m\pm 1$ -neighbors with comparable amplitudes. Then they destructively interfere and attenuate each other almost everywhere, and no single Fourier component can stick out like a sore thumb. The most famously smooth window function is the *Gaussian window function* $W_G(m, \Delta m)$.

$$W_G(m) = e^{-[(m-\bar{m})/\Delta m]^2} \quad (12.2.7a)$$

The resulting wave packet has the following space-time dependence.

$$\Psi(\phi, t) = \langle \phi, t | \Psi \rangle = \sum_{m=-\infty}^{\infty} W_G(m) \langle \phi, t | m \rangle \langle m | \phi_0 \rangle = \frac{1}{2\pi} \sum_{m=-\infty}^{\infty} W_G(m) e^{i(m\phi - m^2\omega_1 t)} e^{-im\phi_0} \quad (12.2.7b)$$

The resulting initial ($t=0$) distribution for centered momentum ($\bar{m}=0$) and mass ($\phi_0=0$) is the following.

$$\Psi(\phi, 0) = \langle \phi, 0 | \Psi \rangle = \frac{1}{2\pi} \sum_{m=-\infty}^{\infty} e^{-m^2/\Delta m^2} e^{im\phi} \quad (12.2.7c)$$

Completing the square of the exponent provides a simpler ϕ -angle wavefunction.

$$\Psi(\phi, 0) = \frac{1}{2\pi} \sum_{m=-\infty}^{\infty} e^{-\left(\frac{m}{\Delta m} - i\frac{\Delta m}{2}\phi\right)^2 - \left(\frac{\Delta m}{2}\phi\right)^2} = \frac{A(\Delta m, \phi)}{2\pi} e^{-\left(\frac{\Delta m}{2}\phi\right)^2} \quad (12.2.7d)$$

Only the lower- m terms with $m < \Delta m$ in the sum $A(\Delta m, \phi)$ have significant $e^{-(m/\Delta m)^2}$ values, but for larger Δm the number of significant terms grows until it approaches a Gaussian integral which is a constant.

$$A(\Delta m, \phi) = \sum_{m=-\infty}^{\infty} e^{-\left(\frac{m}{\Delta m} - i\frac{\Delta m}{2}\phi\right)^2} \xrightarrow{\Delta m \gg 1} \int_{-\infty}^{\infty} dk e^{-\left(\frac{k}{\Delta m}\right)^2} = \sqrt{\pi} \Delta m \quad (12.2.7e)$$

The remaining variable factor $e^{-(\Delta m \phi/2)^2}$ is a Gaussian function of angle ϕ or position x . It is remarkable that the Fourier transform of a Gaussian $e^{-(m/\Delta m)^2}$ is just another Gaussian $e^{-(\phi/\Delta\phi)^2}$. The Gaussian is an eigenvector of the Fourier C_n transformation matrix. (More about this later.) Gaussian function $e^{-(\phi/\Delta\phi)^2}$ has a width parameter $\Delta\phi$. It is the angular wave packet *Half-Width-at-(1/e)-th-Maximum* ($HWeM_\phi = \Delta\phi$). That is, at $\phi = \pm\Delta\phi$, function $e^{-(\phi/\Delta\phi)^2}$ becomes e^{-1} . Also for the Gaussian $e^{-(m/\Delta m)^2}$ the parameter Δm is the *HWeM* of the *momentum* distribution. ($HWeM_m = \Delta m$) Equating $e^{-(\phi/\Delta\phi)^2}$ to $e^{-(\Delta m \phi/2)^2}$ in (12.2.7d) relates half-width $HWeM_m = \Delta m = L\Delta k/2\pi$ of momentum m or wavevector k to the half width $HWeM_\phi = \Delta\phi = 2\pi\Delta x/L$ of angle ϕ or position x . (This re-derives uncertainty relations (5.3.7) and (9.3.15).)

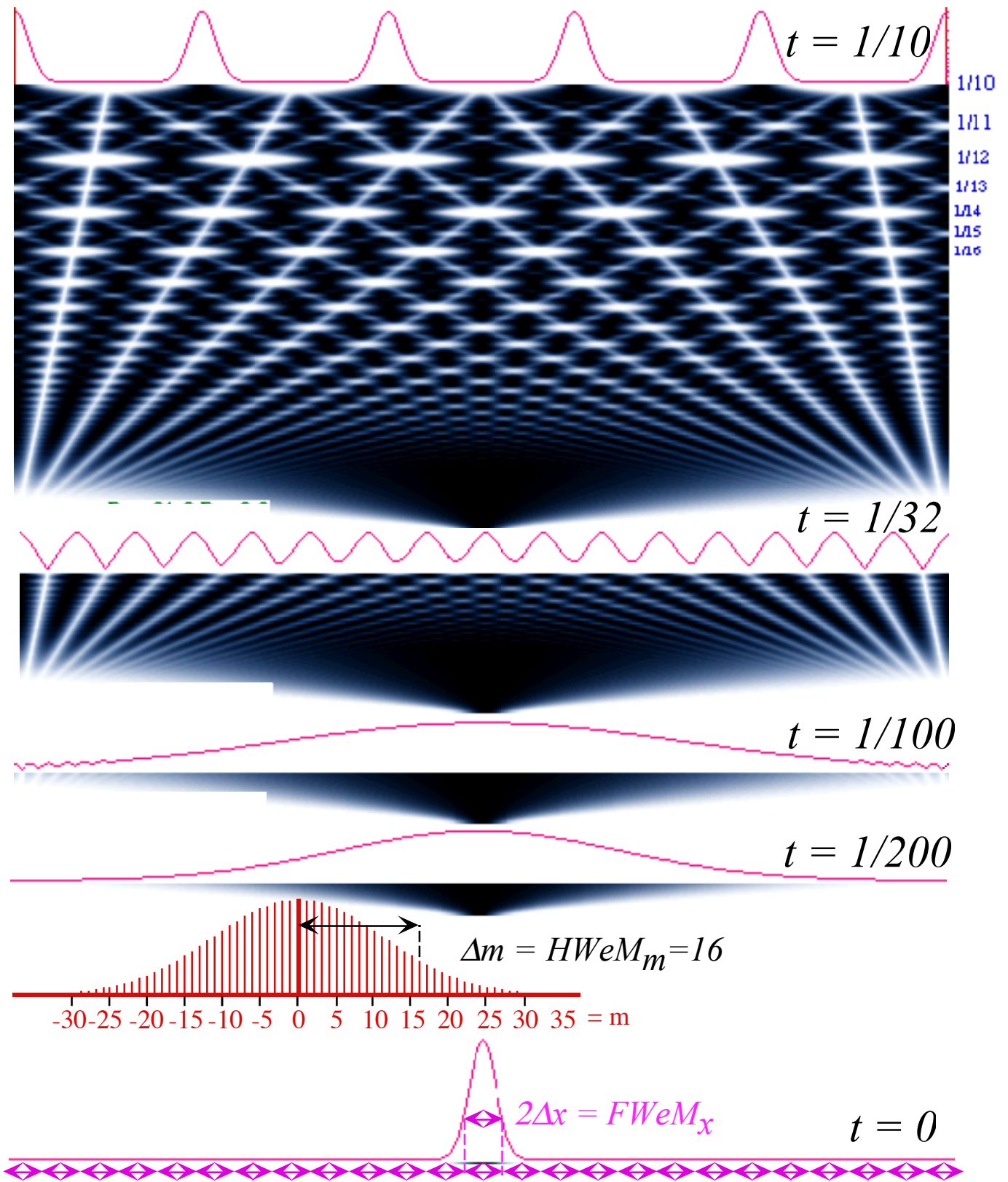


Fig. 12.2.8 (a) Initial evolution for $2\Delta x = 0.04$ and $\Delta m = 16$ "Gaussian" wavepacket for Bohr rotor.

$$\Delta m = 2/\Delta\phi = 1/(\pi\Delta) \quad \text{or:} \quad \Delta\phi \cdot \Delta m = 2 = \Delta x \cdot \Delta k \quad (12.2.8)$$

This is a *Gaussian uncertainty relation* to be compared with the uncertainty product $\Delta x \cdot \Delta k = \pi$ of a "box-car" window in (12.2.5). The Gaussian seems "less uncertain" than the box-car by a factor $2/\pi$, but one has to be careful when being so precise about imprecision! It's a little like comparing apples and oranges.

Often we use full-widths instead of half-widths. Fig. 12.2.8 shows *Full-Width-at-(1/e)-th-Maximum (FWeM=2HWeM)*, or twice the half-width of both the position and momentum Gaussian.

$$FWeM_\phi = 2\Delta\phi, \quad FWeM_m = 2\Delta m \quad (12.2.9)$$

Given momentum quanta excitation of $\Delta m = m_{HWeM} = 16$ or a full momentum width of $FWeM_m = 2\Delta m = 32$ we use (12.2.8) to derive the angular full width $FWeM_\phi$ in units of 2π .

$$FWeM_\phi = 2\Delta\phi = \frac{4}{HWeM_m} = \frac{8}{FWeM_m} = \frac{8}{32} = \frac{1}{8\pi} 2\pi \quad (12.2.10)$$

This predicts $8\pi = 25.1$ packet full-widths fit in the full 2π circle. This is shown at the bottom of Fig. 12.2.8 for $2\Delta m = 32$. Each packet's angular half-width $HWeM_\phi = \Delta\phi = 2\pi\Delta$ is only $\Delta = 2\%$ of a full 2π .

The subsequent evolution of the Gaussian packet in Fig. 12.2.8 is also to be contrasted with that of the box-car packet in Fig. 12.2.7. The box-car wave explodes with a ringing "Bang," but the Gaussian wave gently expands with little or no wrinkling or change of shape until its two oppositely moving "feet" meet at $\phi = \pm\pi$ on the other side of the ring. The m -component waves with $\Delta m = m_{HWeM} = 16$ have group velocity $2m = 32$ by (12.2.16). So they circle the ring in $(1/32)\tau_1$ or go half-way in $(1/64)\tau_1$ at which time the two speeding "feet" first meet each other.

But, the $m = 16$ -component waves aren't the fastest "feet" in this distribution. The m -distribution in the lower left hand part of Fig. 12.2.8 shows higher $m = 17, 18, 19, \dots$ have amplitudes that are less than $(1/e)$ but significant all the way up to $m = 30$ or 31 . Each of these "feet" will meet at $\phi = \pm\pi$ earlier than $(1/64)\tau_1$. So, interference wrinkles due to $m = \dots, 25, 26, 27, \dots$ are visible in Fig. 12.2.8 already at $(1/100)\tau_1$. Finally, by $(1/32)\tau_1$ the $m = 16$ components have made a complete circle so their "feet" meet at origin ($\phi = \pm 2\pi$), and they are staging a fractional revival as a wave having 16 miniature peaks.

By $(1/16)\tau_1$ (near top of Fig. 12.2.8) there is a revival in a wave having 8 miniature Gaussian peaks with 8 long flat nodal regions in between the peaks. As we will see, this is due mainly to the $m = \pm 8$ "feet" and the $m = \pm 16$ "feet" combining. Shortly afterwards, at $(1/15)\tau_1$ there is a revival in a wave having 15 miniature Gaussian peaks followed closely at $(1/14)\tau_1$ by a wave having 7 miniature Gaussian peaks, and so on until the figure stops at $(1/10)\tau_1$ with a 5 peak revival plotted at the top.

The space-time plot of the Gaussian packet in Fig. 12.2.8 has many of the same patterns that are seen in the boxcar packet in Fig. 12.2.7. However, the Gaussian patterns have a clarity and linearity that is obscured in the boxcar patterns. An explanation based upon C_N phases giving the patterns of lines in Fig. 12.2.8 goes to the heart of quantum symmetry and dynamics. This was given in Chapter 9.

(d) Brief history of revival structure and dynamics

Quantum revivals like classical chaos and fractals are a class of phenomena that many saw but few observed. Each has required modern computer simulations and graphics to make a convincing case for their existence. Each of these phenomena is important because they illuminate inadequacies of Newtonian calculus or continuum analysis and favor discrete algebraic-number-theoretic theory.

The term *revival* is a coinage by Joe Eberly to describe unexpected rephasing that appeared in 1976 computer studies of atom-quantum field theory. For the next two decades there were sporadic reports of revival phenomena including *fractional revivals* in quantum treatments of much simpler systems such as rotors and anharmonic vibrators or Rydberg orbitals. The first explanations in 1989 of fractional revival phenomena involved a particle in an infinite square well ("particle-in-a-box"). Finally, in 1996 and 1997, Berry, Schleich and others used the square well simulations to plot "quantum fractal" landscapes and "quantum carpets" which clearly showed that revivals are a phenomena that is begging to be fully understood.

We have given two ways to understand the phenomena. The first uses phase and group velocity of wave zeros and the Farey arithmetic analysis of fractal circle maps in Section 9.3. The second uses cyclic (C_N) group theory and discrete Fourier analysis of Section 9.4. The latter elucidates fractal revival structure while the former illuminates quantum phase behavior. Together they show how wave symmetry and fractal wave behavior are two sides of the same coin.

Now we consider some of the features that are peculiar to the infinite square well.

12.3 Infinite Well Dynamics vs. Bohr Waves

The infinite square-well is a subset of the Bohr rotor system. As shown in Fig. 12.2.6, the square well width W takes up the front half ($0 < \phi < \pi$) or ($0 < x < W$) of the Bohr ring whose circumference of $L=2W$ and angular range of 2π ($-\pi < \phi < \pi$) is twice that of the well. The back half of the Bohr ring, where angle ϕ is negative ($-\pi < \phi < 0$), is an impenetrable region for the square-well.

The Bohr system has energy-degenerate ($E_m = E_l (\pm m)^2$) sine and cosine wave eigenstates $\sin(m\phi)$ and $\cos(m\phi)$, where a quantum number $m=0, 1, 2, 3, \dots$ of wavelengths must fit in one Bohr lap length L . In contrast, the square-well can only keep the sine standing waves for $m=1, 2, 3, \dots$ from the Bohr set. But, the square-well energy spectrum is the same except it is no longer degenerate. Also, the E_0 -level is missing. The square-well system gets to keep only the odd or antisymmetric ($-$)-states which flip their sign if the angle ϕ is reversed. ($\phi \rightarrow -\phi$) These are the sine standing waves from the Bohr set, excluding $m=0$.

$$\sin(-m\phi) = -\sin(m\phi) \tag{12.3.1}$$

For the square well, all waves are pinned to zero at origin ($\phi=0$) and at the other side of the well ($\phi=\pi$). Beyond, those points lies the impenetrable negative- ϕ region where all square well waves must vanish.

$$\Psi_m^{well}(\phi) = 0 \text{ for } \phi < 0. \tag{12.3.2}$$

This zeroing by (12.3.2) seems inconsistent with anti-symmetry conditions (12.3.1). To sort this out, one might need another lesson in Schrodinger wave mechanics.

(a) The Bohr image-wave

It turns out that the Bohr system will reproduce the dynamics of the square-well system in the well region (postive ϕ or x between 0 and $W=L/2$) if we use only its sine wave states that satisfy the anti-symmetry condition (12.3.1). If the two systems are using the same waves and the same spectrum, that is, the same eigenvalues and eigenfunctions, then they must have the same dynamics wherever eigenwaves and spectra are the same.

Still it seems inconsistent that square-well has its wave suppressed in the negative- ϕ region, while the Bohr system is running a negative *image wave* in that region in order “fake” the dynamics in the well. Will not the image wave “leak” out of the negative region and spoil the Bohr’s reproduction in the well?

The buck stops here!

To understand image waves we must take symmetry conditions and associated boundary conditions seriously. Antisymmetry about $\phi=0$ implies the wave is zero at $\phi=0$, that is, $\Psi = -\Psi$ implies that $\Psi=0$. And, a wave zero at even one point cannot “leak” or transmit anything through that point. The buck stops there! Any energy or wave action that is in the well region stays there and the same applies to the nether region.

Perhaps, the coupled pendulum analogy will make this clear. If you weld even one pendulum so it cannot move, then you create an impenetrable wall between the regions on either side. Now one side may “party-on” as loud as they want, and the occupants on the other side will never hear a peep!

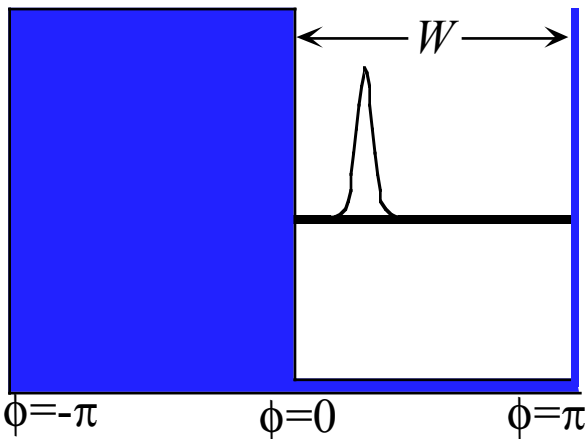
This applies to standard 1D-Schrodinger wave dynamics which is analogous to waves in pendulums coupled only to nearest neighbors through the S -amplitude or effective mass coefficient in (11.5.6). It does not apply to hyper-Schrodinger dynamics which has additional next-nearest coefficients

T, U, \dots as sketched in Fig. 11.3.6. Such hyper-Schrodinger equations have x -derivatives of fourth or higher order which might allow waves to “hop” over one “dead-point” and bypass a single zero boundary point. Blocking hyper-waves requires a zero of the wave *and* its first derivative *and* its second derivative, and so forth, depending on the order of the coupling.

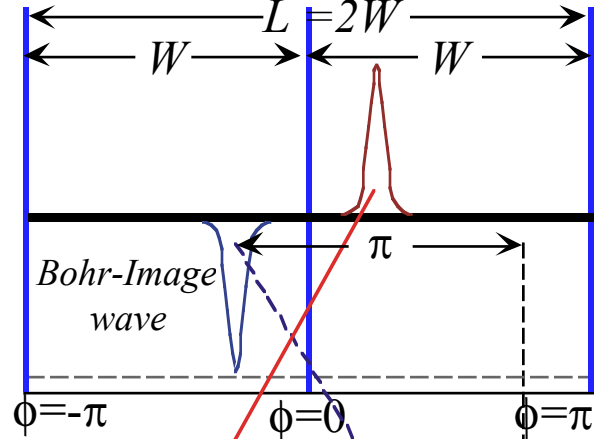
(b) Flipped revivals

Well-wave pulses include *flipped revivals* such as shown in Fig. 12.2.4. The example shown there is the half-time revival of the Bohr image wave as sketched below in Fig. 12.3.1(c).

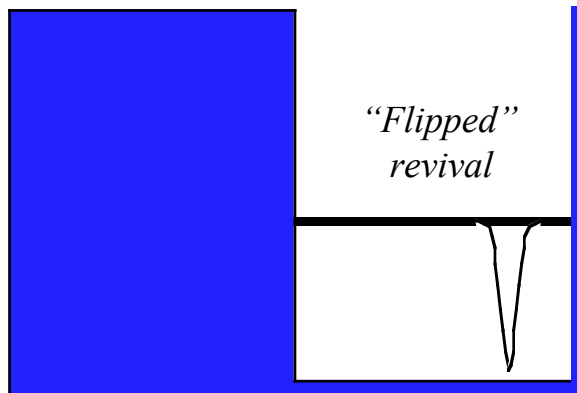
(a) Infinite Square Well at $t=0$



(b) Bohr Rotor at $t=0$



(c) Half-time revival at $t=\tau/2$



(d) Half-time revival at $t=\tau/2$

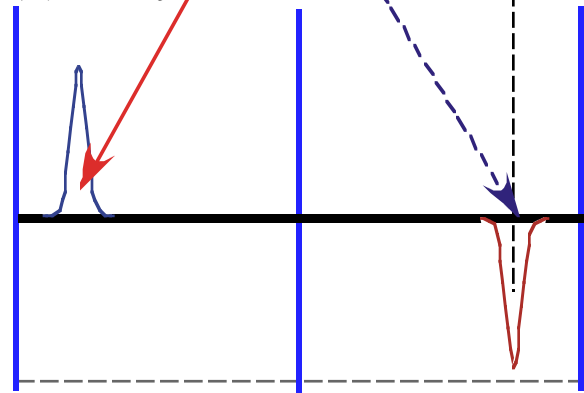


Fig. 12.3.1 Flipped revival is reflection of Bohr-image wave. Real part $Re\Psi$ is being plotted.

The Bohr rotor uses its sine-waves in (b) to copy a wave-packet (a) in the square-well region between $\phi=0$ and $\phi=\pi$. This gives rise to an image wave in (b) on the other side of the origin. Creation of a Bohr packet that only existed on the right hand (positive) side would require the use of its sines *and* cosines, the latter of which are not available in the square-well’s set of eigenfunctions. At half-time each of the Bohr wavepackets revive on the opposite side of the ring at an angle π away from whence they started in Fig. 12.3.1(d). The square well sees a Bohr image’s revival. It’s flipped in sign.

Can this be seen as a passage of the wavepackets through the supposedly impenetrable wall that has been set up at origin? No! That is a Newtonian idea. Either wave motion would not change if the two sides were put a mile apart. Prisoner M has not escaped from either half-cell. He is a Schrodinger cat!

(b) Cloned revivals

A phenomenon related to both Bohr and square-well revivals is that of wave *profile cloning*. We shall see that cloning wavefunctions is problematic; it would violate uncertainty relations for one thing. But, a fractional revival such as the $1/3$ -time revival at the top of Fig. 12.2.5 has a *probability* distribution $\Psi^*\Psi$ or wave *magnitude* $|\Psi|$ that is copied quite perfectly, three times in a row. The phases inside each wavepacket are clearly different from the original and each other. Revival peak phases are precisely given by the C_3 revival phases in the $(t=1/3)$ -row of the Fig. 9.4.2(c). Examples are detailed in Fig. 12.3.2 below.

$$(\text{left peak phase} = -30^\circ, \text{main peak phase} = 90^\circ, \text{right peak phase} = -30^\circ) \quad (12.3.3)$$

All this makes sense if you imagine a wave line is made up of a set of C_N -symmetric coupled pendulums where N is an enormous with lots of factors. We might “pluck” just one of these pendulums to make an “almost-Dirac-delta” function which clones itself. More likely, we pluck out an arbitrary pulse shape to make a combination of several “almost-Diracs” which then spawn cloned copies according to a schedule given in a C_N -revival table like Figures 9.4.2 and 9.5.3.

The important thing to remember is that each of the N starting points, that is, each of the N “quantum dots” is equivalent. Revivals starting from one point look the same as they would starting off down the line somewhere; the whole schedule just shifts accordingly. As a result, low order revivals of narrow packets are usually cloned quite perfectly. The clones are not so perfect if one of them overlaps with a neighbor as will happen if the initial packet is too wide or the revival has too many copies.

Another thing to remember is that the real line is composed of all possible fractions m/N and so a wavepacket function is plucking not just many pendulums but many overlapping sets of many pendulums. The resulting cacophony washes out many of the finer interference effects and helps to make the profiles better copies of the original. But, as seen in the details of Fig. 12.3.2, the phases inside the profiles vary from point to point and from clone to clone in a complicated way.

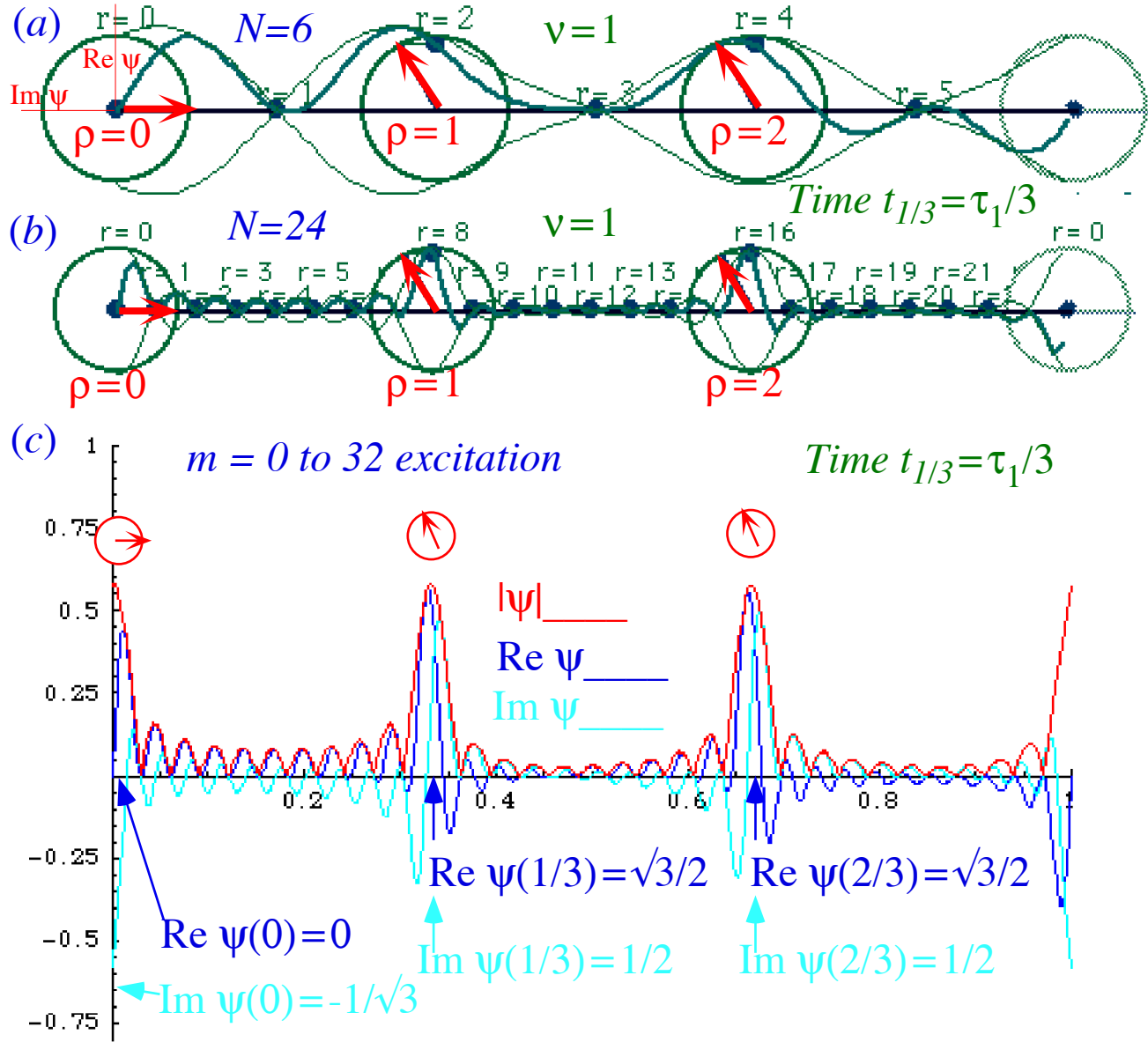


Fig. 12.3.2 Examples of a 1/3-period revival for excitation numbers (a) $N=6$, (b) $N=24$, and (c) $N=32$.

Problems for Chapter 12.

Zero-point-zero

12.1.1 The zero point energy (ZPE) of the infinite well is a feature not seen in the Bohr spectrum. Or is it? Discuss.

- If the cell width is increased how does the ZPE behave?
- What would the ZPE be for a cell of two equal dimensions? (square) ..three dimensions? (cube)

Cell pacing 9-to-5

12.1.2 It was noted after Eq. (3.3.25) that the maximum dipole "pacing" amplitude $\langle \mathbf{x} \rangle$ ($\langle e\mathbf{x} \rangle$ is called an *electric dipole* or *EI* moment) of M was only 18% of cell width W for a 50-50 excitation of the lowest two levels $m=1$ and $m=2$. Does this increase if we excite to higher levels? Consider the following cases. (Caution! Some are trick questions.) Find maximum or *saturated EI* moment $\langle e\mathbf{x} \rangle / W$ for :

- 50-50 excitation of levels $m=1$ and $m=5$.
- 50-50 excitation of levels $m=1$ and $m=10$.
- 50-50 excitation of levels $m=4$ and $m=5$.
- 50-50 excitation of levels $m=4$ and $m=10$.
- 50-50 excitation of levels $m=9$ and $m=10$.
- 50-50 excitation of levels $m=9$ and $m=5$.

Current events

12.1.3. Consider the momentum or *current dipole* (or *MI*) operator \mathbf{p} and its expectation values $\langle \mathbf{p} \rangle$.

(This is related to the *magnetic MI* dipole operator $(e/M) \mathbf{p}$.)

- Derive a formula for the $\langle m|\mathbf{p}|n \rangle$ matrix elements in the square well eigenbasis.
- Derive the time dependent expectation $\langle \mathbf{p}(t) \rangle$ for a 50-50 excitation of levels $m=1$ and $m=2$.
Compare time plot of $\langle \mathbf{p}(t) \rangle$ with $\langle \mathbf{x}(t) \rangle$ derived in Sec. 12.2. Discuss.

More poles

12.1.4. Consider the *electric quadrupole* (or *E2*) operator $e\mathbf{x}^2$ and its expectation values $\langle e\mathbf{x}^2 \rangle$.

(This is related to the *2-photon transition* operator $e^2\mathbf{x}^2$.)

- Derive a formula for the $\langle m|\mathbf{x}^2|n \rangle$ matrix elements in the square well eigenbasis. (You might use the fact that $\langle m|\mathbf{x}^2|n \rangle = \sum_r \langle m|\mathbf{x}|r \rangle \langle r|\mathbf{x}|n \rangle$ to check your results.)
- Find maximum expected *E2*-moment $\langle e\mathbf{x}^2 \rangle$ for 50-50 excitation of levels $m=1$ and $m=2$.
- Find maximum expected *E2*-moment $\langle e\mathbf{x}^2 \rangle$ for 50-50 excitation of levels $m=1$ and $m=3$.

Uncertain uncertainty

12.2.1. Compare the "boxcar-window" spectral uncertainty relation (12.2.5) for a boxcar wave Ψ_{Box} to (9.3.15) for a

Gaussian-window wave Ψ_{Gauss} . Consider the definition of standard deviation $\Delta q = \sqrt{[q - \bar{q}]^2}$ where:

$$\overline{f(q)} = \langle \Psi | f(\mathbf{q}) | \Psi \rangle.$$

- Derive Δx and Δk for each wave. (Give numerical examples if analytic result is problematic.)
- Which is more certain? Discuss.

First-in last-out

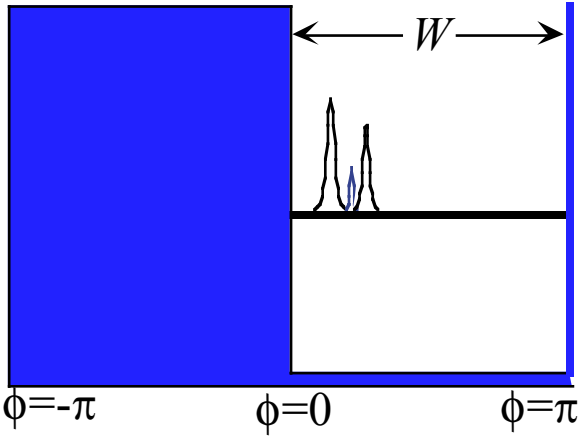
12.2.2. The "last-in-first-out" principle involved the k -integral (12.2.3) from 0 to K_{max} .

- Does a "first-in-last-out" principle apply for a *lower* limit: K_{min} to K_{max} ? Discuss effect on initial pulse shape.
- Discuss how a lower limit K_{min} affects the uncertainty Δx of initial pulse.
- Discuss how a lower limit K_{min} affects the waveforms that emerge from the initial wave

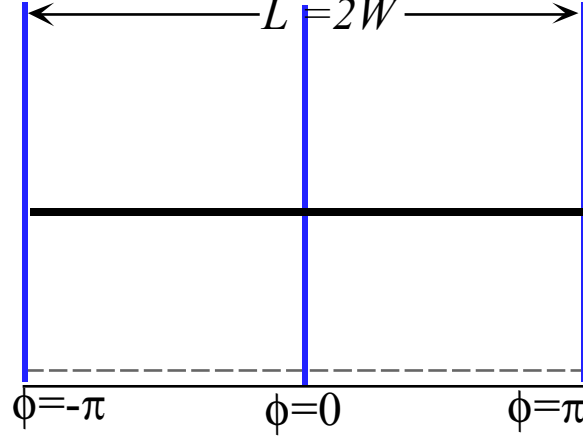
Cloning around

12.3.1. Suppose the initial wave $|\Psi(0)|$ and $\text{Re}\Psi(0)$ are the same at $t=0$. ($\text{Im}\Psi(0)$ is identically zero.) Use the C_2 and C_3 revival schedules in Fig. 9.4.1-2 to sketch $|\Psi(t)|$, $\text{Im}\Psi(t)$, and $\text{Re}\Psi(t)$ in each of the boxes below.

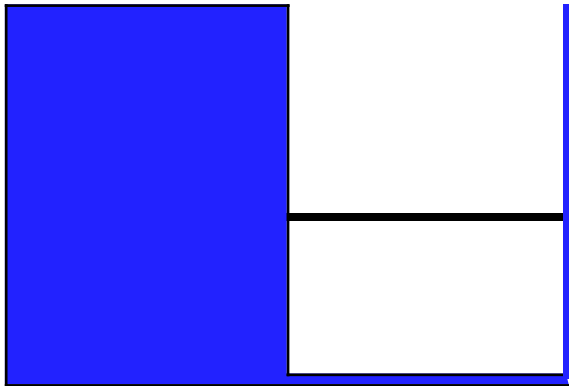
(a) *Infinite Square Well at $t=0$*



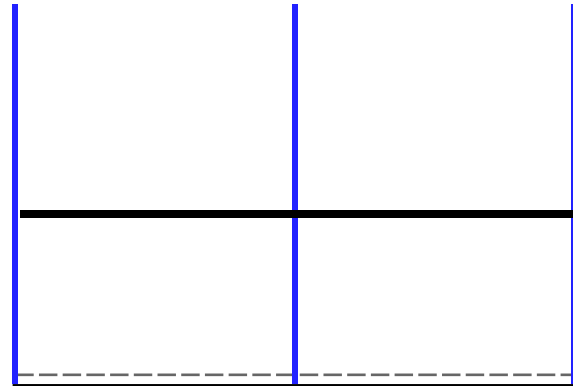
(b) *Bohr Rotor at $t=0$*



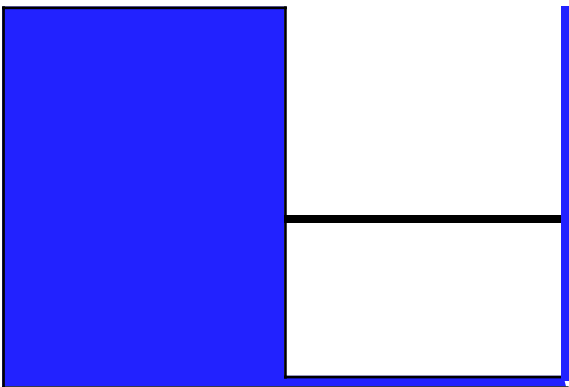
(c) *Half-time revival at $t=\tau/2$*



(d) *Half-time revival at $t=\tau/2$*

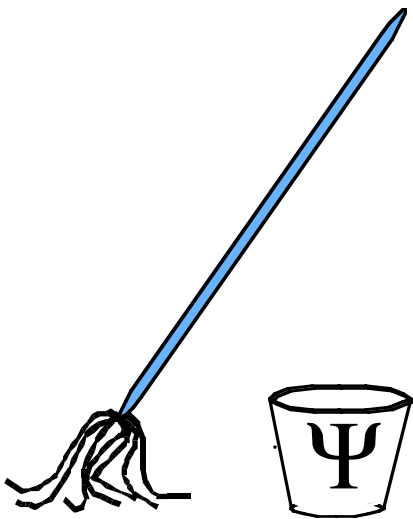


(c) *1/3-time revival at $t=\tau/3$*



(d) *1/3-time revival at $t=\tau/3$*





QM for AMOP

Chapter 13

Step Potential Barriers and Wells

W. G. Harter

The preceding Chapter 12 dealt with the infinitely deep potential well and quantum life in a mythical maximum-security prison. This Chapter 13 deals with less extreme incarceration which have finite walls and wells not altogether unlike those which are designed to house postmodern CEO's. Most of the potential structures described herein are not so escape-proof but have very sharp edges that strongly discourage absenteeism. Also, comings and goings are tracked closely by both C-matrices (which resemble Lorentz matrices) and S-matrices (which resemble rotation matrices). So our guests may be able to run, but they can't hide!

CHAPTER 13. STEP POTENTIAL BARRIERS AND WELLS1

13.1 Waves and Potential Barriers: Crossing Matrices1

- (a) Single boundary potential barrier: C-matrix analysis2
 - (1) Probability current conservation6
 - (2) Momentum vs. frequency or energy normalization7
- (b) Two boundary potential barriers8
 - Perfect transmission Case 1: Symmetric potential ($k = k'$)10
 - Perfect transmission Case 2: Geometric impedance matching ($k' = \sqrt{k k''}$)12
 - The "Stairway-to-Heaven"13
 - Units of Length, Energy and Frequency: meV to EeV 15

13.2 Square wells: bound states vs. free state resonance17

- (a) Ramsauer-Townsend resonances ($E > 0$)21
 - Nearly-grazing states ($E \sim 0$)22
- (b) Bound state quantization ($E < 0$): The sine-line solution22
 - Continuum meets "discreteum"25

13.3 S-Matrix approach to free state resonance dynamics26

- (a) Relating S-Matrix and C-matrix27
- (b) S-Matrix and C-matrix for elementary barrier: $U(2)$ Formulation28
- (c) S-Matrix eigensolutions: Eigenchannels29
- (d) $U(2)$ and $R(3)$ pictures of barrier wavelstates31
- (e) Linear combinations of barrier wavelstates34
 - Remote boundary S-waves: "Sewing" waves together35
- (f) Crossing and Scattering-matrices for square well and hump38
 - Resonance strength, variation and lifetime41

Problems for Chapter 13.43

REVIEW TOPICS & FORMULAS FOR UNIT 446

Chapter 13. Step Potential Barriers and Wells

13.1 Waves and Potential Barriers: Crossing Matrices

Quantum waves behave in strange ways when you change the rules on them. You can make them go faster or slower by putting bumps, barriers or valleys along their paths. The difference between total energy E and potential energy $V(x)$ at each point determines how fast a quantum wave goes or if it goes at all. This follows our discussion of Fig. 11.5.1 to 11.5.3 and the pendulum analogy in Fig. 11.5.4.

The first task in the analysis of a given potential is to find the Schrodinger eigensolutions or stationary states. A stationary state is one which has only a single frequency ω or energy $E = \hbar\omega$. Its wave function oscillates at that single frequency according to $\Psi_E(x,t) = \Psi_E(x,0)e^{-i\omega t}$. Therefore, its probability distribution is completely dead or stationary. The probability distribution

$$\Psi_E(x,t)^*\Psi_E(x,t) = |\Psi_E(x,t)|^2 = |\Psi_E(x,0)|^2 \quad (13.1.1)$$

or envelope $|\Psi_E(x,t)|$ is constant in time, hence the name *stationary* state.

The total energy ($E = T+V$) is assumed constant. However, the kinetic energy $T = \frac{1}{2}mv^2$ of a particle depends upon its position x if the potential $V=V(x)$ is not constant. Kinetic energy must equal the difference between E and V . The non-relativistic approximation to (5.2.5) gives Newtonian KE.

$$T = E - V(x) = \frac{p^2}{2m} = \frac{(\hbar k(x))^2}{2m} \quad (13.1.2)$$

Here we use the DeBroglie relation (5.2.5c) between wave vector k and particle momentum p .

$$m v = p(x) = \hbar k(x) \quad (13.1.3)$$

The magnitude of the wave vector is therefore given by the square-root expression

$$k(x) = [2m(E - V(x))/\hbar^2]^{1/2}. \quad (13.1.4)$$

The square root is real if x lies in what is called a *classical region* for which $E > V(x)$. If $E = V(x)$ then $k(x)$ is zero or, if $E < V(x)$, then $k(x)$ is imaginary. If $k(x)$ is imaginary then we say x lies in a *non-classical region* or *tunneling region*. Recall the waveguide wave in (6.3.10) with imaginary wavevector or the *evanescent - exponential* waves in Fig. 11.4.2-3 being compared to *propagating* waves in Fig. 11.4.1 with real $k(x)$.

For either real- k (propagating) case or the imaginary- k (evanescent) cases, the square root expression (13.1.4) does not determine the sign of k ; it can be either positive ($+k$) or negative ($-k$). Both $\pm k$ is possible at each point and any amount of either is permitted as was indicated in Fig. 11.4.1. Real- k propagating waves have the general "galloping" form discussed first in Sec. 4.2c.

$$\Psi_{\text{propagating}}(x,t) = A_{\rightarrow}(x)e^{i(kx - \omega t)} + A_{\leftarrow}(x)e^{i(-kx - \omega t)}, \quad (13.1.5a)$$

while imaginary- k gives evanescent waves with rising ($e^{\kappa x}$) or dying ($e^{-\kappa x}$) exponentials oscillating in t ,

$$\Psi_{\text{evanescent}}(x,t) = A_{+}(x)e^{\kappa x}e^{-i\omega t} + A_{-}(x)e^{-\kappa x}e^{-i\omega t}, \quad (13.1.5b)$$

where the exponential factor is

$$\kappa = ik = [2m(V(x) - E)/\hbar^2]^{1/2} \quad (\text{for: } E < V(x)). \quad (13.1.5c)$$

Either wave can be regarded as a $U(2)$ system at each point x . $\Psi(x)$ is determined by two complex amplitudes A_{\rightarrow} and A_{\leftarrow} or A_+ and A_- . Note that we do not allow the wavevector k to be complex, that is, it cannot have both real and imaginary parts. Such a complex $K = k + i\alpha$ corresponds to non-conservation of probability as is found in absorptive optical media or laser amplifiers. However, the techniques described below can be applied to such systems, and the program *BandIt* which draws the wave plots seen in this section is equipped to do optical as well as quantum wave dynamics.

Here we use approximation techniques which break up a variable potential $V(x)$ into a series of small steps at boundaries $x=.., a, b,..$ of regions of constant k as shown in Fig. 13.1.1 below. This technique is particularly appropriate (indeed it is exact in some sense) for layered quantum wells or superlattice models. However, it works well for continuously varying potentials if k is less than $\pi/(a-b)$.

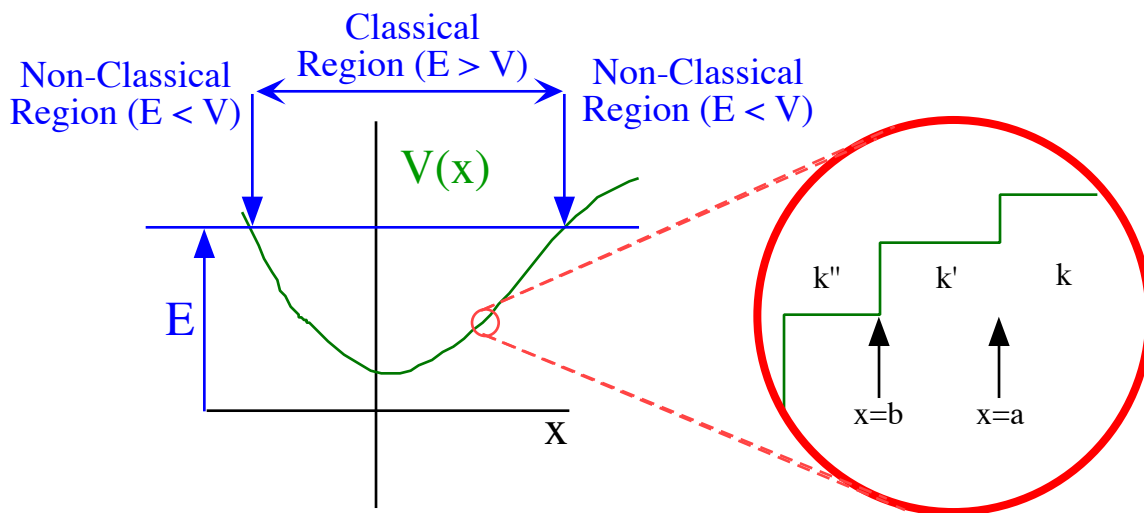


Fig. 13.1.1 Non-constant potential $V(x)$ approximated by a series of small constant- V steps.

Between each step the potential and kinetic energy and k (or $ik = \kappa$, if it's a non-classical region) is assumed constant and the wave function is simply

$$\Psi_E(x,0) = R e^{ikx} + L e^{-ikx} \tag{13.1.6}$$

Now we determine how the right and left amplitudes R and L vary with various kinds of potential steps. The same form is used regardless of whether wavevector k is real or imaginary.

(a) Single boundary potential barrier: C-matrix analysis

The wave function Ψ in (13.1.6) has an x -derivative that we denote by the notation $D\Psi$

$$\frac{\partial}{\partial x} \Psi_E(x,0) = ik R e^{ikx} - ik L e^{-ikx} \equiv D\Psi_E(x,0) \tag{13.1.7}$$

In order to satisfy the Schrodinger wave equation (11.4.5d), Ψ and $D\Psi$ must be continuous at any boundary where the potential $V(x)$ remains finite. A sudden jump in either Ψ and $D\Psi$ corresponds to an infinite curvature or second derivative $D^2\Psi$ and, by Schrodinger's equation, an infinite $V(x)$. A jump in Ψ would require two infinite $V(x)$ jumps, one up and one down as in the derivative of Dirac's delta shown in

Fig. 11.2.1b. A jump in $D\Psi$ itself would require only a single infinite delta "spike" in $V(x)$ such as is shown in Fig. 11.2.1a. Later on we use delta "spike" potentials to model charge and dipole layers.

At each point x , the following relations hold between the pair $(\Psi, D\Psi)$ and amplitudes (R, L) .

$$\begin{pmatrix} \Psi \\ D\Psi \end{pmatrix} = \begin{pmatrix} e^{ikx} & e^{-ikx} \\ ik e^{ikx} & -ik e^{-ikx} \end{pmatrix} \begin{pmatrix} R \\ L \end{pmatrix}, \quad \begin{pmatrix} R \\ L \end{pmatrix} = \frac{i}{2k} \begin{pmatrix} -ike^{-ikx} & -e^{-ikx} \\ -ike^{ikx} & e^{ikx} \end{pmatrix} \begin{pmatrix} \Psi \\ D\Psi \end{pmatrix} \quad (13.1.8a)$$

The same relations hold on the other side of the step boundary using different wave vector k' instead of k , and a different amplitude Ψ' instead of Ψ , R' instead of R , and L' instead of L .

$$\begin{pmatrix} \Psi' \\ D\Psi' \end{pmatrix} = \begin{pmatrix} e^{ik'x} & e^{-ik'x} \\ ik' e^{ik'x} & -ik' e^{-ik'x} \end{pmatrix} \begin{pmatrix} R' \\ L' \end{pmatrix}, \quad \begin{pmatrix} R' \\ L' \end{pmatrix} = \frac{i}{2k'} \begin{pmatrix} -ik' e^{-ik'x} & -e^{-ik'x} \\ -ik' e^{ik'x} & e^{ik'x} \end{pmatrix} \begin{pmatrix} \Psi' \\ D\Psi' \end{pmatrix} \quad (13.1.8b)$$

The wave function amplitudes and k -vectors on either side of a typical boundary point are indicated in Fig. 13.1.2 below.

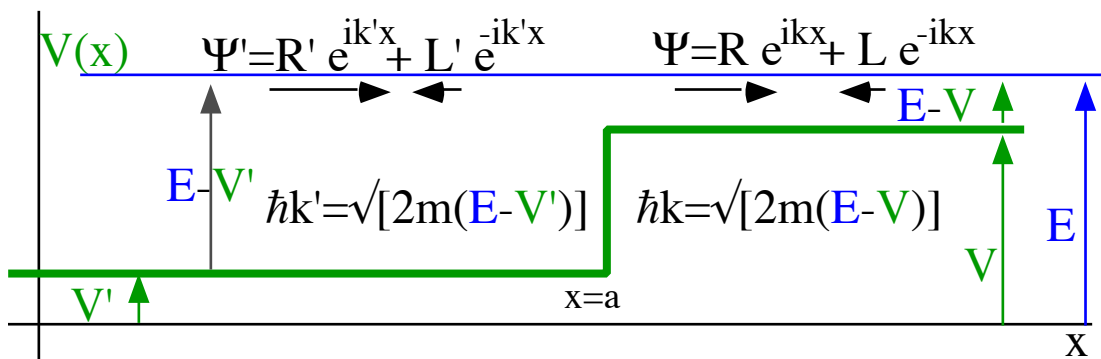


Fig. 13.1.2 Single-step potential $V(x)$ with total energy E greater than either step.

The wave function and derivative on one side of the boundary must equal those on the other side.

$$\begin{pmatrix} \Psi \\ D\Psi \end{pmatrix}_{x=a} = \begin{pmatrix} \Psi' \\ D\Psi' \end{pmatrix}_{x=a} \quad (13.1.9)$$

Using the first and last of equations (13.1.8) we find the following matrix equation between right and left amplitudes on either side of the boundary point ($x=a$).

$$\begin{pmatrix} R' \\ L' \end{pmatrix} = \frac{i}{2k'} \begin{pmatrix} -ik' e^{-ik'a} & -e^{-ik'a} \\ -ik' e^{ik'a} & e^{ik'a} \end{pmatrix} \begin{pmatrix} \Psi \\ D\Psi \end{pmatrix}_{x=a} \quad (13.1.10a)$$

$$\begin{pmatrix} R' \\ L' \end{pmatrix} = \frac{i}{2k'} \begin{pmatrix} -ik' e^{-ik'a} & -e^{-ik'a} \\ -ik' e^{ik'a} & e^{ik'a} \end{pmatrix} \begin{pmatrix} e^{ika} & e^{-ika} \\ ik e^{ika} & -ik e^{-ika} \end{pmatrix} \begin{pmatrix} R \\ L \end{pmatrix}$$

Multiplying the two matrices gives what is called a *crossing matrix relation* for a single boundary point ($x=a$). It gives the right and left amplitudes (R', L') for the left side in terms of the (R, L) for the right.

$$\begin{pmatrix} R' \\ L' \end{pmatrix} = \begin{pmatrix} \left(1 + \frac{k}{k'}\right) \frac{e^{i(k-k')a}}{2} & \left(1 - \frac{k}{k'}\right) \frac{e^{-i(k+k')a}}{2} \\ \left(1 - \frac{k}{k'}\right) \frac{e^{i(k+k')a}}{2} & \left(1 + \frac{k}{k'}\right) \frac{e^{i(k'-k)a}}{2} \end{pmatrix} \begin{pmatrix} R \\ L \end{pmatrix} \quad (13.1.10b)$$

The inverse crossing relation is obtained simply by switching primed and unprimed quantities.

An important special case involves *single input conditions* where no sources or reflectors exist on one side (say, on the right hand side) so no incoming waves exist there (say, $L=0$ but $R=Outgoing \neq 0$.)

$$\begin{pmatrix} R' \\ L' \end{pmatrix} = \begin{pmatrix} \left(1 + \frac{k}{k'}\right) \frac{e^{i(k-k')a}}{2} & \left(1 - \frac{k}{k'}\right) \frac{e^{-i(k+k')a}}{2} \\ \left(1 - \frac{k}{k'}\right) \frac{e^{i(k+k')a}}{2} & \left(1 + \frac{k}{k'}\right) \frac{e^{i(k'-k)a}}{2} \end{pmatrix} \begin{pmatrix} R \\ 0 \end{pmatrix} = \begin{pmatrix} R \left(1 + \frac{k}{k'}\right) \frac{e^{i(k-k')a}}{2} \\ R \left(1 - \frac{k}{k'}\right) \frac{e^{i(k+k')a}}{2} \end{pmatrix} \quad (13.1.10c)$$

We find the *transmitted or output amplitude R* and the *reflected amplitude L'* given an *input amplitude R'*.

$$R = \frac{2k'}{(k+k')} R' e^{i(k'-k)a}, \quad L' = \frac{(k'-k)}{(k+k')} R' e^{2ik'a} \quad (13.1.10d)$$

Squaring gives the *transmission coefficient $T_{transmit}$* and *reflection coefficient $T_{reflect}$* . Here we let $a=0$.

$$T_{transmit} = \frac{|R|^2}{|R'|^2} = \frac{4|k'|^2}{|k+k'|^2}, \quad T_{reflect} = \frac{|L'|^2}{|R'|^2} = \frac{|k'-k|^2}{|k'+k|^2} \quad (13.1.10e)$$

The left channel has the input R' wave interfering with the L' wave to give a *standing wave ratio(SWR)* of

$$SWR = \frac{L' - R'}{L' + R'} = \frac{\frac{2kR'}{k+k'}}{\frac{2k'R'}{k+k'}} = \frac{k}{k'} = \frac{\sqrt{E-V}}{\sqrt{E}} \quad (13.1.10f)$$

An example with $E=25$, $V'=0$, and $V=16$ (or $k'=5.0$ and $k = 3.0$) gives $SWR=3/5$ as shown in Fig. 13.1.3.

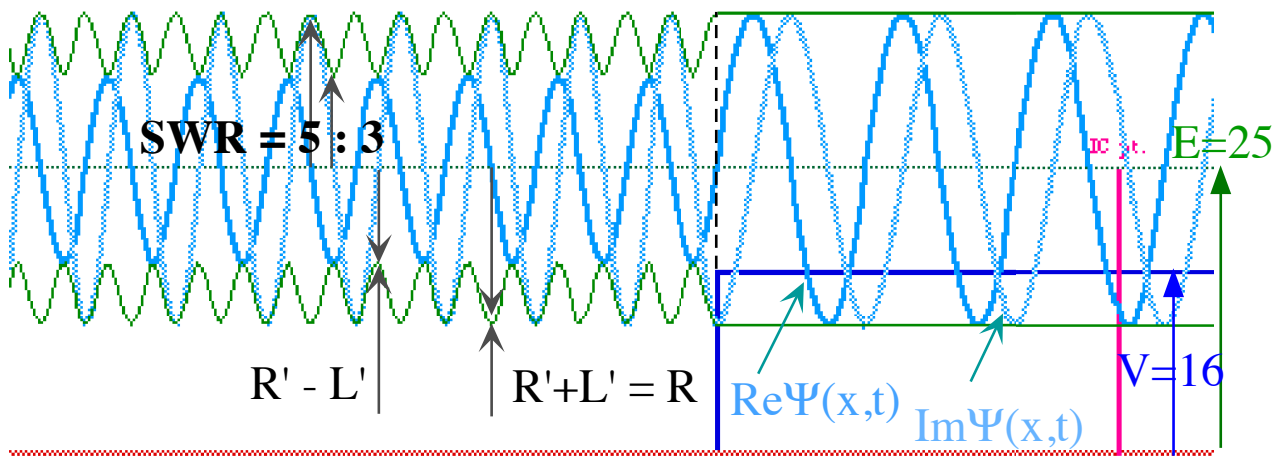


Fig. 13.1.3 Single-step potential $V=16$ and wave sent from left with total energy $E=25$. ($V'=0$).

So, the wave phase velocity "gallops" between $3/5$ and $5/3$ the phase velocity $v'_{phase} = \omega/k' = \omega/5$ on the left hand side. Its slowest speed is $(3/5)\omega/5 = 3\omega/25$. Its fastest speed is $(5/3)\omega/5 = \omega/3$ which exactly

matches the phase velocity $v_{phase} = \omega/k = \omega/3$ on the right hand side. Speeds have to match just as the wave-zero crosses the boundary as is happening to $\text{Re}\Psi$ at the instant shown in Fig. 13.1.3. Note also that the maximum amplitude $L'+R'$ on the left equals the constant amplitude R on the right.

This is valid whether k or k' are real or imaginary or (for classical optics) complex. However, as E approaches the barrier-top energy V the SWR approaches zero as L' become equal to R' and plateau wavevector goes to zero. ($k'=0$) The result is a perfect standing wave on the input side of the barrier as shown on left hand side of Fig. 13.1.4a, and a *grazing-threshold* output wave of zero momentum on the right hand side of Fig. 13.1.4a. (Recall resonate $V=E$ case of “shower curtain” wave in Fig. 11.5.4b.)

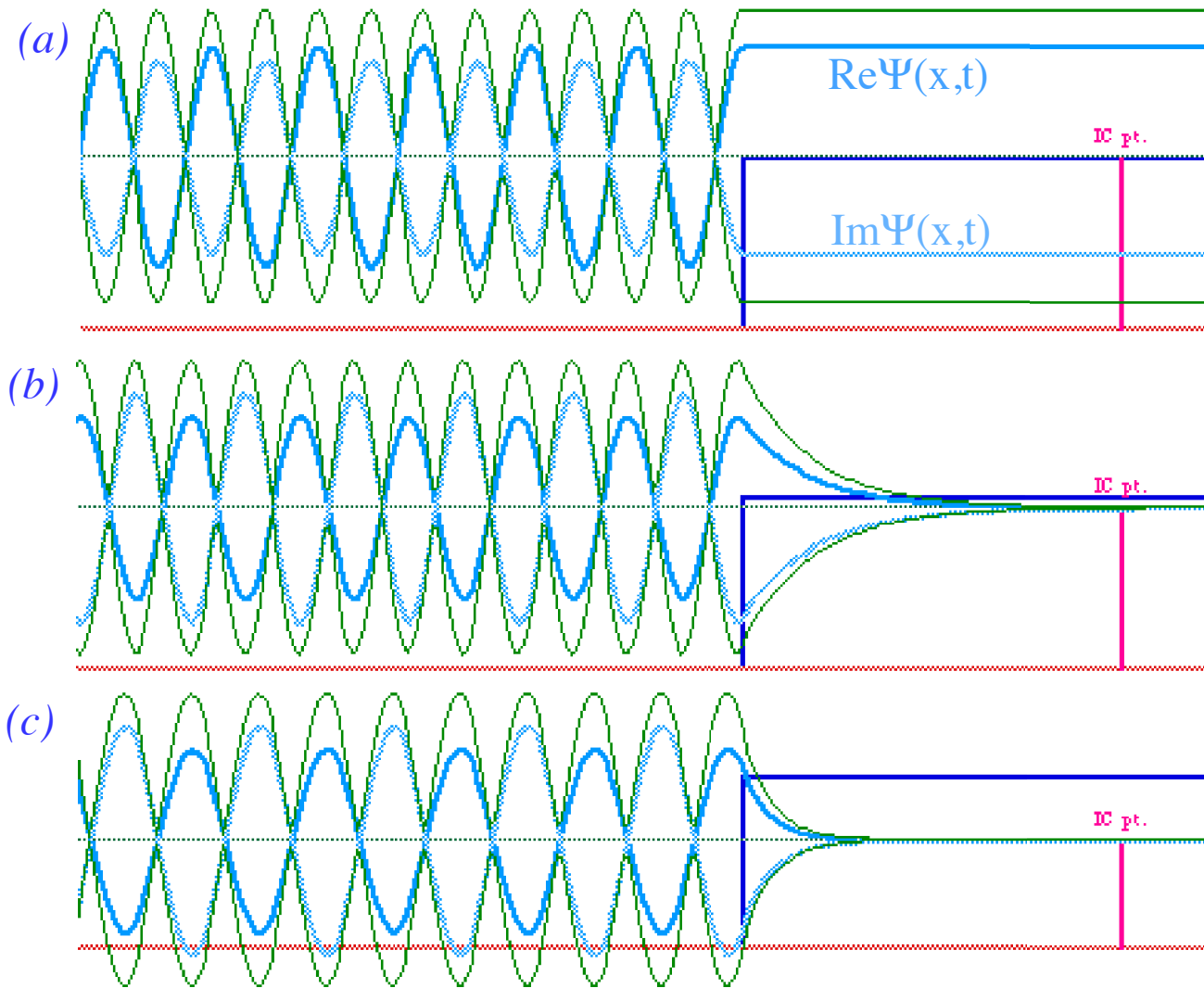


Fig. 13.1.4 Threshold waves (a) Grazing evanescence $E=16= V$ (b) $E=15$ just below $V=16$.(c) $E=10$.

Energy E below V implies imaginary momentum $k = i\kappa$ and exponential decay $e^{ikx} = e^{-\kappa x}$ as shown in Fig. 13.1.4b where $E=15$ is just below $V=16$. On the left of Fig. 13.1.4b the wavevector is $k = \pm\sqrt{(E-V)} = \pm\sqrt{15} = 3.87$, but on the right $k = \pm\sqrt{(15-16)} = \pm 1.0i$ or $\kappa = \pm 1$. Only the decaying ($\kappa = +1$) exponential $\Psi = e^{-\kappa x} = e^{-x}$ is allowed since $e^{\kappa x} = e^x$ would blow up to ∞ at large x . Here energy E and PE $V(x)$ are given in units of *electron Volt* ($1 \text{ eV} = 1.6022 \text{ E-}19 \text{ J}$), the energy one electron gains falling 1Volt. A 1 eV electron has a

wavevector of $k_{1eV} = \sqrt{(2me)/\hbar} = 5.123E9 \text{ rad/m}$ or a wavelength of $\lambda_{1eV} = 2\pi/k_{1eV} = 1.2264E-9 \text{ m} = 1.2264 \text{ nm} = 12.264 \text{ Angstrom}$. (See: Energy Units discussion and tables after (13.1.30).)

The wavelength on the left hand side is $\lambda = 2\pi/k = 2\pi/3.87 = 1.62$ in λ_{1eV} units or $1.62(1.23)=2.0 \text{ nanometers}$. Meanwhile the 95% decay distance on the right hand side ($e^{-\kappa x}=0.05=e^{-3}$) is $d_{5\%} = 3/\kappa=3.0$ in the same units or almost twice the left side wavelength. This is seen in the Fig. 13.1.4b. In Fig. 13.1.4c the energy is reduced further to $E = 10eV$. This gives a slightly lower wavevector of $k=\pm\sqrt{(E-V)}=\pm\sqrt{10}=3.16$, and longer wavelength of $\lambda = 2\pi/k = 2\pi/3.16 = 1.99$ in λ_{1eV} units. But the effect of a greater imaginary $k = \pm\sqrt{(10-16)} = \pm 2.45i$ or $\kappa=2.45$ on the right side is more noticeable. The 95% decay distance decreases to $d_{5\%} = 3/2.45 = 1.22$ in λ_{1eV} units. (To get 4-figure accuracy use the mnemonic $e^{-\pi}=0.4321$.)

Notice also how the left hand standing-wave envelope $|\Psi|$ gets squeezed out of the barrier as E is reduced. This happens so that the incoming-plus-reflected standing-wave envelope $|\Psi(a)|$ at the boundary will have the value *and slope* of the decaying exponential wave contacting the other side of the boundary. Note that, unlike Fig. 13.1.3, no energy or current is transmitted across the boundary in any of the cases shown in Fig. 13.1.4. Pure exponential $e^{\kappa x}$ waves with purely imaginary wavevectors are like perfect metals or perfect mirrors. All their phasors are in phase so no current can flow inside.

(1) Probability current conservation

The current flowing through the barrier is proportional to the difference between the absolute squares of right and left-going amplitudes. Here we let $a=0$ since choice of origin can have no effect.

$$\begin{pmatrix} R' \\ L' \end{pmatrix} = \begin{pmatrix} \left(1 + \frac{k}{k'}\right) \frac{1}{2} & \left(1 - \frac{k}{k'}\right) \frac{1}{2} \\ \left(1 - \frac{k}{k'}\right) \frac{1}{2} & \left(1 + \frac{k}{k'}\right) \frac{1}{2} \end{pmatrix} \begin{pmatrix} R \\ L \end{pmatrix} \quad (13.1.10b)_{\text{repeated for } a=0}$$

Using (13.1.10) and squaring we get (for real k and k' , only)

$$\begin{aligned} |R'|^2 &= \left(1 + \frac{k}{k'}\right)^2 \frac{|R|^2}{4} + \left(1 + \frac{k}{k'}\right) \left(1 - \frac{k}{k'}\right) \frac{R^* L + L^* R}{4} + \left(1 - \frac{k}{k'}\right)^2 \frac{|L|^2}{4} \\ |L'|^2 &= \left(1 - \frac{k}{k'}\right)^2 \frac{|R|^2}{4} + \left(1 + \frac{k}{k'}\right) \left(1 - \frac{k}{k'}\right) \frac{R^* L + L^* R}{4} + \left(1 + \frac{k}{k'}\right)^2 \frac{|L|^2}{4} \end{aligned}$$

Subtracting the two gives

$$|R'|^2 - |L'|^2 = (k/k')(|R|^2 - |L|^2) \quad (13.1.11a)$$

$$k'|R'|^2 - k|L'|^2 = k|R|^2 - k|L|^2. \quad (13.1.11b)$$

The *current* in a given direction R or L is proportional to product of the local wavevector k and the squared amplitude $|R|^2$ or $|L|^2$. Total current (13.1.11b) is right moving current minus left moving current.

This defines quantum current in terms of wave function and its derivative. According to (13.1.8a) the difference between the absolute squares of right and left-going amplitudes is

$$|R|^2 - |L|^2 = \frac{i}{2k}(D\Psi^* \Psi - \Psi^* D\Psi) \quad , \quad |R'|^2 - |L'|^2 = \frac{i}{2k'}(D\Psi'^* \Psi' - \Psi'^* D\Psi') \quad (13.1.12)$$

This becomes the standard 3-dimensional definition of probability current for a wavefunction.

$$j = \frac{-i\hbar}{2m} (\Psi^* (\nabla\Psi) - \Psi (\nabla\Psi)^*) = \frac{1}{2m} (\Psi^* \mathbf{p}\Psi + \Psi\mathbf{p}\Psi^*) \quad (13.1.13)$$

By comparing the preceding equations we derive the current in terms of the right and left coefficients. It has to be conserved across each boundary.

$$j = \frac{\hbar k}{m} (|R|^2 - |L|^2) = \frac{\hbar k'}{m} (|R'|^2 - |L'|^2) \quad (13.1.14)$$

The coefficient of each squared amplitude is just the expected particle velocity ($v = p/m = \hbar k/m$). Smaller kinetic energy and velocity mean greater wavefunction amplitude as seen in later Fig. 13.1.6. Where particles go slowly they often have a higher probability $\Psi^*\Psi$ to be found but less current $\text{Re}\Psi^*\mathbf{p}\Psi$.

It is convenient for some problems to make the square root of this coefficient part of the amplitudes. That is, right and left current amplitudes are defined by

$$I_R = \sqrt{\frac{\hbar k}{m}} R, \quad I_L = \sqrt{\frac{\hbar k}{m}} L, \quad I_{R'} = \sqrt{\frac{\hbar k'}{m}} R', \quad I_{L'} = \sqrt{\frac{\hbar k'}{m}} L', \quad (13.1.15a)$$

so that the current relation is simplified.

$$j = |I_R|^2 - |I_L|^2 = |I_{R'}|^2 - |I_{L'}|^2 \quad (13.1.15b)$$

(2) *Momentum vs. frequency or energy normalization*

Plane wave functions with coefficients defined in terms of I amplitudes can also be normalized with respect to angular frequency ω or energy $E = \hbar\omega$. Simple plane waves $e^{\pm ikx}$ are normalized with respect to momentum or wavevector k . k -orthogonality relations (Recall (2.6.17) are

$$\int_{-X}^X dx (e^{ik'x})^* (e^{ikx}) = \frac{e^{i(k-k')x}}{i(k-k')} \Big|_{-X}^X = \frac{2 \sin(k-k')X}{k-k'} \xrightarrow{X \rightarrow \infty} 2\pi\delta(k-k')$$

while k -completeness relations are

$$\int_{-K}^K dk (e^{ikx'})^* (e^{ikx}) = \frac{e^{ik(x-x')}}{i(x-x')} \Big|_{-K}^K = \frac{2 \sin K(x-x')}{x-x'} \xrightarrow{K \rightarrow \infty} 2\pi\delta(x-x')$$

These are derived from the integral $\int_{-\infty}^{\infty} dx \frac{\sin x}{x} = \pi$ and Dirac's delta function definition $\int_{-\infty}^{\infty} dx \delta(x) = 1$.

The k -integral is converted to an angular frequency or energy integral by a simple change of variable using $E = \hbar\omega = \hbar^2 k^2 / (2m)$.

$$\int dk (e^{ikx'})^* (e^{ikx}) = \int d\omega \frac{dk}{d\omega} (e^{ikx'})^* (e^{ikx}) = \int d\omega \left(\sqrt{\frac{m}{\hbar k}} e^{ikx'} \right)^* \left(\sqrt{\frac{m}{\hbar k}} e^{ikx} \right) = 2\pi\delta(x'-x)$$

So the general 1D monochromatic "galloping" wavefunctions can be written as follows using (13.1.15a),

$$\Psi = R e^{ikx} + L e^{-ikx} = I_R \sqrt{\frac{m}{\hbar k}} e^{ikx} + I_L \sqrt{\frac{m}{\hbar k}} e^{-ikx} = I_R \psi_k(x) + I_L \psi_{-k}(x) \quad (13.1.16a)$$

Here we use frequency normalized plane wave functions:

$$\psi_k(x) = \sqrt{\frac{m}{\hbar k}} e^{ikx} \quad (13.1.16b)$$

These satisfy *frequency orthonormalization*

$$\int_{-\infty}^{\infty} d\omega \psi_k^*(x) \psi_k(x) = \int_{-\infty}^{\infty} d\omega \left(\sqrt{\frac{m}{\hbar k}} e^{ikx'} \right)^* \left(\sqrt{\frac{m}{\hbar k}} e^{ikx} \right) = 2\pi \delta(x'-x) \quad (13.1.16c)$$

and completeness

$$\int_{-\infty}^{\infty} dx \psi_k^*(x) \psi_k(x) = \int_{-\infty}^{\infty} dx \left(\sqrt{\frac{m}{\hbar k'}} e^{ik'x} \right)^* \left(\sqrt{\frac{m}{\hbar k}} e^{ikx} \right) = 2\pi \delta(\omega'-\omega) \quad (13.1.16d)$$

We use the following Dirac identity (prove it!).

$$\delta(x) = \delta(f(x)) \frac{df}{dx}, \quad \text{or:} \quad \delta(\omega'-\omega) = \delta(k'-k) \frac{m}{\hbar k} \quad (13.1.16e)$$

Then the coefficients I_R and I_L of ω -orthonormalized waves satisfy conservation relations (13.1.15b). Note that normalization (13.1.16c-d) is to 2π instead of 1.0. To get rid of that 2π simply replace the \hbar in (13.1.16) by $h = 2\pi\hbar$. E -normalization needs an additional \hbar in the denominator of $\psi_k(x)$'s scale factor.

The presence of multiple definitions of normalization is one of the consequences of having unbounded (Banach-space) norms like $\langle x|x \rangle = \infty$. With discrete norms like $\langle x_p|x_p \rangle = 1$ all the bases have unit length and that's that; no arguments! But, with ∞ -length vectors we might as well have norm 2∞ , or 3∞ , and so forth because that is still just ∞ . It's a convenient feature, but watch it carefully!

(b) Two boundary potential barriers

For two successive boundaries at $(x=a)$ and $(x=b)$ such as is shown in Fig. 13.1.5 it is necessary to multiply two such crossing matrices, one for each boundary point. Two such points $(x=a)$ and $(x=b)$ are present in the potential sketched in Fig. 13.1.5.

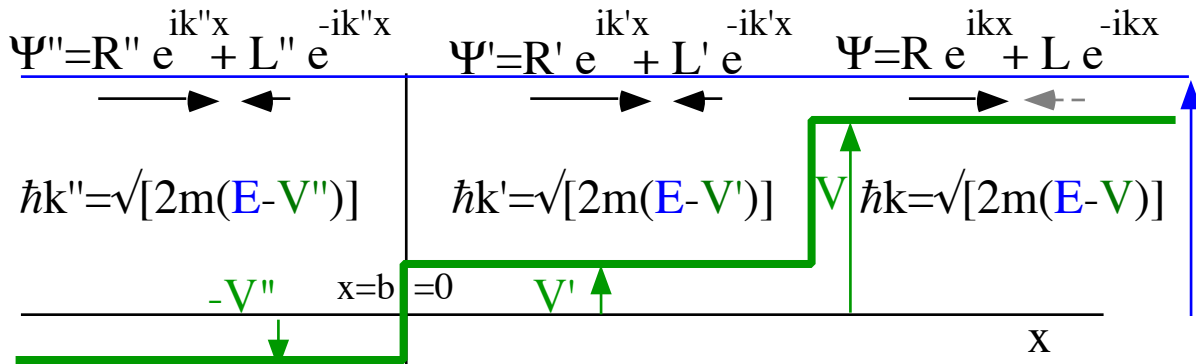


Fig. 13.1.5 Two step square potential boundaries

The resulting matrix product relates the amplitudes (R,L) in the right hand channel to the corresponding (R'',L'') for the wave in the left hand channel. The intermediate amplitudes (R',L') are then eliminated.

$$\begin{pmatrix} R'' \\ L'' \end{pmatrix} = \begin{pmatrix} \left(1 + \frac{k'}{k''}\right) \frac{e^{i(k'-k'')b}}{2} & \left(1 - \frac{k'}{k''}\right) \frac{e^{-i(k'+k'')b}}{2} \\ \left(1 - \frac{k'}{k''}\right) \frac{e^{i(k+k'')b}}{2} & \left(1 + \frac{k'}{k''}\right) \frac{e^{i(k''-k')b}}{2} \end{pmatrix} \begin{pmatrix} \left(1 + \frac{k}{k'}\right) \frac{e^{i(k-k')a}}{2} & \left(1 - \frac{k}{k'}\right) \frac{e^{-i(k+k')a}}{2} \\ \left(1 - \frac{k}{k'}\right) \frac{e^{i(k+k')a}}{2} & \left(1 + \frac{k}{k'}\right) \frac{e^{i(k'-k)a}}{2} \end{pmatrix} \begin{pmatrix} R \\ L \end{pmatrix} \quad (13.1.24)$$

This is simplified by letting one of the boundary points be origin $(b=0)$ as in the figure above.

$$\begin{pmatrix} R'' \\ L'' \end{pmatrix} = \frac{1}{2} \begin{pmatrix} \left(1 + \frac{k'}{k''}\right) & \left(1 - \frac{k'}{k''}\right) \\ \left(1 - \frac{k'}{k''}\right) & \left(1 + \frac{k'}{k''}\right) \end{pmatrix} \begin{pmatrix} \left(1 + \frac{k}{k'}\right) \frac{e^{i(k-k')a}}{2} & \left(1 - \frac{k}{k'}\right) \frac{e^{-i(k+k')a}}{2} \\ \left(1 - \frac{k}{k'}\right) \frac{e^{i(k+k')a}}{2} & \left(1 + \frac{k}{k'}\right) \frac{e^{i(k-k')a}}{2} \end{pmatrix} \begin{pmatrix} R \\ L \end{pmatrix}$$

Matrix multiplication yields a single crossing matrix. Here the first column of the result is given.

$$\begin{pmatrix} R'' \\ L'' \end{pmatrix} = \frac{1}{2} \begin{pmatrix} \left(1 + \frac{k'}{k''}\right) \left(1 + \frac{k}{k'}\right) \frac{e^{i(k-k')a}}{2} + \left(1 - \frac{k'}{k''}\right) \left(1 - \frac{k}{k'}\right) \frac{e^{i(k+k')a}}{2} & \dots \\ \left(1 - \frac{k'}{k''}\right) \left(1 + \frac{k}{k'}\right) \frac{e^{i(k-k')a}}{2} + \left(1 + \frac{k'}{k''}\right) \left(1 - \frac{k}{k'}\right) \frac{e^{i(k+k')a}}{2} & \dots \end{pmatrix} \begin{pmatrix} R \\ L \end{pmatrix}$$

Further reduction of the terms in the first column of the crossing matrix gives the following.

$$\begin{pmatrix} R'' \\ L'' \end{pmatrix} = \frac{1}{4} \begin{pmatrix} e^{ika} \left[\left(1 + \frac{k'}{k''} + \frac{k}{k'} + \frac{k}{k''}\right) e^{-ik'a} + \left(1 - \frac{k'}{k''} - \frac{k}{k'} + \frac{k}{k''}\right) e^{ik'a} \right] & \dots \\ e^{ika} \left[\left(1 - \frac{k'}{k''} + \frac{k}{k'} - \frac{k}{k''}\right) e^{-ik'a} + \left(1 + \frac{k'}{k''} - \frac{k}{k'} - \frac{k}{k''}\right) e^{ik'a} \right] & \dots \end{pmatrix} \begin{pmatrix} R \\ L \end{pmatrix} \tag{13.1.25a}$$

$$\begin{pmatrix} R'' \\ L'' \end{pmatrix} = \frac{1}{2} \begin{pmatrix} e^{ika} \left[\left(1 + \frac{k}{k''}\right) \cos k'a - i \left(\frac{k'}{k''} + \frac{k}{k'}\right) \sin k'a \right] & \dots \\ e^{ika} \left[\left(1 - \frac{k}{k''}\right) \cos k'a + i \left(\frac{k'}{k''} - \frac{k}{k'}\right) \sin k'a \right] & \dots \end{pmatrix} \begin{pmatrix} R \\ L \end{pmatrix}$$

Once again we suppose that the wave function is entirely due to sources off to the left. So, the left hand moving wave amplitude in the right hand channel must vanish ($L=0$) if the right channel contributes nothing and only the R -amplitude (transmitted wave) can be non-zero. (The amplitude L is indicated by the gray arrow in Fig. 13.1.5.)

The sources in the left hand channel can give rise to both right moving ($R'' \neq 0$) and left moving ($L'' \neq 0$) waves in the regions to the left of point ($x=a$) because the potential barriers at ($x=a$) and at ($x=b=0$) may cause reflections. However, under certain conditions it is possible to zero amplitude L'' for the reflected wave moving to the left from the point ($x=b=0$). According, to (13.1.25a) with $L=0$ we have the reflected amplitude

$$L'' = \frac{1}{2} e^{ika} \left[\left(1 - \frac{k}{k''}\right) \cos k'a + i \left(\frac{k'}{k''} - \frac{k}{k'}\right) \sin k'a \right] R \tag{13.1.25b}$$

L'' will be zero only if both terms in the brackets vanish. For real k -values there are two cases: In the first case(1), the first term can be killed by having

$$\left(1 - \frac{k}{k''}\right) = 0 \text{ or } k = k'', \quad \text{with } \sin k'a = 0 \tag{13.1.25c}$$

so the second term is killed, too. In the second case(2), the second term can be killed by having

$$\left(\frac{k'}{k''} - \frac{k}{k'}\right) = 0 \text{ or } k' = \sqrt{kk''}, \quad \text{with: } \cos k'a = 0 \tag{13.1.25d}$$

killing the first term, too. We consider these two cases separately below. The transmission coefficient is the ratio of transmitted current $\sim k|R|^2$ to the incident current $\sim k''|R''|^2$ as defined by (13.1.15).

$$\frac{k}{k''} \left| \frac{R}{R''} \right|^2 = \frac{4}{\left| \frac{k''}{k} \left(\left(1 + \frac{k}{k''} \right) \cos k'a - i \left(\frac{k'}{k''} + \frac{k}{k'} \right) \sin k'a \right) \right|^2} = \frac{4kk''}{(k+k'')^2 \cos^2 k'a + \left(\frac{kk''}{k'} + k' \right)^2 \sin^2 k'a} \quad (13.1.25e)$$

Perfect transmission Case 1: Symmetric potential (k = k'')

The first case corresponds to a C₂-symmetric potential well. Perfect transmission occurs only when *sin k'a* is zero, or *k'a = 0, π, 2π, 3π, 4π, ... nπ*. There must be an integral number *n* of half waves in the potential well between *x=0* and *x=a*. An example with one half-wave (*k'a = π*) on the barrier is shown in Fig. 13.1.6a below. Two halves or a whole-wave sit on the barrier in Fig. 13.1.6b.

The transmission function (13.1.25e) is plotted as function of energy E with the E-axis running vertically. The first transmission maximum (see arrow) corresponds to the *k'a=π* half-wave piled up on the barrier. The next transmission maximum is the *k'a=2π* (whole-wave) resonance shown in Fig. 13.1.6b.

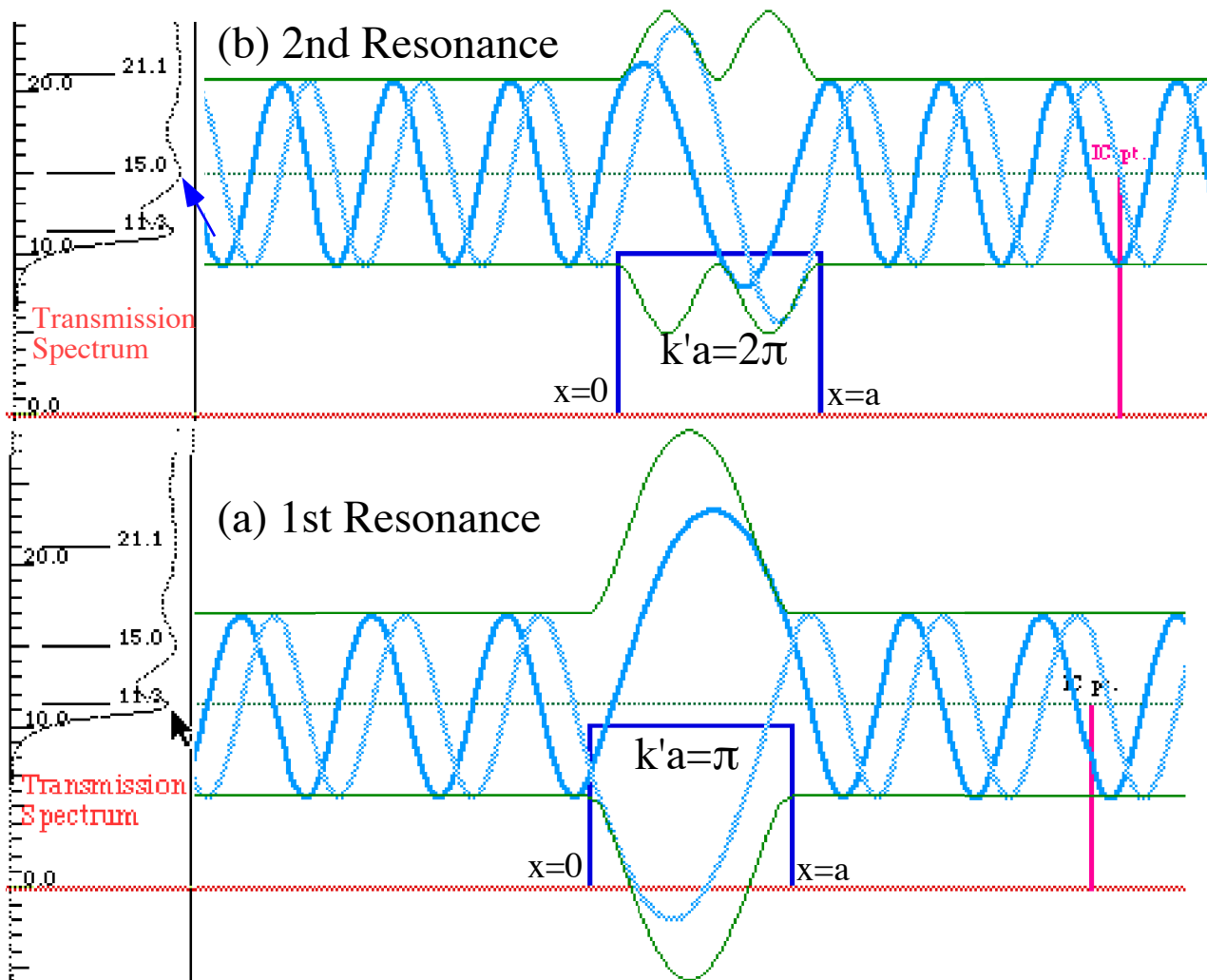


Fig. 13.1.6 Resonance waves over square barrier

Notice that the transmission peak for the first resonance is sharper and the wave amplitude is larger for the first resonance peak (lower arrow) than it is for the second one in (b). The third one is even smaller. The piling up of probability amplitude on top of a barrier is due to the fact that the particle goes

more slowly there and is therefore has higher probability to be there. As energy E increases above V , the potential has less effect on particle speed and transmission function whose wiggles die off accordingly.

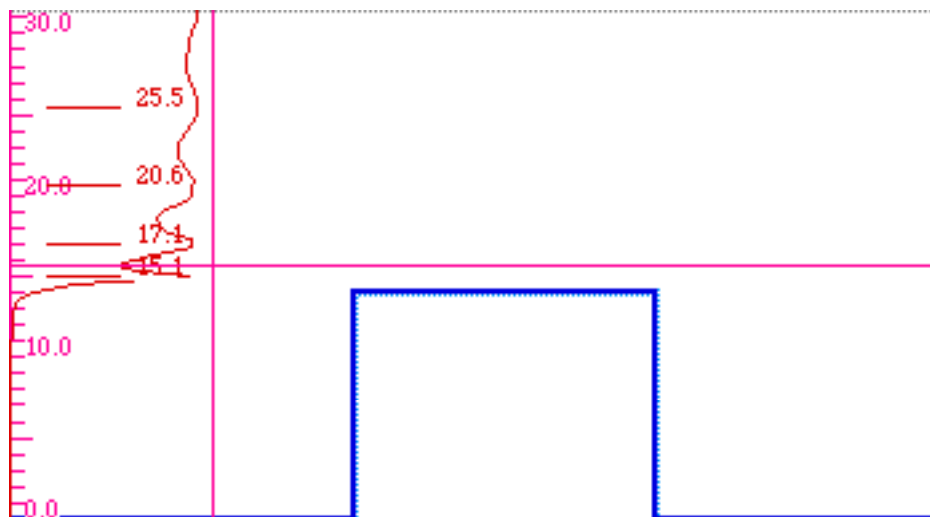
That a potential has any effect on transmission for $E > V$ is actually quite remarkable. A classical particle approaching a barrier with sufficient energy E to pass it will do so 100% of the time even if E is arbitrarily close to the barrier top value V . The oscillations in the transmission function are due a steep or "sharp" potential slope, and they practically disappear if $V(x)$ is "dulled" as in Fig. 13.1.7 b and c.

Potential barriers which change significantly in the space of a wavelength will disrupt wave transmission even if the energy is well above the barrier top. This is true even for a single barrier shown in Fig. 13.1.3. Wave reflection increases when the k -value changes by a large percentage, that is, when $\Delta k/k$ is large. According to (13.1.10e) the reflection from a square jump goes as $|\Delta k|^2 / |2k|^2$.

It is surprising that a reflection probability like (13.1.10e) does not depend upon Planck's constant \hbar . Quantum effects are usually as tiny as Planck's constant $\hbar = 1.05 \cdot 10^{-35} \text{ J.s.}$ and become important only when momenta are tiny, too. Taxi cabs usually don't reflect off road bumps unless they are subatomic taxi cabs. So you might think that quantum reflection formulas should vanish when momenta are many \hbar .

Generally, deBroglie waves for classical momenta are too fine to be "cut" by a normal classical potential which is usually not "sharp" enough to cause quantum reflection. However, a square barrier potential is an exception because its slope or "sharpness" is *infinite*; no deBroglie wave is fine enough to behave classically when its energy approaches a truly square potential barrier. This explains why (13.1.10) is not explicitly a function of \hbar . A perfect square barrier, like a perfect Dirac-delta function, is an impossibility representing an *infinite* force, and it could reflect everything including full size taxi cabs!

Reflection formula (13.1.10) does not require truly square walls; only walls that rise much steeper than the wavefunction. Indeed, reflection of optical photons is an everyday occurrence observed on video camera lenses or from soap bubble films which reflect photons having wavelengths that are long ($\sim 0.5\mu\text{m}$) compared to the optical surface "roughness." Indeed, the reflection from optical surfaces is something of a nuisance; quality lens makers try to get rid of it. Let's see how.



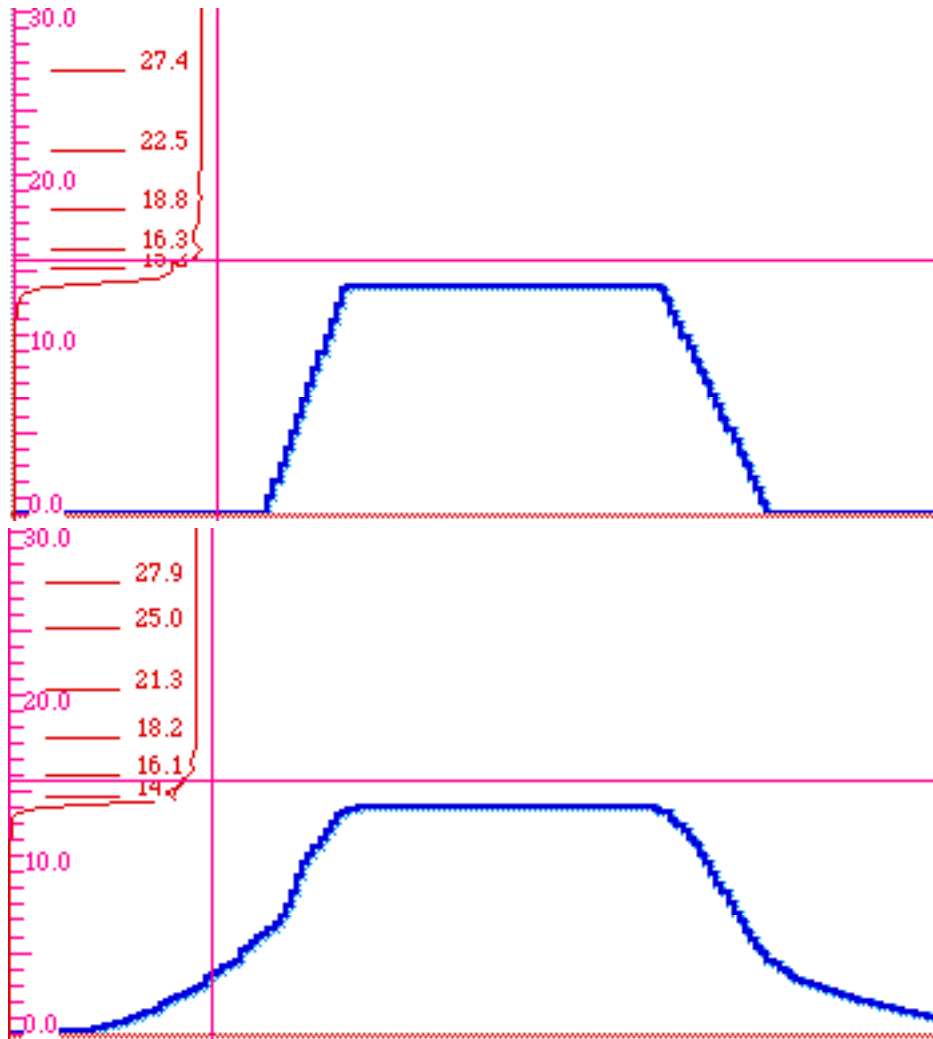


Fig. 13.1.7 Transmission quickly approaches 100% above potential barriers that are less "sharp."

Perfect transmission Case 2: Geometric impedance matching ($k' = \sqrt{k k''}$)

The second case (13.1.25d) of perfect transmission has the intermediate wavevector k' equal to the geometric mean $k' = \sqrt{k k''}$ of the input k and output k'' wavevectors. The wave will transmit 100% if the intermediate step length a is an odd integral multiple of quarter-wavelengths, that is : $\cos k'a=0$ or $k'a = (2n+1)\pi/2$. An example is shown below in Fig. 13.1.8.

It should be noted that it is necessary to have perfect frequency matching to get perfect 100% transmission. Even a slight deviation will result in some reflective galloping in the input channel as shown in Fig. 13.1.9. This is why non-reflective lens coatings are purplish. They are designed to transmit 100% of the green light so some of the red and blue get reflected and we see a purple sheen.

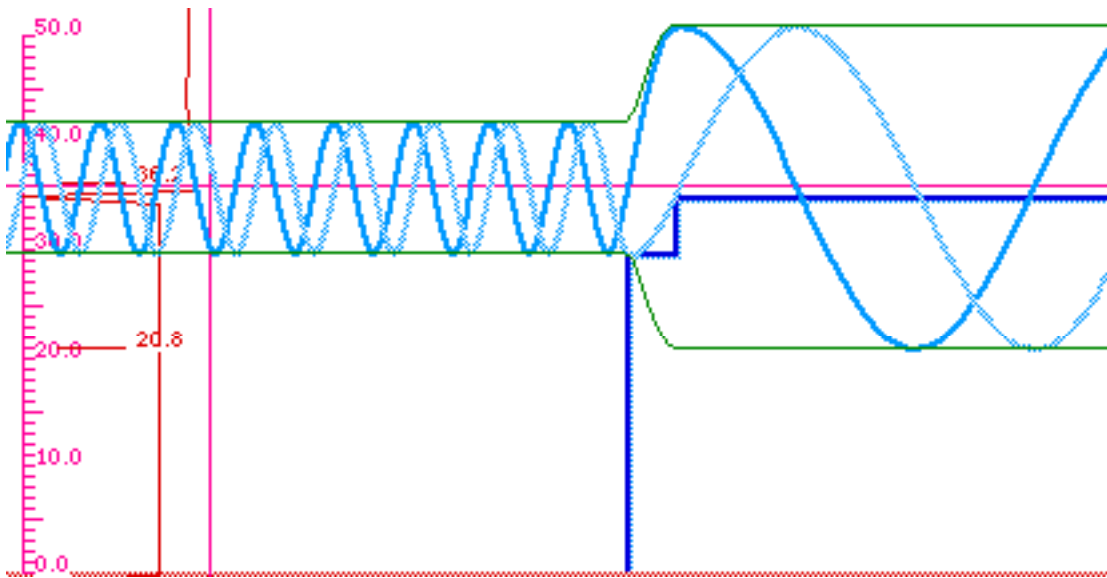


Fig. 13.1.8 100% Transmission using single intermediate quarter-wave geometric mean wave step

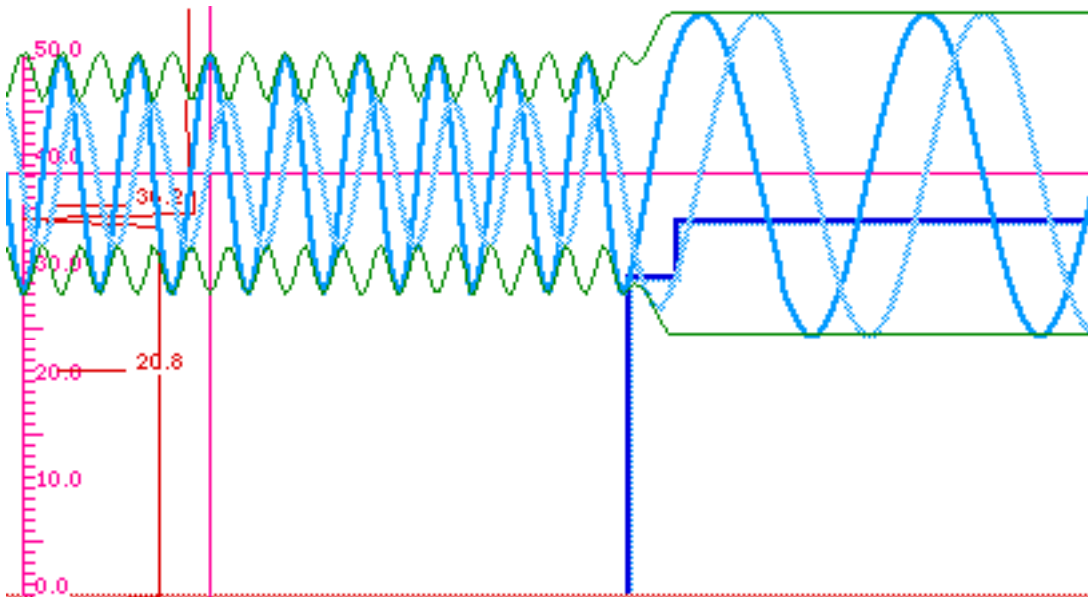


Fig. 13.1.9 Detuned wave has less than 100% transmission through wave step

The "Stairway-to-Heaven"

Geometric wavevector matching can be continued indefinitely using a series of steps that reduce the wave vector and increase the step length by the same ratio at each jump. In the example shown by Fig. 13.1.10 the total energy is $E=36$ above the initial plain of $V_1=0$. The first step was chosen to be $V_2=15$. The resulting wavevector ratio sets the next step $k_3 = 3.5$ and the rest of the stairway as far as it goes.

$$k_2/k_1 = \sqrt{(E-V_2)}/\sqrt{(E-V_1)} = \sqrt{(21)}/\sqrt{(36)} = \sqrt{(0.583)} = 0.764$$

While this square-stepped stairway does give a perfect 100% transmission of $E=36$ particles, it is sensitive to any change in the energy.

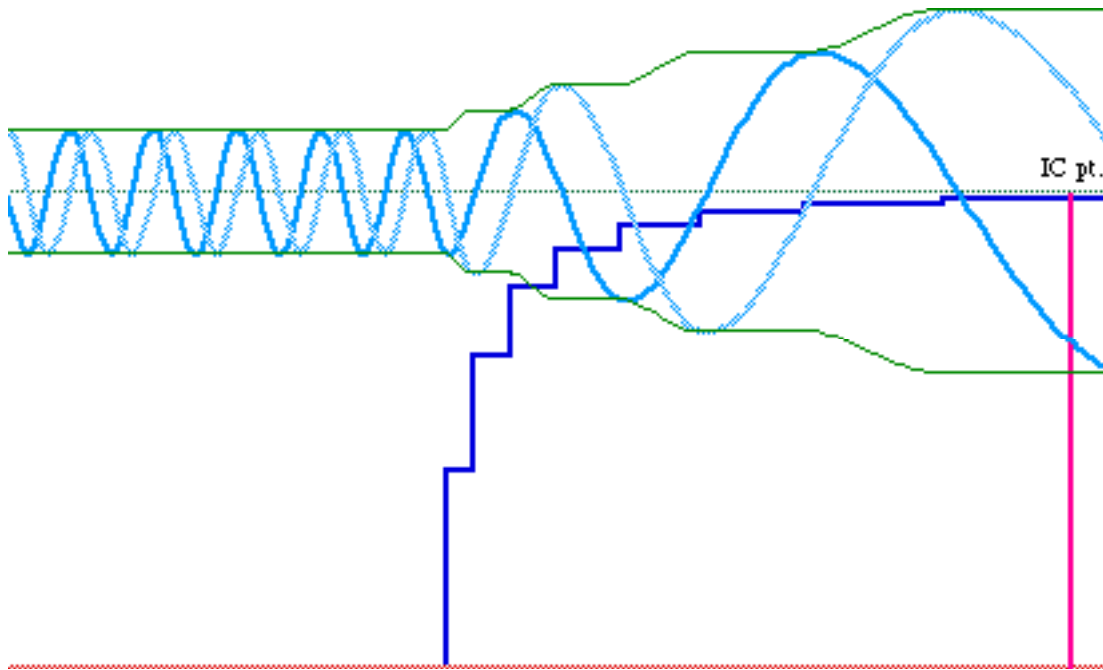


Fig. 13.1.10 Stairway to Heaven makes large change in wavevector with 100% transmission.

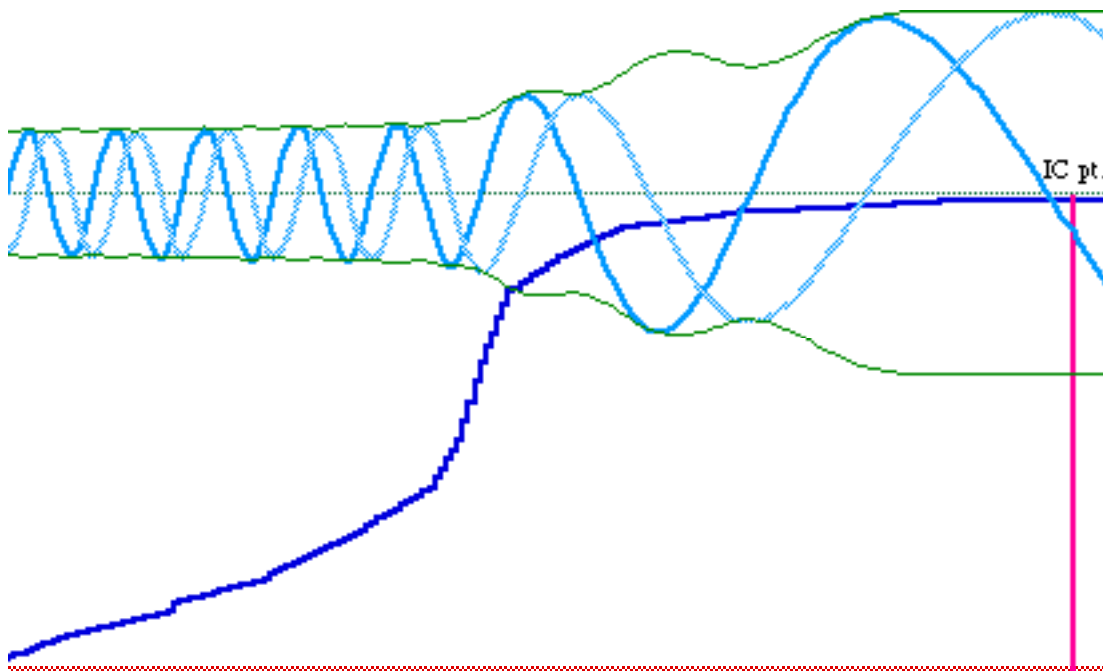


Fig. 13.1.11 "Ramp to Heaven" passes a range of wavevectors with nearly 100% transmission.

Nature has a way to get very nearly 100% transmission without so much sensitivity to frequency, and this provides another lesson in wave mechanics. Our eyes do not have a purplish sheen seen on camera lenses because our lens index or "potential" varies gradually with depth. The eye is layered like an onion with graded wavevector, and so it can avoid reflection over a wider spectrum. A simulated example constructed more or less randomly using *BandIt* is shown in Fig. 13.1.11 below. Like the examples in Fig. 13.1.7 the "ramp to Heaven" is not absolutely 100% but very close to 100% for a wide range of frequency.

Units of Length, Energy and Frequency: meV to EeV

It is conventional to use energy units of *electron Volts* or eV in most of physics where $1eV = (e) \text{ Joule} = 1.602E-19 J$ is based on the quantum of electronic or nuclear charge of $e=1.602177E-19$ Coulomb.

Sub-fields of physics may be characterized by prefix they attach to eV in their most commonly used energy quanta. Common prefixes are listed in the table below. Note: One eV is about 0.16 attoJoule .

A non-relativistic electron (β -ray) of energy E and potential V , has wavevector k_β or wavelength λ_β .

$$k_\beta = \sqrt{\frac{2m}{\hbar^2}(E_\beta - V)} = \sqrt{\frac{2me}{\hbar^2}(E - V)_{in eV}} \quad (\text{non-relativistic } KE \ll mc^2) \quad (13.1.26a)$$

$$\lambda_\beta(E, V) = \frac{2\pi}{k_\beta} = \frac{2\pi\hbar}{\sqrt{2me(E - V)_{in eV}}} = \frac{h}{\sqrt{2me}} \frac{1}{\sqrt{(E - V)_{in eV}}} = 1.23nm \frac{1}{\sqrt{(E - V)_{in eV}}} \quad (13.1.26b)$$

The wavelength $\lambda_\beta = 2\pi/k_\beta$ of a $1eV$ electron is $1.2264 E-9m$ or about $1.23nm$. It is easily memorized.

Wavelength λ_γ of a $1eV$ photon (γ -ray) is $1.2398 E-6m$ or about $1.24\mu m$. It is also easily memorized!

$$\lambda_\gamma(E_\gamma) = \frac{2\pi}{k_\gamma} = \frac{2\pi\hbar c}{e(E)_{in eV}} = \frac{hc}{e} \frac{1}{(E)_{in eV}} = 1.24\mu m \frac{1}{(E)_{in eV}} \quad (13.1.27a)$$

For gamma, beta, or any kind of radiation, $1 eV$ of energy corresponds to the following frequency values.

$$\omega(E) = \frac{E}{\hbar} = \frac{e}{\hbar}(E)_{in eV} = (E)_{in eV} 1.52 \cdot 10^{15} \frac{\text{radian}}{s}, \quad \nu(E) = \frac{E}{h} = \frac{e}{h}(E)_{in eV} = (E)_{in eV} 0.242PHz \quad (13.1.27b)$$

Below are units of photon and electron energy E , frequency ν , and wavelengths λ used in various realms.

We often use "theorist" or "natural" units in which m/\hbar^2 , $\hbar c/e$, \hbar^2/me or all three are set equal to one. The question, of course, is one *what?* For example, a "theorist" formula for electronic (beta) wavelength might replace (13.1.26b) by the following.

$$\lambda(\text{theorist}) = \frac{2\pi}{\sqrt{2(E - V)_{theorist}}} \quad (13.1.28)$$

BandIt use such units to avoid numerical overflow. Then (13.1.26b) in $1.23nm$ units of length is

$$\lambda_\beta(E, V) = \frac{1}{\sqrt{(E - V)_{in eV}}} \text{ (in } 1.23nm \text{ units)} \quad (13.1.29)$$

Equations (13.1.26b) imply that $1 eV$ is $2\pi^2 = 19.74$ theorist energy units. If you prefer $1.0nm$ length units, then an energy of $1 eV$ is, in that system, $2\pi^2/(1.226)^2 = 13.13$ units.

$$(E - V)_{theorist} = 2\pi^2 (E - V)_{in eV} = 19.74 (E - V)_{in eV} \quad (13.1.30)$$

Similar conversions may be made so theorist units make sense for any realm of physics or any size distance units. These are listed below.

Energy Units.

Conventional E Units

milli: $meV = 10^{-3} eV$
 micro: $\mu eV = 10^{-6} eV$
 nano: $neV = 10^{-9} eV$
 pico: $peV = 10^{-12} eV$
 femto: $feV = 10^{-15} eV$
 atto: $aeV = 10^{-18} eV$

Physics

far infrared, solid state
 molecular rotation
 molecular tunneling
 Bose condensates

$1eV=1.602177 \cdot 10^{-19}J$
 kilo: $keV = 10^3 eV$
 Mega: $MeV = 10^6 eV$
 Giga: $GeV = 10^9 eV$
 Tera: $TeV = 10^{12} eV$
 Peta: $PeV = 10^{15} eV$
 Exa: $EeV = 10^{18} eV$

optics, near IR to near UV
 atomic, X-ray
 nuclear, γ -ray
 heavy ion accelerator
 high energy accelerator
 astrophysics
 monsters

Photon Optical Waves. (γ -Rays)

Photon E,v, λ Units

$meV=0.24THz$ or: $\lambda_\gamma=1.24mm$
 $\mu eV=0.24GHz$ or: $\lambda_\gamma=1.24m$
 $neV=0.24MHz$ or: $\lambda_\gamma=1.24km$
 $peV=0.24kHz$ or: $\lambda_\gamma=1239km$
 $feV=0.24Hz$ or: $\lambda_\gamma=1239Mm$
 $aeV=0.24mHz$ or: $\lambda_\gamma=1239Gm$

Physics

$8cm^{-1}$, solids, far-IR to μ wave
 molecular rotation, high rf
 molecular tunneling, AM
 Bose condensates

$1eV=0.24PHz$ or: $\lambda_\gamma=1.24\mu m$
 $keV=0.24EHZ$ or: $\lambda_\gamma=1.24nm$
 $MeV=242EHZ$ or: $\lambda_\gamma=1.24pm$
 $GeV=24E22Hz$ or: $\lambda_\gamma=1.24fm$
 $TeV=24E25Hz$ or: $\lambda_\gamma=1.24am$
 $PeV = 10^{15} eV$
 $EeV = 10^{18} eV$

$=8066cm^{-1}$, optics, IR to UV
 $=12.4 \text{ \AA}$, atomic, X-ray
 nuclear, γ -ray
 heavy ion accelerator
 high energy accelerator
 astrophysics
 monsters

Electron Matter Waves. (β -Rays)

Electron E,v, λ Units

$meV=0.24THz$ or: $\lambda_\beta=38.8nm$
 $\mu eV=0.24GHz$ or: $\lambda_\beta=1.23um$
 $neV=0.24MHz$ or: $\lambda_\beta=38.8um$
 $peV=0.24kHz$ or: $\lambda_\beta=1.23mm$

Physics

far infrared, solid state
 molecular rotation
 molecular tunneling
 Bose condensates

$1eV=0.24PHz$ or: $\lambda_\beta=1.23nm$
 $keV=0.24EHZ$ or: $\lambda_\beta=38.8pm$
 $MeV=242EHZ$: $\dagger \lambda_\beta \sim 1.23pm$
 $GeV=24E22Hz$: $\dagger \lambda_\beta \sim 38.8fm$
 $TeV \sim 24E25Hz$: $\dagger \lambda_\beta \sim 1.23fm$

optics, UV
 atomic, X-ray
 nuclear, γ -ray
 heavy ion accelerator
 high energy accelerator

\dagger Incorrectly using nonrelativistic $E=(\hbar k)^2/2M$.. Above 1keV you need to use $E=\sqrt{[(\hbar kc)^2+(Mc^2)^2]}$. Then λ_β approaches λ_γ . (See Ch. 5.)

13.2 Square wells: bound states vs. free state resonance

The two successive stairway barriers in Fig. 13.1.5 may also be borders of a *potential well* or trap as shown in Fig. 13.2.1 below. If the total energy E is above the left hand and right hand potentials V'' and V , ($E > V > V''$) as shown in part (a), then waves can propagate across the system. If the total energy E is above the left hand potential V'' but below the right hand potential V , ($V > E > V''$) as shown in part (b), then waves will reflect from barrier V at $x=a$ and barrier V contains only evanescent (exponential) waves. If the total energy E is below both the left hand potential V'' and the right hand potential V , ($V > V'' > E$) as shown in part (c), the system will have a *trapped* or *bound state* in the region between $x=0$ and $x=a$ and evanescent waves with energy under the barriers on either side.

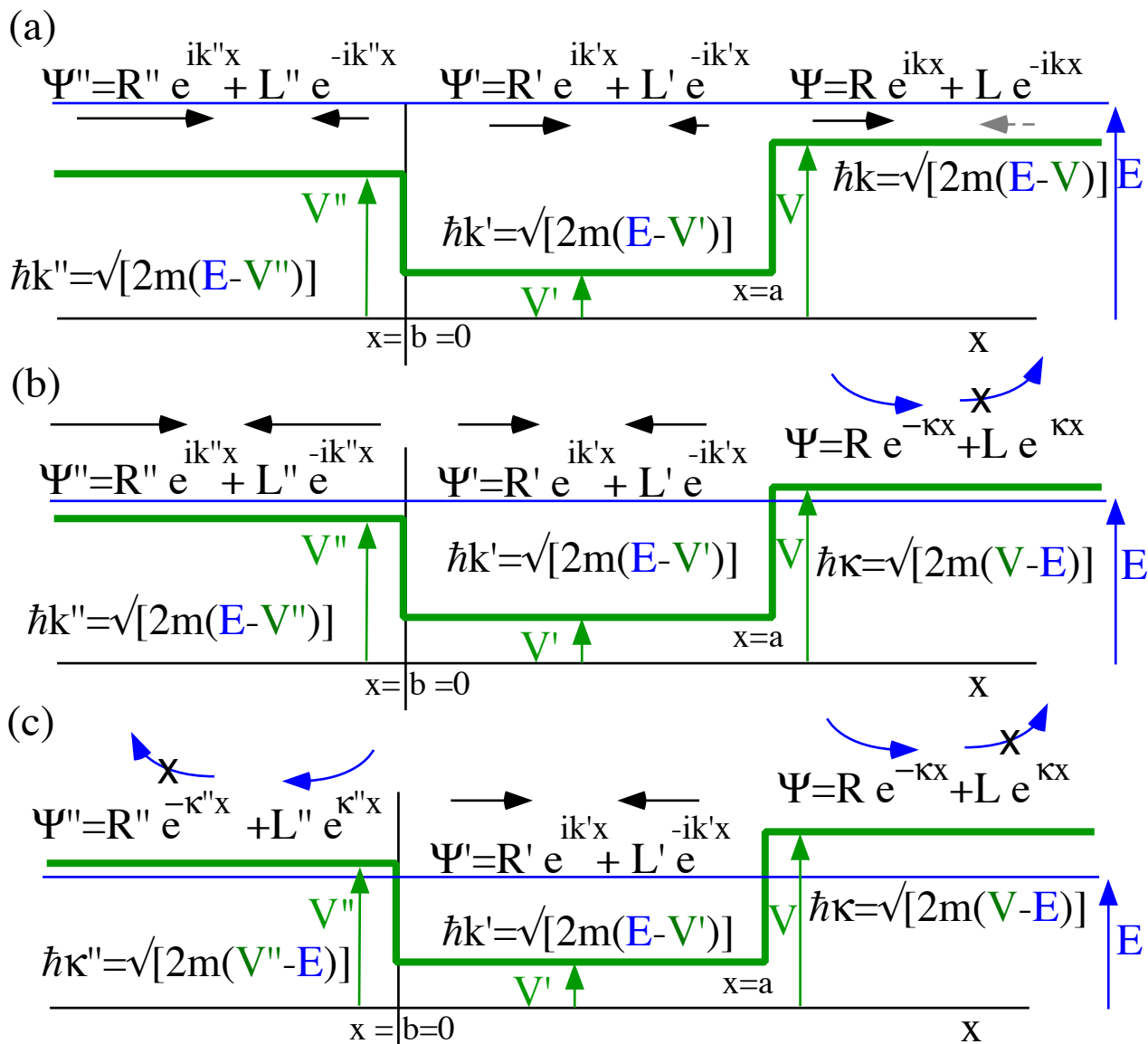


Fig. 13.2.1 Quantum well with energy E (a) above both barriers, (b) below one, and (c) below both..

The double barrier crossing matrix (13.1.25a) is valid for all three cases depicted in Fig. 13.2.1 if, for evanescent (non-classical) cases, we write k in terms of exponential extinction factors κ as follows.

$$k \rightarrow i\kappa, \quad ik \rightarrow -\kappa, \quad -ik \rightarrow \kappa,$$

$$\text{where: } \hbar k = \sqrt{[2m(E-V)]}, \text{ and } \hbar \kappa = \sqrt{[2m(V-E)]}, \quad (13.2.1)$$

This is necessary whenever the potential V exceeds the total energy E . If the right barrier extends to $+\infty$ then an exploding exponential $Le^{\kappa x}$ cannot exist and we must have $L=0$ in Fig. 13.2.1 b and c. Similarly, if the left barrier extends to $-\infty$ then the exponential $R''e^{-\kappa x}$ in Fig. 13.2.1c blows up unless $R''=0$.

The transmission function (13.1.25e) should then also blow up if R'' goes to zero.

$$T = \frac{k}{k''} \left| \frac{R}{R''} \right|^2 = \frac{4}{\left| \frac{k''}{k} \left[\left(1 + \frac{k}{k''} \right) \cos k'a - i \left(\frac{k'}{k''} + \frac{k}{k'} \right) \sin k'a \right] \right|^2} \rightarrow \infty, \text{ if: } R'' \rightarrow 0 \quad (13.2.2)$$

We shall use this shortly to help derive quantum well quantization conditions. We now derive transmission functions for two cases which have C_2 reflection symmetry, that is ($V=V''$), or depending on the case: ($k=k''$) or ($\kappa=\kappa''$). In the first case the energy E is above the potential top V and we have from (13.1.25e)

$$T = \left| \frac{R}{R''} \right|^2 = \frac{1}{\cos^2 k'a + \frac{(k^2 + k'^2)^2}{4k^2 k'^2} \sin^2 k'a} = \frac{1}{1 + \frac{(k^2 - k'^2)^2}{4k^2 k'^2} \sin^2 k'a}, \quad (13.2.3a)$$

where wavevectors k' and k are given in terms of energy $E = \varepsilon \frac{\hbar^2}{m}$ and potential-top $V = v \frac{\hbar^2}{m}$.

$$k' = \sqrt{\frac{2Em}{\hbar^2}} = \sqrt{2\varepsilon}, \quad k'' = k = \sqrt{\frac{2(E-V)m}{\hbar^2}} = \sqrt{2(\varepsilon - v)}, \quad k'^2 - k^2 = \sqrt{\frac{2Vm}{\hbar^2}} = \sqrt{2v} \quad (13.2.3b)$$

In the second case the energy E is below the potential-top V and we have from (13.2.1-27)

$$T = \frac{4}{\left| 2 \cos k'a - i \left(\frac{k'}{i\kappa} + \frac{i\kappa}{k'} \right) \sin k'a \right|^2} = \frac{1}{\left| \cos k'a - \frac{k'^2 - \kappa^2}{2k'\kappa} \sin k'a \right|^2}, \quad (13.2.4a)$$

where wavevector k' and extinction κ are given in terms of energy E and potential-top V as follows.

$$k' = \sqrt{\frac{2Em}{\hbar^2}} = \sqrt{2\varepsilon}, \quad \kappa'' = \kappa = \sqrt{\frac{2(V-E)m}{\hbar^2}} = \sqrt{2(v - \varepsilon)}, \quad k'^2 - \kappa^2 = 2(2\varepsilon - v) \quad (13.2.4b)$$

Below, in terms of energy, are two cases for a C_2 -square-well *inverse transmission function* $1/T$.

$$\text{The Bound Case: } E < V \quad (13.2.5a) \quad \text{The Free Case: } E > V \quad (13.2.5b)$$

$$\frac{1}{T} = \left| \cos \sqrt{2\varepsilon}a - \frac{(2\varepsilon - v)}{2\sqrt{\varepsilon(v - \varepsilon)}} \sin \sqrt{2\varepsilon}a \right|^2, \quad \frac{1}{T} = 1 + \frac{(v)^2}{4(\varepsilon - v)\varepsilon} \sin^2 \sqrt{2\varepsilon}a,$$



In Fig. 13.2.2 these two T -functions and their inverses $1/T$ are plotted versus rationalized energy ε for the bound-case (13.2.5a) on the left and the free case (13.2.5b) on the right. (The E in the figure is in units of m/\hbar^2) The plot of $T(E)$ has two 100% ($T=1$) transmission maxima on the right hand (free) side and four infinite ($T=\infty$) maxima on the left hand (bound) side. The transmission maxima are like the

resonance-peaks pointed out in Fig. 13.1.6, and like the ones there, they are the beginning of an infinite sequence that grows weaker as energy E becomes much larger than V . The infinities or poles of $T(E)$ represent *bound*-or *quantized-states* and, for this case ($V=8.23$, $a=3.05$), there are exactly four of these singular energy values. The energy values are located by the zeros of the inverse ($1/T$)-function

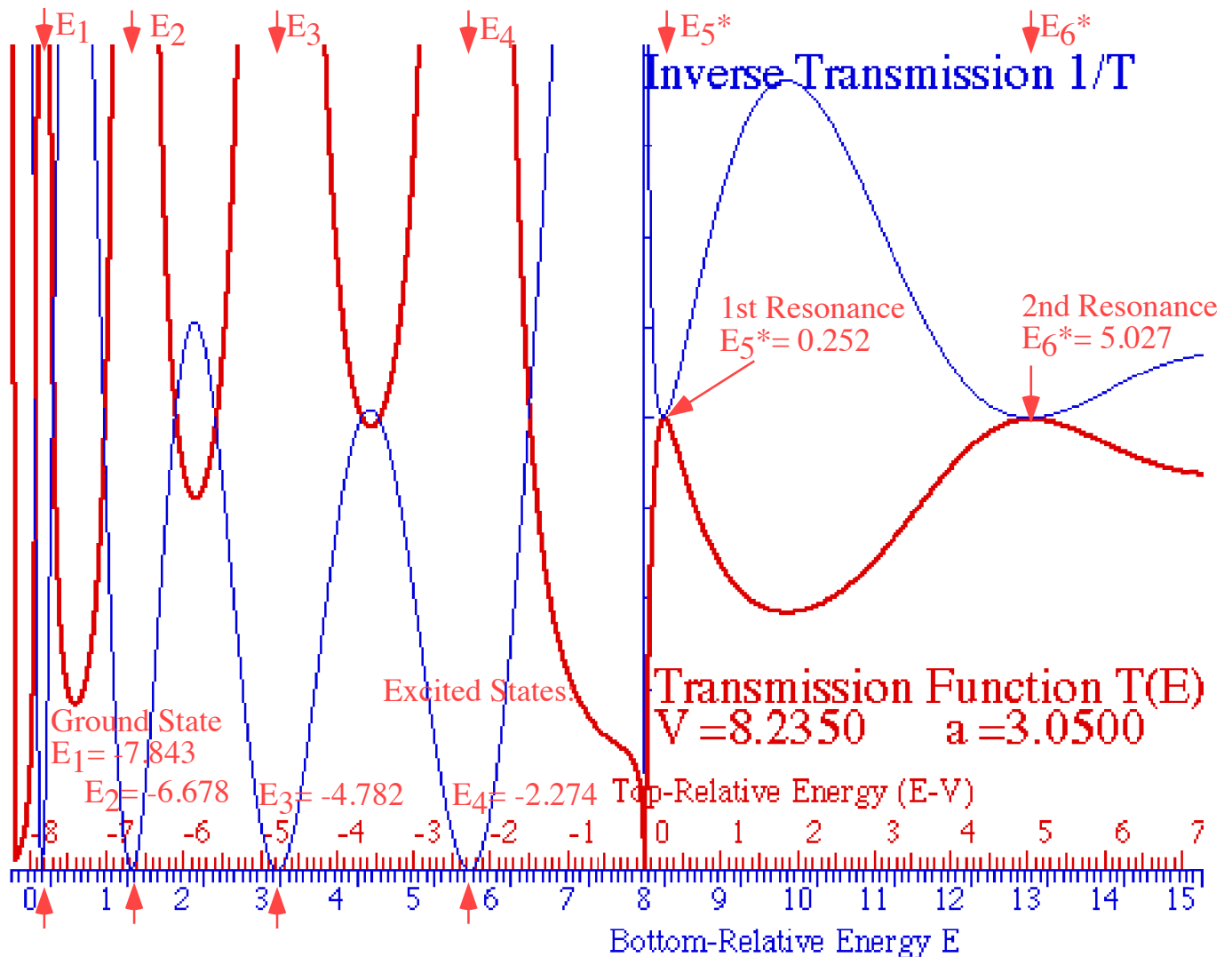


Fig. 13.2.2 C_2 -Quantum well T and $1/T$ functions of energy E for bound ($E < V$) and free ($E > V$) states..

The four bound state eigenfunctions plotted in Fig. 13.2.3a-d compare to the first eigenfunctions $\sin k_n x$ of the infinite square well shown in Figs. 12.1.1. T -functions of Fig. 13.2.2 are on the left of Fig. 13.2.3.

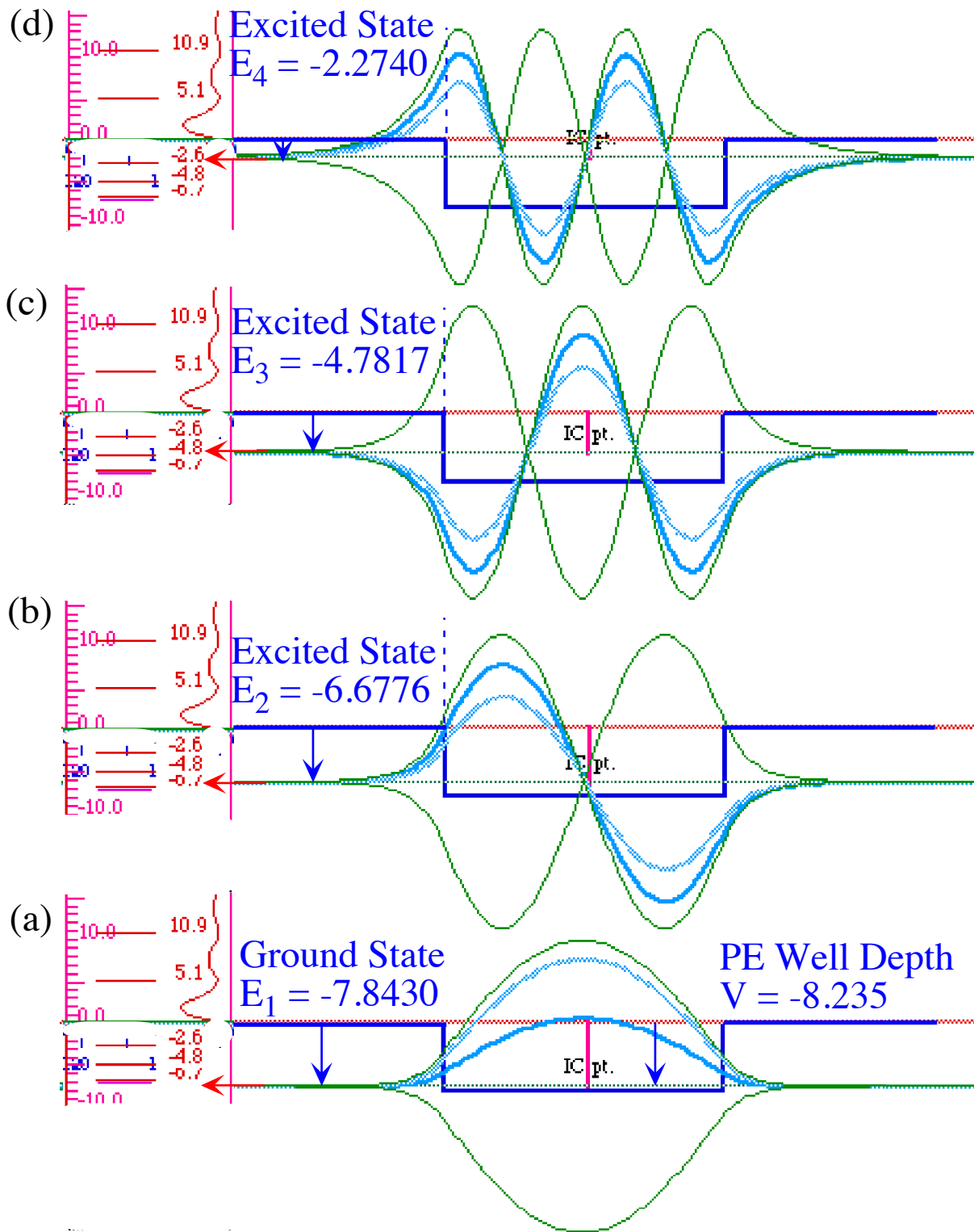


Fig. 13.2.3 C_2 -Quantum well T functions and energy eigenfunctions $|E\rangle$ for bound states ($E_j < V$)

As E_k increases, the wave intrudes or “tunnels” more into the non-classical regions of the barrier where the evanescent or exponential “tails” are seen wagging at the angular frequency $\omega_k = E_k/\hbar$.

(a) Ramsauer-Townsend resonances ($E > 0$)

The infinite square well allowed absolutely no evanescent wave function to "sneak" or "tunnel" into the potential barrier, but a finite V permits more and more tunneling as $(V-E)$ approaches zero. Finally, as the energy exceeds the barrier-top virtually all the wavefunction appears outside the potential-well as shown in the first two resonance states plotted in Fig. 13.2.4. (Once prisoner-M gets above the barrier, he's outa' here. Free! Thank God, free at last!) The resonances shown in Fig. 13.2.4 below are different than the ones associated with barriers that were displayed in Fig. 13.1.7. In the latter, the probability "piled up" on the barrier top since the particle slows down while passing over it. In contrast, the resonance waves in Fig. 13.2.4 below have less probability per unit distance to be found in the well than outside since they speed up inside. Such effects are called *Ramsauer-Townsend* resonances to distinguish a purely kinetic transmission enhancement from *barrier trapping* that we will study shortly.

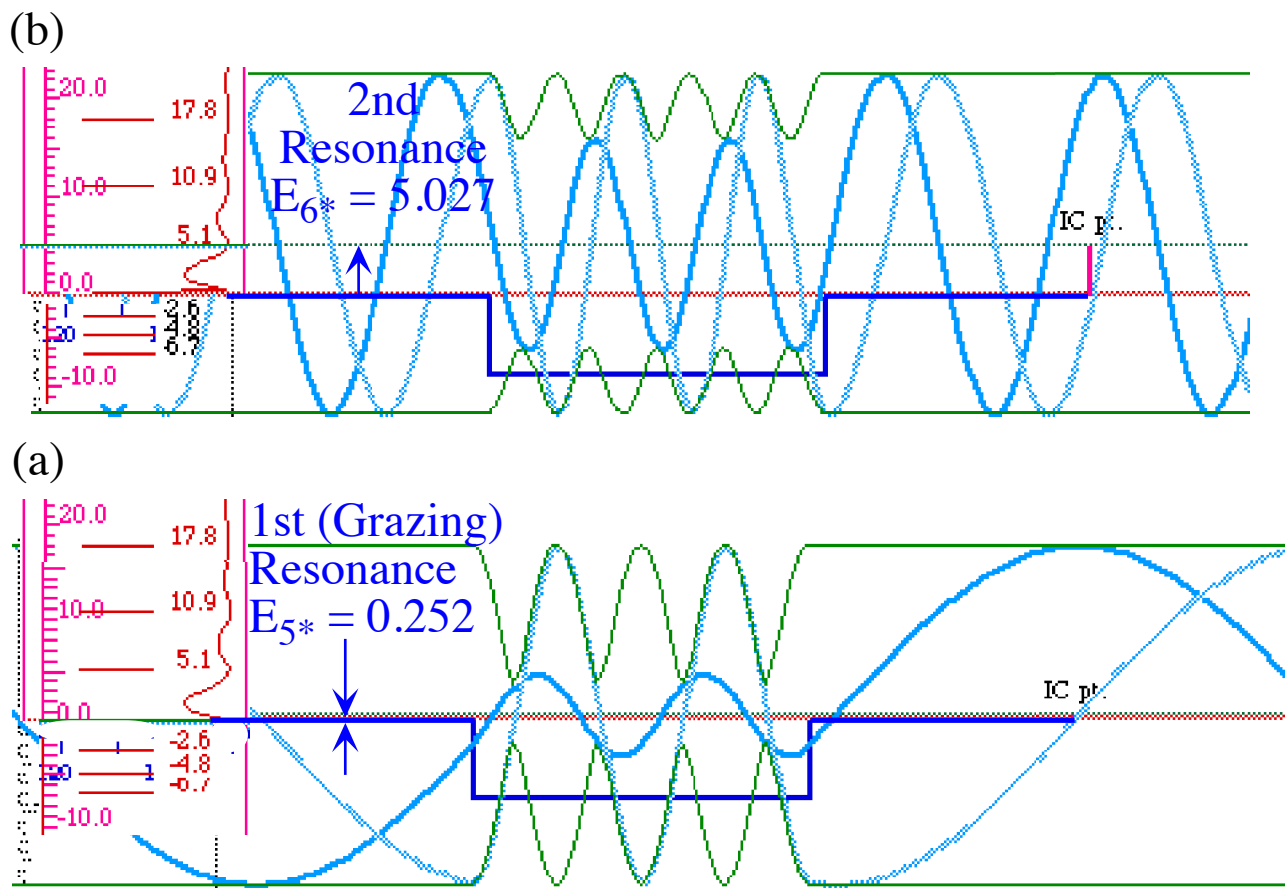


Fig. 13.2.4 C_2 -Quantum well T functions and energy eigenfunctions $|E\rangle$ for resonant free states ($E_j > V$)

For systems with bound states one often measures energy down from the potential-top rather than up from its bottom. This is done in Fig. 13.2.2 and the two which follow it. The two energy scales are compared along the bottom of Fig. 13.2.2. Top-relative energy is not possible for the infinite square well which has no top, nor is bottom-relative energy possible for a Coulomb potential $V = -k/r$ which has no bottom. Then, as here, the energy zero is taken to be at the top which is the potential V at $r = \infty$.

Nearly-grazing states ($E \sim 0$)

If we use a top-relative energy scale with $V(\infty)=0$, then *bound states* are those with negative energy eigenvalues ($E < 0$), while *free states* are those which have positive energy values ($E > 0$). At the boundary between these two sets lies a curious zero-measure set of *grazing states* with exactly zero energy ($E = 0$). The resonance wave with $E_{5^*} = 0.252$ in Fig. 13.2.4a is nearly grazing; it is within 0.252 of being exactly grazing. Near-grazing states are characterized by extreme sensitivity of the transmission function to the potential barrier V or the particle energy E . Note the extreme slope of $T(E)$ between the resonance value E_{5^*} and the value $E = 0$. For $E_{5^*} < 0$, state $|E_{5^*}\rangle$ becomes a bound state with infinite E -sensitivity of T .

However, another word of caution should be said about anything that uses the word infinite since we have already seen some of the pitfalls associated with having blind faith in the ability of calculus to describe quantum physics. If a state is truly and exactly bound then you are prohibited from touching or seeing any part of it; it may as well not exist at all. Perhaps, this is the quantum version of the (pseudo-) philosophical (quasi-) concept of the "tree falling in the (unoccupied) forest." Only, unlike that poorly formed idea, we know the answer to this one: an exactly bound state, by definition, cannot communicate at all with the outside world since infinite T means zero for the ratio between $\Psi(\text{outside})$ and $\Psi(\text{inside})$.

Also, some extra care is needed to understand grazing states and even more to produce or apply them in a laboratory. We noted that square-well walls cannot be infinitely sharp, and neither can ordinary atomic matter make perfectly flat tops. And, even if perfectly flat potential-top is made it still requires infinite precision in energy to produce an exactly grazing wave like the flat pendulum wave in Fig. 11.5.4b or the wave in Fig. 13.1.4a. Such a wave means a particle with exactly zero kinetic energy must put itself with equal probability everywhere in a vast ($V-E=0$) region. Such an incredibly symmetric situation is just as incredibly sensitive to any of the many tiny perturbations which we ignore here but would be present in a laboratory experiment attempting such a state. It is like a tennis court that seems perfectly flat to the players but appears randomly flawed to rainwater that puddles hither and yon. The best we can hope for is to cleverly exploit the large (but probably not infinite) sensitivity of nearly (but probably not perfectly) grazing states ability to transmit information.

(b) Bound state quantization ($E < 0$): The sine-line solution

We noted that the bound-state eigenvalues occur at the infinite poles of the transmission function $T(E)$ or at the zeros of the inverse I/T function. From (13.2.5a) this is the same as requiring

$$\cos\sqrt{2\varepsilon}a + \frac{(2\varepsilon - v)}{2\sqrt{\varepsilon(v - \varepsilon)}} \sin\sqrt{2\varepsilon}a = 0, \quad \text{or:} \quad \tan\sqrt{2\varepsilon}a = \frac{2\sqrt{\varepsilon(v - \varepsilon)}}{(v - 2\varepsilon)} \quad (13.2.6)$$

Or else we can use the wavevector-dependent equation (13.2.4a) to find zeros of I/T .

$$\tan k'a = \frac{2k'\kappa}{(k'^2 - \kappa^2)} \quad (13.2.7)$$

This is the form that is solved graphically in many texts. However, it is fairly clumsy and fails to provide much beyond the desired energy values. There is an easier and simpler solution based partly on C_2 symmetry which more quickly provides eigenvalues and exposes some other things, as well.

The presence of C_2 reflection symmetry around $x=a/2$ means that the reflection operation σ commutes with Hamiltonian \mathbf{H} and so \mathbf{H} eigenkets $|\epsilon_n\rangle$ are eigenkets of σ , too, with (+1) or (-1) eigenvalues since $\sigma^2 = \mathbf{1}$. (Recall: C_2 symmetry was used to help find eigensolutions (10.2.6a-c) in Ch. 10.)

$$\sigma|\epsilon_{n^+}\rangle = (+1)|\epsilon_{n^+}\rangle \text{ for } n^+=1,3,5, \dots; \sigma|\epsilon_{n^-}\rangle = (-1)|\epsilon_{n^-}\rangle \text{ for } n^-=2,4,6, \dots \quad (13.2.8)$$

So, the eigenfunctions in Fig. 13.2.3 are symmetric for E_1 and E_3 but anti symmetric for E_2 and E_4 .

$$\langle x | \sigma |\epsilon_{n^+}\rangle = \langle a-x | \epsilon_{n^+}\rangle = (+1)\langle x | \epsilon_{n^+}\rangle \quad ; \quad \langle x | \sigma |\epsilon_{n^-}\rangle = \langle a-x | \epsilon_{n^-}\rangle = (-1)\langle x | \epsilon_{n^-}\rangle \quad (13.2.8a)$$

$$\sigma\Psi_{n^+}(x) = \Psi_{n^+}(a-x) = (+1)\Psi_{n^+}(x) \quad ; \quad \sigma\Psi_{n^-}(x) = \Psi_{n^-}(a-x) = (-1)\Psi_{n^-}(x) \quad (13.2.8b)$$

The right hand ($x=a$)-wall wave $\Psi_{n^\pm}(a)$ is (\pm) the left hand ($x=0$)-wall wave $\Psi_{n^\pm}(0)$. The dead-center wave $\Psi_{n^\pm}(a/2)$ is a zero-node for $n^-=2,4, \dots$ or an anti-node for $n^+=1,3, \dots$ as seen in the Fig. 13.2.3.

$$\Psi_{n^\pm}(0) = \pm\Psi_{n^\pm}(a) \quad \text{and} \quad \Psi_{n^\pm}(a/2) = \pm\Psi_{n^\pm}(a/2) \quad (13.2.8c)$$

To complete the analysis for the C_2 -well we notice that the wavefunctions in the wells all have the form of sine waves $\sin(kx+\delta)$ that are shifted by some amount δ to the left as sketched in Fig. 13.2.5.

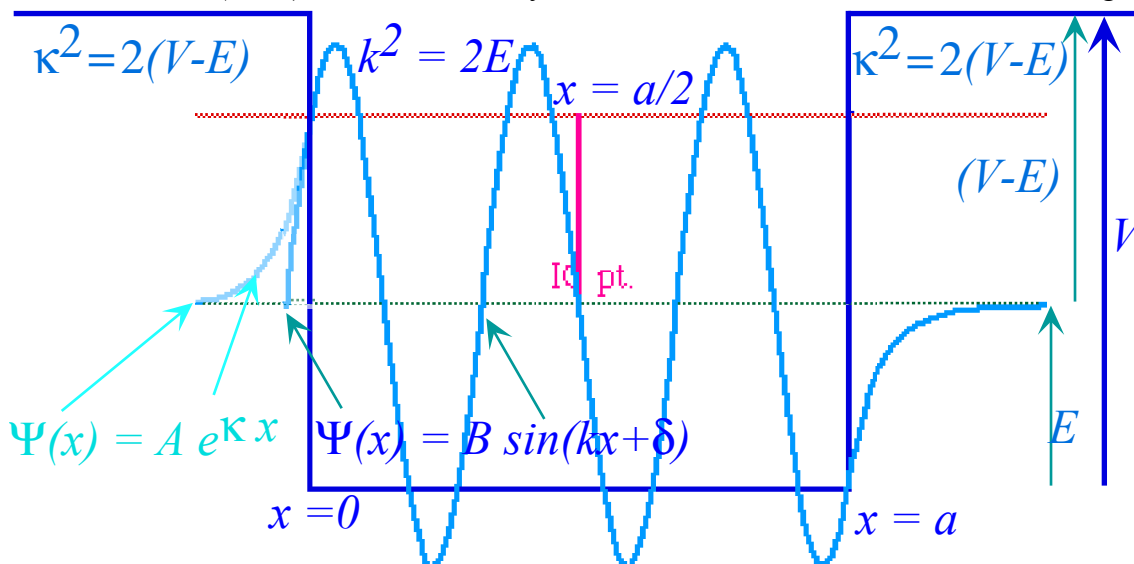


Fig. 13.2.5 C_2 -Quantum well energy eigenfunctions for typical bound state (E and V in units of \hbar^2/m)

The δ -shifted-sine wave has (\pm)-equal amplitudes at the walls $x=0$ and $x=a$ by (13.2.8c)

$$A e^{k\cdot 0} = B \sin(k\cdot 0 + \delta) = \pm B \sin(k a + \delta) \quad ,$$

$$\text{or :} \quad A = B \sin \delta = \pm B \sin(k a + \delta) \quad , \quad \text{and:} \quad \sin \delta = \pm \sin(k a + \delta) \quad (13.2.9a)$$

A similar (\pm) relation holds of the derivatives of Ψ at the walls, except (\pm) becomes $-(\pm)$.

$$A \kappa e^{k\cdot 0} = B k \cos(k\cdot 0 + \delta) = -\pm B k \cos(k a + \delta)$$

$$\text{or :} \quad A \kappa = B k \cos \delta \quad , \quad \text{and:} \quad \kappa \sin \delta = k \cos \delta = -\pm k \cos(k a + \delta) \quad (13.2.9b)$$

Squaring the relation ($\kappa \sin \delta = k \cos \delta$) and using $k^2 = 2E$ and $\kappa^2 = 2(V-E)$ gives

$$\kappa^2 \sin^2 \delta = k^2 \cos^2 \delta \text{ or: } k^2 = (k^2 + \kappa^2) \sin^2 \delta = 2V \sin^2 \delta \quad (13.2.9c)$$

The relations (13.2.9a-b) reduce to linear $k - \delta$ relations which are plotted as 45° lines in Fig. 13.2.6.

$$k a + \delta = n \pi - \delta, \text{ or: } k a/2 = n \pi/2 - \delta \quad (n = 1, 2, 3, \dots) \quad (13.2.9d)$$

The 45° lines are plotted on top of a sine curve that represents (13.2.9c). Circles enclose intersections.

$$k a/2 = a/2 \sqrt{(2V)} \sin \delta \quad (13.2.9d)$$

Intersections provide quantized values for wavevector k (and energy $E = k^2/2 - V$), exponential extinction factor κ , and the sine wave phase shift δ . To recover mks units, put m/\hbar^2 on V and E .

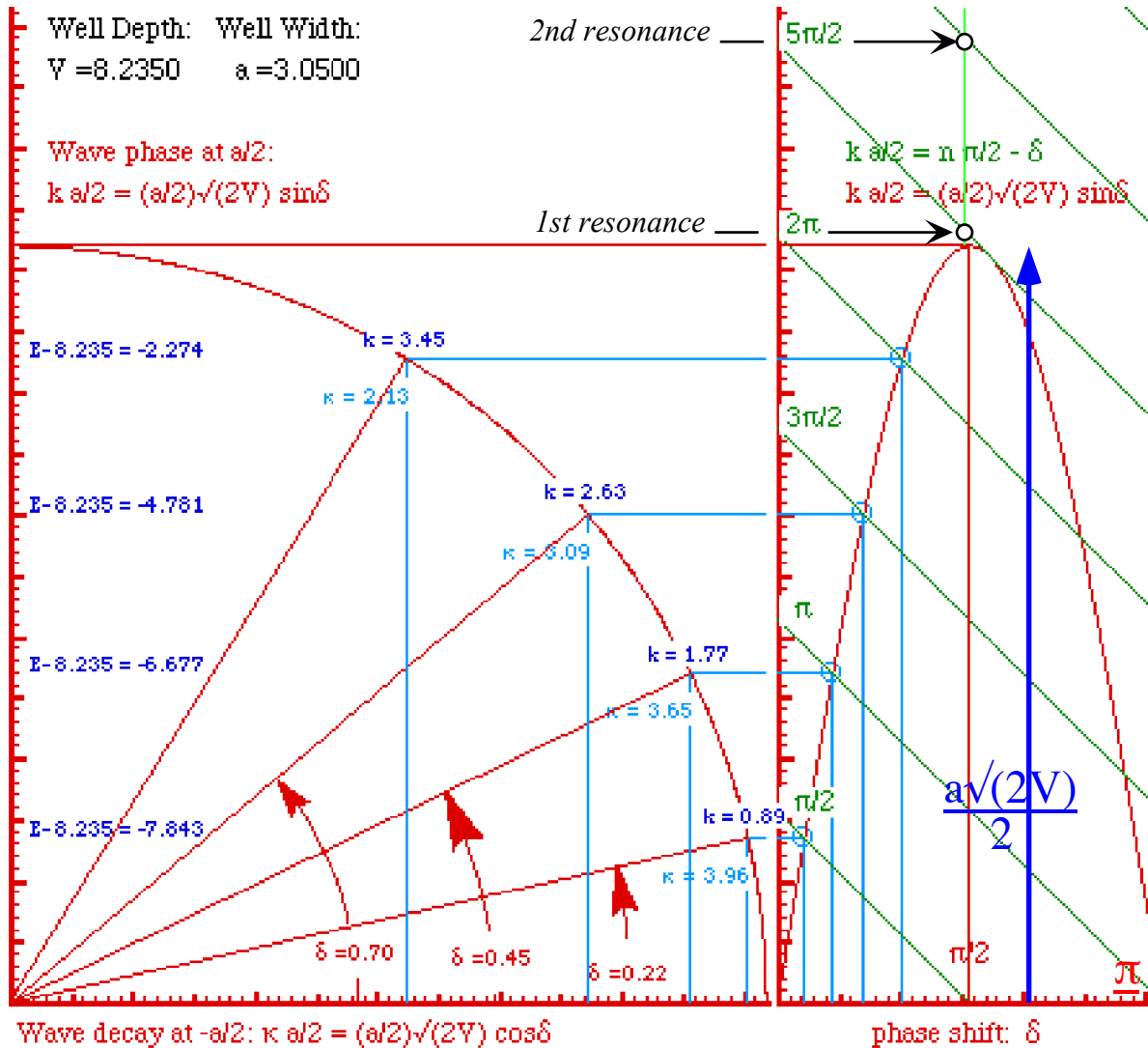


Fig. 13.2.6 C_2 -Quantum well eigenvalues obtained graphically by lines and sine in $(ka/2$ vs. $\delta)$ plot.

This solution also shows part of the sine eigenfunction as well as the eigenvalues. Each $\delta = \text{const.}$ intersection represents the precise position of the actual sine wavefunction with respect to the potential wall at $x=0$ or $x=a$. Compare the four intersections in Fig. 13.2.6 to the actual intersections of the wall and the sine waves in Fig. 13.2.3.

Also note that the quantity $ka/2$, which is the vertical axis in Fig. 13.2.6, is the wave phase of the sine wave at $x = a/2$ in the center of the well if it had started at the barrier $x=0$ instead of inside the barrier at $x = -k/\delta$ to the left. For example, for the ground state level $E_{1+} = -7.843$, the phase is $ka/2 = 1.36$ which

is a little below the infinite square well value of $\pi/2 = 1.57$. However, for the fourth level $E_{4-} = -2.274$, the phase is $ka/2 = 5.26$ which is way below the infinite square well value of $2\pi = 6.28$.

Finally, the quantity $\kappa a/2$, which is the horizontal axis for the circle plot on the left in Fig. 13.2.6, is the wave decay of the evanescent wave at $x = -a/2$ to the left of the wall. For example, for the ground state level $E_{1+} = -7.843$, the decay exponent is $\kappa a/2 = 3.96 \cdot 3.05/2 = 6.0$. It helps to use the "5% mnemonic" ($e^{-3} \sim 0.05$). This wave is reduced to 5% in half of the distance $a/2$. In contrast, for the fourth level $E_{4+} = -7.843$, the decay exponent is $\kappa a/2 = 2.13 \cdot 3.05/2 = 3.2$. This wave is reduced to 5% in roughly the distance $a/2$. This may be verified by looking at the waves in Fig. 13.2.3.

Continuum meets "discreteum"

The square well is a peculiar quantum system in that an infinite free-continuum meets a very limited bound "discreteum" at $E=0$. The differences between the free ($E>0$) and bound ($E<0$) states could hardly be more pronounced. Each energy level of the free continuum is associated with a two-state $U(2)$ degeneracy which allows any type of standing, moving, or galloping wave shown in Fig. 3.2.1. (Recall also Ch. 2-Sec. 2.9-10.) However the discrete levels for bound states are each restricted to be a single standing sine wave which wags two evanescent tails. The free waves can carry steady current and (with arbitrarily small bandwidth) transmit information from either side to the other. In contrast, the discrete waves are strictly stationary and prevented from any communication with the outside world.

We should, at this point note something else about the continuum resonances. All the resonances, that is all the peaks of the $(E>0)-T(E)$ function, belong to waves with precisely an integral number of half-waves in the well region ($0<x<a$). In other words, the resonant sine waves all have a phase shift δ relative to the wall that is exactly a multiple of $\pi/2$. The two circles on the $\delta=\pi/2$ axis above the sine curve in Fig. 13.2.6 mark the $ka/2$ values of exactly 2π and $5\pi/2$, respectively, for the first two resonances shown in Fig. 13.2.4. In contrast, the four bound state circles on the sine curve below $E=0$ fall away from integral half-wave values because of bound state barrier penetration and related non-zero values of phase shift δ which are confined to the range ($0<\delta<\pi/2$).

So it is, perhaps, understandable why grazing resonant waves ($E\sim 0$) lying just above the boundary between these two archetypes are so sensitive. A slight increase in the potential V in Fig. 13.2.6 will "capture" the first resonance into a fifth bound state. It won't go back to jail without a fuss!

13.3 S-Matrix approach to free state resonance dynamics

Another approach to wave dynamics complements the usual crossing matrix or C -matrix with the so-called *scattering or S-matrix*. One advantage of this is that the S -matrix generally is unitary so the $U(2)$ description introduced in Chapter 10 can be applied.

A comparison of C -matrix and S -matrix relations is given first. We imagine a "black-box" representing a general potential region and suppose that we need to connect the free wave functions $\Psi_2(x)|_{x=a_2}$ and $\Psi_1(x)|_{x=a_1}$ on the left and right hand sides ($x=a_2$) and ($x=a_1$) of the region.

$$\begin{aligned} \Psi_2(x_{\leq a_2}) &= L_2(a_2) e^{-ik_2x} + R_2(a_2) e^{ik_2x}, & \Psi_1(x_{\geq a_1}) &= L_1(a_1) e^{-ik_1x} + R_1(a_1) e^{ik_1x}, \\ &= I_2^L / \sqrt{k_2} e^{-ik_2x} + I_2^R / \sqrt{k_2} e^{ik_2x}, & &= I_1^L / \sqrt{k_1} e^{-ik_1x} + I_1^R / \sqrt{k_1} e^{ik_1x}. \end{aligned} \quad (13.3.1a)$$

Wavevector-normalized amplitudes proportional to (13.1.15) are defined at ($x=a_1$) and ($x=a_2$).

$$I_2^L = L_2(a_2)\sqrt{k_2}, \quad I_2^R = R_2(a_2)\sqrt{k_2}, \quad I_1^L = L_1(a_1)\sqrt{k_1}, \quad I_1^R = R_1(a_1)\sqrt{k_1}. \quad (13.3.1b)$$

We look at two kinds of relations between amplitudes $\{I_1^L, I_1^R, I_2^L, I_2^R\}$. The first is a C -matrix relation like (13.1.10) shown on the left below, and the second is an S -matrix relation shown on the right.

$$\begin{pmatrix} I_2^R \\ I_2^L \end{pmatrix} = \begin{pmatrix} C_{11} & C_{12} \\ C_{21} & C_{22} \end{pmatrix} \begin{pmatrix} I_1^R \\ I_1^L \end{pmatrix}, \quad (13.3.2a) \quad \begin{pmatrix} I_1^R \\ I_2^L \end{pmatrix} = \begin{pmatrix} S_{11} & S_{12} \\ S_{21} & S_{22} \end{pmatrix} \begin{pmatrix} I_1^L \\ I_2^R \end{pmatrix}, \quad (13.3.2b)$$

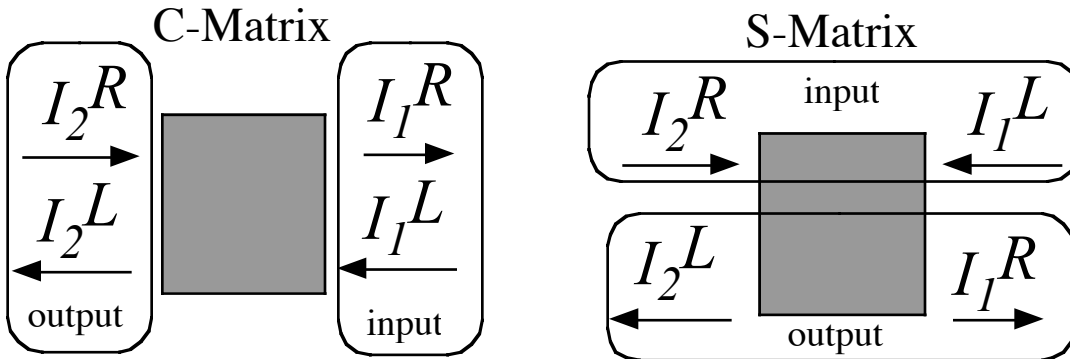


Fig. 13.3.1 Comparison of current relations for (a) C -Matrix, and (b) S -Matrix.

The C -matrix relates amplitudes on left side to those on the right side. The S -matrix relates amplitudes of *incoming waves* to amplitudes of *outgoing waves* relative to the potential region.

The *fundamental C-matrix* for a single potential jump at $x=a$ is given below. It is based upon (13.1.10), only now we include the \sqrt{k} -normalization defined by (13.3.1).

$$\begin{pmatrix} I_2^R \\ I_2^L \end{pmatrix} = \frac{1}{2\sqrt{k_1 k_2}} \begin{pmatrix} (k_2 + k_1) e^{-i(k_2 - k_1)a} & (k_2 - k_1) e^{-i(k_1 + k_2)a} \\ (k_2 - k_1) e^{i(k_1 + k_2)a} & (k_2 + k_1) e^{i(k_2 - k_1)a} \end{pmatrix} \begin{pmatrix} I_1^R \\ I_1^L \end{pmatrix} \quad (13.3.3a)$$

Our shorthand notation for the fundamental C -matrix is as follows.

$$\begin{pmatrix} I_2^R \\ I_2^L \end{pmatrix} = \begin{pmatrix} C_{11} & C_{12} \\ C_{21} & C_{22} \end{pmatrix} \begin{pmatrix} I_1^R \\ I_1^L \end{pmatrix} = \frac{1}{\Pi} \begin{pmatrix} \Sigma e^{-i\Delta a} & \Delta e^{-i\Sigma a} \\ \Delta e^{i\Sigma a} & \Sigma e^{i\Delta a} \end{pmatrix} \begin{pmatrix} I_1^R \\ I_1^L \end{pmatrix} \quad (13.3.3b)$$

where sum: $\Sigma = k_2 + k_1$, difference: $\Delta = k_2 - k_1$, and product: $\Pi = 2\sqrt{(k_2 k_1)}$ satisfy the identities

$$\Sigma^2 - \Delta^2 = \Pi^2, \quad \text{or: } \Sigma^2 = \Delta^2 + \Pi^2. \quad (13.3.3c)$$

This guarantees that the fundamental C -matrix and all those built from C -products are *unimodular*.

$$\det C = I \quad (13.3.3d)$$

As we have seen in (13.1.24) and (13.1.25) the C -matrix for more complicated potentials is a matrix product of fundamental C -matrices. The determinant product identity ($(\det C)(\det C') = \det(C C')$) means all such crossing matrices are unimodular, too. The same is true for the inverse C -matrix

$$\begin{pmatrix} C_{11} & C_{12} \\ C_{21} & C_{22} \end{pmatrix}^{-1} = \begin{pmatrix} C_{11}^{-1} & C_{12}^{-1} \\ C_{21}^{-1} & C_{22}^{-1} \end{pmatrix} = \begin{pmatrix} C_{22} & -C_{12} \\ -C_{21} & C_{11} \end{pmatrix} = \frac{1}{\Pi} \begin{pmatrix} \Sigma e^{i\Delta a} & -\Delta e^{-i\Sigma a} \\ -\Delta e^{i\Sigma a} & \Sigma e^{-i\Delta a} \end{pmatrix} \quad (13.3.4)$$

Note that the C -matrix is generally not unitary. Unitarity is a property of the S -matrix as we'll see next.

(a) Relating S -Matrix and C -matrix

The S -matrix may be derived by using the C -matrix and its inverse to make the S -matrix relations in (13.3.2b). The first of these is treated as follows.

$$\begin{aligned} I_1^R &= C_{11}^{-1} I_2^R + C_{12}^{-1} I_2^L = C_{12}^{-1} (C_{21} I_1^R + C_{22} I_1^L) + C_{11}^{-1} I_2^R \\ (1 - C_{12}^{-1} C_{21}) I_1^R &= C_{12}^{-1} C_{22} I_1^L + C_{11}^{-1} I_2^R \end{aligned}$$

The unit C -determinant (13.3.3d) and the C -inverse (13.3.4) is then used.

$$I_1^R = \frac{C_{12}^{-1} C_{22} I_1^L + C_{11}^{-1} I_2^R}{(1 + C_{12} C_{21})} = \frac{-C_{12} C_{22} I_1^L + C_{22} I_2^R}{C_{11} C_{22}} = -\frac{C_{12}}{C_{11}} I_1^L + \frac{1}{C_{11}} I_2^R$$

The result is the first row of the S -matrix in terms of C_{ij} 's. Continuing in this way gives conversion formulas for both S and its transpose conjugate S^\dagger . Note the symmetry ($S_{ij} = S_{ji}$) of both S and S^\dagger .

$$\begin{pmatrix} S_{11} = -\frac{C_{12}}{C_{11}} & S_{12} = \frac{1}{C_{11}} \\ S_{21} = \frac{1}{C_{11}} & S_{22} = \frac{C_{21}}{C_{11}} \end{pmatrix} \quad (13.3.5a) \quad \begin{pmatrix} S_{11} & S_{12} \\ S_{21} & S_{22} \end{pmatrix}^{-1} = \begin{pmatrix} S_{11}^\dagger = -\frac{C_{21}}{C_{22}} & S_{12}^\dagger = \frac{1}{C_{22}} \\ S_{21}^\dagger = \frac{1}{C_{22}} & S_{22}^\dagger = \frac{C_{12}}{C_{22}} \end{pmatrix} = \begin{pmatrix} S_{11}^* & S_{21}^* \\ S_{12}^* & S_{22}^* \end{pmatrix} \quad (13.3.5b)$$

Also, note that complex conjugation of C_{ij} 's simply interchanges 1's and 2's. The inverse conversion is

$$\begin{pmatrix} C_{11} = \frac{1}{S_{12}} & C_{12} = \frac{-S_{11}}{S_{12}} \\ C_{21} = \frac{S_{22}}{S_{12}} & C_{22} = \frac{1}{S_{12}^*} \end{pmatrix} \quad (13.3.5c) \quad \begin{pmatrix} C_{11} & C_{12} \\ C_{21} & C_{22} \end{pmatrix}^{-1} = \begin{pmatrix} C_{22} = \frac{1}{S_{12}^*} & -C_{12} = \frac{S_{11}}{S_{12}} \\ -C_{21} = \frac{-S_{22}}{S_{12}} & C_{11} = \frac{1}{S_{12}} \end{pmatrix} = \begin{pmatrix} \frac{1}{S_{21}^*} & \frac{S_{22}^*}{S_{12}^*} \\ \frac{S_{11}^*}{S_{12}^*} & \frac{1}{S_{21}} \end{pmatrix} \quad (13.3.5d)$$

The fact that S is unitary ($S^\dagger S = I$) is a general result of choosing the k -normalization so that current conservation (13.1.15b) can also be written as an absolute value sum like probability conservation.

$$j_R - j_L = |I_1^R|^2 - |I_1^L|^2 = |I_2^R|^2 - |I_2^L|^2 \Rightarrow j_{OUT} = |I_1^R|^2 + |I_2^L|^2 = |I_2^R|^2 + |I_1^L|^2 = j_{IN} \quad (13.3.5e)$$

In other words, the sum of the incoming current must equal the sum of the outgoing. While the C -matrix conserves a difference of squares, the S -matrix conserves a (different) sum., but the two are equivalent.

(b) S-Matrix and C-matrix for elementary barrier: U(2) Formulation

The C-matrix and S-matrix for an elementary barrier follow from (13.3.3b) and (13.3.5a-b).

$$\begin{pmatrix} C_{11} & C_{12} \\ C_{21} & C_{22} \end{pmatrix} = \begin{pmatrix} \frac{\Sigma}{\Pi} e^{-i\Delta a} & \frac{\Delta}{\Pi} e^{-i\Sigma a} \\ \frac{\Delta}{\Pi} e^{i\Sigma a} & \frac{\Sigma}{\Pi} e^{i\Delta a} \end{pmatrix}, \text{ where: } \begin{matrix} \Sigma = k_2 + k_1 \\ \Delta = k_2 - k_1 \\ \Pi = 2\sqrt{k_2 k_1} \end{matrix}, \quad (13.3.6a)$$

$$\begin{pmatrix} S_{11} & S_{12} \\ S_{21} & S_{22} \end{pmatrix} = \begin{pmatrix} \frac{-\Delta}{\Sigma} e^{-i(\Sigma-\Delta)a} & \frac{\Pi}{\Sigma} e^{i\Delta a} \\ \frac{\Pi}{\Sigma} e^{i\Delta a} & \frac{\Delta}{\Sigma} e^{i(\Sigma+\Delta)a} \end{pmatrix} = e^{i\Delta a} \begin{pmatrix} \frac{-\Delta}{\Sigma} e^{-i\Sigma a} & \frac{\Pi}{\Sigma} \\ \frac{\Pi}{\Sigma} & \frac{\Delta}{\Sigma} e^{i\Sigma a} \end{pmatrix}$$

The C-matrix is unimodular (but not unitary) and the S-matrix is unitary (but not unimodular) because

$$\Sigma^2 = \Delta^2 + \Pi^2. \quad (13.3.6b)$$

The S-matrix determinant gives a phase factor.

$$\det S = -e^{i2\Delta a} \quad (13.3.7)$$

S is not unimodular unless $\Delta a = \pi/2$. For $\Delta a = 0$ it is *anti*-unimodular like a pure mirror-plane reflection. If the elementary barrier has no step ($\Delta = k_1 - k_2 = 0$) then S is a σ_X reflection and C to a unit matrix.

$$\begin{pmatrix} C_{11} & C_{12} \\ C_{21} & C_{22} \end{pmatrix} = \begin{pmatrix} 1 & 0 \\ 0 & 1 \end{pmatrix}, \text{ and: } \begin{pmatrix} S_{11} & S_{12} \\ S_{21} & S_{22} \end{pmatrix} = \begin{pmatrix} 0 & 1 \\ 1 & 0 \end{pmatrix} \text{ for: } \Delta = k_2 - k_1 = 0 \quad (13.3.8)$$

Following Chapter 10, the S-matrix is expanded into Hamilton-Pauli reflection operators σ_μ .

$$\begin{aligned} S &= e^{i\Delta a} \left[\mathbf{1} \left(i \frac{\Delta}{\Sigma} \sin \Sigma a \right) + \sigma_X \frac{\Pi}{\Sigma} + \sigma_Y \cdot 0 - \sigma_Z \frac{\Delta}{\Sigma} \cos \Sigma a \right] \\ &= ie^{i\Delta a} \left[\mathbf{1} \left(\frac{\Delta}{\Sigma} \sin \Sigma a \right) - i \left(\sigma_X \frac{\Pi}{\Sigma} - \sigma_Z \frac{\Delta}{\Sigma} \cos \Sigma a \right) \right] \end{aligned} \quad (13.3.9)$$

Without the overall phase $ie^{i\Delta a}$, the bracketed factor of S has the form of the SU(2) rotation (10.5.25b) or (10.5.25c) with $\varphi=0$. This rotation "crank" axis has only Θ_X and Θ_Z components and only polar angle ϑ .

$$\begin{aligned} \mathbf{R}[\varphi\vartheta\Theta] &= \begin{pmatrix} \cos \frac{\Theta}{2} - i\hat{\Theta}_Z \sin \frac{\Theta}{2} & -i\hat{\Theta}_X \sin \frac{\Theta}{2} \\ -i\hat{\Theta}_X \sin \frac{\Theta}{2} & \cos \frac{\Theta}{2} + i\hat{\Theta}_Z \sin \frac{\Theta}{2} \end{pmatrix}, \text{ where: } \begin{matrix} \hat{\Theta}_X = \sin \vartheta \\ \hat{\Theta}_Z = \cos \vartheta \end{matrix} \\ &= \mathbf{1} \cos \frac{\Theta}{2} - i \left(\sigma_X \hat{\Theta}_X \sin \frac{\Theta}{2} + \sigma_Z \hat{\Theta}_Z \sin \frac{\Theta}{2} \right) \end{aligned}$$

We relate the kinematic parameters Σ , Δ , and Π to rotation axis polar angle ϑ and angle Θ of rotation.

$$\begin{aligned} \frac{\Delta}{\Sigma} \sin \Sigma a = \cos \frac{\Theta}{2}, \quad \frac{\Pi}{\Sigma} = \hat{\Theta}_X \sin \frac{\Theta}{2}, \quad \frac{-\Delta}{\Sigma} \cos \Sigma a = \hat{\Theta}_Z \sin \frac{\Theta}{2} \\ = \sin \vartheta \sin \frac{\Theta}{2}, \quad = \cos \vartheta \sin \frac{\Theta}{2}. \end{aligned} \quad (13.3.10)$$

The eigenstates of $\mathbf{R}[\varphi\vartheta\Theta]$ are spin-up $|\uparrow(\varphi\vartheta)\rangle$ or spin-down $|\downarrow(\varphi\vartheta)\rangle$ along the Θ -axis. (Recall sentence after (10.5.20).) The spin-up eigenstate $|\uparrow(\varphi\vartheta)\rangle$ has Euler angles ($\alpha=\varphi, \beta=\vartheta$) of the U(2) state

(10.5.8a) equal to polar angles (φ, ϑ) of the Θ -axis. For spin-down $|\downarrow(\varphi\vartheta)\rangle$ the spin polar angle ϑ is flipped by $\pm\pi$ to $(\alpha=\varphi, \beta=\vartheta\pm\pi)$. For $\varphi=0$ the following $\mathbf{R}[\varphi\vartheta\Theta]$ eigen-equations yield AB -type states.

$$\begin{aligned} \mathbf{R}[0\vartheta\Theta]|\uparrow(\varphi\vartheta)\rangle &= \begin{pmatrix} \cos\frac{\Theta}{2} - i\cos\vartheta\sin\frac{\Theta}{2} & -i\sin\vartheta\sin\frac{\Theta}{2} \\ -i\sin\vartheta\sin\frac{\Theta}{2} & \cos\frac{\Theta}{2} + i\cos\vartheta\sin\frac{\Theta}{2} \end{pmatrix} \begin{pmatrix} \cos\frac{\vartheta}{2} \\ \sin\frac{\vartheta}{2} \end{pmatrix} = e^{-i\frac{\Theta}{2}} \begin{pmatrix} \cos\frac{\vartheta}{2} \\ \sin\frac{\vartheta}{2} \end{pmatrix} \\ \mathbf{R}[0\vartheta\Theta]|\downarrow(\varphi\vartheta)\rangle &= \begin{pmatrix} \cos\frac{\Theta}{2} - i\cos\vartheta\sin\frac{\Theta}{2} & -i\sin\vartheta\sin\frac{\Theta}{2} \\ -i\sin\vartheta\sin\frac{\Theta}{2} & \cos\frac{\Theta}{2} + i\cos\vartheta\sin\frac{\Theta}{2} \end{pmatrix} \begin{pmatrix} \sin\frac{\vartheta}{2} \\ -\cos\frac{\vartheta}{2} \end{pmatrix} = e^{+i\frac{\Theta}{2}} \begin{pmatrix} \sin\frac{\vartheta}{2} \\ -\cos\frac{\vartheta}{2} \end{pmatrix} \end{aligned} \quad (13.3.11a)$$

The eigenvalues of operator $\mathbf{R}[\varphi\vartheta\Theta]$ are phase factors $e^{\pm i\Theta/2}$. The S -matrix has an extra factor $ie^{i\Delta a}$.

Eigenvector :	Eigenvalue of $\mathbf{R}[0\vartheta\Theta]$:	Eigenvalue of S :
$\begin{pmatrix} \cos\vartheta/2 \\ \sin\vartheta/2 \end{pmatrix}$	$e^{-i\frac{\Theta}{2}}$	$e^{i\mu_1} = e^{i\left(\frac{-\Theta}{2} + \Delta a + \frac{\pi}{2}\right)}$
$\begin{pmatrix} \sin\vartheta/2 \\ -\cos\vartheta/2 \end{pmatrix}$	$e^{+i\frac{\Theta}{2}}$	$e^{i\mu_2} = e^{i\left(\frac{\Theta}{2} + \Delta a + \frac{\pi}{2}\right)}$

(13.3.11b)

(c) S-Matrix eigensolutions: Eigenchannels

The eigenvalues and eigenvectors of the S -matrix are helpful for understanding wave-barrier dynamics. The left hand (Ψ_2) and right hand (Ψ_1) channels each have right and left-moving waves.

$$\Psi_{2(LLEFT)} = \left(I_2^L e^{-ik_2x} + I_2^R e^{ik_2x} \right) / \sqrt{k_2}, \quad \Psi_{1(RIGHT)} = \left(I_1^L e^{-ik_1x} + I_1^R e^{ik_1x} \right) / \sqrt{k_1} \quad (13.3.12)$$

We now use special combinations of left-right input coefficients (I_{1v}^L, I_{2v}^R) of incoming waves that are eigenvectors of the unitary S -matrix. Because $(S^\dagger S = I)$, S must have phase factors $s = e^{i\mu}$ for eigenvalues.

$$\begin{pmatrix} I_{1v}^R \\ I_{2v}^L \end{pmatrix} = \begin{pmatrix} S_{11} & S_{12} \\ S_{21} & S_{22} \end{pmatrix} \begin{pmatrix} I_{1v}^L \\ I_{2v}^R \end{pmatrix} = s_v \begin{pmatrix} I_{1v}^L \\ I_{2v}^R \end{pmatrix} = e^{i\mu_v} \begin{pmatrix} I_{1v}^L \\ I_{2v}^R \end{pmatrix} \quad (13.3.13)$$

So, output coefficients (I_{1v}^R, I_{2v}^L) become equal to the inputs (I_{1v}^L, I_{2v}^R) times a phase factor $s_v = e^{i\mu_v}$.

$$\left(I_{1v}^R = s_v I_{1v}^L = e^{i\mu_v} I_{1v}^L, \quad I_{2v}^L = s_v I_{2v}^R = e^{i\mu_v} I_{2v}^R \right) \quad (13.3.14)$$

The results are called *eigenchannel waves* Ψ^v each with an individual *eigenchannel phase shift* $\mu_v/2$.

$$\begin{aligned} \Psi_{(LEFT)}^v &= \left(e^{i\mu_v} I_{2v}^R e^{-ik_2x} + I_{2v}^R e^{ik_2x} \right) / \sqrt{k_2} & \Psi_{(RIGHT)}^v &= \left(I_{1v}^L e^{-ik_1x} + e^{i\mu_v} I_{1v}^L e^{ik_1x} \right) / \sqrt{k_1} \\ &= I_{2v}^R \left(e^{-i(k_2x - \mu_v)} + e^{ik_2x} \right) / \sqrt{k_2} & &= I_{1v}^L \left(e^{-ik_1x} + e^{i(k_1x + \mu_v)} \right) / \sqrt{k_1} \\ &= I_{2v}^R e^{i\mu_v/2} 2\cos(k_2x - \mu_v/2) / \sqrt{k_2} & &= I_{1v}^L e^{i\mu_v/2} 2\cos(k_1x + \mu_v/2) / \sqrt{k_1} \end{aligned} \quad (13.3.15a) \quad (13.3.15b)$$

eigenchannel wave amplitudes (I_{1v}^L, I_{2v}^R) and eigenchannel phase shifts $\mu_v/2$ follow from (13.3.11b).

Eigenchannel	Eigenchannel Amplitudes	Eigenchannel Phase Shifts
$\nu = 1$	$\begin{pmatrix} I_{1\nu}^L / \sqrt{k_1} \\ I_{2\nu}^R / \sqrt{k_2} \end{pmatrix} = \begin{pmatrix} (1/\sqrt{k_1}) \cos \vartheta / 2 \\ (1/\sqrt{k_2}) \sin \vartheta / 2 \end{pmatrix}$	$\mu_1 = \frac{-\Theta}{2} + \Delta a + \frac{\pi}{2}$
$\nu = 2$	$\begin{pmatrix} I_{1\nu}^L / \sqrt{k_1} \\ I_{2\nu}^R / \sqrt{k_2} \end{pmatrix} = \begin{pmatrix} (1/\sqrt{k_1}) \sin \vartheta / 2 \\ -(1/\sqrt{k_2}) \cos \vartheta / 2 \end{pmatrix}$	$\mu_2 = \frac{\Theta}{2} + \Delta a + \frac{\pi}{2}$

(13.3.15c)

The angles are found using (13.3.10) with (13.3.3c).

$$\Theta = 2 \cos^{-1} \left(\frac{\Delta \sin \Sigma a}{\Sigma} \right), \quad \sin \vartheta = \frac{\Pi}{\Sigma \sin \frac{\Theta}{2}}, \quad \cos \vartheta = \frac{-\Delta \cos \Sigma a}{\Sigma \sin \frac{\Theta}{2}}. \quad (13.3.15d)$$

The half-angle eigenchannel amplitude values needed for (13.3.15c) follow.

$$\cos \frac{\vartheta}{2} = \sqrt{\frac{1 + \cos \vartheta}{2}} = \sqrt{\frac{\Sigma \sin \frac{\Theta}{2} - \Delta \cos \Sigma a}{2 \Sigma \sin \frac{\Theta}{2}}}, \quad \sin \frac{\vartheta}{2} = \sqrt{\frac{1 - \cos \vartheta}{2}} = \sqrt{\frac{\Sigma \sin \frac{\Theta}{2} + \Delta \cos \Sigma a}{2 \Sigma \sin \frac{\Theta}{2}}} \quad (13.3.15e)$$

Eigenchannel waves are standing waves provided $+k$ and $-k$ waves have the same frequency. (No chiral, circular, cyclotron, Coriolis or other C-type symmetry breaking is present.) For positive phase shift $\mu_\nu/2$, the RIGHT channel k_1 -standing wave part of the eigenchannel wave gets pulled to the left toward the barrier at $x=a$, while the LEFT-channel k_2 -standing wave gets pushed to the right, also toward the barrier. In this way, the eigenchannel phase-shift $\mu_\nu/2$ becomes a measure of the effective "attraction" (or "repulsion", if negative) of the potential barrier to the eigenchannel state- ν .

Consider an example of waves with $k_1 = 1$ in the right hand channel and $k_2 = 4$ in the channel to the left of $a=0$. This could be due to an energy of $E=8$ (in units with $\hbar^2/m=1$) over a right hand potential step of $V_1 = 7.5$ from a left hand $V_2 = 0$ plane so $k_1 = \sqrt{2(E-V_1)} = \sqrt{[1]}$ and $k_2 = \sqrt{2(E-V_2)} = \sqrt{[16]}$. This amounts to a kinematic sum $\Sigma = k_2 + k_1 = 5$, difference $\Delta = k_2 - k_1 = 3$, and product $\Pi = 2\sqrt{(k_2 k_1)} = 4$, from (13.3.3c). Inserting these values along with $a=0$ into (13.3.15d) gives $U(2)$ rotation and polar angles.

$$\Theta = 2 \cos^{-1}(0) = \pi, \quad \sin \vartheta = 4/5, \quad \cos \vartheta = -3/5, \quad \vartheta = -127^\circ \quad (13.3.16)$$

The eigenchannel amplitudes in (13.3.15c) require half-angle functions (13.3.15e). For $a=0$ they simplify.

$$\begin{aligned} \cos \frac{\vartheta}{2} &= \sqrt{\frac{\Sigma - \Delta}{2\Sigma}} = \sqrt{\frac{k_1}{\Sigma}}, & \sin \frac{\vartheta}{2} &= \sqrt{\frac{\Sigma + \Delta}{2\Sigma}} = \sqrt{\frac{k_2}{\Sigma}}, \quad (\text{for: } a=0) \\ &= \sqrt{\frac{1}{5}}, & &= \sqrt{\frac{4}{5}}, \quad (\text{for: } k_1=1, k_2=4) \end{aligned} \quad (13.3.17)$$

We first check that these are the correct components for S -matrix eigenvectors and verify the eigenvalues which are the eigen-channel phase shift factors $e^{i\mu_\nu}$ predicted by (13.3.15) through (13.3.16).

$$\begin{pmatrix} \frac{-3}{5} & \frac{4}{5} \\ \frac{4}{5} & \frac{3}{5} \end{pmatrix} \begin{pmatrix} \frac{1}{\sqrt{5}} \\ \frac{2}{\sqrt{5}} \end{pmatrix} = (e^{i0}) \begin{pmatrix} \frac{1}{\sqrt{5}} \\ \frac{2}{\sqrt{5}} \end{pmatrix}, \quad \begin{pmatrix} \frac{-3}{5} & \frac{4}{5} \\ \frac{4}{5} & \frac{3}{5} \end{pmatrix} \begin{pmatrix} \frac{2}{\sqrt{5}} \\ \frac{-1}{\sqrt{5}} \end{pmatrix} = (e^{i\pi}) \begin{pmatrix} \frac{2}{\sqrt{5}} \\ \frac{-1}{\sqrt{5}} \end{pmatrix} \quad (13.3.18)$$

Then the eigenchannel amplitudes and phase shifts are as follows. (Recall that $k_2=4$ and $k_1=1$, here.)

<i>Eigenchannel</i>	<i>Eigenchannel Amplitudes</i>	<i>Eigenchannel Phase Shifts</i>
$\nu = 1$	$\begin{pmatrix} I_{1\nu}^L / \sqrt{k_1} \\ I_{2\nu}^R / \sqrt{k_2} \end{pmatrix} = \begin{pmatrix} \sqrt{\frac{1}{5}} / \sqrt{1} \\ \sqrt{\frac{4}{5}} / \sqrt{4} \end{pmatrix} = \begin{pmatrix} 1 \\ 1 \end{pmatrix} / \sqrt{5}$	$\mu_1 = 0$
$\nu = 2$	$\begin{pmatrix} I_{1\nu}^L / \sqrt{k_1} \\ I_{2\nu}^R / \sqrt{k_2} \end{pmatrix} = \begin{pmatrix} \sqrt{\frac{4}{5}} / \sqrt{1} \\ -\sqrt{\frac{1}{5}} / \sqrt{4} \end{pmatrix} = \begin{pmatrix} 2 \\ -1/2 \end{pmatrix} / \sqrt{5}$	$\mu_2 = \pi$

(13.3.19)

According to (13.3.15a-b) the ($\nu=1$) eigenchannel standing waves are two cosines with equal amplitudes.

$$\begin{aligned} \Psi_{(LEFT)}^{\nu=1} &= \frac{2I_{21}^R e^{i\mu_1/2}}{\sqrt{k_2}} \cos(k_2 x - \mu_1 / 2), & \Psi_{(RIGHT)}^{\nu=1} &= \frac{2I_{11}^L e^{i\mu_1/2}}{\sqrt{k_1}} \cos(k_1 x + \mu_1 / 2) \\ &= \frac{2}{\sqrt{5}} \cos(k_2 x) & &= \frac{2}{\sqrt{5}} \cos(k_1 x) \end{aligned} \quad (13.3.20a)$$

The ($\nu=2$) eigenchannel waves are two sine waves with 1:4 amplitude ratio, each with a -90° phase lag.

$$\begin{aligned} \Psi_{(LEFT)}^{\nu=2} &= \frac{2I_{22}^R e^{i\mu_2/2}}{\sqrt{k_2}} \cos(k_2 x - \mu_2 / 2), & \Psi_{(RIGHT)}^{\nu=2} &= \frac{2I_{12}^L e^{i\mu_2/2}}{\sqrt{k_1}} \cos(k_1 x + \mu_2 / 2) \\ &= \frac{2}{\sqrt{5}} \left(\frac{-e^{i\pi/2}}{2} \right) \cos(k_2 x - \pi / 2) & &= \frac{2}{\sqrt{5}} \left(2e^{i\pi/2} \right) \cos(k_1 x + \pi / 2) \\ &= \frac{2}{\sqrt{5}} \left(\frac{-i}{2} \right) \sin(k_2 x) & &= \frac{2}{\sqrt{5}} (-2i) \sin(k_1 x) \end{aligned} \quad (13.3.20b)$$

The $(-i)$ factors on the standing waves do not affect the envelope or probability distribution of the eigenchannel states. However, they do give a -90° time phase lag which is very important when we mix the eigenchannel "normal-modes" to make all the other possible scattering states and waves.

(d) U(2) and R(3) pictures of barrier wavestates

The eigenchannel states (13.3.19) and waves (13.3.20) are analogous to the $U(2)$ AB -type 2-state eigenstates discussed in Sec. 10.3 or A or B -type 2-state eigenstates shown in Sec. 10.2a-b. The ($\nu=1$) and ($\nu=2$) eigenchannel states provide a basis for describing all states of a given energy since all states must be $U(2)$ linear combinations of the eigenchannels. Each different $U(2)$ combination has a different S -vector on $R(3)$ sphere that characterizes the $U(2)$ state. (Recall $U(2)$ Fig. 10.5.8a and $R(3)$ Fig. 10.5.8b.)

Both are pure standing waves with equal-but-opposite currents on either side of the barrier so the net currents sum to zero on either side because eigenchannel states $|\epsilon_v\rangle$ are eigenvectors of the S -matrix as in (13.3.18) which is repeated below.

$$\begin{aligned} S|\epsilon_1\rangle &= (+1)|\epsilon_1\rangle, & S|\epsilon_2\rangle &= (-1)|\epsilon_2\rangle \\ \begin{pmatrix} -3 & 4 \\ 5 & 5 \end{pmatrix} \begin{pmatrix} 1 \\ \sqrt{5} \end{pmatrix} &= (+1) \begin{pmatrix} 1 \\ \sqrt{5} \end{pmatrix}, & \begin{pmatrix} -3 & 4 \\ 5 & 5 \end{pmatrix} \begin{pmatrix} 2 \\ \sqrt{5} \end{pmatrix} &= (-1) \begin{pmatrix} 2 \\ \sqrt{5} \end{pmatrix} \end{aligned} \quad (13.3.22)$$

Currents in channel $m=1$ or 2 of eigenchannel state $|\epsilon_v\rangle$ are squares $|\langle m|\epsilon_v\rangle|^2 = |I_{mv}|^2$ of I -amplitudes I_{mv} .

$$\begin{aligned} |\epsilon_1\rangle & \begin{cases} I_{channel\ 1} \\ I_{channel\ 2} \end{cases} = \begin{cases} \langle 1|\epsilon_1\rangle^2 \\ \langle 2|\epsilon_1\rangle^2 \end{cases} = \begin{cases} \frac{1}{5} \\ \frac{4}{5} \end{cases}, & |\epsilon_1\rangle & \begin{cases} I_{channel\ 1} \\ I_{channel\ 2} \end{cases} = \begin{cases} \langle 1|S|\epsilon_1\rangle^2 \\ \langle 2|S|\epsilon_1\rangle^2 \end{cases} = \begin{cases} \frac{1}{5} \\ \frac{4}{5} \end{cases} \end{aligned} \quad (13.3.23a)$$

$$\begin{aligned} |\epsilon_2\rangle & \begin{cases} I_{channel\ 1} \\ I_{channel\ 2} \end{cases} = \begin{cases} \langle 1|\epsilon_2\rangle^2 \\ \langle 2|\epsilon_2\rangle^2 \end{cases} = \begin{cases} \frac{4}{5} \\ \frac{1}{5} \end{cases}, & |\epsilon_2\rangle & \begin{cases} I_{channel\ 1} \\ I_{channel\ 2} \end{cases} = \begin{cases} \langle 1|S|\epsilon_2\rangle^2 \\ \langle 2|S|\epsilon_2\rangle^2 \end{cases} = \begin{cases} \frac{4}{5} \\ \frac{1}{5} \end{cases} \end{aligned} \quad (13.3.23b)$$

Inputs of the $|\epsilon_1\rangle$ eigenchannel are 1/5 or 20% from the right and 4/5 or 80% from the left, while inputs of the $|\epsilon_2\rangle$ eigenchannel are 4/5 or 80% from the right and 1/5 or 20% from the left. Outputs are the same.

The upper-left and lower-right hand corners of Fig. 13.3.2 show the *right-source channel state* $|1\rangle$ and *left-source channel state* $|2\rangle$. The inputs of the right-source channel state $|1\rangle$ are 100% from the right and 0% from the left and *vice-versa* for left-source channel state $|2\rangle$. Neither are S -eigenstates. The output states $S|1\rangle$ and $S|2\rangle$ are π -rotations or reflections of $|1\rangle$ and $|2\rangle$, respectively, through the S operator axis.

$$S|1\rangle = \begin{pmatrix} -3 & 4 \\ 5 & 5 \end{pmatrix} \begin{pmatrix} 1 \\ 0 \end{pmatrix} = \begin{pmatrix} -3 \\ 5 \end{pmatrix}, \quad S|2\rangle = \begin{pmatrix} -3 & 4 \\ 5 & 5 \end{pmatrix} \begin{pmatrix} 0 \\ 1 \end{pmatrix} = \begin{pmatrix} 4 \\ 5 \end{pmatrix} \quad (13.3.24a)$$

Output currents of $|1\rangle$ are 9/25=36% left and 16/25=64% right or, *vice-versa* for $|2\rangle$.

$$\begin{aligned} |1\rangle & \begin{cases} I_{channel\ 1} \\ I_{channel\ 2} \end{cases} = \begin{cases} \langle 1|1\rangle^2 \\ \langle 2|1\rangle^2 \end{cases} = \begin{cases} 1 \\ 0 \end{cases}, & |1\rangle & \begin{cases} I_{channel\ 1} \\ I_{channel\ 2} \end{cases} = \begin{cases} \langle 1|S|1\rangle^2 \\ \langle 2|S|1\rangle^2 \end{cases} = \begin{cases} \frac{9}{25} \\ \frac{16}{25} \end{cases} \end{aligned} \quad (13.3.24b)$$

$$\begin{aligned} |2\rangle & \begin{cases} I_{channel\ 1} \\ I_{channel\ 2} \end{cases} = \begin{cases} \langle 1|2\rangle^2 \\ \langle 2|2\rangle^2 \end{cases} = \begin{cases} 0 \\ 1 \end{cases}, & |2\rangle & \begin{cases} I_{channel\ 1} \\ I_{channel\ 2} \end{cases} = \begin{cases} \langle 1|S|2\rangle^2 \\ \langle 2|S|2\rangle^2 \end{cases} = \begin{cases} \frac{16}{25} \\ \frac{9}{25} \end{cases} \end{aligned} \quad (13.3.24c)$$

The $U(2)$ description of S -matrix scattering states is similar in mathematical form to that of the Hamiltonian H -matrix dynamics, but there are some important differences. First, all the states in Fig. 13.3.2 as well as any $U(2)$ combinations thereof, are H -eigenstates. Second, and perhaps the greatest

source of confusion, is the fact that all states come as input-output pairs. There must always be an output state $|O\rangle = S|I\rangle$ related by S to every input state $|I\rangle$, and, together, they to make the complete barrier wavefunction according to the following generalization of (13.3.15).

$$\begin{aligned}\Psi_{(LEFT)}^{I,O} &= \frac{\langle 2|S|I\rangle}{\sqrt{k_2}} e^{-ik_2x} + \frac{\langle 2|I\rangle}{\sqrt{k_2}} e^{ik_2x} \\ &= \frac{\langle 2|O\rangle}{\sqrt{k_2}} e^{-ik_2x} + \frac{\langle 2|I\rangle}{\sqrt{k_2}} e^{ik_2x}\end{aligned}\quad (13.3.25a)$$

$$\begin{aligned}\Psi_{(RIGHT)}^{I,O} &= \frac{\langle 1|I\rangle}{\sqrt{k_1}} e^{-ik_1x} + \frac{\langle 1|S|I\rangle}{\sqrt{k_1}} e^{ik_1x} \\ &= \frac{\langle 1|I\rangle}{\sqrt{k_1}} e^{-ik_1x} + \frac{\langle 1|O\rangle}{\sqrt{k_1}} e^{ik_1x}\end{aligned}\quad (13.3.25b)$$

Finally, each amplitude $\langle m|I\rangle$ or $\langle m|O\rangle$ must be divided by a square root $\sqrt{k_m}$ of its local wavevector before becoming a phasor amplitude of a moving wave in (13.3.25). This is why a wave with a given current $|\langle I|I\rangle|^2$ or $|\langle I|O\rangle|^2$ on the right ($k_I=I$) side has twice the amplitude of a wave with the same current $|\langle 2|I\rangle|^2$ or $|\langle 2|O\rangle|^2$ on the left ($k_2=4$) side.

(e) Linear combinations of barrier wavestates

In spite of their complicated structure, the wavefunctions in a barrier may be combined like any other quantum states. For example, the transformation matrix T between eigenchannel states $\{|\varepsilon_1\rangle, |\varepsilon_2\rangle\}$ and base states $\{|1\rangle, |2\rangle\}$ in Fig. 13.3.2 follow from the eigenvector columns in (13.3.22).

$$T = \begin{pmatrix} \langle 1|\varepsilon_1\rangle & \langle 1|\varepsilon_2\rangle \\ \langle 2|\varepsilon_1\rangle & \langle 2|\varepsilon_2\rangle \end{pmatrix} = \begin{pmatrix} 1/\sqrt{5} & 2/\sqrt{5} \\ 2/\sqrt{5} & -1/\sqrt{5} \end{pmatrix} = \begin{pmatrix} \langle \varepsilon_1|1\rangle & \langle \varepsilon_1|2\rangle \\ \langle \varepsilon_2|1\rangle & \langle \varepsilon_2|2\rangle \end{pmatrix} = T^{-1} = T^\dagger \quad (13.3.26)$$

(This T is another of those Hermitian-unitary reflection matrices.) This shows how the base states are made of combinations of the eigenchannel states and vice-versa with the same matrix. Let us see an abstract relation like $|1\rangle = (1/\sqrt{5})|\varepsilon_1\rangle + (2/\sqrt{5})|\varepsilon_2\rangle$ as a wavefunction combination.

$$\begin{aligned}\Psi_{(LEFT)}^{Base1} &= \frac{1}{\sqrt{5}} \Psi_{(LEFT)}^{\varepsilon_1} + \frac{2}{\sqrt{5}} \Psi_{(LEFT)}^{\varepsilon_2}, & \Psi_{(RIGHT)}^{Base1} &= \frac{1}{\sqrt{5}} \Psi_{(RIGHT)}^{\varepsilon_1} + \frac{2}{\sqrt{5}} \Psi_{(RIGHT)}^{\varepsilon_2} \\ &= \frac{1}{\sqrt{5}} \left(\frac{1}{\sqrt{5}} e^{-i4x} + \frac{1}{\sqrt{5}} e^{i4x} \right), & &= \frac{1}{\sqrt{5}} \left(\frac{1}{\sqrt{5}} e^{-ix} + \frac{1}{\sqrt{5}} e^{ix} \right) \\ &+ \frac{2}{\sqrt{5}} \left(\frac{1}{2\sqrt{5}} e^{-i4x} - \frac{1}{2\sqrt{5}} e^{i4x} \right), & &+ \frac{2}{\sqrt{5}} \left(\frac{2}{\sqrt{5}} e^{-ix} - \frac{2}{\sqrt{5}} e^{ix} \right) \\ &= \frac{2}{5} e^{-i4x} + 0, & &= \frac{5}{5} e^{-ix} - \frac{3}{5} e^{ix}.\end{aligned}$$

On the left is a pure left-moving wave of amplitude $L_2=2/5$ carrying a current of $16/25$ units. (Recall that current is $|L_2|^2 k_2$, and $k_2=4$.) On the right is a galloping wave of $SWR = (5-3)/(5+3) = 1/4$ carrying a unit current to the left and a current of $9/25$ to the right as shown in the upper left of Fig. 13.3.2.

Remote boundary S-waves: "Sewing" waves together

The S -matrix eigensolutions given so far (13.3.17) to (13.3.20) assumed boundary coordinate $a=0$. Now we consider cases in which the origin is not right on the potential barrier. This will show some of the power and subtleties of S -matrix methods. The example will be the opposite extreme to the preceding one in which the first 1-term containing $\sin\Sigma a$ in the S -operator expansion (13.3.10a) was zero. Here, we let

$$\Sigma a = 5a = \pi/2 \text{ or: } a = \pi/10 \quad (13.3.28)$$

so the last σ_Z term containing $\cos\Sigma a$ goes to zero instead. This swings the S -vector up to $\vartheta=\pi/2$ since it now only has a σ_X term. The resulting eigenvectors in (13.3.11b) assume a very simple form of a bilaterally symmetric (B -type) S -operator. Indeed, the form of the S -operator (4.4.41) is that of B -symmetric operators in (2.9.10) and has eigenvectors $|\varepsilon_\nu\rangle$ in which the left amplitudes are \pm the right ones.

$$e^{i3a} \begin{pmatrix} \frac{3i}{5} & \frac{4}{5} \\ \frac{4}{5} & \frac{3i}{5} \end{pmatrix} \begin{pmatrix} \frac{1}{\sqrt{2}} \\ \frac{1}{\sqrt{2}} \end{pmatrix} = e^{i\mu_1} \begin{pmatrix} \frac{1}{\sqrt{2}} \\ \frac{1}{\sqrt{2}} \end{pmatrix}, \quad e^{i3a} \begin{pmatrix} \frac{3i}{5} & \frac{4}{5} \\ \frac{4}{5} & \frac{3i}{5} \end{pmatrix} \begin{pmatrix} \frac{1}{\sqrt{2}} \\ -\frac{1}{\sqrt{2}} \end{pmatrix} = e^{i\mu_2} \begin{pmatrix} \frac{1}{\sqrt{2}} \\ -\frac{1}{\sqrt{2}} \end{pmatrix} \quad (13.3.29a)$$

The eigenchannel phases for a barrier displaced by $a = \pi/10$ are easily found to be

$$e^{i\mu_1} = e^{i3a} \left(\frac{3i}{5} + \frac{4}{5} \right) = e^{i3\pi/10} \left(e^{i0.6435} \right), \quad e^{i\mu_2} = e^{i3a} \left(\frac{3i}{5} - \frac{4}{5} \right) = e^{i3\pi/10} \left(e^{i2.498} \right) \quad (13.3.29b)$$

$$= e^{i1.585}, \quad = e^{i3.443}$$

This immediately gives the corresponding eigenchannel waves according to (13.3.15a).

$$\Psi_{(LEFT)}^{\varepsilon_1} = \frac{2e^{i0.793}}{\sqrt{2}\sqrt{4}} \cos(4x - 0.793), \quad \Psi_{(RIGHT)}^{\varepsilon_1} = \frac{2e^{i0.793}}{\sqrt{2}\sqrt{1}} \cos(x + 0.793) \quad (13.3.29c)$$

$$\Psi_{(LEFT)}^{\varepsilon_2} = \frac{-2e^{i1.722}}{\sqrt{2}\sqrt{4}} \cos(4x - 1.722), \quad \Psi_{(RIGHT)}^{\varepsilon_2} = \frac{2e^{i1.722}}{\sqrt{2}\sqrt{1}} \cos(x + 1.722) \quad (13.3.29d)$$

Graphs of the cosine functions are displayed in Fig. 13.3.3. Notice how the *RIGHT* and *LEFT* waves contact perfectly at the barrier boundary ($x=a=\pi/10$). This tricky "sewing" together of the two waves is done quite effortlessly using the S -matrix formulation. The corresponding eigenchannel waves are plotted in Fig. 13.3.4 for comparison with the analysis.

The ($a=\pi/(2\Sigma)=\pi/10$) eigenchannel states in Fig. 13.3.4 differ from the ($a=0$) ones in Fig. 13.3.2 in a number of ways. The ($a=\pi/10$) waves have currents divided equally ($1:1$) between the two sides of the barrier instead of ($1:4$) or ($4:1$). The $U(2)$ rotation angles Θ have a non-zero $\cos(\Theta/2) = \Delta/\Sigma = 3/5$; and so $\Theta = \pm 1.85$ (or $\pm 106^\circ$) is smaller than π (or 180°). Also, the overall phase shift $a\Delta = 3\pi/10$ is nonzero so the eigenchannel phase shifts $\mu_1 = 1.585$ and $\mu_2 = 3.443$ differ accordingly from 0 and $\pi/2$.

All these differences are due to simply translating the barrier from origin ($x=0$) to point ($x=a$)! A change in origin makes a big difference to the eigenchannel waves because it means moving the nodes of standing waves relative to the barrier and having to "re-sew" the contact point with each change in translation a . Suppose you simply demand that a standing wave of amplitude A_l have a node at point x_l . Changing x_l may cause the amplitude and locations of the waves on the other side to oscillate wildly.

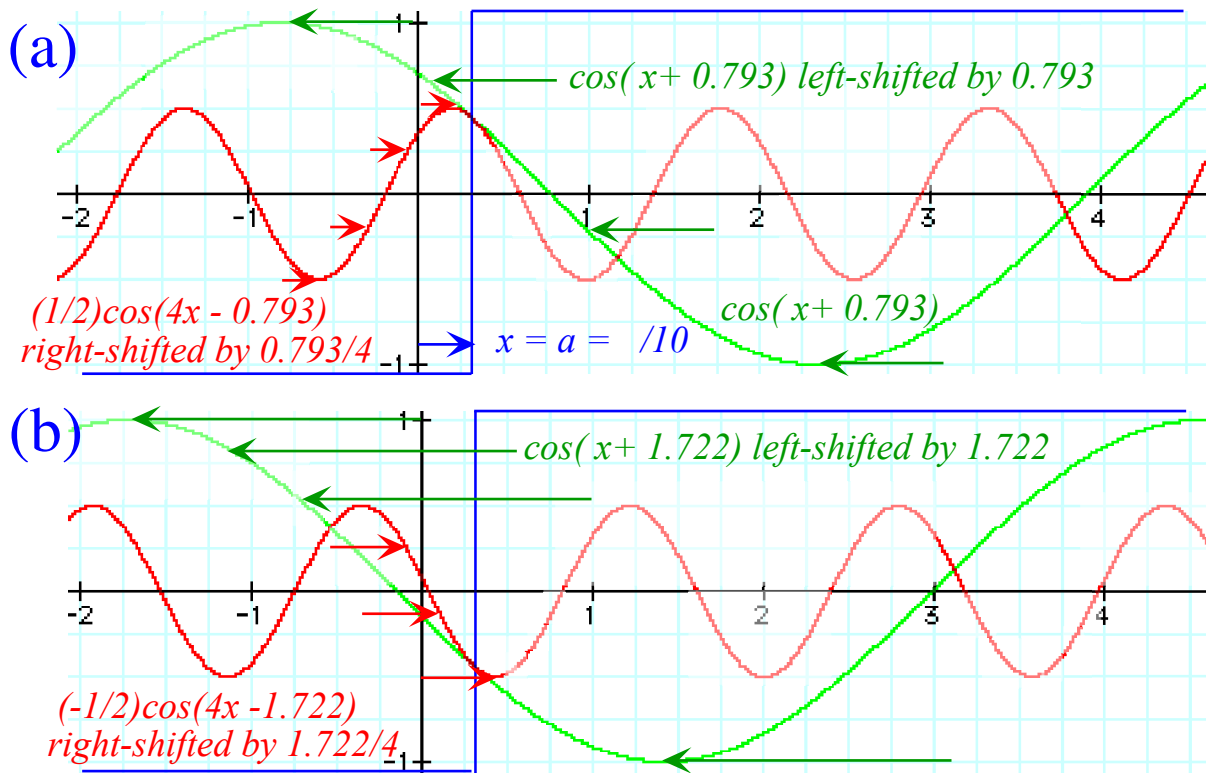


Fig. 13.3.3 Cosine components of eigenchannel waves showing boundary contact and phase shifts.

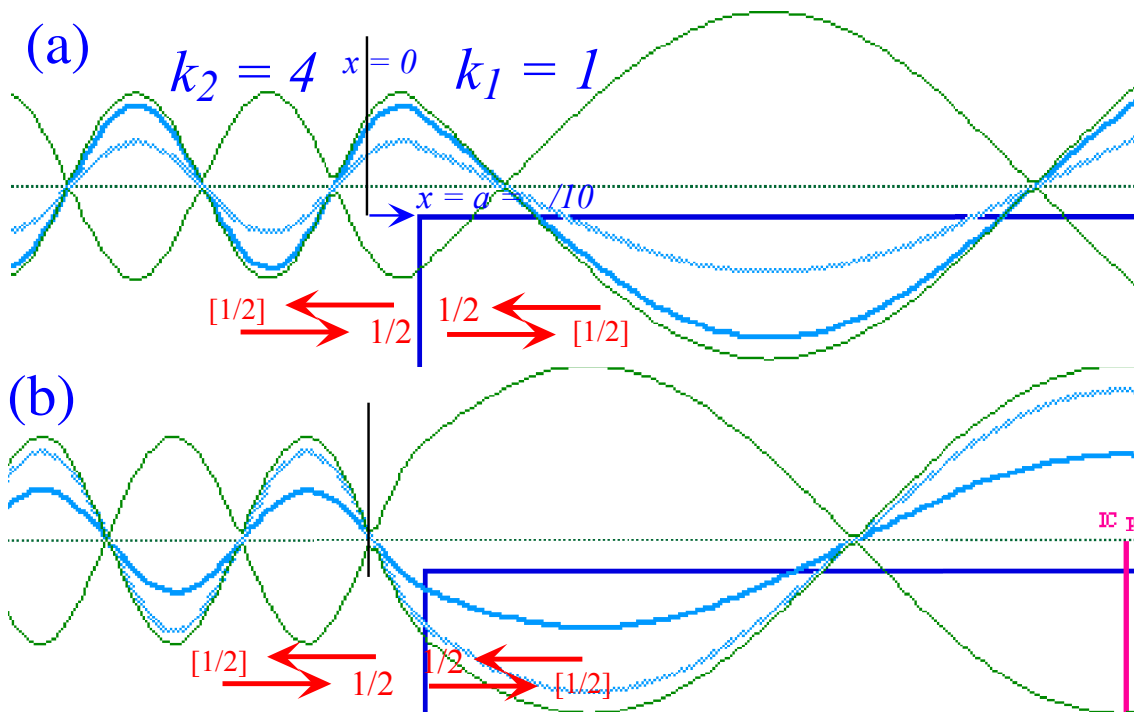


Fig. 13.3.4 Barrier eigenchannel waves with remote origin $a = \pi/10$.

It is this oscillation that is described by the S -matrix eigensolutions. The oscillations become more pronounced as the energy E approaches values which closely "graze" the barrier top V , that is, as the difference ratio $\Delta/\Sigma = (k_2 - k_1)/(k_2 + k_1) = [\sqrt{E} - \sqrt{E-V}]/[\sqrt{E} + \sqrt{E-V}]$ becomes large compared to the

$$\mathbf{S}_X(\Sigma a) = \frac{\Pi}{\Sigma} = \sin \vartheta \sin \frac{\Theta}{2}, \quad (13.3.31)$$

So vector $\mathbf{S}(\Sigma a)$ follows a vertical straight line as Σa increases while its companion vector $\Sigma(\Sigma a)$ follows the smaller radius- Δ/Σ circle but has the same vertical component. The horizontal component of $\Sigma(\Sigma a)$ is

$$\Sigma_X(\Sigma a) = \frac{\Delta}{\Sigma} \sin \Sigma a = \cos \frac{\Theta}{2}. \quad (13.3.32)$$

$\Sigma_X(\Sigma a)$ is measured relative to $X = \Pi/\Sigma$ at the center of the smaller radius- Δ/Σ circle. A vertical dashed line is drawn through the tip of the $\Sigma(\Sigma a)$ vector in the lower left hand side of Fig. 13.3.5. This is an altitude of length $\sin\Theta/2$ of a unit-hypotenuse right triangle which contains the angle $\Theta/2$. (The base is $\cos\Theta/2$ from (13.3.32) above.) Meanwhile, an $\mathbf{S}(\Sigma a)$ -vector triangle has base $\mathbf{S}_X(\Sigma a)$, altitude $\mathbf{S}_Z(\Sigma a)$ and hypotenuse $\sin\Theta/2$. The triangle contains angle $\vartheta - \pi/2$ at the origin and angle $\pi - \vartheta$ at the tip of the $\mathbf{S}(\Sigma a)$ -vector.

The two quantities $\sin\Theta/2$ and $\sin\vartheta$ are related to eigenchannel phase shift $\mu = \pm\Theta/2 + \Delta a + \pi/2$ and current symmetry ratio $I_1^L : I_2^R = \cos\vartheta/2 : \sin\vartheta/2$, both from (13.3.15c). From the above formulas and diagram it can be seen how the two quantities $\sin\Theta/2$ and $\sin\vartheta$ play "leapfrog" as translation angle Σa advances, with each taking turns oscillating between the values of 1 and Π/Σ . Lower values of Π/Σ (or greater values of $|\Delta/\Sigma|$) cause more extreme oscillations. At $\Sigma a = 0$ or π (top and bottom of Fig. 13.3.5) the phase "rotation" angle Θ is $\pm\pi$ so $\sin\Theta/2 = 1$ is maximum while a minimum value Π/Σ occurs for the parameter $\sin\vartheta$ which determines left-right current symmetry. At in-between values of $\Sigma a = \pm\pi/2$ (center of Fig. 13.3.5) phase parameter $\sin\Theta/2$ is minimum value Π/Σ , but current symmetry parameter $\sin\vartheta$ is at its maximum value $\sin\vartheta = 1$. This is the point where left and right current magnitudes are equal as was shown before in Fig. 13.3.4.

(f) Crossing and Scattering-matrices for square well and hump

The C -matrix for a square well from $x=b$ and to $x=a$ as sketched in Fig. 13.3.6(a) is as follows.

$$C = \begin{pmatrix} e^{ikL} [\cos \ell L - i \cosh 2\alpha \sin \ell L] & -ie^{-ik(a+b)} \sinh 2\alpha \sin \ell L \\ ie^{ik(a+b)} \sinh 2\alpha \sin \ell L & e^{-ikL} [\cos \ell L + i \cosh 2\alpha \sin \ell L] \end{pmatrix} \quad (13.3.33a)$$

Here $L = a - b$ is well-length and wavevector k (outside) and ℓ (inside) have E measured relative to ∞ .

$$k = \sqrt{\frac{2mE}{\hbar^2}}, \quad \ell = \sqrt{\frac{2m(E - V)}{\hbar^2}} \quad \left(= \sqrt{\frac{2m(E + |V|)}{\hbar^2}} \text{ for } V < 0 \right) \quad (13.3.33b)$$

A notation using hyperbolic functions

$$\cosh 2\alpha = \frac{1}{2} \left(\frac{\ell}{k} + \frac{k}{\ell} \right) = \frac{\ell^2 + k^2}{2k\ell}, \quad \sinh 2\alpha = \frac{1}{2} \left(\frac{\ell}{k} - \frac{k}{\ell} \right) = \frac{\ell^2 - k^2}{2k\ell}, \quad (13.3.33c)$$

is convenient for doing wavevector algebra. Previous quantities Σ , Δ , and Π use related functions of α .

$$\cosh \alpha = \frac{k + \ell}{2\sqrt{k\ell}} = \frac{\Sigma}{\Pi}, \quad \sinh \alpha = \frac{\ell - k}{2\sqrt{k\ell}} = \frac{\Delta}{\Pi} \quad (13.3.33d)$$

These follow from hyperbolic identities $\cosh 2a = 2 \cosh^2 a - 1$, and $\sinh 2a = 2 \sinh a \cosh a$. Also, the hyperbolic functions of 4α are useful shorthand notation for some calculations.

$$\cosh 4\alpha = \frac{1}{2} \left(\frac{\ell^2}{k^2} + \frac{k^2}{\ell^2} \right), \quad \sinh 4\alpha = \frac{1}{2} \left(\frac{\ell^2}{k^2} - \frac{k^2}{\ell^2} \right) \quad (13.3.33e)$$

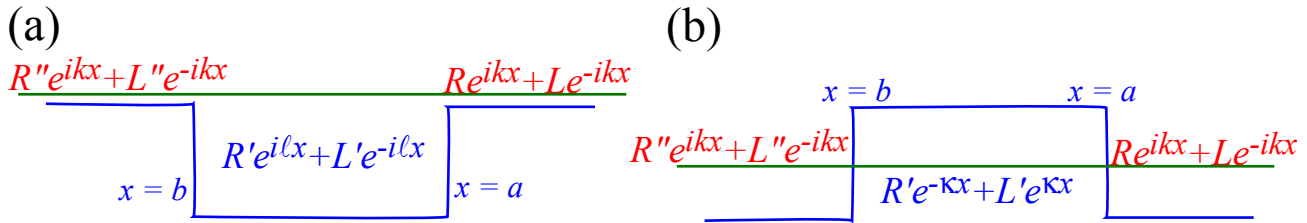


Fig. 13.3.6 (a) C_2 -symmetric square well (b) C_2 -symmetric square barrier.

If E is below a square barrier V , then wavevector ℓ is replaced by evanescent parameter $i\kappa$.

$$C = \begin{pmatrix} e^{i\kappa L} [\cosh \kappa L + i \sinh 2\beta \sinh \kappa L] & i e^{-i\kappa(a+b)} \cosh 2\beta \sinh \kappa L \\ -i e^{i\kappa(a+b)} \cosh 2\beta \sinh \kappa L & e^{-i\kappa L} [\cosh \kappa L - i \sinh 2\beta \sinh \kappa L] \end{pmatrix} \quad (13.3.34a)$$

where:
$$k = \sqrt{\frac{2mE}{\hbar^2}}, \quad -i\ell = \kappa = \sqrt{\frac{2m(V-E)}{\hbar^2}} \quad (\text{for } V > E > 0) \quad (13.3.34b)$$

Again, $L=a-b$ and a convenient notation uses hyperbolic functions.

$$\cosh 2\beta = \frac{1}{2} \left(\frac{\kappa}{k} + \frac{k}{\kappa} \right) = \frac{\kappa^2 + k^2}{2k\kappa}, \quad \sinh 2\beta = \frac{1}{2} \left(\frac{\kappa}{k} - \frac{k}{\kappa} \right) = \frac{\kappa^2 - k^2}{2k\kappa} \quad (13.3.34c)$$

$$\cosh \beta = \frac{k + \kappa}{2\sqrt{k\kappa}} \equiv \frac{\sigma}{\rho}, \quad \sinh \beta = \frac{\kappa - k}{2\sqrt{k\kappa}} \equiv \frac{\delta}{\rho} \quad (13.3.34d)$$

$$\cosh 4\beta = \frac{1}{2} \left(\frac{\kappa^2}{k^2} + \frac{k^2}{\kappa^2} \right), \quad \sinh 4\beta = \frac{1}{2} \left(\frac{\kappa^2}{k^2} - \frac{k^2}{\kappa^2} \right) \quad (13.3.34e)$$

Note, once again, how wavevector ℓ is replaced by evanescent parameter $i\kappa$, or equivalently, $i\ell$ with $-\kappa$. We replace $i\ell$ with $-\kappa$ instead of $+\kappa$ because the wavefunction in Fig. 13.3.6 connects R -amplitudes having positive $i\ell$ and negative exponentials (dying: $-\kappa$) while L -amplitudes go with negative $-i\ell$ and positive (rising: $+\kappa$) exponential evanescent waves.

The scattering or S -matrix follows from the crossing matrix using connection formulas (13.3.5). For the square well (or the square barrier at energy above ($E > V$) its top) the S -matrix is as follows.

$$\begin{pmatrix} S_{11} = -\frac{C_{12}}{C_{11}} & S_{12} = \frac{1}{C_{11}} \\ S_{21} = \frac{1}{C_{11}} & S_{22} = \frac{C_{21}}{C_{11}} \end{pmatrix} = \begin{pmatrix} \frac{i e^{-i\kappa(a+b)} \sinh 2\alpha \sin \ell L}{e^{i\kappa L} [\cos \ell L - i \cosh 2\alpha \sin \ell L]} & \frac{1}{e^{i\kappa L} [\cos \ell L - i \cosh 2\alpha \sin \ell L]} \\ \frac{1}{e^{i\kappa L} [\cos \ell L - i \cosh 2\alpha \sin \ell L]} & \frac{i e^{i\kappa(a+b)} \sinh 2\alpha \sin \ell L}{e^{i\kappa L} [\cos \ell L - i \cosh 2\alpha \sin \ell L]} \end{pmatrix}$$

$$\langle S \rangle = \frac{i e^{-i\kappa L}}{[\cos \ell L - i \cosh 2\alpha \sin \ell L]} \begin{pmatrix} e^{-i\kappa(a+b)} \sinh 2\alpha \sin \ell L & -i \\ -i & e^{i\kappa(a+b)} \sinh 2\alpha \sin \ell L \end{pmatrix}$$

The S -matrix expands into a unitary combination of Hamilton-Pauli spinors.

$$\langle S \rangle = \frac{ie^{-ikL} [\cos \ell L + i \cosh 2\alpha \sin \ell L]}{1 + \sinh^2 2\alpha \sin^2 \ell L} \times \left[\cos k(a+b) \sinh 2\alpha \sin \ell L \begin{pmatrix} 1 & 0 \\ 0 & 1 \end{pmatrix} - i \begin{pmatrix} 0 & 1 \\ 1 & 0 \end{pmatrix} - i \sin k(a+b) \sinh 2\alpha \sin \ell L \begin{pmatrix} 1 & 0 \\ 0 & -1 \end{pmatrix} \right]$$

or (13.3.35a)

$$\mathbf{S} = \frac{ie^{-ikL} [\cos \ell L + i \cosh 2\alpha \sin \ell L]}{1 + \sinh^2 2\alpha \sin^2 \ell L} \times \left[\mathbf{1} \cos k(a+b) \sinh 2\alpha \sin \ell L - i [\sigma_X + \sigma_Z \sin k(a+b) \sinh 2\alpha \sin \ell L] \right] \quad (13.3.35b)$$

As in the preceding example (13.3.9), there is an overall phase μ_0 due to the factors outside the [] braces.

$$e^{i\mu_0} = \frac{ie^{-ikL} [\cos \ell L + i \cosh 2\alpha \sin \ell L]}{\sqrt{1 + \sinh^2 2\alpha \sin^2 \ell L}} \quad (13.3.36)$$

This μ_0 is to be added to eigenphases $\pm\Theta/2$ coming from the rotational operator terms inside the [] braces.

$$\mathbf{S} = e^{i\mu_0} \frac{\left[\mathbf{1} \cos k(a+b) \sinh 2\alpha \sin \ell L - i [\sigma_X + \sigma_Z \sin k(a+b) \sinh 2\alpha \sin \ell L] \right]}{\sqrt{1 + \sinh^2 2\alpha \sin^2 \ell L}} \quad (13.3.37)$$

The operators determine $\Theta/2$ and the polar angles ϑ for eigenchannels, as in the first example (13.3.10).

$$\begin{aligned} \frac{\cos k(a+b) \sinh 2\alpha \sin \ell L}{\sqrt{1 + \sinh^2 2\alpha \sin^2 \ell L}}, & \quad \frac{1}{\sqrt{1 + \sinh^2 2\alpha \sin^2 \ell L}}, & \quad \frac{\sin k(a+b) \sinh 2\alpha \sin \ell L}{\sqrt{1 + \sinh^2 2\alpha \sin^2 \ell L}} \\ = \cos \frac{\Theta}{2}, & \quad = \hat{\Theta}_X \sin \frac{\Theta}{2}, & \quad = \hat{\Theta}_Z \sin \frac{\Theta}{2}, \\ & \quad = \sin \vartheta \sin \frac{\Theta}{2}, & \quad = \cos \vartheta \sin \frac{\Theta}{2}. \end{aligned} \quad (13.3.38)$$

For grazing states or a deep well, ℓ is much larger than k and $\sinh 2\alpha = (\ell^2 - k^2)/2k\ell$ becomes large. This makes the σ_Z -component of (13.3.35b) potentially much larger than the σ_X -component. So polar angle ϑ for the \mathbf{S} -vector that points to eigenchannel states will swing widely up and down around $\pi/2$ as the *kinetic factor* $\sin \ell L$ and *translation factor* $\sin k(a+b)$ each oscillate through ± 1 and 0. Then as ϑ oscillates, so, generally, will the ratio $\cos^2 \vartheta/2 : \sin^2 \vartheta/2$ of currents or charge on either side of the barrier for the eigenchannel. (Here the \sqrt{k} factors are the same on both sides.)

One exception occurs if the translation factor $\sin k(a+b)$ vanishes. This happens if the origin of reference is at the center of the well so $a=-b$. Then the \mathbf{S} -vector gets pinned to the $\pm X$ -axis and the polar angle is pinned to right angles ($\vartheta = \pm\pi/2$) for all values of well length $L=a-b$ and internal well momentum ℓ . Then all eigenchannel states have 1:1 charge ratio, just as you would expect from C_2 -symmetry analysis. Under these conditions, only two components of (13.3.38) remain.

$$\begin{aligned} \frac{\sinh 2\alpha \sin \ell L}{\sqrt{1 + \sinh^2 2\alpha \sin^2 \ell L}}, & \quad \frac{1}{\sqrt{1 + \sinh^2 2\alpha \sin^2 \ell L}}, & \quad \text{(for: } a=-b) \\ = \cos \frac{\Theta}{2}, & \quad = \sin \frac{\Theta}{2}. \end{aligned} \quad (13.3.39)$$

Eigenchannel phase shifts $\mu_{\pm} = \mu_0 \pm \Theta/2$ undergo sudden 2π jumps due to the kinetic factors $\sin \ell L$ and $\cos \ell L$ varying through ± 1 and 0 as E or V varies. The situation is complicated by a factor e^{-ikL} in the

overall phase factor (13.3.36), but, it is the other factors in $e^{i\mu_0}$ and particularly the $\pm\Theta/2$ variation of (13.3.39) that accounts for most of the jumps in total eigenchannel phase shifts μ_{\pm} .

Resonance strength, variation and lifetime

Each jump in μ_{\pm} by 2π represents a possible resonance as another half-wave ($\mu_{\pm}/2=\pm\pi$) gets sucked into (or out of) the well according to (13.3.15). The suddenness of the jump determines the strength or *lifetime* of the resonance. Sudden variation over small ΔE means long beating or dephasing times Δt for states composed of mixtures of energy states within the resonance interval ΔE . (Recall that beat frequency is proportional to the difference ΔE so the beat period Δt is inversely proportional to ΔE .)

A resonance will be strong or long-lived if the *amplification factor* $\sinh 2\alpha = (\ell^2 - k^2)/2k\ell$ is large compared to 1. Then the first component $\cos\Theta/2 = A \sinh 2\alpha \sin \ell L$ varies from positive to negative when kinetic factor $\sin \ell L$ varies from +1 thru 0 to -1. Meanwhile, the first component $\sin\Theta/2 = A$ is proportionately constant and relatively small. Only when $\sin \ell L$ is very much smaller than $\sinh 2\alpha$ does the phase angle $\Theta/2$ swing rapidly through $\pi/2$. The point where $\Theta/2 = \pi/2$ is the *resonance peak* and the amplitude for one of the eigenchannel states achieves a maximum in the potential well.

The two eigenchannel phases $\mu_{\pm} = \mu_0 \pm \Theta/2$ play leapfrog with one leaping while the other remains quiescent. It is very much like the galloping motion of real and imaginary wave components in space-time as discussed in Ch. 4 Sec. 4.3. The overall phase μ_0 increases stepwise, and at each step of μ_0 , $+\Theta/2$ flops suddenly up or down (or $-\Theta/2$ flops down or up) as shown in Fig. 13.3.7(a). If $+\Theta/2$ flops up it is in step with μ_0 and μ_+ does a big jump, but then $-\Theta/2$ is out of step with μ_0 so μ_- jumps only a little.

For even numbers ($\ell L = 2\pi, 4\pi, 6\pi, \dots$) of well half-waves, angle $+\Theta/2$ flops up in step with μ_0 and $\mu_+ = \mu_0 + \Theta/2$ does a big jump, but for odd numbers ($\ell L = 3\pi, 5\pi, 7\pi, \dots$) it is $\mu_- = \mu_0 - \Theta/2$ that makes a big jump. They have to take turns because a Ramsauer-Townsend resonance occurs only for those special values of ℓ which put wave anti-nodes right on both the well boundaries. (Recall Fig. 13.2.4.) A symmetric resonance has an even number of half waves while an anti-symmetric resonance has an odd number, so they must take turns as ℓ grows with a deepening well. Fig. 13.3.7 shows that they both have more abrupt jumps at their respective resonances as the well gets deeper.

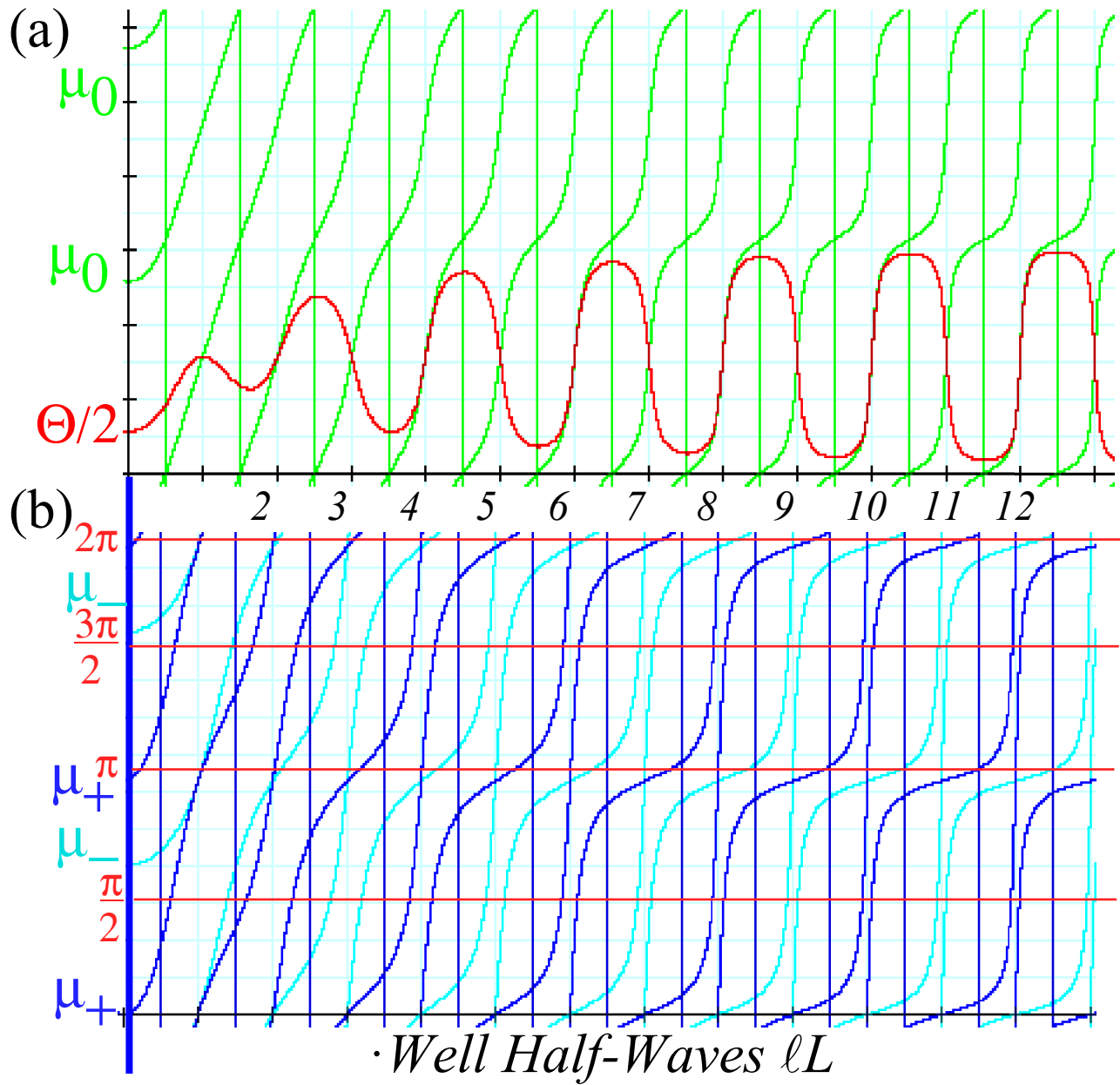


Fig. 13.3.7 (a) Separate phase angles (b) Combined phase angles give eigenchannel phase jumps.

Problems for Chapter 13.

Current current

13.1.1.(a) The concept of current $\mathbf{j} = \frac{-i\hbar}{2m}(\Psi^*(\nabla\Psi) - \Psi(\nabla\Psi)^*)$ introduced in (13.1.13) is as important as density or probability $\rho = \Psi^*\Psi$. Use the Schrodinger wave equations (11.4.5) to show that these two quantities satisfy a continuity equation. $\nabla \cdot \mathbf{j} + \frac{\partial \rho}{\partial t} = 0$.

(b) Is the continuity equation relativistically invariant? How can \mathbf{j} and ρ be made into a Lorentz 4-vector?

Standing Wave Rationale

13.1.2. Suppose you are propagating an electron wave left-to-right with energy $10\text{meV} = 10^{-2}\text{eV}$ above a potential-zero "floor" region toward a square step barrier that is V meV higher than the floor. Electrons, which get past the barrier interface, continue on indefinitely with no other sources or reflectors to the right.

(a) Suppose your counters detect a standing wave ratio (SWR) of 10:1 in the source region. (Let the detection electronics give ψ -amplitude values instead of particle number $\Psi^*\Psi$.)

Estimate the step value V of the barrier. Derive and sketch the wavefunction ψ and wave envelope $|\psi|$ before and after the barrier. (Show Re and Im parts for a couple of times.)

Show the distances between the barrier and the first and second wave envelope minima.

Calculate the relative probability or branching ratio for each electron to be turned back or to pass over the barrier. If possible, give answers in form of a rational fraction like $7/11$; $4/11$.

(b) Suppose you lower your electron energy so it falls just as much below the barrier as it was above it in the preceding exercise (a).

What happens to the SWR and the amplitude minima compared to their values in (a)? Derive and sketch the resulting wavefunction on either side of the barrier.

Calculate and indicate the distance into the barrier where the wave amplitude falls to 95% of its value at the interface. Do the same for the electron probability density.

(c). Suppose you are propagating an electron wave of energy $10\text{meV} = 10^{-2}\text{eV}$ left-to-right in a potential-free "floor" region toward a square barrier that is V meV lower than the floor.

Do exercise (a) for these new experimental conditions.

(d) Exercises (a) and (c) contain a purely outgoing moving wave propagating away from the barrier on one side or the other. In either or both these cases, would it be possible to have a purely incoming wave propagating toward the barrier? If not, explain which or why not. If so, explain how it might be accomplished experimentally and for which case(s).

Stairway to Hell

13.1.3. Suppose we reverse the "stairway to heaven" idea (Recall Fig. 13.1.10) and let a particle with an initially small momentum, say $k=1$, accelerate by falling into a deep well while increasing its k in small steps so as to give 100% transmission probability at each step. Must the step length Δx vary with k ?

(a) If the wavevector k increases by the same fraction or percentage p after each step describe how k and the potential must vary as a function of distance x . Suppose the percentage is small, say $\sim 1\%$, and derive an approximate differential equation $dk/dx=f(k,p)$. Solve the equation and see if there is a point x where this descent "blows-down," that is, ends with infinite kinetic energy.

(b) Is it possible to vary the percentage change $p(x)$ of k discretely every step or every other step in order to obtain more gentle wavelength variation, but still guarantee 100% transmission? Is $\lambda(x) \sim e^{-ax}$ or $\lambda(x) \sim 1/x$ a possibility?

Stump

13.2.1. Consider a barrier whose *height* equals the depth ($V=8.235$) of the well in Fig. 13.2.2 and whose width ($a=3.050$) is the same. (Use rationalized units for which m/\hbar^2 is unity.)

- (a) Derive and plot vs. energy E the transmission function $T(E)$ and its inverse for the barrier. Compare and comment on the similarities and/or differences between your results and Fig. 13.2.2.
- (b) Now consider real laboratory energy units, say, $V=8.235\text{eV}$. Suppose your $T(E)$ curves apply to an electron whose effective mass equals its *en-vacuo* value of $9E-31$ kg. What are the units of distance, and how long is the barrier in mks units?
- (c) How far below the barrier can the energy be and still give 5% transmission? Compare this transmission fall-off to a simple exponential $|e^{-\sqrt{2m(V-E)/\hbar^2}a}|^2$ fall-off. Give a simple $T(E)$ formula for the long- a limit.

Square Well by Sine-Line

13.2.2. Consider electrons with energy measured relative to an $E=0$ plane containing a square well of depth $V=-1$ eV and width $L=2$ units where the unit of distance is 1.23 nm. Use sine-line solutions.

- (a) Derive and sketch the lowest (ground) state wavefunction and energy eigenvalue. Include analytic approximations for the energy, wavevector, and 5% fall-off distance for the evanescent tails.
- (b) Give rough but reasonably accurate sketches of the remaining bound states.
- (c) Derive and sketch the lowest two positive energy resonance wavefunctions and energy values.

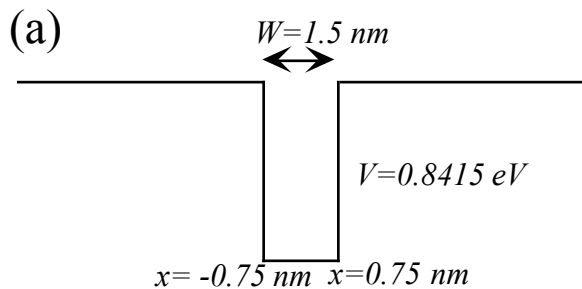


Fig.2.3

Resonating Inside and Out

13.2.3. Consider the well of depth $V = -0.8415$ eV and width $W = 1.5\text{nm}$. (See above Fig. 2.3)

(To compare with BandIt, give V in theorist units with m/\hbar^2 set to unity and while using a distance unit of nm.)

- (a) Use the sine-line method to characterize the bound states and first two resonance states. Plot or sketch the resulting wavefunctions showing their δ -shifts and κ -evanescences. (Useful for the next set.)
- (b) Compare with a plot of transmission functions T and $1/T$ for the E -range of interest.

C-to-S and Back

13.3.1. Verify the C-matrix to S-matrix transformation relations (13.3.5) and their inverses.

Crossing Elsewhere

13.3.2. Crossing matrices depend upon the choice of reference origin. If the origin for the plane waves x -coordinate is translated by distance a , or if a barrier boundary is moved the other way, then the C-matrix changes.

- (a) Derive a set of a-transformation relations in terms of a which you describe how to transform a general C-matrix which connects a k_1 -region on the right to a k_2 -region on its left.
- (b) Do the same for a general S-matrix.

Wave well

13.3.3. For the potential well of problem 13.2.3 derive C-matrix and S-matrix in terms of E and potential depth V , and width W . Consider waves for $V = -0.8415$ eV and width $W = 1.5\text{nm}$.

- (a) Calculate and plot both S-matrix eigenchannel waves for the first (lowest) resonance. Compare symmetry and other properties of the lowest "resonant" and "anti-resonant" eigenchannels. Sketch or plot the wavefunctions.

- (b) Combine the eigenchannel states so they make a left-source-channel waves and plot them.
- (d) Do a plot of both the eigenchannel phase shifts for a range of potential energy E that includes two or three of the lowest resonances. (See, for example, Fig. 13.3.7.)

Delta stumps

13.3.4. The effect of a Dirac-delta function potential $V(x) = \delta(x-a)$ may be derived directly using the analysis of Sec. 13.1.a or considered as a limit of very narrow "stump" potential.

- (a) Derive the C -matrix and S -matrix for a Dirac-delta function potential $V(x) = A \delta(x-a)$.
- (b) Compare your result to that of a "stump" (Problem 13.2.1) in the appropriate limit.
- (c) Discuss the S -matrix eigenfunctions for $V(x) = \delta(x-a)$ and $k=1$, first for $a=0$, and then for general values of $a=\pi/2$. Sketch the wavefunctions.

Sine-line shifts revisited

13.3.5. One can "sew" waves at a PE-jump (like the one at $x=a$ in Fig. 13.3.3) by solving

$$\Psi_1(x) = A_1 \cos(k_1 x' + \delta_1) = A_2 \cos(k_2 x' + \delta_2) = \Psi_2(x) \text{ at } x=a \text{ or } x'=x-a=0,$$

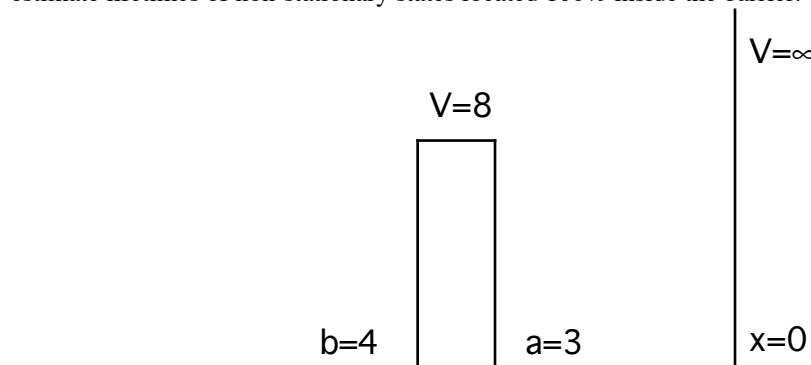
and a similar equation for the derivatives, to find (A_1, δ_1) in terms of (A_2, δ_2) and (k_1, k_2) .

- (a) Given the left channel wave $1/2 \cos(4x-0.793) = 1/2 \cos(4x'+0.4636)$ (where: $x'=x-a$ and $a=\pi/10$) find the right-channel wavefunction and compare to Fig. 13.3.3 (a).
- (b) Do the same for the wavefunction in Fig. 13.3.3 (b), and then sum the two wavefunctions (50-50 or $1/\sqrt{2}:1/\sqrt{2}$) and identify the result.
- (c) Derive general relations between (δ_1, δ_2) and S -matrix quantities $(\Theta, \Sigma; a)$ in (13.3.15). (Other parameters like $\Delta; a$ should drop out.)

Square molecule

13.3.6. A crude approximation to molecular vibration potentials and alpha-nuclear decay can be made using the square barriers shown in the figure below.

- (a) Construct a crossing matrix relation connecting the amplitudes propagating outside the barrier region and those inside. (Assume energy below barrier, at first.)
- (b) What restriction does the infinite right-hand barrier put on the wave amplitudes inside? Use this to derive a ratio between inside and outside probability for an eigenfunction of arbitrary energy E . Plot your result using the usual theoretician units with $m/\hbar^2=1$. Pay particular attention to the widths of resonant peaks in your plots. Use them to estimate lifetimes of non-stationary states located 100% inside the barrier.



Review Topics & Formulas for Unit 4

Dirac-delta representation of differential operators

$$\int_{y=a}^{y=b} dy \langle x | h(x) \mathbf{1} | y \rangle \psi(y) = \int_{y=a}^{y=b} dy h(x) \delta(y, x) \psi(y) = h(x) \psi(x) \quad (11.2.14a)$$

$$\int_{y=a}^{y=b} dy \langle x | g(x) \mathbf{D} | y \rangle \psi(y) = \int_{y=a}^{y=b} dy g(x) \frac{d\delta(y, x)}{dy} \psi(y) = g(x) \frac{d\psi(x)}{dx} \quad (11.2.14b)$$

$$\int_{y=a}^{y=b} dy \langle x | f(x) \mathbf{D}^2 | y \rangle \psi(y) = \int_{y=a}^{y=b} dy f(x) \frac{d^2\delta(y, x)}{dy^2} \psi(y) = f(x) \frac{d^2\psi(x)}{dx^2} \quad (11.2.14c)$$

Adjoint operator $\langle x | \mathbf{L}^\dagger | y \rangle = f^*(y) \frac{d^2\delta(x, y)}{dx^2} + g^*(y) \frac{d\delta(x, y)}{dx} + h^*(y) \delta(x, y)$ (11.2.18)

$$L^\dagger \cdot \psi(x) = \frac{d^2(f^*(x)\psi(x))}{dx^2} - \frac{d(g^*(x)\psi(x))}{dx} + h^*(x)\psi(x) \quad (11.2.20a)$$

Fourier transform of $\psi(x)$ $\langle k | \psi \rangle = \int_{-\infty}^{+\infty} dx \langle k | x \rangle \langle x | \psi \rangle = \int_{-\infty}^{+\infty} dx \frac{e^{-ikx}}{\sqrt{2\pi}} \langle x | \psi \rangle = \frac{1}{\sqrt{2\pi}} \int_{-\infty}^{+\infty} dx e^{-ikx} \psi(x)$

Momentum p-op. in x-basis $\langle x | \mathbf{p} | \psi \rangle = \frac{\hbar}{i} \frac{\partial}{\partial x} \psi(x)$ Coordinate x-op. in k-basis $\langle k | \mathbf{x} | \psi \rangle = i \frac{\partial}{\partial k} \psi(k)$

Schrodinger's time-dependent $\Psi(x, t) = \langle x | \Psi(t) \rangle$ wave equation.

$$i\hbar \langle x | \frac{\partial}{\partial t} | \Psi \rangle = \langle x | \frac{\mathbf{p}^2}{2M} + V(\mathbf{x}) | \Psi \rangle, \quad \text{or:} \quad i\hbar \frac{\partial \Psi(x, t)}{\partial t} = \frac{-\hbar^2}{2M} \frac{\partial^2 \Psi(x, t)}{\partial x^2} + V(x) \Psi(x, t) \quad (11.4.5c)$$

Schrodinger's time-independent $\psi_\epsilon(x) = \langle x | \epsilon \rangle$ wave eigenequation.

$$\langle x | \mathbf{H} | \epsilon \rangle = \epsilon \langle x | \epsilon \rangle, \quad \text{or:} \quad \frac{-\hbar^2}{2M} \frac{\partial^2 \psi_\epsilon(x)}{\partial x^2} + V(x) \psi_\epsilon(x) = \epsilon \psi_\epsilon(x) \quad (11.4.5d)$$

Bilateral B-type hyper-Schrodinger equations have even derivatives.

$$i\hbar \frac{\partial \Psi(x, t)}{\partial t} = d_0 \Psi(x, t) + d_2 \frac{\partial^2 \Psi(x, t)}{\partial x^2} + d_4 \frac{\partial^4 \Psi(x, t)}{\partial x^4} + d_6 \frac{\partial^6 \Psi(x, t)}{\partial x^6} + \dots \quad (11.5.10c)$$

Circulating or Complex C-type hyper-Schrodinger equations. (The odd-k d_k are imaginary.)

$$i\hbar \frac{\partial \Psi(x, t)}{\partial t} = d_0 \Psi(x, t) + d_1 \frac{\partial \Psi(x, t)}{\partial x} + d_2 \frac{\partial^2 \Psi(x, t)}{\partial x^2} + d_3 \frac{\partial^3 \Psi(x, t)}{\partial x^3} + d_4 \frac{\partial^4 \Psi(x, t)}{\partial x^4} + \dots \quad (11.5.13)$$

Asymmetric or A-type Schrodinger equations have q -dependent connectivity terms $d_{k,l,\dots}(q_m)$.

$$i\hbar \frac{\partial \Psi(q_m, t)}{\partial t} = \sum_{k,l} d_{k,l,\dots}(q_m) \frac{\partial^{k+l} \Psi(q_m, t)}{\partial q_1^k \partial q_2^l \dots} \quad (11.5.15)$$

Infinite square well eigensolutions $\langle x | \epsilon_n \rangle = \psi_n(x) = A \sin(k_n x) = A \sin\left(\frac{n\pi x}{W}\right)$ ($n=1,2,3,\dots$) (12.1.1c)

$$\epsilon_n = \frac{\hbar^2}{2M} k^2 = \frac{\hbar^2 n^2 \pi^2}{2MW^2} = \left(1^2, 2^2, 3^2, \dots \text{or } n^2\right) \frac{\hbar^2}{8MW^2} \quad (12.1.1d)$$

Dipole expectation $\langle x \rangle_\Psi = \langle \Psi | \mathbf{x} | \Psi \rangle = \sum_{m=1}^{\infty} \sum_{n=1}^{\infty} \langle \Psi | \epsilon_m \rangle \langle \epsilon_m | \mathbf{x} | \epsilon_n \rangle \langle \epsilon_n | \Psi \rangle$ (12.1.11)

$$\begin{aligned} \langle \Psi | \mathbf{x} | \Psi \rangle &= (|\alpha|^2 + |\beta|^2) \frac{W}{2} + \langle \varepsilon_1 | \mathbf{x} | \varepsilon_2 \rangle (\alpha^* \beta + \beta^* \alpha) \\ &= \frac{W}{2} + \frac{8W \cdot 1 \cdot 2}{\pi^2 (1^2 - 2^2)^2} 2|\alpha(0)\beta(0)| \cos(\omega_1 - \omega_2)t \xrightarrow{\alpha=\beta} \frac{W}{2} + 0.18W \cos(\omega_1 - \omega_2)t \end{aligned} \quad (12.1.15b)$$

Delta function: $\delta(x - a) = \langle x | a \rangle = \sum_{n=1}^{\infty} \langle x | \varepsilon_n \rangle \langle \varepsilon_n | a \rangle = \sum_{n=1}^{\infty} a_n \sin k_n x$, $a_n = (2/W) \sin k_n a$ (12.2.1a)

Approximate delta: $\Psi(x) \equiv \frac{2}{\pi} \int_0^{K_{\max}} dk \sin ka \sin kx \equiv \frac{\sin K_{\max}(x-a)}{\pi(x-a)}$ for: $x \approx a$ (12.2.3)

Heisenberg uncertainty relation $\Delta x \cdot |K_{\max}| = \Delta x \cdot \Delta k = \pi$ or: $\Delta x \cdot \Delta p = \pi \hbar = h/2$ (12.2.5)

Schrodinger's integral eigen-equation. $\frac{\hbar^2}{2M} k^2 \langle k | \varepsilon \rangle + \int dk' V(k - k') \langle k' | \varepsilon \rangle = \varepsilon \langle k | \varepsilon \rangle$ (11.4.13a)

where $V(k - k') = \langle k | V | k' \rangle = \frac{1}{2\pi} \int dx e^{-i(k-k')x} V(x)$ (11.4.13b)

Square potential boundary relations

$$\begin{pmatrix} \Psi \\ D\Psi \end{pmatrix} = \begin{pmatrix} e^{ikx} & e^{-ikx} \\ ike^{ikx} & -ike^{-ikx} \end{pmatrix} \begin{pmatrix} R \\ L \end{pmatrix}, \quad \begin{pmatrix} R \\ L \end{pmatrix} = \frac{i}{2k} \begin{pmatrix} -ike^{-ikx} & -e^{-ikx} \\ -ike^{ikx} & e^{ikx} \end{pmatrix} \begin{pmatrix} \Psi \\ D\Psi \end{pmatrix} \quad (13.1.8a)$$

Elementary *crossing matrix relation* for a single boundary point ($x=a$).

$$\begin{pmatrix} R' \\ L' \end{pmatrix} = \begin{pmatrix} \left(1 + \frac{k}{k'}\right) \frac{e^{i(k-k')a}}{2} & \left(1 - \frac{k}{k'}\right) \frac{e^{-i(k+k')a}}{2} \\ \left(1 - \frac{k}{k'}\right) \frac{e^{i(k+k')a}}{2} & \left(1 + \frac{k}{k'}\right) \frac{e^{i(k'-k)a}}{2} \end{pmatrix} \begin{pmatrix} R \\ L \end{pmatrix} \quad (13.1.10b)$$

Standing wave ratio (SWR) due to single boundary $SWR = \frac{L' + R'}{L' - R'} = \frac{2k'R'}{k + k'} = \frac{k'}{k} = \frac{\sqrt{E}}{\sqrt{E-V}}$ (13.1.10f)

Double step boundary $L'' = \frac{1}{2} e^{ika} \left[\left(1 - \frac{k}{k''}\right) \cos k'a + i \left(\frac{k'}{k''} - \frac{k}{k'}\right) \sin k'a \right] R$ (13.1.25b)

$(1 - k/k'')=0$ or $k=k''$, with $\sin k'a=0$ (3.4.25c) $k'=\sqrt{(kk'')}$ with: $\cos k'a=0$ (3.4.25d)

The Bound Case: $E < V$ (13.2.5a) *The Free Case: $E > V$* (13.2.5b)

$$\frac{1}{T} = \left| \cos \sqrt{2\varepsilon a} - \frac{(2\varepsilon - v)}{2\sqrt{\varepsilon(v - \varepsilon)}} \sin \sqrt{2\varepsilon a} \right|^2, \quad \frac{1}{T} = 1 + \frac{(v)^2}{4(\varepsilon - v)\varepsilon} \sin^2 \sqrt{2\varepsilon a},$$



Bound case: Sine-line square well solution

$ka + \delta = n\pi - \delta$, or: $ka/2 = n\pi/2 - \delta$ ($n = 1, 2, 3, \dots$) (13.2.9d)

$ka/2 = a/2\sqrt{(2V)} \sin \delta$ (13.2.9d)

C-matrix and S-matrix for single boundary and General C-to-S relations

$$\begin{pmatrix} C_{11} & C_{12} \\ C_{21} & C_{22} \end{pmatrix} = \begin{pmatrix} \frac{\Sigma}{\Pi} e^{-i\Delta a} & \frac{\Delta}{\Pi} e^{-i\Sigma a} \\ \frac{\Delta}{\Pi} e^{i\Sigma a} & \frac{\Sigma}{\Pi} e^{i\Delta a} \end{pmatrix}, \text{ where: } \begin{matrix} \Sigma = k_2 + k_1 \\ \Delta = k_2 - k_1 \\ \Pi = 2\sqrt{k_2 k_1} \end{matrix}, \quad \Sigma^2 = \Delta^2 + \Pi^2$$

$$\begin{pmatrix} S_{11} & S_{12} \\ S_{21} & S_{22} \end{pmatrix} = \begin{pmatrix} \frac{-\Delta}{\Sigma} e^{-i(\Sigma-\Delta)a} & \frac{\Pi}{\Sigma} e^{i\Delta a} \\ \frac{\Pi}{\Sigma} e^{i\Delta a} & \frac{\Delta}{\Sigma} e^{i(\Sigma+\Delta)a} \end{pmatrix} = e^{i\Delta a} \begin{pmatrix} \frac{-\Delta}{\Sigma} e^{-i\Sigma a} & \frac{\Pi}{\Sigma} \\ \frac{\Pi}{\Sigma} & \frac{\Delta}{\Sigma} e^{i\Sigma a} \end{pmatrix}$$

$$\begin{pmatrix} S_{11} = -\frac{C_{12}}{C_{11}} & S_{12} = \frac{1}{C_{11}} \\ S_{21} = \frac{1}{C_{11}} & S_{22} = \frac{C_{21}}{C_{11}} \end{pmatrix}, \quad \begin{pmatrix} S_{11} & S_{12} \\ S_{21} & S_{22} \end{pmatrix}^{-1} = \begin{pmatrix} S_{11}^\dagger = -\frac{C_{21}}{C_{22}} & S_{12}^\dagger = \frac{1}{C_{22}} \\ S_{21}^\dagger = \frac{1}{C_{22}} & S_{22}^\dagger = \frac{C_{12}}{C_{22}} \end{pmatrix} = \begin{pmatrix} S_{11}^* & S_{21}^* \\ S_{12}^* & S_{22}^* \end{pmatrix} \quad (13.3.5)$$

$$\begin{pmatrix} C_{11} = \frac{1}{S_{12}} & C_{12} = \frac{-S_{11}}{S_{12}} \\ C_{21} = \frac{S_{22}}{S_{12}} & C_{22} = \frac{1}{S_{12}^*} \end{pmatrix}, \quad \begin{pmatrix} C_{11} & C_{12} \\ C_{21} & C_{22} \end{pmatrix}^{-1} = \begin{pmatrix} C_{22} = \frac{1}{S_{12}^*} & -C_{12} = \frac{S_{11}}{S_{12}} \\ -C_{21} = \frac{-S_{22}}{S_{12}} & C_{11} = \frac{1}{S_{12}} \end{pmatrix} = \begin{pmatrix} \frac{1}{S_{21}^*} & -\frac{S_{22}^*}{S_{12}^*} \\ \frac{S_{11}^*}{S_{12}^*} & \frac{1}{S_{21}} \end{pmatrix}$$

Pauli-Hamilton expansion of S-Matrix (Single boundary)

$$S = ie^{i\Delta a} \left[\mathbf{1} \left(\frac{\Delta}{\Sigma} \sin \Sigma a \right) - i \left(\sigma_X \frac{\Pi}{\Sigma} - \sigma_Z \frac{\Delta}{\Sigma} \cos \Sigma a \right) \right]$$

Kinematic parameters Σ , Δ , and Π and rotation axis polar angle ϑ and angle Θ of rotation.

$$\begin{aligned} \frac{\Delta}{\Sigma} \sin \Sigma a &= \cos \frac{\Theta}{2}, & \frac{\Pi}{\Sigma} &= \hat{\Theta}_X \sin \frac{\Theta}{2}, & \frac{-\Delta}{\Sigma} \cos \Sigma a &= \hat{\Theta}_Z \sin \frac{\Theta}{2} \\ &= \sin \vartheta \sin \frac{\Theta}{2}, & & & &= \cos \vartheta \sin \frac{\Theta}{2}. \end{aligned} \quad (13.3.9)$$

Eigenvector :	Eigenvalue of $\mathbf{R}[0\vartheta\Theta]$:	Eigenvalue of S :
$\begin{pmatrix} \cos \vartheta / 2 \\ \sin \vartheta / 2 \end{pmatrix}$	$e^{-i\frac{\Theta}{2}}$	$e^{i\mu_1} = e^{i\left(\frac{-\Theta}{2} + \Delta a + \frac{\pi}{2}\right)}$
$\begin{pmatrix} \sin \vartheta / 2 \\ -\cos \vartheta / 2 \end{pmatrix}$	$e^{+i\frac{\Theta}{2}}$	$e^{i\mu_2} = e^{i\left(\frac{\Theta}{2} + \Delta a + \frac{\pi}{2}\right)}$

(13.3.11b)

Eigenchannel waves Ψ^v each with an individual **eigenchannel phase shift $\mu_v/2$** .

$$\begin{aligned} \Psi_{(LEFT)}^v &= \left(e^{i\mu_v} I_{2v}^R e^{-ik_2 x} + I_{2v}^R e^{ik_2 x} \right) / \sqrt{k_2}, & \Psi_{(RIGHT)}^v &= \left(I_{1v}^L e^{-ik_1 x} + e^{i\mu_v} I_{1v}^L e^{ik_1 x} \right) / \sqrt{k_1} \\ &= I_{2v}^R \left(e^{-i(k_2 x - \mu_v)} + e^{ik_2 x} \right) / \sqrt{k_2} & &= I_{1v}^L \left(e^{-ik_1 x} + e^{i(k_1 x + \mu_v)} \right) / \sqrt{k_1} \\ &= I_{2v}^R e^{i\mu_v/2} 2 \cos(k_2 x - \mu_v/2) / \sqrt{k_2} & &= I_{1v}^L e^{i\mu_v/2} 2 \cos(k_1 x + \mu_v/2) / \sqrt{k_1} \end{aligned}$$

Eigenchannel	Eigenchannel Amplitudes	Eigenchannel Phase Shifts
$\nu = 1$	$\begin{pmatrix} I_{1\nu}^L / \sqrt{k_1} \\ I_{2\nu}^R / \sqrt{k_2} \end{pmatrix} = \begin{pmatrix} (1/\sqrt{k_1}) \cos \vartheta / 2 \\ (1/\sqrt{k_2}) \sin \vartheta / 2 \end{pmatrix}$	$\mu_1 = \frac{-\Theta}{2} + \Delta a + \frac{\pi}{2}$
$\nu = 2$	$\begin{pmatrix} I_{1\nu}^L / \sqrt{k_1} \\ I_{2\nu}^R / \sqrt{k_2} \end{pmatrix} = \begin{pmatrix} (1/\sqrt{k_1}) \sin \vartheta / 2 \\ -(1/\sqrt{k_2}) \cos \vartheta / 2 \end{pmatrix}$	$\mu_2 = \frac{\Theta}{2} + \Delta a + \frac{\pi}{2}$

(13.3.15c)

The angles are found using (3.4.45) with (3.4.38c).

$$\Theta = 2 \cos^{-1} \left(\frac{\Delta \sin \Sigma a}{\Sigma} \right), \quad \sin \vartheta = \frac{\Pi}{\Sigma \sin \frac{\Theta}{2}}, \quad \cos \vartheta = \frac{-\Delta \cos \Sigma a}{\Sigma \sin \frac{\Theta}{2}}. \quad (13.3.15d)$$

$$\cos \frac{\vartheta}{2} = \sqrt{\frac{1 + \cos \vartheta}{2}} = \sqrt{\frac{\Sigma \sin \frac{\Theta}{2} - \Delta \cos \Sigma a}{2 \Sigma \sin \frac{\Theta}{2}}}, \quad \sin \frac{\vartheta}{2} = \sqrt{\frac{1 - \cos \vartheta}{2}} = \sqrt{\frac{\Sigma \sin \frac{\Theta}{2} + \Delta \cos \Sigma a}{2 \Sigma \sin \frac{\Theta}{2}}} \quad (13.3.15e)$$

The C-matrix for a square well from $x=b$ and to $x=a$ as sketched in Fig. 13.3.6(a) is as follows.

$$C = \begin{pmatrix} e^{ikL} [\cos \ell L - i \cosh 2\alpha \sin \ell L] & -ie^{-ik(a+b)} \sinh 2\alpha \sin \ell L \\ ie^{ik(a+b)} \sinh 2\alpha \sin \ell L & e^{-ikL} [\cos \ell L + i \cosh 2\alpha \sin \ell L] \end{pmatrix}$$

(13.3.33a)

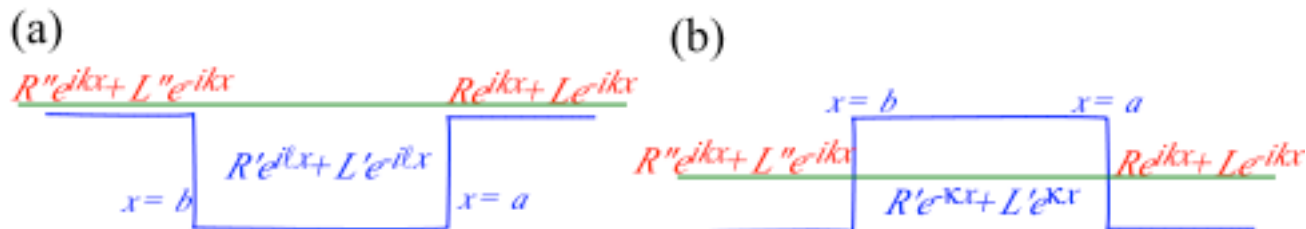
$$k = \sqrt{\frac{2mE}{\hbar^2}}, \quad \ell = \sqrt{\frac{2m(E-V)}{\hbar^2}} \quad \left(= \sqrt{\frac{2m(E+|V|)}{\hbar^2}} \text{ for } V < 0 \right) \quad (13.3.33)$$

A notation using hyperbolic functions

$$\cosh 2\alpha = \frac{1}{2} \left(\frac{\ell}{k} + \frac{k}{\ell} \right) = \frac{\ell^2 + k^2}{2k\ell}, \quad \sinh 2\alpha = \frac{1}{2} \left(\frac{\ell}{k} - \frac{k}{\ell} \right) = \frac{\ell^2 - k^2}{2k\ell}, \quad (13.3.33c)$$

$$\cosh \alpha = \frac{k + \ell}{2\sqrt{k\ell}} = \frac{\Sigma}{\Pi}, \quad \sinh \alpha = \frac{\ell - k}{2\sqrt{k\ell}} = \frac{\Delta}{\Pi} \quad (13.3.33d)$$

$$\cosh 4\alpha = \frac{1}{2} \left(\frac{\ell^2}{k^2} + \frac{k^2}{\ell^2} \right), \quad \sinh 4\alpha = \frac{1}{2} \left(\frac{\ell^2}{k^2} - \frac{k^2}{\ell^2} \right) \quad (13.3.33e)$$



If E is below a square barrier V : $C = \begin{pmatrix} e^{ikL} [\cosh \kappa L + i \sinh 2\beta \sinh \kappa L] & ie^{-ik(a+b)} \cosh 2\beta \sinh \kappa L \\ -ie^{ik(a+b)} \cosh 2\beta \sinh \kappa L & e^{-ikL} [\cosh \kappa L - i \sinh 2\beta \sinh \kappa L] \end{pmatrix}$

(13.3.34a)

where: $k = \sqrt{\frac{2mE}{\hbar^2}}$, $-i\ell = \kappa = \sqrt{\frac{2m(V-E)}{\hbar^2}}$ (for: $V > E > 0$) (13.3.34b)

Again, $L=a-b$ and a convenient notation uses hyperbolic functions.

$$\cosh 2\beta = \frac{1}{2} \left(\frac{\kappa}{k} + \frac{k}{\kappa} \right) = \frac{\kappa^2 + k^2}{2k\kappa}, \quad \sinh 2\beta = \frac{1}{2} \left(\frac{\kappa}{k} - \frac{k}{\kappa} \right) = \frac{\kappa^2 - k^2}{2k\kappa} \quad (13.3.34c)$$

$$\cosh \beta = \frac{k + \kappa}{2\sqrt{k\kappa}} \equiv \frac{\sigma}{\rho}, \quad \sinh \beta = \frac{\kappa - k}{2\sqrt{k\kappa}} \equiv \frac{\delta}{\rho} \quad (13.3.34d)$$

$$\cosh 4\beta = \frac{1}{2} \left(\frac{\kappa^2}{k^2} + \frac{k^2}{\kappa^2} \right), \quad \sinh 4\beta = \frac{1}{2} \left(\frac{\kappa^2}{k^2} - \frac{k^2}{\kappa^2} \right) \quad (13.3.34e)$$

S-matrix: $\mathbf{S} = e^{i\mu_0} \frac{\mathbf{1} \cos k(a+b) \sinh 2\alpha \sin \ell L - i [\sigma_X + \sigma_Z \sin k(a+b) \sinh 2\alpha \sin \ell L]}{\sqrt{1 + \sinh^2 2\alpha \sin^2 \ell L}}$

$$e^{i\mu_0} = \frac{ie^{-ikL} [\cos \ell L + i \cosh 2\alpha \sin \ell L]}{\sqrt{1 + \sinh^2 2\alpha \sin^2 \ell L}}$$

$$\frac{\cos k(a+b) \sinh 2\alpha \sin \ell L}{\sqrt{1 + \sinh^2 2\alpha \sin^2 \ell L}}, \quad \frac{1}{\sqrt{1 + \sinh^2 2\alpha \sin^2 \ell L}}, \quad \frac{\sin k(a+b) \sinh 2\alpha \sin \ell L}{\sqrt{1 + \sinh^2 2\alpha \sin^2 \ell L}}$$

$$= \cos \frac{\Theta}{2}, \quad = \sin \vartheta \sin \frac{\Theta}{2}, \quad = \cos \vartheta \sin \frac{\Theta}{2}.$$